

**Metabolic engineering of *Cupriavidus necator* H16
for the production of C5 platform chemicals**

Christian Jürgen Egon Gude, MSc.

**Thesis submitted to the University of Nottingham for the degree of Doctor
of Philosophy**

October 2020

Declaration

Unless otherwise acknowledged, the work presented in this thesis is my own.

No part has been submitted for another degree at the University of Nottingham or any other institute of learning.

Christian Gude, October 2020

Acknowledgements

To my supervisors, Kati Kovacs, Nigel Minton and Alexander Conradie. For your dedication, your guidance and your support.

To my parents, who were always at my side, no matter how far away I was.

To Isobel, who made this journey possible and decided to join my side for life.

To the wise whisper that lights my paths.

Abstract

Raising demand for plastics, especially in developing countries, poses a challenge for suppliers to satisfy the need in a sustainable way. Developing carbon-neutral C5 platform chemicals for the production of easily recyclable biopolymers is an integral part of this mission.

In this work, *Cupriavidus necator* H16 was metabolic engineered to produce the C5 precursors 5-aminovaleric acid and 5-hydroxyvaleric acid for plastic production from industrial waste gases. *C. necator* H16 was selected as host organism for metabolic engineering because of its ability to grow lithoautotrophically, using CO₂ waste gas as carbon source, ammonia as nitrogen source and hydrogen as energy source.

The novel pathway designs for these C5 platform chemicals were first tested in background hosts such as the *C. necator* H16 wildtype and engineered deletion mutant strains. Once all pathways were designed, tested and chassis strains engineered, optimisations were made. Synthetic biology tools such as the use of synthetic ribosomal binding sites, use of the promoters P_{trp} and P_{trc} and feedback-resistant enzyme mutants were introduced to the pathways

The production of 5-hydroxyvaleric acid (5-OHV), a precursor for biodegradable polyesters was investigated, using a novel reverse beta-oxidation chain elongation pathway from β -alanine. An engineered *C. necator* H16 Δ *phaCAB* Δ *mmsA1* Δ *mmsA2* Δ *mmsA3* strain expressing the genes *ydfG_{EC}*, *bapat_{CV}*, *prpE_{EC}*, *bktB_{CN}*, *phaB_{CN}*, *crt3_{CN}* and *ter_{TD}* produced 5-OHV with a yield of 17.1 mg L⁻¹ from 20 mM β -alanine.

The production of 5-aminovaleric acid (5-AV) via L-lysine was investigated. 5-AV is a precursor for the industrial production of the polyamide nylon-5. Feedback-resistant variants of the lysine biosynthesis pathway enzymes aspartate kinase (LysC) and DHDPS (DapA) were introduced. Furthermore, a bypass pathway using DAPDH (Ddh) enhanced L-lysine biosynthesis. The enzymes DavB and DavA, encoding a lysine monooxygenase and a δ -aminovaleramidase, completed the pathway from L-lysine to 5-AV. Lastly, disruption of the gene *gabT*, encoding a GABA aminotransferase with activity towards 5-AV, eliminated 5-AV degradation. As a result of the above modifications, this work showed the first to date production of 5-AV from *C. necator* H16 central metabolism with a yield of 10.5 mg L⁻¹ from 10 g L⁻¹ mM sodium gluconate.

Furthermore, a novel transcription-factor based biosensor design with fluorescent output for the detection of 5-AV and quantities >50 mM was investigated. This work also demonstrates a second biosensor design with the ability to detect δ -valerolactam in a graded manner for quantities >2 mM.

List of Figures and Tables

Figure 1.1 Simplified Calvin-Benson-Bassham cycle and its three stages.

Figure 1.2 *Cupriavidus necator* H16 metabolism under aerobic lithoautotrophic conditions for the production of products from CO₂.

Figure 1.3 TEM micrograph of *C. necator* H16 before (left) and after (right) PHB granule accumulation.

Figure 1.4 Chemical structures of 5-hydroxyvaleric acid and poly-5-hydroxyvalerate. (p. 27)

Figure 1.5 Chemical structures of 5-aminovaleric acid and nylon-5.

Figure 1.6 DavB catalyses the formation of 5-aminovaleramide from L-lysine.

Figure 1.7 DavA catalyses the formation of 5-aminovaleric acid from 5-aminovaleramide.

Figure 1.8 The Dav degradation pathway of L-lysine in *Pseudomonas putida*.

Figure 1.9 L-lysine biosynthesis pathways in bacteria.

Table 2.1 Bacterial strains used in this study.

Table 2.2 List of antibiotics that were used in this study.

Table 2.3 Plasmids used in this study.

Table 2.4 HiFi fragments used to generate plasmids described in this study.

Table 2.5 Sequences of primers used in this study.

Figure 3.1 Proposed pathways for the production of 5-hydroxyvaleric acid from β -alanine.

Figure 3.2 Conversion of β -alanine to 3-HP through malonic semialdehyde in *Cupriavidus necator* H16.

Figure 3.3 Transfer of CoA to 3-HP through either one of two proposed reactions.

Figure 3.4 (A) Desired chain elongation by two carbon atoms mediated by β -ketothiolase BktB and 3-oxoadipyl-CoA thiolase PaaJ. (B) Native reactions catalysed by BktB and PaaJ.

Figure 3.5 Reverse beta oxidation chain lengthening converts 3-HP-CoA to 5-hydroxyvaleryl-CoA through a series of reactions A-E.

Figure 3.6 5-hydroxypentanoyl-CoA is hydrolysed.

Figure 3.7 The *Cupriavidus necator* H16 $\Delta mmsA1 \Delta mmsA2 \Delta mmsA3$ deletion strain prevents the degradation of malonic semialdehyde to acetyl-CoA in the 5-OHV pathway.

Figure 3.8 Gene combinations used for the *E. coli* DH5 α double transformant strains.

Table 3.1 Overview of detected analytes after 48 h fermentation of transgenic *E. coli* DH5 α expressing potential metabolic pathways for 5-hydroxyvalerate production.

Figure 3.9 Gene combinations used for the *C. necator* H16 wildtype and $\Delta 4$ double transformant strains.

Table 3.2 Overview of detected analytes after 48 h fermentation of transgenic *C. necator* H16 wildtype and $\Delta 4$, expressing potential metabolic pathways for 5-hydroxyvalerate production.

Figure 3.10 Growth profiles and gluconate consumption of the double empty vector transformed *Cupriavidus necator* wildtype and its $\Delta phaCAB$ and $\Delta 4$ knockout mutants.

Figure 3.11 Growth profiles of the double empty vector transformed *Cupriavidus necator* $\Delta 4$ mutant (CN21 $\Delta 4$), the 3-HP producing strain CN19 $\Delta 4$ and the 5-hydroxyvalerate producing strain CN11 $\Delta 4$.

Figure 3.12 Quantified levels of β -alanine, 3-hydroxypropanoic acid and 5-hydroxyvaleric acid after 24h of resting cell fermentation in 20 mM β -alanine supplemented and non-supplemented *C. necator* H16 $\Delta 4$ cultures.

Figure 3.13 Configuration of the final 5-hydroxyvalerate producing pathway.

Figure 3.14 Quantified levels of pathway relevant metabolites during 60 h fermentation of 20 mM β -alanine supplemented *Cupriavidus necator* H16 strain CN22 $\Delta 4$.

Figure 4.1 Metabolic pathway for the production of 5-AV from glucose in *E. coli* as used by Adkins et al.

Figure 4.2 The Dav degradation pathway of L-lysine in *P. putida*.

Figure 4.3 Pairwise alignment of native *Escherichia coli* DHDPS and *Corynebacterium glutamicum* DHDPS.

Figure 4.4 Optical density of resting cell *Cupriavidus necator* H16 micro fermentation cultures over 40 h in the presence of 5-AV in CNMM-P medium.

Figure 4.5 Growth curves of *Cupriavidus necator* H16 wildtype in CNMM medium with and without 5-AV supplementation over 40 h.

Figure 4.6 Growth curves of *Cupriavidus necator* H16 wildtype in limiting media conditions and 5-AV supplementation.

Figure 4.7 Vector pL1: Pathway for the production of 5-AV from L-lysine.

Figure 4.8 Aspartate, L-lysine and 5-AV levels in aspartate-fed *Escherichia coli* and *Cupriavidus necator* H16 cultures harbouring the pL1 plasmid.

Figure 4.9 Aspartate, L-lysine and 5-AV levels in L-lysine-fed *Escherichia coli* and *Cupriavidus necator* H16 cultures harbouring the pL1 plasmid.

Figure 4.10 Aerobic resting cell fermentation in minimal 20 mM aspartate supplemented medium using phosphate limitation in *Cupriavidus necator* H16 $\Delta phaCAB$.

Figure 4.11 *Cupriavidus necator* H16 $\Delta phaCAB$ and $\Delta phaCAB \Delta gabT$ carrying pL1 in aerobic fermentations with 20 mM aspartate supplemented minimal medium.

Figure 4.12 Proposed 5-AV biosynthesis pathway in *Cupriavidus necator* H16 $\Delta phaCAB \Delta gabT$.

Figure 4.13 Synthetic pathways for the production of 5-AV in *Cupriavidus necator* H16 Δ phaCAB Δ gabT.

Figure 4.14 5-aminovaleric acid levels in *Cupriavidus necator* H16 Δ phaCAB Δ gabT growing cell fermentations using CNMM^{Tet} supplemented with 10 mM aspartic acid.

Figure 4.15 5-aminovaleric acid levels in *Cupriavidus necator* H16 Δ phaCAB Δ gabT growing cell L9 fermentations: Unsupplemented CNMM^{Tet} medium and supplemented CNMM^{Tet} medium with 10 mM aspartic acid.

Figure 4.16 Proposed uracil synthesis route in *Cupriavidus necator* H16 resting cells from aspartate and gluconate.

Figure 5.1 A plasmid-based 5-AV biosensor.

Figure 5.2 Biosensor pBS1 assembly design.

Figure 5.3 *E. coli* DH5 α cells expressing the BS1 biosensor in the presence of δ -valerolactam. (p. 216)

Figure 5.4 Biosensor pBS2 assembly design.

Figure 5.5 Quantified levels of δ -valerolactam in aerobic *E. coli* cells harbouring pBS2 and pL1 in LB^{cm} supplemented with 20 mM L-lysine.

Figure 5.6 Western-blot of His-tagged ORF26 in soluble and insoluble fractions of Lemo21 cells.

Figure 5.7 Biosensor BS3 assembly design.

Figure 5.8 *E. coli* DH5 α cells expressing the pBS3 biosensor in the presence of δ -valerolactam at different temperatures.

Figure 5.8 SDS-PAGE of His-tagged ChnR in soluble and insoluble fractions of Rosetta-gamiTM cells.

Figure 5.9 δ -valerolactam and its analogues.

Figure 5.10 Fluorescence of DH5 α cells (OD normalised) expressing biosensor pBS3 in microfermentation using ECMM^{cm}, supplemented with δ -valerolactam and its analogues.

Figure 5.11 Relationship between δ -valerolactam concentration and fluorescence.

Figure 6.1 Main outcomes of this study: Engineered pathways for the production of 5-AV, 5-OHV and a 5-AV biosensor.

Figure A1 H1-NMR spectrum of chemically synthesised 5-OHV

Figure A2 Mass spectrum of 1 mM β -alanine standard reagent

Figure A3 Mass spectrum of 1 mM 3-HP standard reagent

Figure A4 Mass spectrum of 1 mM 5-OHV standard reagent

Figure A5 Mass spectrum of 1 mM 5-AV standard reagent

Figure A6 Alanine mass spectra of 50 mM β -alanine supplemented (top) and unsupplemented (bottom) EC21 (no plasmid control) *E. coli* fermentations, 48 h timepoint.

Figure A7 3-HP mass spectra of 50 mM β -alanine supplemented (top) and unsupplemented (bottom) EC21 (no plasmid control) *E. coli* fermentations, 48 h timepoint.

Figure A8 5-OHV mass spectra of 50 mM β -alanine supplemented (top) and unsupplemented (bottom) EC21 (no plasmid control) *E. coli* fermentations, 48 h timepoint.

Figure A9 Alanine mass spectra of 50 mM β -alanine supplemented EC11 (top) and EC12 (bottom) *E. coli* fermentations, 48 h timepoint.

Figure A10 3-HP mass spectra of 50 mM β -alanine supplemented EC11 (top) and EC12 (bottom) *E. coli* fermentations, 48 h timepoint.

Figure A11 5-OHV mass spectra of 50 mM β -alanine supplemented EC11 (top) and EC12 (bottom) *E. coli* fermentations, 48 h timepoint.

Figure A12 Alanine mass spectra of 50 mM β -alanine supplemented (top) and unsupplemented (bottom) CN21 Δ 4 (no plasmid control) fermentations, 48 h timepoint.

Figure A13 3-HP mass spectra of 50 mM β -alanine supplemented (top) and unsupplemented (bottom) CN21 Δ 4 (no plasmid control) fermentations, 48 h timepoint.

Figure A14 5-OHV mass spectra of 50 mM β -alanine supplemented (top) and unsupplemented (bottom) CN21 Δ 4 (no plasmid control) fermentations, 48 h timepoint.

Figure A15 3-HP mass spectra of 50 mM β -alanine supplemented CN1 Δ 4 (top) and CN2 Δ 4 (bottom) fermentations, 48 h timepoint.

Figure A16 5-OHV mass spectra of 50 mM β -alanine supplemented CN1 Δ 4 (top) and CN2 Δ 4 (bottom) fermentations, 48 h timepoint.

Figure A17 Alanine mass spectra of 50 mM β -alanine supplemented (top) and unsupplemented (bottom) CN11 Δ 4 fermentations, 48 h timepoint.

Figure A18 Alanine mass spectra of 50 mM β -alanine supplemented CN11 Δ 4 (top) and CN12 Δ 4 (bottom) fermentations, 48 h timepoint.

Figure A19 3-HP mass spectra of 50 mM β -alanine supplemented (top) and unsupplemented (bottom) CN11 Δ 4 fermentations, 48 h timepoint.

Figure A20 3-HP mass spectra of 50 mM β -alanine supplemented CN11 Δ 4 (top) and CN12 Δ 4 (bottom) fermentations, 48 h timepoint.

Figure A21 5-OHV mass spectra of 50 mM β -alanine supplemented CN11 Δ 4 (top) and CN12 Δ 4 (bottom) fermentations, 48 h timepoint.

Figure A22 5-OHV mass spectra of 50 mM β -alanine supplemented CN17 Δ 4 fermentations, 48 h timepoint.

Figure A23 5-AV mass spectra of 20 mM L-lysine supplemented L7 fermentations, 20 h timepoint.

Figure A24 δ -valerolactam mass spectra of 20 mM L-lysine supplemented L7 + pBS2 fermentations, 20 h timepoint.

Figure A25 δ -valerolactam mass spectra of 20 mM L-lysine supplemented L1 without pBS2 fermentations, 20 h timepoint.

Figure A26 Growth curves of *E. coli* DH5 α EC1 in ECMM medium with 50 mM β -alanine supplementation over 48 h.

Figure A27 Growth curves of *E. coli* DH5 α EC2 in ECMM medium with 50 mM β -alanine supplementation over 48 h.

Figure A28 Growth curves of *E. coli* DH5 α EC3 in ECMM medium with 50 mM β -alanine supplementation over 48 h.

Figure A29 Growth curves of *E. coli* DH5 α EC4 in ECMM medium with 50 mM β -alanine supplementation over 48 h.

Figure A30 Growth curves of *E. coli* DH5 α EC5 in ECMM medium with 50 mM β -alanine supplementation over 48 h.

Figure A31 Growth curves of *E. coli* DH5 α EC6 in ECMM medium with 50 mM β -alanine supplementation over 48 h.

Figure A32 Growth curves of *E. coli* DH5 α EC7 in ECMM medium with 50 mM β -alanine supplementation over 48 h.

Figure A33 Growth curves of *E. coli* DH5 α EC8 in ECMM medium with 50 mM β -alanine supplementation over 48 h.

Figure A34 Growth curves of *E. coli* DH5 α EC9 in ECMM medium with 50 mM β -alanine supplementation over 48 h.

Figure A35 Growth curves of *E. coli* DH5 α EC10 in ECMM medium with 50 mM β -alanine supplementation over 48 h.

Figure A36 Growth curves of *E. coli* DH5 α EC11 in ECMM medium with 50 mM β -alanine supplementation over 48 h.

Figure A37 Growth curves of *E. coli* DH 5 α EC12 in ECMM medium with 50 mM β -alanine supplementation over 48 h.

Figure A38 Growth curves of *E. coli* DH5 α EC13 in ECMM medium with 50 mM β -alanine supplementation over 48 h.

Figure A39 Growth curves of *E. coli* DH5 α EC14 in ECMM medium with 50 mM β -alanine supplementation over 48 h.

Figure A40 Growth curves of *E. coli* DH5 α EC15 in ECMM medium with 50 mM β -alanine supplementation over 48 h.

Figure A41 Growth curves of *E. coli* DH5 α EC16 in ECMM medium with 50 mM β -alanine supplementation over 48 h.

Figure A42 Growth curves of *E. coli* DH5 α EC17 in ECMM medium with 50 mM β -alanine supplementation over 48 h.

Figure A43 Growth curves of *E. coli* DH5 α EC18 in ECMM medium with 50 mM β -alanine supplementation over 48 h.

Figure A44 Growth curves of *E. coli* DH5 α EC19 in ECMM medium with 50 mM β -alanine supplementation over 48 h.

Figure A45 Growth curves of *E. coli* DH5 α EC20 in ECMM medium with 50 mM β -alanine supplementation over 48 h.

Figure A46 Growth curves of *E. coli* DH5 α EC21 in ECMM medium with 50 mM β -alanine supplementation over 48 h.

Figure A47 Growth curves of *C. necator* H16 CN1 Δ 4 in CNMM medium with 50 mM β -alanine supplementation over 48 h.

Figure A48 Growth curves of *C. necator* H16 CN2 Δ 4 in CNMM medium with 50 mM β -alanine supplementation over 48 h.

Figure A49 Growth curves of *C. necator* H16 CN3 Δ 4 in CNMM medium with 50 mM β -alanine supplementation over 48 h.

Figure A50 Growth curves of *C. necator* H16 CN4 Δ 4 in CNMM medium with 50 mM β -alanine supplementation over 48 h.

Figure A51 Growth curves of *C. necator* H16 CN5 Δ 4 in CNMM medium with 50 mM β -alanine supplementation over 48 h.

Figure A52 Growth curves of *C. necator* H16 CN6 Δ 4 in CNMM medium with 50 mM β -alanine supplementation over 48 h.

Figure A53 Growth curves of *C. necator* H16 CN7 Δ 4 in CNMM medium with 50 mM β -alanine supplementation over 48 h.

Figure A54 Growth curves of *C. necator* H16 CN8 Δ 4 in CNMM medium with 50 mM β -alanine supplementation over 48 h.

Figure A55 Growth curves of *C. necator* H16 CN9 Δ 4 in CNMM medium with 50 mM β -alanine supplementation over 48 h.

Figure A56 Growth curves of *C. necator* H16 CN10 Δ 4 in CNMM medium with 50 mM β -alanine supplementation over 48 h.

Figure A57 Growth curves of *C. necator* H16 CN11 Δ 4 in CNMM medium with 50 mM β -alanine supplementation over 48 h.

Figure A58 Growth curves of *C. necator* H16 CN12 Δ 4 in CNMM medium with 50 mM β -alanine supplementation over 48 h.

Figure A59 Growth curves of *C. necator* H16 CN13 Δ 4 in CNMM medium with 50 mM β -alanine supplementation over 48 h.

Figure A60 Growth curves of *C. necator* H16 CN14 Δ 4 in CNMM medium with 50 mM β -alanine supplementation over 48 h.

Figure A61 Growth curves of *C. necator* H16 CN15 Δ 4 in CNMM medium with 50 mM β -alanine supplementation over 48 h.

Figure A62 Growth curves of *C. necator* H16 CN16 Δ 4 in CNMM medium with 50 mM β -alanine supplementation over 48 h.

Figure A63 Growth curves of *C. necator* H16 CN17 Δ 4 in CNMM medium with 50 mM β -alanine supplementation over 48 h.

Figure A64 Growth curves of *C. necator* H16 CN18 Δ 4 in CNMM medium with 50 mM β -alanine supplementation over 48 h.

Figure A65 Growth curves of *C. necator* H16 CN19Δ4 in CNMM medium with 50 mM β-alanine supplementation over 48 h.

Figure A66 Growth curves of *C. necator* H16 CN20Δ4 in CNMM medium with 50 mM β-alanine supplementation over 48 h.

Figure A67 Growth curves of *C. necator* H16 CN21Δ4 in CNMM medium with 50 mM β-alanine supplementation over 48 h.

Figure A68 Growth curves of *C. necator* H16 CN1 in CNMM medium with 50 mM β-alanine supplementation over 48 h.

Figure A69 Growth curves of *C. necator* H16 CN2 in CNMM medium with 50 mM β-alanine supplementation over 48 h.

Figure A70 Growth curves of *C. necator* H16 CN3 in CNMM medium with 50 mM β-alanine supplementation over 48 h.

Figure A71 Growth curves of *C. necator* H16 CN4 in CNMM medium with 50 mM β-alanine supplementation over 48 h.

Figure A72 Growth curves of *C. necator* H16 CN5 in CNMM medium with 50 mM β-alanine supplementation over 48 h.

Figure A73 Growth curves of *C. necator* H16 CN6 in CNMM medium with 50 mM β-alanine supplementation over 48 h.

Figure A74 Growth curves of *C. necator* H16 CN7 in CNMM medium with 50 mM β-alanine supplementation over 48 h.

Figure A75 Growth curves of *C. necator* H16 CN8 in CNMM medium with 50 mM β-alanine supplementation over 48 h.

Figure A76 Growth curves of *C. necator* H16 CN9 in CNMM medium with 50 mM β-alanine supplementation over 48 h.

Figure A77 Growth curves of *C. necator* H16 CN10 in CNMM medium with 50 mM β-alanine supplementation over 48 h.

Figure A78 Growth curves of *C. necator* H16 CN11 in CNMM medium with 50 mM β-alanine supplementation over 48 h.

Figure A79 Growth curves of *C. necator* H16 CN12 in CNMM medium with 50 mM β-alanine supplementation over 48 h.

Figure A80 Growth curves of *C. necator* H16 CN13 in CNMM medium with 50 mM β-alanine supplementation over 48 h.

Figure A81 Growth curves of *C. necator* H16 CN14 in CNMM medium with 50 mM β-alanine supplementation over 48 h.

Figure A82 Growth curves of *C. necator* H16 CN15 in CNMM medium with 50 mM β-alanine supplementation over 48 h.

Figure A83 Growth curves of *C. necator* H16 CN16 in CNMM medium with 50 mM β-alanine supplementation over 48 h.

Figure A84 Growth curves of *C. necator* H16 CN17 in CNMM medium with 50 mM β-alanine supplementation over 48 h.

Figure A85 Growth curves of *C. necator* H16 CN18 in CNMM medium with 50 mM β -alanine supplementation over 48 h.

Figure A86 Growth curves of *C. necator* H16 CN19 in CNMM medium with 50 mM β -alanine supplementation over 48 h.

Figure A87 Growth curves of *C. necator* H16 CN20 in CNMM medium with 50 mM β -alanine supplementation over 48 h.

Figure A88 Growth curves of *C. necator* H16 CN21 in CNMM medium with 50 mM β -alanine supplementation over 48 h. CN21

Figure A89 Plasmid map of vector pMTL71301.

Figure A90 Plasmid map of vector pMTL4111.

Figure A91 Plasmid map of vector pET-16b.

Abbreviations

°C	Degrees Celcius
μF	Microfarad
3-HP	3-hydroxypropanoic acid, 3HP
5-AV	5-aminovaleric acid
5-OHV	5-hydroxyvaleric acid
A.U.	arbitrary unit, arb unit
ADP	Adenosine diphosphate
AK	Aspartate kinase
AMP	Adenosine monophosphate
Amp	Ampicillin
AMV	Aminovalerate pathway
ATCC	American Type Culture Collection
ATP	Adenosine triphosphate
BBSRC	Biotechnology and Biological Sciences Research Council
BDOs	Butanediols
BSA	Bovine serum albumin
C3	An organic chemical with three carbon atoms
C5	An organic chemical with five carbon atoms
CBB	CBB cycle – Calvin-Benson-Bessham cycle
cfu	Colony forming units
Cm	Chloramphenicol
CNMM	<i>C. necator</i> minimal medium
CoA	Coenzyme A
DAP-AT	<i>meso</i> -diaminopimelate aminotransferase
DAPDC	Diaminopimelate decarboxylase
DAPDH	Diaminopimelate dehydrogenase
DAPE	Diaminopimelate epimerase
DARPA	Defense Advanced Research Projects Agency
DCM	Dichlormethane
DHDPR	Dihydrodipicolinate reductase
DHDPS	Dihydrodipicolinate synthase
DNA	Desoxyribonucleic acid, carrier of genetic information
DSMZ	Deutsche Sammlung von Mikroorganismen und Zellkulturen
ECMM	<i>E. coli</i> minimal medium
EDTA	Ethylenediaminetetraacetic acid
EPSRC	Engineering and Physical Sciences Research Council
ESI	Electrospray ionisation
FACS	Flow cytometric cell sorting
GA3P	Glycerolaldehyde-3-phosphate
GABA	Gamma-aminobutyric acid
GCMS	GC-MS, gas chromatography–mass spectrometry
HEPES	4-(2-hydroxyethyl)-1-piperazineethanesulfonic acid

HILIC	Hydrophilic interaction chromatography
His-tag	Poly-Histidine-tag, 6x-His-tag, affinity tag
HPLC	High-performance liquid chromatography
HRP	Horseradish peroxidase
HTPA	4-hydroxy-2,3,4,5-tetrahydrodipicolinate
Hz	Hertz
IPTG	Isopropyl β -D-1-thiogalactopyranoside
J	Coupling constant
kbp	Kilo-base pairs
KEGG	Kyoto Encyclopaedia of Genes and Genomes
kV	Kilovolt
L	Liter
LCMS	LC-MS, liquid chromatography–mass spectrometry
LL-DAP	L,L-2,6-diaminopimelate
m/z	mass to charge ratio
MBP	Maltose binding protein, affinity tag, solubility tag
Mbp	Mega base pairs
<i>m</i> -DAP	<i>meso</i> -diaminopimelate
mg	Milligram
MIC	Minimal inhibitory concentration
ml	Milliliter
mm	Millimeter
mM	Millimolar
mmol	Millimol
MOPS	3-(N-morpholino)propanesulfonic acid
MW	Molecular weight
NADH	Nicotinamide adenine dinucleotide
NADPH	Nicotinamide adenine dinucleotide phosphate
NCBI	National Center for Biotechnology Information
NEB	New England Biolabs
nm	Nanometer
nmol	Nanomol
NMR	Nuclear magnetic resonance
NO _x	Nitrous oxide gases
NSAKP	N-succinyl-L-2-amino-ketopimelate
NSDAP	N-succinyl-L,L-2,6,-diaminopimelate
NSDAP-AT	N-succinyldiaminopimelate aminotransferase
OD	Optical density, mostly referring to OD ₆₀₀ (at 600 nm)
OPA	ortho-phtalaldehyde
PA	Polyamide
PAGE	Polyacrylamide gel electrophoresis
PBS	Phosphate buffered saline
PCR	Polymerase chain reaction
PDOs	Propanediols

pH3B	Poly-3-hydroxybutyrate, PHB
PHA	Polyhydroxyalkanoate
PHB	Poly-3-hydroxybutyrate, p3HB
PIC	Protease Inhibitor Cocktail
pmol	Picomol
pMTL	Modular Clostron plasmid system
poly-5HV	Poly-5-hydroxyvalerate
PVDF	Polyvinylidene fluoride
RBS	Ribosomal binding site
RFP	Red fluorescent protein
RNA	Ribonucleic acid
RuBisCo	Ribulose-1,5-bisphosphate carboxylase/oxygenase
S	Svedberg
SACPATH	Saccharopine pathway
SDAP-DS	Succinyldiaminopimelate desuccinylase
SDS	Sodium dodecyl sulphate-polyacrylamide
SL7	Trace element solution for <i>Cupriavidus necator</i>
SOP	Standard operating procedure
TAE	Buffer containing Tris base, acetic acid and EDTA
TCA	TCA cycle – Tricarboxylic acid cycle, Krebs cycle
Tet	Tetracycline
THDP	Tetrahydrodipicolinate
THPC-NST	2,3,4,5-tetrahydropyridine-2-carboxylate N-succinyltransferase
TMB	Tetramethyl benzidine chromogen
Tween-20	Polysorbate 20, PEG(20)sorbitan monolaurate
UMP	Uracil monophosphate
UV	Ultraviolet light
V	Volt
xg	times gravity
$\Delta 3$	$\Delta mmsA2 \Delta mmsA1 \Delta mmsA3$
$\Delta 4$	$\Delta mmsA2 \Delta mmsA1 \Delta mmsA3 \Delta phaCAB$
δ -VL	δ -valerolactam
μ g	Microgram
μ l	Microliter
μ m	Micrometer
μ M	Micromolar
Ω	Ohm

Table of contents

Declaration	2
Acknowledgements	3
Abstract.....	4
List of Figures and Tables.....	6
Abbreviations.....	14
Chapter 1 – Introduction	23
1.1 Synthetic biology in the bioeconomy – what is it and what is it good for?. 23	
1.2 Gas fermentation and its uses in sustainable production of platform chemicals	31
1.3 <i>Cupriavidus necator</i> H16 – the perfect candidate for aerobic gas fermentation?.....	33
1.4 Sustainable 5-hydroxyvaleric acid production.....	38
1.5 Sustainable 5-aminovaleric acid production	40
1.6 The L-lysine metabolism of <i>Cupriavidus necator</i> H16 and other species....	43
1.6.1 L-lysine degradation	43
1.6.2 L-lysine biosynthesis	47
1.7 Quorum sensing in bacteria.....	52
1.8 Biosensors.....	54
1.9 Aims of the project	56
Chapter 2 – Materials and methods	58
2.1 Bacterial cell manipulation: strains, media, growth conditions	58
2.1.1 Bacterial strains	58
2.1.2 General chemicals.....	59
2.1.3 Media and buffers	59
2.1.4 General growth conditions and culturing.....	61
2.1.5 Spectrometric OD ₆₀₀ measurements	61
2.1.6 Strain storage conditions.....	61
2.2 Antibiotics.....	62
2.3 Molecular biology	63
2.3.1 Plasmids	63
2.3.2 Oligonucleotide primers	69
2.3.3 Plasmid DNA isolation.....	74
2.3.4 Chromosomal DNA isolation of 5-AV adapted strains.....	74
2.3.5 Polymerase Chain Reaction (PCR).....	74

2.3.8	Agarose gel electrophoresis	75
2.3.9	Purification of DNA after gel electrophoresis.....	75
2.3.10	Restriction digest of plasmid and amplified DNA.....	75
2.3.11	Ligation	75
2.3.12	HiFi-assembly.....	76
2.3.13	DNA quantification	76
2.4	Transformation of bacterial strains	77
2.4.2	Preparation of chemically competent <i>E. coli</i> strains	77
2.4.3	Preparation of electrocompetent <i>C. necator</i> strains.....	77
2.4.4	Transformation of chemically competent <i>E. coli</i> strains	77
2.4.5	Transformation of electrocompetent <i>Cupriavidus necator</i> H16 strains	78
2.5	Protein expression and analysis	79
2.5.1	Growth conditions for recombinant protein expression.....	79
2.5.2	Protein extraction.....	79
2.5.2	Protein purification.....	79
2.5.3	Denaturing SDS-PAGE and blotting.....	79
2.5.4	Western blot	80
2.6	Chemistry.....	81
2.6.1	Synthesis and purification 5-hydroxyvaleric acid sodium salt by ring-opening polymerisation and subsequent hydrolysis of 5-valerolactam.....	81
2.6.2	H1-NMR analysis of synthesised 5-hydroxyvaleric acid sodium salt ...	81
2.7	Analytics.....	82
2.7.1	Amino acid content analysis from fermentation supernatants using HPLC	82
2.7.2	Gluconate and 3-HP quantification using HPLC.....	82
2.7.3	5-aminovaleric acid content analysis from fermentation supernatants using GCMS.....	82
2.7.4	Metabolite analysis using LC-MS	83
2.8	Assays.....	85
2.8.1	Toxicity assays with BioLector	85
2.8.2	RFP assays with TECAN	85
2.8.3	Growth assays: calculation of growth rates	85
2.9	Bioinformatics.....	86
2.9.1	Plasmid map analysis and genome alignments	86
2.9.2	Sequence databases	86
2.9.3	BLAST analysis.....	86

2.9.4	Design of RBS motifs.....	86
2.9.5	Statistical analysis.....	86
2.9.6	Quantitative and qualitative analysis of metabolites using LC-MS and XCalibur™ and TraceFinder.....	87
Chapter 3 - Metabolic engineering of <i>Cupriavidus necator</i> H16 for 5-hydroxyvaleric acid production from β -alanine.....		90
3.1	Introduction.....	90
3.1.1	General introduction.....	90
3.1.2	Introduction to the pathway.....	93
3.1.3	3-HP synthesis from β -alanine.....	95
3.1.4	3-HP thioester formation.....	97
3.1.5	Reverse beta-oxidation chain lengthening.....	100
3.1.6	Thioester hydrolysis and product formation.....	102
3.1.7	Results in <i>E. coli</i> may predict results in <i>Cupriavidus necator</i> H16.....	104
3.1.9	The resting cell condition.....	106
3.1.10	Aim of the Chapter.....	107
3.2	Results.....	108
3.2.1	Experimental design choices.....	108
3.2.2	2 of 20 pathways for 5-hydroxyvaleric acid production yield the final product in <i>Escherichia coli</i>	114
3.2.2	5 of 20 pathways for 5-hydroxyvaleric acid production yield the final product in <i>Cupriavidus necator</i> H16, suggesting that some results obtained in <i>Escherichia coli</i> are transferable to <i>Cupriavidus necator</i> H16.....	121
3.2.3	The $\Delta 4$ deletion strain grows slower than the $\Delta phaCAB$ deletion strain and the wildtype.....	126
3.2.3	Resting cell fermentation conditions allow for 5-OHV formation in <i>Cupriavidus necator</i> H16 $\Delta 4$, but cause undesired accumulation of uracil.....	131
3.2.4	Enhanced 5-hydroxyvaleric acid production using P_{trc} and P_{trp} promoters and synthetic RBS sites.....	135
3.3	Discussion.....	140
3.3.1	5-OHV production in <i>Escherichia coli</i> and analytical challenges.....	140
3.3.2	5-OHV production in <i>Cupriavidus necator</i> H16 and the transferability of results obtained in <i>Escherichia coli</i>	146
3.3.3	The fitness costs of synthetic pathways and <i>mmsA</i> knockouts in <i>Cupriavidus necator</i> H16.....	151
3.3.4	The resting cell condition for 5-OHV production in <i>Cupriavidus necator</i> H16 is unsuitable.....	153
3.3.4	Stronger promoters and synthetic RBS sites boost 5-OHV production	156

Chapter 4 - Metabolic engineering of <i>Cupriavidus necator</i> H16 for 5-aminovaleric acid production	160
4.1 Introduction	160
4.1.1 5-AV toxicity and degradation in <i>Cupriavidus necator</i> H16.....	160
4.1.2 Deregulation and optimisation of the <i>Cupriavidus necator</i> H16 L-lysine biosynthesis pathway	162
4.1.3 Antimicrobial activity of 5-AV and 5-AV degradation.....	163
4.1.4 <i>Cupriavidus necator</i> H16 quorum sensing.....	164
4.1.5 5-AV biosynthesis pathways	166
4.1.6 The $\Delta gabT$ knockout may reduce 5-AV degradation <i>Cupriavidus necator</i> H16 $\Delta phaCAB$	169
4.1.7 Engineering the <i>Cupriavidus necator</i> H16 L-lysine biosynthesis pathway	171
4.1.8 Engineering of L-lysine biosynthesis pathway regulation	173
4.1.9 Aim of this Chapter	176
4.2 Results.....	177
4.2.1 5-AV has no significant bactericidal or bacteriostatic effect on <i>Cupriavidus necator</i> H16 wildtype	177
4.2.2 5-AV shows no bacteriostatic effect on <i>Cupriavidus necator</i> H16 wildtype	182
4.2.3 <i>Cupriavidus necator</i> H16 adapts in 7 days to 5-AV as a nitrogen source and 10 days as a carbon source.....	184
4.2.4 DavA and DavB convert L-lysine to 5-aminovaleric acid in <i>Escherichia coli</i> and <i>Cupriavidus necator</i> H16.....	187
4.2.5 Aerobic resting cell 5-AV production in minimal supplemented medium using phosphate limitation in <i>Cupriavidus necator</i> $\Delta phaCAB$	193
4.2.6 The $\Delta gabT$ knockout in <i>Cupriavidus necator</i> H16 $\Delta phaCAB$ improves 5-AV yield in aerobic fermentation using aspartate supplemented minimal medium	197
4.2.7 Enhancing 5-AV production from <i>Cupriavidus necator</i> H16 $\Delta phaCAB$ $\Delta gabT$ central metabolism by using feedback-resistant enzyme variants, P_{trc} and P_{trp} promoters and synthetic RBS sites	200
4.3 Discussion	206
4.3.1 5-AV toxicity and degradation in <i>Cupriavidus necator</i> H16.....	206
4.3.2 DavA and DavB convert L-lysine to 5-aminovaleric acid in <i>Escherichia coli</i> and <i>Cupriavidus necator</i> H16.....	209
4.3.3 Aerobic resting cell fermentation in minimal supplemented medium using phosphate limitation in <i>Cupriavidus necator</i> $\Delta phaCAB$ is not a suitable condition for 5-AV production	211
4.3.4 The $\Delta gabT$ knockout in <i>Cupriavidus necator</i> H16 $\Delta phaCAB$ improves 5-AV yield in aerobic fermentation using aspartate supplemented minimal medium	215

4.3.5 Enhancing 5-AV production from <i>Cupriavidus necator</i> H16 Δ <i>phaCAB</i> Δ <i>gabT</i> central metabolism by using feedback-resistant enzyme variants, P _{trc} and P _{trp} promoters and synthetic RBS sites	217
Chapter 5 - Development of a 5-aminovalerate biosensor	221
5.1 Introduction	221
5.2 Results.....	225
5.2.1 BS1 can sense extracellular levels of δ -VL, but not 5-AV.....	225
5.2.2 Extracellular 5-AV is not converted to δ -valerolactam in <i>E. coli</i> harbouring BS2	228
5.2.3 Intracellularly produced 5-AV is slowly converted to δ -valerolactam in <i>E. coli</i> harbouring BS2 and L1.	229
5.2.4 ORF26 could not be characterised due to poor solubility	231
5.2.5 Characterisation of a redesigned biosensor using CaiC.....	234
5.2.6 Characterisation of the <i>ChnR</i> /P _{ChnB} -RFP sensor module was not possible due to poor solubility of ChnR.....	236
5.2.7 Characterisation of ChnR specificity reveals a broad substrate spectrum	238
5.3 Discussion	241
5.4 Key outcomes of the biosensor development.....	244
Chapter 6: General discussion and future work	247
6.1 General outcomes of this study.....	247
6.2 5-OHV production in <i>C. necator</i> H16	250
6.3 5-AV production in <i>C. necator</i> H16.....	254
6.4 A novel 5-AV biosensor.....	256
Acknowledgements	257
References	258
Appendix.....	282
Figures and tables.....	282
Plasmid maps.....	326
Sequences.....	331

Chapter 1

Introduction

Chapter 1 – Introduction

1.1 Synthetic biology in the bioeconomy – what is it and what is it good for?

The field of synthetic biology has gathered an increasing amount of interest over the last two decades. Synthetic biology allows for the redesign and engineering of biological systems [1] and lies at the centre of what is referred to as “the bioeconomy of the 21st century” [2]. Synthetic biology is a technology field in its infancy, dedicated to newly designing, constructing or redesigning biological systems for useful purposes such as the production of drugs or sustainable chemical platform chemicals using genetically modified organisms [3].

Historically, biotechnology has been explored since ancient times. After domestication of animals and plants, the use of bacteria for cheesemaking or the use of yeasts for baking, winemaking and brewing allowed to preserve food [4]. In the 1800s, the observation of nature and application of the scientific method led to discoveries that would further the understanding of how traits (for example in crop plants) are inherited. Gregor John Mendel observed phenomena in pea plants that would be consolidated to basic “Laws of Inheritance” and Charles Darwin’s “Theory of Evolution” furthered our understanding of how traits develop over time [5]. It was understood that observed traits in species do not occur randomly and that this basis of inheritance can allow for selective breeding that would shape traits of a

population over time. In search of the physical basis of these traits, botanist Robert Brown discovered the cell nucleus in 1868 (although it should be noted that sketches of structures resembling a cell nucleus existed since the early 1700s) [6] and Friedrich Miescher first isolated nucleic acids [7]. Twenty years later, in 1888, Heinrich Wilhelm Gottfried Von Waldeyer-Hartz described and named the “chromosome” (and “neuron”, for that matter) [8]. It wasn’t until 1953, however, that the molecular structure of DNA would be solved by Watson, Crick and Franklin [9] [10].

Synthetic biology, however, is functionally different from biotechnology. Its an interdisciplinary field that aims to apply engineering principles to biology [11, 12]. These principles are almost always applied on a *genetic* basis (e.g. in form of altering the DNA of an organism). In particular, the Design-Build-Test-Learn cycle approach is adopted from engineering and represents an efficient way to engineer strains in synthetic biology [13]. This approach divides an engineering strategy in four stages that are repeated iteratively. During the design phase, problems are defined and desired pathways and hosts are selected [14]. In the build phase, appropriate parts for the pathways are synthesised, cloned or otherwise selected and assembled for incorporation in the host [14]. In the learning phase, the strains validated in regards to production performance and in the learning stage, test data is analysed to inform the next design phase [14].

Synthetic biology studies how to build *artificial* biological systems and uses the same tools as other fields. For example, the simulation and modelling of complex biological systems that has been developed in the field of systems biology is now expanded to simulate how *artificial* metabolic pathways or

artificial regulatory networks can impact an organism as a whole [15]. Equally, molecular biology has given rise to toolkits and techniques used to manipulate and alter the DNA of an organism. These same techniques are now used in the context of synthetic biology to synthesise new genes (or even whole genomes) [16] or alter the genetic information of an organism. The focus lies more heavily on building simple, standardised parts of biological systems and then combining them as building blocks or components of a new, engineered biological system or circuit [17, 18].

Thus, synthetic biology can be summarised to use standardised biological parts and to build novel biological systems. Furthermore, to apply engineering principles to the re-design of existing biological parts, such as promoters or proteins to help synthesise natural products. Lastly, a third subset of synthetic biology is interested in designing and constructing entire artificial genomes or simplifying existing genomes of natural organisms (the so-called minimal genome) [16, 19, 20]. All *methods* used to achieve these ends, from breeding to computer simulations and genetic modification stem from other fields, ranging from applied biology to systems biology, molecular biology and many more. Eventually, synthetic biology ties into industrial biotechnology – a field that aims to use the natural ability of organisms and their enzymes to catalyse chemical reactions [21]. Industrial biotechnology is thus an important field to transition a petroleum-based economy to a bio-based economy and synthetic biology helps to provide the necessary organisms for this transition [22].

Up until the 1970s, humans have been sourcing molecules for fragrances, flavouring, vitamins and medicine either by harvesting or processing living organisms or by processing fossilised life using petrochemistry [23].

This sourcing of molecules has become increasingly unsustainable due to the rising demand for products from these molecules and a simultaneously decreasing abundance of area that is suitable to farm the plants or animals that are needed to make them. Petrochemistry in the 20th century offered a short-term solution to source molecules of interest by converting limited fossil sources to platform chemicals that are used to synthesise useful products. Cotton and wool for clothing were widely replaced by polyester and polyamide fibres and cosmetics such as lipstick are now based on paraffin wax instead of bee wax, often requiring refining processes that are harmful to the environment and release CO₂, a greenhouse gas that contributes majorly to global warming [24].

Nylon, for example, is a popular family of polyamide (PA) fibres and usually synthesised from the reaction of a dicarboxylic acid with a diamine or by ring-opening polymerisation of lactams, which are mostly produced by petrochemistry [25, 26]. Adipic acid that is used for Nylon6,6 for instance, is mainly produced by oxidation of benzene (a fossil source) via cyclohexanol [27]. This process requires the use of nitric acid and produces harmful NO_x gases as a by-product [28]. Hexamethylene diamine, the second ingredient of Nylon 66, is obtained by hydrogenation of adiponitrile, which can be sourced from propylene or butadiene, two other fossil sources [28]. Nylon synthesis is this a very energy-intensive process and the harsh acidic reaction conditions produce

large amounts of waste salts – all of which could be avoided with a cell-based production process on the basis of enzymatic catalysis [29].

Synthetic biology offers a new and innovative approach for engineering biological systems to produce these molecules - that could to date only be delivered via petrochemistry - in a sustainable process [1]. The increasing interest in the field of synthetic biology is however not only justified by rising environmental concerns over petrochemistry and high energy prices. It is also motivated by a desire to understand biological systems from a scientific point of view.

Insulin is another good example of how synthetic biology helps industries to transition to more environmentally friendly or more ethical production solutions. In 1906, Georg Ludwig Zülzer performed the first insulin injection in humans [30]. The insulin used was a pancreatic extract from calves (after killing the animal) and caused fevers in patients due to immunogenic reactions towards impurities in the extract [31]. Helmut Zahn then performed the first total chemical synthesis in 1963 [32], but the process was too laborious and expensive to compete with animal insulin. In 1982, however, genetically modified bacteria were engineered by synthetic biologists for the first cheap, safe and ethical production of insulin (Humulin® R and N) [33].

Today, metabolic engineering of life is already capable of providing advanced biofuels, L-amino acids and simple alcohols, now produced biologically through fermentation instead of using oil as feedstock [34-37]. Metabolic engineering is a subfield of synthetic biology, which aims to apply engineering principles to

metabolic pathways for the production of small molecules. In a pressure test administered by the U.S. Defense Advanced Research Projects Agency (DARPA), synthetic biologists of a biofoundry (a centralised facility for genetic engineering) were assessed and asked to produce ten molecules in 90 days, ranging from lubricants and solvents to complex antitumour drugs and antibiotics [38]. The scientists were able to deliver six of the ten, proving that metabolic engineering can contribute to a fast and flexible response when rapid routes to complex pharmaceuticals are needed in times of crisis [38]. Genetic modification of organisms, targeted engineering of metabolic pathways, computer and artificial intelligence-aided design, automated DNA synthesis and genome construction, strain development and high-throughput assaying are core technologies of synthetic biology [38]. Prices for these technologies are dropping rapidly, making the future development of biological solutions for chemical problems even more attractive [38]. In recent years, synthetic biology and genetic engineering have even begun to become cheap enough to gain popularity outside of academic laboratories, as a growing number of “biohackers” (amateur molecular biologists) join the synthetic biology movement from home or from community laboratories [39].

The most dominant market for fermented bio-products is in L-amino acids, which are difficult to synthesise chemically due to their chirality. For example, L-lysine is an essential amino acid that is produced with a market size of 1.5 – 2 million tons per year [40]. Manipulations of the core carbon metabolism and elimination of competing pathways have led to the appearance of highly improved L-lysine producer strains of *Escherichia coli* (*E. coli*) and

Corynebacterium glutamicum (*Co. glutamicum*) [34, 41, 42]. L-threonine is produced industrially in organisms such as *E. coli* with an annual production of 330,000 tons (2017) [43]. Data from genome, transcriptome and proteome analysis helped to design an in-silico flux response model, in which key regulators of the endogenous *E. coli* L-threonine pathway, other competing pathways, and reuptake transporters were inhibited [44]. Elimination of undesired pathways, deregulation of desired pathways and upregulation of key enzymes are classic synthetic biology approaches that paved a path to high-performance strains [34, 45, 46]. A third example for amino acids, L-glutamate, is known as important flavour enhancer and is currently (2015) produced at 2.5 million tons per year [47]. The industrial fermentation of L-glutamate relies on *Co. glutamicum* strains which were specifically isolated for this purpose [41, 48-50].

A second class of noteworthy chemicals that have already been successfully generated by fermentation through the use of synthetic pathways for the bioeconomy are alcohols such as ethanol [51, 52], PDOs [53-55], such as 1,3-Propanediol and 1,2-Propanediol, BDOs, such as 2,3-Butanediol [56], and isobutanol [57]. In 2007, 120,000 tons of Bio-PDOs were produced and production from corn syrup in genetically engineered *E. coli* strains won the DuPont Tate and Lyle BioProducts research teams the “Heroes of Chemistry Award” [58, 59]. PDOs can, amongst uses as antifreeze or in cosmetics, also serve as polymerization building blocks and are readily available. The main carbon source for the production of such simple alcohols is glycerol. Butanediols (BDOs) are platform chemicals for the production of cosmetics,

solvents and polymers. Isopropanol can be fermented through the manipulation of branched amino acid pathways [34, 60-63].

The third class of small molecule compounds that are being produced sustainably by metabolic engineering are organic acids, such as adipic acid, which, as we learned, is one of two ingredients for Nylon66 synthesis [64]. Multiple organic acids have drawn interest of the bioeconomy for biological production and most of these compounds are key metabolites of the central carbon metabolism, especially the TCA cycle. For example, succinic acid fermentation has been achieved in an industrial scale in *E. coli*, yeast and the aptly named *Basfia succiniciproducens* [34, 65-68]. Possible carbon sources range from glycerol to lignocellulose. Citric acid, used as acidulant in cosmetics and food, is fermented on a scale of 1.5 million tons per year and its production can be traced back as far as the 1930s, when *Aspergillus niger* was first established as a producer [69-71]. Another organic acid with established fermentation in *Aspergillus sp.* is itaconic acid, the five-carbon chain length dicarboxylic acid, which is used in rubber and polyacrylate production. Recently engineered strains in *E. coli*, yeast, *Co. glutamicum* and other organisms have emerged as alternative hosts for the production of itaconic acid [34, 72-74].

1.2 Gas fermentation and its uses in sustainable production of platform chemicals

Many products of the bioeconomy are produced by fermentation with carbohydrate feedstocks such as glucose from corn starch and sugar cane or by enzymatic treatment of cellulose biomass [75-77]. Some problems are raised by these processes however: Biomass containing cellulose often also contains non-biodegradable material such as lignin and the enzymatic pre-treatment is costly. Also, the use of corn starch, which requires farmable land, water and fertilizer, defeats the original purpose of bio-based production: Reducing the environmental footprint of the end-product. As an alternative carbon source, synthesis gas was investigated. Syngas is a mixture of CO₂, CO and H₂ and can be sustainably sourced from steel-work off-gases [78] or from municipal solid waste biomass [79] and has been used for the production of synthetic fuels [80]. For example, CO₂ and hydrogen can be used as substrates in bacteria such as *C. necator* H16 and excess carbon monoxide can be transformed to carbon dioxide and hydrogen using the water-gas shift reaction [81]. Syngas is thus a fantastic feedstock for the sustainable production of chemicals – it contains a carbon source (CO₂) and a source of reduction equivalents (H₂). Furthermore, the individual components of syngas are not only produced in limited quantity as industrial off-gases, they can also be captured (CO₂) or produced by electrolysis (H₂) in large quantities, and given the use of an adequate sustainable energy source (such as wind, solar or hydro power), completely waste-free and sustainable. Syngas can also be sourced by gasification of municipal waste [82], agricultural waste and recalcitrant biomass (e.g.

lignocellulose) [83, 84]. Furthermore, there is a known organism (*C. necator* H16), which can grow using syngas when CO-adapted [85] and thus presents the perfect synthetic biology engineering target for the production of chemicals using syngas.

1.3 *Cupriavidus necator* H16 – the perfect candidate for aerobic gas fermentation?

C. necator H16 is a rod-shaped, gram-negative, facultatively anaerobic and facultatively lithoautotrophic β -proteobacterium. It was first described as “Knallgasbakterium” (“Oxyhydrogen bacterium”) when it was isolated, for its ability to generate reduction equivalents from molecular hydrogen with oxygen as main electron acceptor [86, 87]. Despite several name changes of the species, it is nowadays most commonly referred to as *Ralstonia eutropha* or *C. necator* [88].

The second interesting property of *C. necator* is its capability to grow on a very broad range of industrially relevant carbon and energy sources, including sugars, glycerol and, owing to its lithoautotrophic metabolism, CO₂ and H₂, two components of syngas [89, 90], but not glucose, of which the wildtype is intolerant [91]. Its remarkable flexibility for utilizing different nutrient and energy sources and its capability to fix carbon through the Calvin-Benson-Bassham (CBB) cycle make *C. necator* an ideal host to engineer for production of value-added products from CO₂-containing waste gases as sole carbon source [92]. *C. necator* strains carry two circular chromosomes of ~4 Mbp and ~3 Mbp size. Also, one mega plasmid (pHG1) with a size of ~450 kbp is present. In addition to carrying hydrogenase (*hox*) genes that are necessary for H₂ utilisation, the mega plasmid pHG1 also contributes in other ways to the diversity of the metabolism in *C. necator* H16: Duplicates of the CBB cycle can be found on pHG1, as well as nitrite and nitrate reductase genes, which allow for anaerobic respiration [93].

The hydrogenases in *C. necator* contribute to its energy metabolism by generating NADH from NAD⁺. Three hydrogenases have been described in *C. necator*. The regulatory hydrogenase is a “hydrogen sensor” and signals to the cell that hydrogen is present. It is bound to a kinase subunit that activates downstream response regulators which promote transcription of the other two hydrogenases [94, 95]. The membrane bound hydrogenase is part of the respiratory chain and contributes electrons to oxidative phosphorylation [96]. The soluble [NiFe] hydrogenase uses H₂ to reduce NAD⁺ to NADH and is, like the other hydrogenases in *Cupriavidus* sp., evolved to be oxygen-tolerant, which is not typical for [NiFe] hydrogenases in other organisms because of the tendency of oxygen to bind tightly to the active site [97-99]. Under lithoautotrophic conditions, transhydrogenases that catalyse the formation of NADPH from NADH are upregulated [100]. NADPH is the main contributor of reductive power in anabolic reactions for the formation of biomass.

From six different CO₂-fixing pathways that have been described to date in bacteria, the Calvin-Benson-Bassham cycle that is present in *Cupriavidus* sp. is one of the best investigated pathways due to its importance in plant metabolism [101].

Figure 1.1 illustrates the CBB cycle in *C. necator* H16, in which 3 molecules CO₂ are converted to one molecule glycerolaldehyde-3-phosphate using 9 ATP and 6 NADPH. NADPH is mainly sourced from soluble hydrogenases and transhydrogenases under lithoautotrophic conditions and ATP is produced by oxidative phosphorylation with O₂ as main electron acceptor.

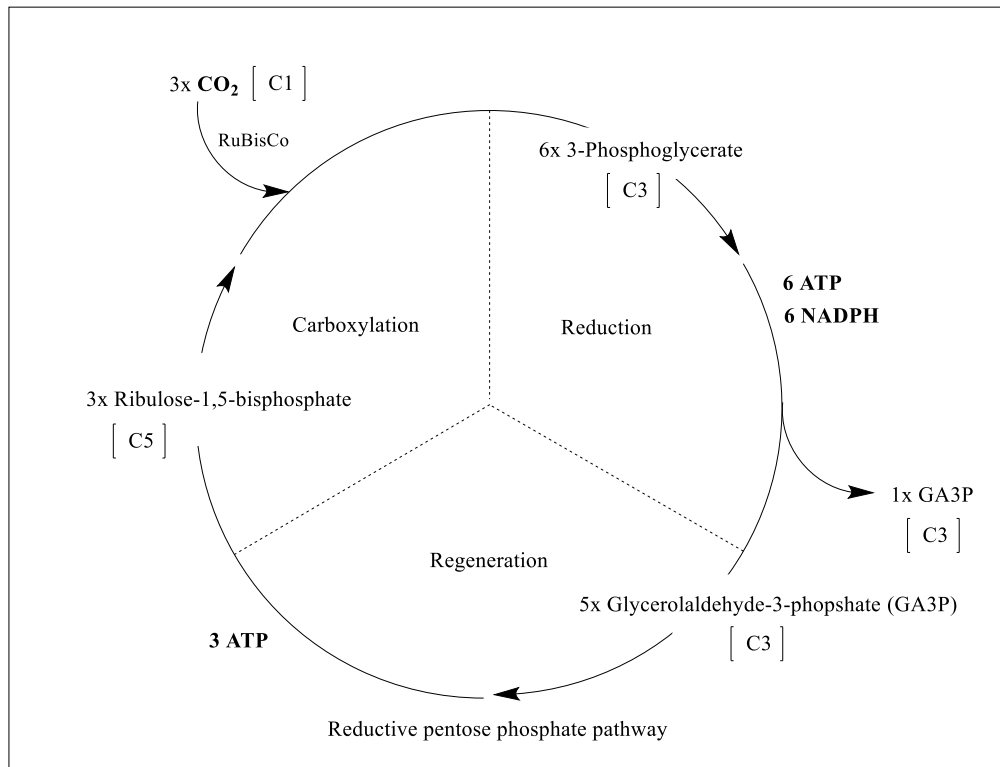


Figure 1.1 Simplified Calvin-Benson-Bassham cycle and its three stages. *C. necator* H16 fixes CO_2 with the aid of the ribulose-1,5-bisphosphate carboxylase/oxygenase and produces 6 molecules 3-Phosphoglycerate from 3 molecules ribulose-1,5-bisphosphate and 3 CO_2 in the carboxylation stage. In the reduction stage, 6 molecules of 3-phosphoglycerate are reduced to 6 molecules of glycerolaldehyde-3-phosphate, of which one leaves the cycle and enters either glycolysis or gluconeogenesis pathways. The reduction stage utilises 6 ATP and 6 NADPH. 3 molecules ribulose-1,5-bisphosphate are regenerated from the remaining 5 molecules glycerolaldehyde-3-phosphate by the reductive pentose phosphate pathway, the regeneration stage of the CBB cycle. These reactions use 3 ATP. In total, 3 molecules CO_2 are converted to one molecule glycerolaldehyde-3-phosphate using 9 ATP and reducing equivalents in form of 6 NADPH. The design of this figure was derived from Soo Youn Lee et al. [102], Figure 2.

Figure 1.2 illustrates the use of *C. necator* H16 metabolism under aerobic lithoautotrophic conditions and carbon flow for the production of value-added products from CO₂.

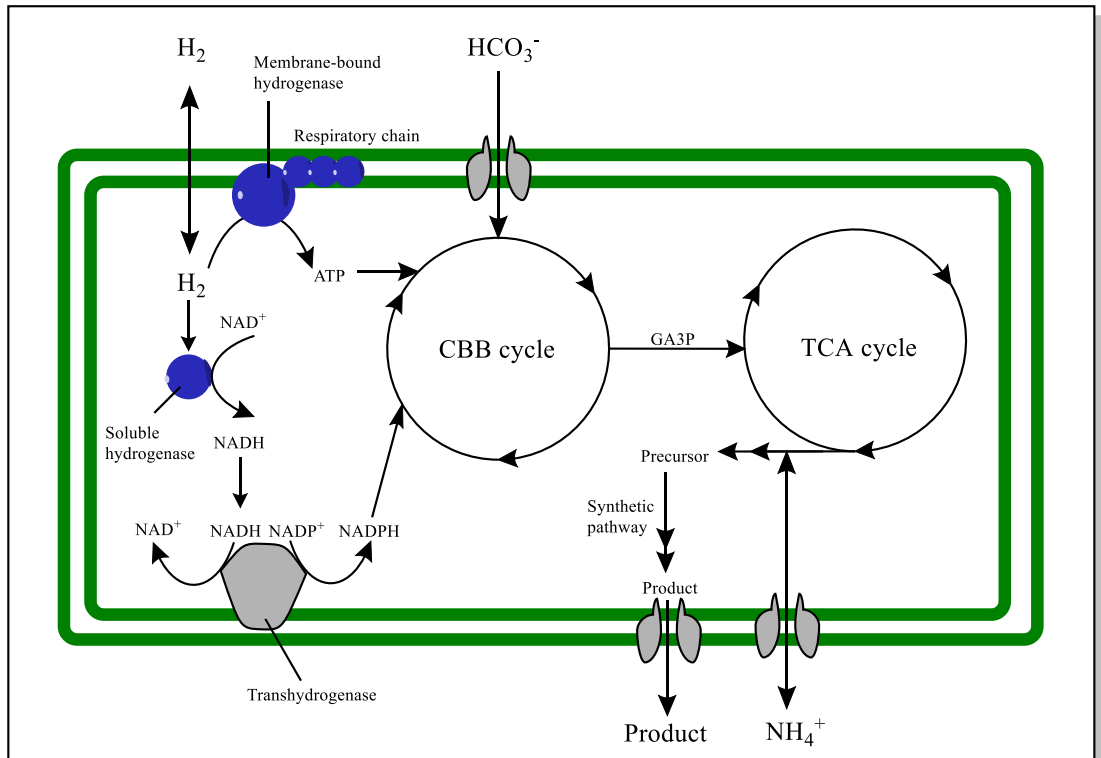


Figure 1.2 *Cupriavidus necator* H16 metabolism under aerobic lithoautotrophic conditions for the production of products from CO₂. H₂ is used as an energy source to generate ATP with a membrane-bound hydrogenase, which contributes to the transmembrane proton gradient of the cell via the respiratory chain and therefore to ATP production. The soluble hydrogenase oxidises H₂ to generate NADH reducing equivalents, which can be transformed to NADPH by action of a transhydrogenase. NADPH is then used for anabolic reactions such as in the reduction of CO₂ in the CBB cycle. ATP is generated through the respiratory chain with O₂ as electron acceptor, using all available sources of NADH formation. NADPH and ATP are used to fix CO₂ from carbonate in the Calvin-Bassham-Benson cycle. Glycerol-3-phosphate (GA3P) is produced, enabling subsequent anaplerotic reactions and used for biomass formation. TCA cycle intermediates such as acetyl-CoA, aspartic acid or succinic acid act as precursors for introduced biosynthetic pathways that yield value-added products, which are exported to the supernatant of the culturing medium.

The third interesting property that sets apart *C. necator* as a host strain in synthetic biology is its natural capability to synthesize the polyhydroxyalkanoate (PHA) poly-3-hydroxybutyrate (PHB) as a storage compound. PHB is stored in the form of intracellular granules and can make up to 80% of the dry cell weight in CO₂/H₂ fermentation [103]. PHB is produced from acetyl-CoA by the enzymes PhaA, PhaB and PhaC [104-106]. **Figure 1.3** shows transmission electron microscopy pictures taken of *C. necator* pH16 before and after PHB accumulation by Mravec et al [107]. The granules are visible as white circular shapes.

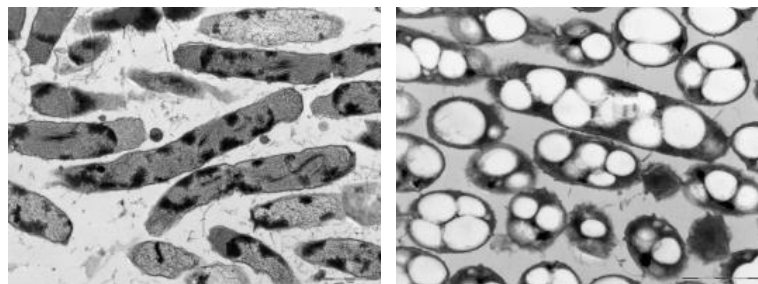


Figure 1.3 TEM micrograph of *C. necator* H16 before (left) and after (right) PHB granule accumulation. Pictures were taken from Mravec et al. [107].

Their genes are organised in a single *phaCAB* operon, which has been successfully used in *E. coli* for PHB production [106, 108, 109]. Due to the high brittleness of PHB, it has only very limited use as a biopolymer. However, it was found that p3HP, the C3 analogue of PHB, has improved properties and was thus described as a target for production in *E. coli* and *C. necator* [110]. Robust engineered production of 3-HP in *C. necator* H16 was the foundation of one of the engineered pathways that will be presented in this work.

1.4 Sustainable 5-hydroxyvaleric acid production

5-hydroxyvaleric acid (5-OHV) is a monomer for the production of poly-5HV, which is classed as a polyester.

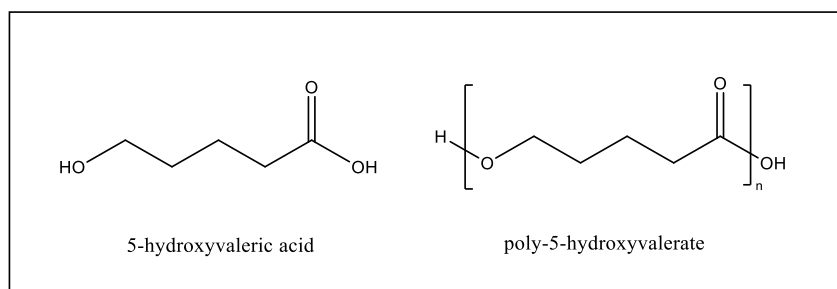


Figure 1.4 Chemical structures of 5-hydroxyvaleric acid and poly-5-hydroxyvalerate

5-OHV has been described in the literature as a substrate of the 5-hydroxyvalerate CoA-transferase in *Clostridium aminovalericum* [111] and as intermediate in cyclopentanol metabolism of *Pseudomonas* strain NCIB 9872. Its properties have been much less studied than those of its isomer 3-hydroxyvaleric acid, which has been investigated as a co-polymer in polyhydroxyalkanoates, although, in recent years, advances were made to include 5-hydroxyvalerate units as co-polymer in PHAs as well [112]. Nonetheless, one important prediction can be made about the poly-5HV polymer. It belongs to the family of linear aliphatic polyesters, which are well known for being biodegradable by esterases and lipases [113, 114].

To date, only one study shows 5-hydroxyvaleric acid production in metabolically engineered bacteria. Yu Jung Sohn et al. [115] produced 51.1 g L⁻¹ 5-hydroxyvaleric acid in *Co. glutamicum* fed-batch fermentation. This was

achieved by using a 5-aminovaleric acid producing background strain (using *davAB* in an L-lysine overproducer) and expanding the pathway with DavT, yielding glutaric semialdehyde and YahK, a semialdehyde reductase, yielding 5-OHV. In this work, I aimed to demonstrate the production of 5-OHV through a novel pathway that is based on employing reverse beta-oxidation chain elongation to yield 5-OHV from a C3 feedstock, in an organism that, unlike *Co. glutamicum*, is able to produce from the renewable source syngas.

1.5 Sustainable 5-aminovaleric acid production

In this work, I aimed to establish the production of C5 platform chemicals in *C. necator* H16, because of its ability to synthesise compounds sustainably from waste gases. Apart from 3-hydroxypropanoic acid production [110], *C. necator* H16 has been successfully engineered for production of cyanophycin [116], 2-methylcitric acid [117], and solvents such as isopropanol, isobutanol, methyl ketones and branched-chain alcohols [118-121].

The two C5 molecules that I aimed to produce are 5-aminovaleric acid and 5-hydroxyvaleric acid, which are used as monomers for the production of the polyamide fibre Nylon-5 and the polyester poly-5-hydroxyvalerate, respectively.

5-Aminovaleric acid (5-AV) is a monomer for the production of nylon-5 or copolymers such as nylon-6,5 and nylon-10,5 and a non-proteinogenic ω -amino acid with potential use as a five-carbon (C5) platform chemical.

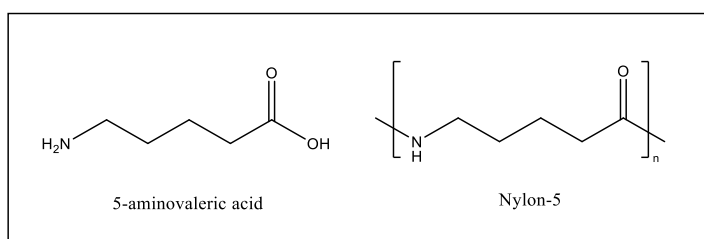


Figure 1.5 Chemical structures of 5-aminovaleric acid and nylon-5

Through intramolecular cyclisation it can be easily converted to δ -valerolactam (δ -VL), a reactive monomer for nylon-5 production [122-124]. Nylon-5 shows

both higher melting points and increased thermostability over nylon-6 and other common nylon copolymers [125].

Due to the difficulty to prepare the C5 monomer from fossil oil feedstocks, not very much research has been conducted towards identifying basic properties of the polyamide fibre, such as thermal conductivity, tensile strength, elasticity, hardness, glassy transition temperature and various electrical properties. It is however predicted to have similar pyroelectric and piezoelectric properties to other uneven carbon number nylons such as nylon-7 and nylon-11 [126, 127].

The most common approach of 5-aminovalerate synthesis uses the L-lysine degradation pathway of *Pseudomonas putida* [128], in which L-lysine is oxidised to δ -aminovaleramidate by lysine oxygenase (DavB) and subsequently degraded to 5-aminovalerate by δ -aminovaleramidase (DavA). This approach has been followed in the well-established L-lysine producing host *Co. glutamicum* and also in *E. coli* [123, 124, 129-132] and will also be followed in this work.

Additionally to the L-lysine pathway, an alternative pathway was suggested in a patent application by Invista Technologies S.A.R.L., in which a C3 backbone such as malonyl-CoA is shielded by a methylester group and then enzymatically converted to glutaryl-CoA, glutaryl-semialdehyde and subsequently 5-AV by a transaminase [133]. 5-AV was also postulated to be producible from cadaverine analogous to GABA (γ -aminobutyric acid) production via the putrescine route using the transaminase PatA and dehydrogenase PatB [29, 134]. Cheng et al. [135] report production of 5-AV from L-lysine in a pathway expressing the enzymes RaiP (lysine α -oxidase), KivD (α -ketoacid decarboxylase) and PadA

(aldehyde dehydrogenase), however their pathway produced 5-AV in all negative controls, e.g. regardless of the individual presence of any of the three enzymes. In this work, I show 5-AV production from *C. necator* H16 central metabolism via the previously mentioned L-lysine biosynthesis route.

1.6 The L-lysine metabolism of *Cupriavidus necator* H16 and other species

1.6.1 L-lysine degradation

L-lysine degradation has been well studied in many organisms and a large variety of degradation pathways are known today. In mammals and higher plants, the saccharopine pathway (SACPATH) converts L-lysine to aminoadipate and ultimately to glutaryl-CoA [136]. In bacteria, L-lysine can be degraded through the AMA-pathway, which results into a conversion of L-lysine to D-lysine and a subsequent degradation through 2-aminoadipate and glutaric acid [128]. The other L-lysine degrading pathway, named AMV pathway, has been well studied in *Pseudomonas* sp. since the 1970s and degrades L-lysine to 5-aminovaleric acid and then to glutaric acid [137-139].

The enzymes DavA and DavB, part of the AMV pathway, have been first reported in *Pseudomonas putida* as part of the L-lysine catabolism in 2005 [128]. The authors reported that in a first step, L-lysine is oxidised to 5-aminovaleramide by DavB. (**Figure 1.6**). The mechanism of this oxidation reaction was elucidated by Matsui et al. in 2014, when crystallographic analysis of DavB suggested molecular oxygen as the oxidising agent [140].

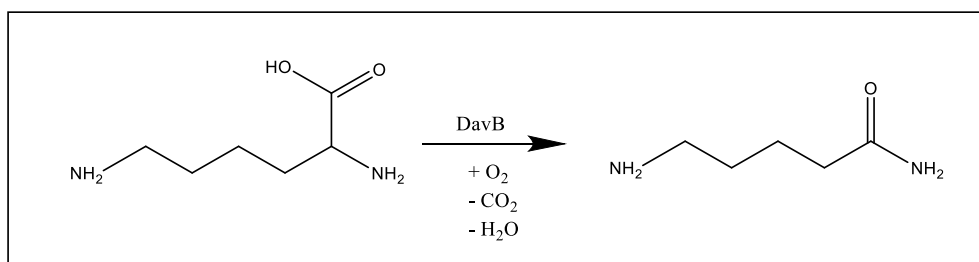


Figure 1.6 DavB catalyses the formation of 5-aminovaleramide from L-lysine. The monooxygenase DavB uses molecular oxygen and releases the carboxyl group of L-Lysine as CO₂.

This effectively restricts the use of DavB in synthetic pathways to organisms that can be fermented aerobically – a restriction that does not apply to the aerobe *C. nector* H16. DavA then hydrolyses 5-aminovaleramide to 5-AV and releases free ammonia (**Figure 1.7**)

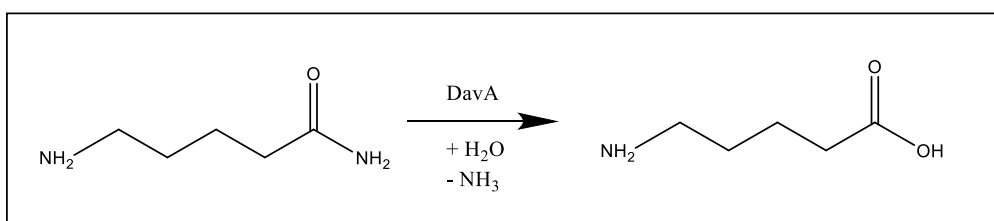


Figure 1.7 DavA catalyses the formation of 5-aminovaleric acid from 5-aminovaleramide. Hydrolysis of 5-aminovaleramide releases ammonia and 5-AV.

These two catalysed steps make DavA and DavB very interesting enzymes for a synthetic pathway for the production of 5-aminovaleric acid. The release of gaseous products (NH₃ and CO₂) make these reactions also irreversible. In order to build upon the L-lysine metabolism in *C. nector* 5-AV production, this work will make use of DavA and DavB. The enzymes have been used by synthetic

biologists for 5-AV and glutaric acid production in *E. coli* and *Co. glutamicum* [122, 123, 129-132].

A further degradation of 5-aminovaleric acid to glutaric acid has been studied in *Pseudomonas putida* and forms part of the Dav degradation pathway of L-lysine (**Figure 1.8**) [128, 141]. The *davTD* operon in *Pseudomonas putida* and the homologue *gabTD* in *Bacillus subtilis* are under control of the *gabR* regulator, which responds to GABA [124, 142, 143]. In *C. necator*, a *gabT* homologue was identified by Diego Orol and knocked out in the *C. necator* H16 Δ *phaCAB* strain, yielding the engineered *C. necator* H16 Δ *phaCAB* Δ *gabT* strain which was investigated in the context of a possible β -alanine degradation pathway but showed no affinity to β -alanine [144]. Research by Mayer et al. on the *gabT* and *gabD* homologues in *C. necator* H16 revealed that they are active in the context of homotaurine degradation and *gabT* recognised homotaurine as a substrate. Homotaurine, GABA and 5-AV acid all share a common terminal amino group that is recognised as target for transamination by GabT, followed by an aliphatic chain of 3 (Homotaurine, GABA) or 4 (5-AV) carbon atom length and a terminal, negatively charged acidic moiety - sulfonic acid in case of homotaurine and a carboxyl group in case of GABA and 5-AV.

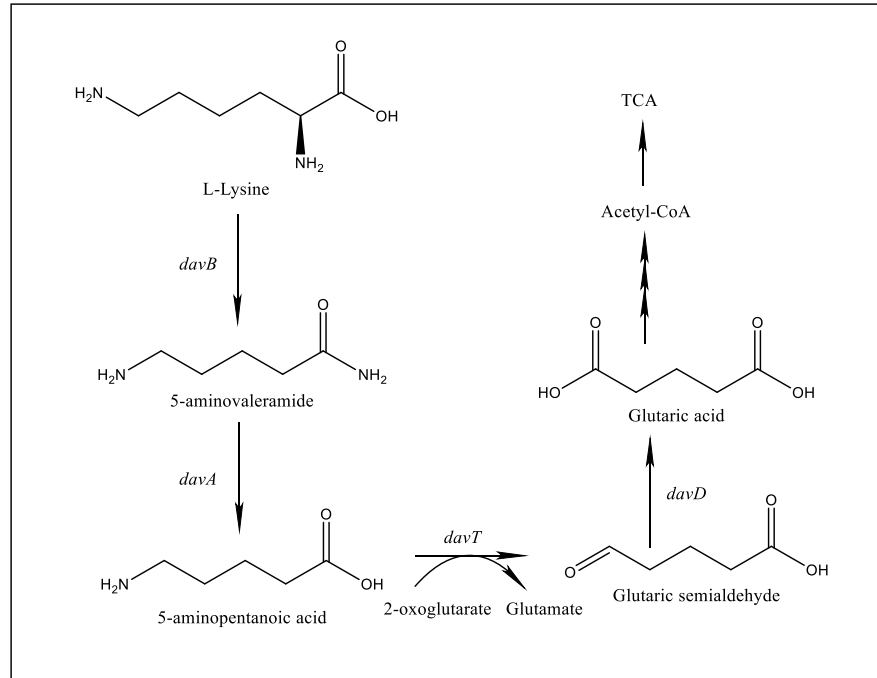


Figure 1.8 The Dav degradation pathway of L-lysine in *Pseudomonas putida*. L-Lysine is degraded to 5-AV by the catalysis of DavB and DavA. 5-AV can be converted to glutaric semialdehyde by *davT* (*C. necator* H16 homologue: *gabT*). The reactive semialdehyde is then converted to glutaric acid by *davD* and subsequently a degradation to Acetyl-CoA leads into the TCA cycle.

1.6.2 L-lysine biosynthesis

Three related L-lysine biosynthesis pathways exist in bacteria. (**Figure 1.9**).

The pathways share a common entry point, aspartate, which is phosphorylated by aspartate kinase AK encoded by *lysC* [H16_A1225] (**1**) as committing step towards L-lysine biosynthesis. AK is regulated by allosteric end-product feedback-inhibition [145]. L-aspartyl-phosphate is converted to aspartate semialdehyde by the *asd* encoded aspartate semialdehyde dehydrogenase [H16_A2618](**2**). The dihydrodipicolinate synthase DHDPS (**3**) converts the semialdehyde by condensation with pyruvate to 4-hydroxy-2,3,4,5-tetrahydrodipicolinate (HTPA) [146-149]. DHDPS is also end-product feedback inhibited by L-lysine [150]. Three copies of this enzyme are annotated in the *C. necator* H16 genome: *dapA1* [H16_A1204], *dapA3* [H16_B0891] and *dapA4* [H16_B1831]. After non-enzymatic dehydration to dihydrodipicolinate, the dihydrodipicolinate reductase DHDPR, (**4**) encoded by *dapB* [H16_A3141] and [H16_A3348], then yields tetrahydrodipicolinate (THDP) [151-153].

From Tetrahydrodipicolinate onwards, the four bacterial synthesis pathways diverge as the succinylase, acetylase, aminotransferase and dehydrogenase pathways [154, 155]. The **succinylase pathway (I)** is the main pathway used by most bacteria species for *mDAP*/L-lysine biosynthesis [156], including *C. necator* H16 and *E. coli*, where it is the only annotated pathway.

(legend continued) Figure adapted from Scapin et al.: *Enzymology of bacterial lysine biosynthesis* [156]. I) Succinylase pathway (II) Acetylase pathway (III) Aminotransferase pathway (IV) Dehydrogenase pathway. Dashed lines indicate negative feedback relationship. Homologs for enzymes in red are found in *C. necator* H16 but have not been experimentally verified. They are assumed to be functional as the strain is an L-lysine prototroph. Enzymes in blue are not found in *C. necator* H16, but in other bacterial species. AK – aspartate kinase. HTPA - 4-hydroxy-2,3,4,5-tetrahydrodipicolinate. DHDPS - dihydrodipicolinate synthase. DHDPR - dihydrodipicolinate reductase. THDP – tetrahydrodipicolinate. THPC-NST - 2,3,4,5-tetrahydropyridine-2-carboxylate *N*-succinyltransferase. NS-AKP - *N*-succinyl-L-2-amino-ketopimelate. NSDAP-AT - *N*-succinyldiaminopimelate aminotransferase. NSDAP - *N*-succinyl-L,L-2,6,-diaminopimelate. SDAP-DS - succinyldiaminopimelate desuccinylase. NAAKP - *N*-acetyl-(*S*)-2-amino-6-ketopimelate. NADAP - *N*-acetyl-(2*S*)-2,6,-diaminopimelate. DAPDH - diaminopimelate dehydrogenase. DAP-AT – diaminopimelate aminotransferase. DAPE - diaminopimelate epimerase. *m*-DAP – *meso*-diaminopimelate. DAPDC - diaminopimelate decarboxylase. DavA - δ -aminovaleramidase. DavB - lysine monooxygenase.

Tetrahydrodipicolinate is converted to *N*-succinyl-L-2-amino-ketopimelate (NSAKP) **(5)**, catalysed by the 2,3,4,5-tetrahydropyridine-2-carboxylate *N*-succinyltransferase (THPC-NST) under consumption of succinyl-CoA [157-159]. This enzyme is encoded by the gene *dapD* [H16_A2066] in *C. necator* H16. NSAKP is then transaminated **(6)** by the action of the *N*-succinyldiaminopimelate aminotransferase (NSDAP-AT) under consumption of glutamate, which yields 2-oxoglutaric acid and *N*-succinyl-L,L-2,6,-diaminopimelate (NSDAP) [160]. NSDAP-AT is encoded by *dapC* [H16_A2065] in *C. necator* H16, however the *N*-acetylornithine aminotransferase encoded by *argD* is known to be a bifunctional enzyme that can catalyse this step as well [161] and is annotated as [H16_A3025] in *C. necator* H16. NSDAP is desuccinylated **(7)** by the succinyldiaminopimelate desuccinylase SDAP-DS that is encoded as *dapE* [H16_A2069]. This reaction forms L,L-2,6-diaminopimelate (LL-DAP), where the succinylase and aminotransferase pathway join [162]. LL-DAP is then converted to *meso*-DAP (*m*-DAP) **(8)** by the diaminopimelate

epimerase DAPE, which is encoded by *dapF* [H16_A0227] in *C. necator* H16. *meso*-DAP, where the acetylase pathway and hydrogenase pathway re-join, can then be converted to L-lysine by decarboxylation **(9)** [163, 164] [165]. This is catalysed by the diaminopimelate decarboxylase DAPDC, encoded by on the *C. necator* H16 megaplasmid as *lysA* [PHG121] and also by a chromosomal copy, *lysA2* [H16_A3443].

The **acetylating pathway (II)** follows the succinylating pathway exactly, except for the acetylation of THDP instead of succinylation. This pathway can be found in several *Bacillus* species [166, 167]. Because of its extensive length of 4 reaction steps from THDP to DAP **(10-12)** it is of low priority as a metabolic engineering target. The reactions are parallel to the existing succinylating pathway in *C. necator* H16 and none of the enzymes are potentially interchangeable.

The **aminotransferase pathway (III)** is a sub-pathway found mainly in plants, *Eubacteria* sp., *Methanococci* and some other archae [168, 169]. Through the action of a single aminotransferase, DAP-AT, the open-ring form of THDP (1,2-amino-6- ketopimelate) is directly converted to m-DAP, thereby re-joining the other pathways. The gene *dapL* that codes for this aminotransferase is present in ca. 13% of bacteria in the NCBI database (2014), but not in *C. necator* H16 [170]. In two studies published by Hudson et al., the kinetic properties of DAP-AT were investigated. The enzyme activity of DAP-AT from all orthologs characterised to date has shown that DAP-AT is more efficient by a factor of 20-60 in reverse (catabolic) direction in terms of V_{max} . Nonetheless, a copy of DAP-AT can save a $\Delta dapDE$ L-lysine auxotrophic mutant [171] [172]. Unfortunately,

even if a single-enzyme bridge seems an attractive target in metabolic engineering, due to the adverse kinetics of enzyme, this pathway can also only be a low-priority to employ for a lysine overproducing strain.

The **dehydrogenase pathway (IV)**, which can be found in *Cornynebacterium* sp. and *Bacillus* sp. catalyses the reaction from THDP to m-DAP through the action of the diaminopimelate dehydrogenase DAPDH encoded by *ddh* in *Co. glutamicum* [173-176]. This enzyme is not present in *Cupriavidus* species. As opposed to the aminotransferase bypass, the dehydrogenase is more suited for metabolic engineering of lysine overproducing strains. In a study by Xu et al. [177], *ddh* was introduced to *E. coli* and increased the carbon yield of L-lysine production by 13.8% with a thermostable *ddh* variant, which accounts for the differences of culturing conditions between *E. coli* (37°C) and *Co. glutamicum* (30°C). the *ddh* gene is therefore particularly suited to be introduced to *C. necator* H16, because *C. necator* H16 and *Co. glutamicum* share an optimal growth temperature of 30 °C. Only few bacteria use the dehydrogenase pathway for lysine formation, including, for example, *Brevibacterius* sp., *Bacillus* sp. and *Co. glutamicum* [178], of which some use several pathways for L-lysine formation at once. For example, *Co. glutamicum* uses both the succinylating and the dehydrogenase pathway in parallel [179]. Other bacteria are also known to use the dehydrogenase in parallel with the acetylating pathway [180]. More information about the regulation of L-lysine biosynthesis and about methods for deregulating the pathway for metabolic engineering is given in **Chapter 4.1.8** in the context of 5-AV production.

1.7 Quorum sensing in bacteria

Quorum sensing in bacteria allows for the regulation of genes based on cell density. Bacteria can produce and secrete signal molecules called autoinducers, which stimulate a change in gene expression in other bacterial cells [181]. This allows bacteria to communicate and act as a collective, which, according to Miller et al. [181], can impact the regulation of processes such as “symbiosis, virulence, competence, conjugation, antibiotic production, motility, sporulation, and biofilm formation”.

Quorum sensing is an important topic in the context of biotechnology, as industrial production of chemicals is often done at high cell densities [182]. This means that quorum sensing can interfere with product formation and has to be taken into account when engineering attempts of organisms with a quorum sensing system are undertaken.

In Gram-positive bacteria, these autoinducers are released in form of polypeptides and interact with regulators such as phosphatases and transcription factors, which change transcription of genes in the cell [183]. While these peptides contribute to bacterial communication, cross-talk between Gram-positive bacteria and their hosts via these signal peptides is under investigation [184].

Quorum sensing in Gram-negative bacteria, such as *C. necator* H16, is realised by a different class of autoinducers. These are synthesised mainly from S-adenosylmethionine, like acyl-homoserine lactones [185]. An example for a well-studied quorum sensing circuit in Gram-negative bacteria is the *Vibrio*

fischeri LuxI/LuxR bioluminescence system [186]. For example, in symbiotic relationship with the eukaryotic host, *V. fischeri* is supplied with nutrients by the squid *Euprymna scolopes* - and provides its host with a light organ based on its quorum sensing circuit [187]. The emission of light (bioluminescence) is strictly dependent on a critical cell density of *V. fischeri* and can reach up to 10^{11} cells per mL [188]. The luciferase enzymes necessary for light emission are encoded by the *luxCDABE* operon and regulated by two proteins, LuxI and LuxR, of which the former is the biosynthesis enzyme of the autoinducer and the later [181]. Once a critical concentration of autoinducer (in this case, *N*-(3-oxohexanoyl)-homoserine lactone) of $1-10 \mu\text{g mL}^{-1}$ is reached, the binding affinity of the compound is sufficient to bind to the cytoplasmatic LuxR protein, subsequently allowing LuxR to then bind to the *luxCDABE* operon promoter and activate transcription [181].

Another quorum sensing circuits well described in the literature is the *Pseudomonas aeruginosa* LasI/LasR-RhlI/RhlR virulence system [189], which is based on the same autoinducer as *V. fischeri*, and, additionally, on 2-heptyl-3-hydroxy-4-quinolone, an exception that is not based on *S*-adenosylmethionine [190]. For more detailed information about quorum sensing in the context of *C. necator* H16, see **Chapter 4.1.4**.

1.8 Biosensors

Biosensors are analytical tools that convert a biological response into an electrical or optical signal [191]. In the last decades, various types of biosensors have been described in the literature, which can be enzyme-based, tissue-based, immunosensors, DNA biosensors or thermal and piezoelectric biosensors [191]. Biosensors generate signals proportional to the concentration of a small molecule analyte [192] and can therefore be used in high-throughput screening applications.

Fields that biosensors see use are, for example, quality assurance in food production [193], water quality checks [194] and landmine detection [195]. Another category of biosensors was developed for rapid and mobile medical diagnostics, cutting down treatment time for diseases ranging from influenza to a range of cancers [196].

Biosensors exist since the 1960s and the first enzyme-based sensor was developed by Updike and Hicks [197] as a miniature chemical transducer, which could measure the concentration of glucose *in vitro* and output an electrical signal. Cell-based sensors were firstly developed on the basis of ethanol oxidation by Diviès [198], using *Acetobacter xylinum* [191, 198]. Today, cell-based sensors often rely on the two-component system of a histidine kinase that binds a target molecule and a response regulator that expresses a reporter gene [199]. Tissue-based sensors were introduced by *Rechnitz* [200] with electrical output. Immunosensors relied on the high affinity of antibodies for their antigens as a means to measure analyte concentrations, and DNA

biosensors work based on the principle that ssDNA hybridizes with complementing DNA strands, which it helps to detect [191].

In synthetic biology and metabolic engineering, biosensors are used to enable high-throughput screening of diverse (bacterial) populations for the production of a desired product [191]. First, enzymatic assays with spectroscopic output were developed, but had limited throughput [191]. Genetically encoded fluorescent biosensors, however, enabled the monitoring of bacterial metabolism and desired phenotypes by fluorescence-activated cell sorting (FACS) [191, 201]. For these biosensors, a transcription factor/promoter system that is naturally activated by the analyte is cloned into a different host and drives the expression of a heterologous reporter gene, such as green fluorescent protein (GFP) [202]. These biosensors are limited by the natural range of transcription factor – promoter pairs available and not all natural products activate genes by these systems [196]. Additionally, they can suffer from off-target activation and must therefore be carefully validated before use [196]. One such novel biosensor design of this type for the detection of the small molecule 5-AV is described in this work in **Chapter 5**. The last, and arguably, most complex type of biosensor are nucleic acid-based biosensors for small molecules on the basis of aptamers, single stranded DNA or RNA with an affinity to the target analyte [203, 204]. DNA and RNA sequences can be evolved systematically to bind target analytes using the SELEX method, meaning that this class of biosensors is less constrained than transcription-factor based biosensors [205].

1.9 Aims of the project

Rising demands for value-added chemicals and the environmental concerns over petrochemical synthesis routes have led to a booming industry for the production of chemicals in microorganisms. This work aimed to add the production of 5-hydroxyvaleric acid, a precursor for biodegradable polyesters and 5-aminovaleric acid (5-AV), a nylon-5 precursor, to the portfolio of bio-based chemicals we can produce in an environmentally friendly way.

In this study, *C. necator* H16 was engineered for the production of two value-added products because of its unique ability to produce under aerobic lithoautotrophic conditions using waste gases.

This work aimed introduce an engineered pathway for 5-AV production from *C. necator* H16 central metabolism based on the L-lysine biosynthesis route and a novel pathway for the production of 5-hydroxyvaleric acid (5-OHV) based on a reverse beta-oxidation chain elongation pathway from β -alanine. I also aimed to showcase a “top-down” approach to synthetic biology, which expedites the process for pathway screening and optimisation. A design for a biosensor for one of the products, 5-AV was introduced in this work. Biosensors are useful tools in synthetic biology that aid in high-throughput screening of strains for the production of a desired product, thus potentially enabling automated next-generation techniques for strain and pathway development.

Chapter 2

Materials and methods

Chapter 2 – Materials and methods

2.1 Bacterial cell manipulation: strains, media, growth conditions

2.1.1 Bacterial strains

All strains used in this study are shown in **table 2.1**.

Table 2.1 Bacterial strains used in this study

Strain	Genotype / Description	Reference / Source
<i>E. coli</i>		
DH5 α	<i>fhuA2</i> Δ (<i>argF-lacZ</i>)U169 <i>phoA glnV44</i> Φ 80 Δ (<i>lacZ</i>)M15 <i>gyrA96 recA1</i> <i>relA1 endA1 thi-1 hsdR17</i>	New England Biolabs C2987H
Rosetta-gami™ 2 (DE3)	Δ (<i>ara-leu</i>)7697 Δ <i>lacX74</i> Δ <i>phoA PvuII phoR araD139</i> <i>ahpC galE galK rpsL</i> (DE3) F'[<i>lac+ lacIq pro</i>] <i>gor522::Tn10 trxB</i> pRARE2 (CamR, StrR, TetR)	Novagen
Lemo21 (DE3)	<i>fhuA2 [lon] ompT gal</i> (λ DE3) [<i>dcm</i>] Δ <i>hsdS</i> / <i>pLemo</i> (CamR) λ DE3 = λ <i>sBamHI</i> Δ <i>EcoRI-B</i> <i>int::(lacI::PlacUV5::T7</i> <i>gene1) i21</i> Δ <i>nin5</i> <i>pLemo</i> = <i>pACYC184-PrhaBAD-lysY</i>	New England Biolabs
<i>C. necator</i>		
H16	wildtype	DSM 428
Δ <i>phaCAB</i>	H16 Δ <i>phaCAB</i>	Christian Arenas López, University of Nottingham [110]
Δ 3	H16 Δ <i>mmsA2</i> Δ <i>mmsA1</i> Δ <i>mmsA3</i>	Christian Arenas López, University of Nottingham [110]

$\Delta 4$	H16 $\Delta mmsA2 \Delta mmsA1 \Delta mmsA3 \Delta phaCAB$	Christian Arenas López, University of Nottingham [110]
$\Delta phaCAB \Delta gabT$	H16 $\Delta phaCAB \Delta gabT$	Diego Orol, University of Nottingham [144]
<i>Corynebacterium glutamicum</i>	ATCC® 13032™	Stephan Heeb, University of Nottingham [206]
<i>Clostridium acetobutylicum</i>	ATCC® 824™	Nigel Minton, University of Nottingham
<i>Clostridium saccharoperbutylacetonicum</i>	ATCC® 27021™	Tom Wilding Steele, University of Nottingham [207]
<i>Chromobacterium violaceum</i>	ATCC® 12472™	Diego Orol, University of Nottingham [144]

2.1.2 General chemicals

All chemicals were purchased from Sigma Aldrich unless stated otherwise and stored at their recommended temperature.

2.1.3 Media and buffers

2.1.3.1 Media plates

All media plates were casted by addition of 15 g L⁻¹ bacteriological technical agar No. 3 (Oxoid™, Thermo Fisher) to any liquid medium.

2.1.3.2 Lysogeny broth medium (LB)

Lysogeny Broth (LB) medium consisted of: 10 g L⁻¹ tryptone (Oxoid™, Thermo Fisher), 5 g L⁻¹ yeast extract (Oxoid™, Thermo Fisher) and 10 g L⁻¹ NaCl. LB was adjusted to pH 7 with NaOH, sterilised by autoclaving and stored at room temperature.

2.1.3.3 Hannahan's broth (SOB)

Hannahan's broth was used to prepare competent cells of *C. necator* H16 strains and reconstituted from powder. SOB consisted of: 20 g L⁻¹ tryptone, 5 g L⁻¹ yeast extract, 2.4 g L⁻¹ MgSO₄, 500 mg L⁻¹ NaCl and 186 mg L⁻¹ KCl. SOB was sterilised by autoclaving and stored at room temperature.

2.1.3.4 M9 minimal medium for *E. coli* (ECMM)

ECMM was used in fermentations with *E. coli* and contains 17.1 g L⁻¹ Na₂HPO₄ x 12 H₂O, 3 g L⁻¹ KH₂PO₄, 500 mg L⁻¹ NaCl, 1 g L⁻¹ NH₄Cl, 4 g L⁻¹ Glucose, 2 mM MgSO₄, 100 μM CaCl₂ and 100 mg L⁻¹ thiamine. ECMM was sterilised by filtration and stored at room temperature.

2.1.3.5 Trace element solution (SL7)

Trace element solution was used to make *C. necator* H16 minimal media. SL7 contains: 1.3 mL L⁻¹ HCl (25% w/v), 63 mg L⁻¹ H₃BO₃, 190 mg L⁻¹ CoCl₂ x 6 H₂O, 17 mg L⁻¹ CuCl₂ x 2 H₂O, 100 mg L⁻¹ MnCl₂ x 4 H₂O, 36 mg L⁻¹ Na₂MoO₄ x 2 H₂O, 24 mg L⁻¹ NiCl₂ x 6 H₂O and 70 mg L⁻¹ ZnCl₂ 70 mg/L. The recipe was *derived* from the trace element SL7 solution of DSMZ media 1129 (phototrophic medium) [208].

2.1.3.6 Minimal medium for *C. necator* H16 (CNMM)

CNMM was used in fermentations with *C. necator* H16 and contains 10 g L⁻¹ sodium gluconate, 9 g L⁻¹ Na₂HPO₄ x 12 H₂O, 1.5 g L⁻¹ KH₂PO₄, 1 g L⁻¹ NH₄Cl, 200 mg L⁻¹ MgSO₄ x 7 H₂O, 20 mg CaCl₂, 1.2 mg L⁻¹ Fe(III)NH₄-citrate and 1 mL L⁻¹ SL7 trace element solution. CNMM was adjusted to pH 6.9 with NaOH, sterilised by filtration and stored at room temperature. The medium was adapted from Lenz et al. [209] and López et al. [210].

2.1.3.7 Phosphate limited minimal medium for *C. necator* H16 resting cells (CNMM-P)

CNMM-P was used in fermentations with *C. necator* H16 resting cells and contains 10 g L⁻¹ sodium gluconate, 10.4 g L⁻¹ MOPS, 2.5 g L⁻¹ NH₄Cl, 200 mg L⁻¹ MgSO₄ x 7 H₂O, 20 mg CaCl₂, 1.2 mg L⁻¹ Fe(III)NH₄-citrate and 1 mL L⁻¹ SL7 trace element solution. CNMM-P was adjusted to pH 6.9 with NaOH, sterilised by filtration and stored at room temperature.

2.1.3.8 Carbon limited minimal medium for *C. necator* H16 (CNMM-C)

CNMM-C was used to test 5-AV metabolisation in *C. necator* H16 as sole carbon source. It contains: 9 g L⁻¹ Na₂HPO₄ x 12 H₂O, 1.5 g L⁻¹ KH₂PO₄, 1 g L⁻¹ NH₄Cl, 200 mg L⁻¹ MgSO₄ x 7 H₂O, 20 mg CaCl₂, 1.2 mg L⁻¹ Fe(III)NH₄-citrate and 1 mL L⁻¹ SL7 trace element solution. CNMM-C was adjusted to pH 6.9 with NaOH, sterilised by filtration and stored at room temperature.

2.1.3.9 Nitrogen limited minimal medium for *C. necator* H16 (CNMM-N)

CNMM-C was used to test 5-AV metabolisation in *C. necator* H16 as sole nitrogen source. It contains: 10 g L⁻¹ sodium gluconate, 9 g L⁻¹ Na₂HPO₄ x 12 H₂O, 1.5 g L⁻¹ KH₂PO₄, 200 mg L⁻¹ MgSO₄ x 7 H₂O, 20 mg CaCl₂, 1.2 mg L⁻¹ Fe(III)NH₄-citrate and 1 mL L⁻¹ SL7 trace element solution. CNMM-N was adjusted to pH 6.9 with NaOH, sterilised by filtration and stored at room temperature.

2.1.3.10 *E. coli* transformation buffer 1 (EC-T1)

Used to prepare chemically competent cells. Contains 12 g L⁻¹ RbCl, 10 g L⁻¹ MnCl₂ x 4 H₂O, 3 mL 1M potassium acetate solution (pH 7.5). 1.5 g L⁻¹ CaCl₂ x 2 H₂O and 120 mL L⁻¹ glycerol. The buffer was adjusted to pH 5.8 using 0.2M acetic acid and filter sterilised. The buffer was stored at 4 °C.

2.1.3.11 *E. coli* transformation buffer 2 (EC-T2)

Used to prepare chemically competent cells. Contains 2.1 g L⁻¹ MOPS, 1.2 g L⁻¹ RbCl, 11 g L⁻¹ CaCl₂ and 120 mL L⁻¹ glycerol. The buffer was adjusted to pH 6.8 using NaOH and filter sterilised. The buffer was stored at 4 °C.

2.1.4 General growth conditions and culturing

All *E. coli* and *C. necator* H16 strains were grown aerobically in a Thermo Scientific™ MaxQ™ 8000 Incubated Stackable Shaker at 37 °C (*E. coli*) or 30 °C (*C. necator* H16) at 200 rpm. When grown as precultures, 50 mL falcon tubes (Greiner Bio-One) were used and filled to 5 mL to allow for plenty of headspace for oxygenation. For shake flask fermentations, 250 mL baffled Duran® shake flasks were used and filled to a maximum of 10% volume (25 mL). For resting cell precultures, 2000 mL unbaffled erlenmeyer flasks were used and filled to 10% volume. *C. glutamicum* was cultured at 30 °C on LB medium.

Biological triplicates originate from separate single colonies that were obtained by streaking 10^{-3} to 10^{-6} dilutions of precultures on LB plates or minimal media plates; or by streaking frozen cryostock beads directly on LB plates. LB plates were kept up to 4-6 weeks.

From single colonies, 5 mL precultures were grown in appropriate medium in 50 mL falcon tubes and incubated at 200 rpm over night or until growth was observed at the appropriate temperature for the strain. Precultures were used to inoculate main cultures at the OD₆₀₀ (optical density at 600 nm) described by the experiment.

2.1.5 Spectrometric OD₆₀₀ measurements

Optical density at 600 nm (OD₆₀₀) was recorded using a BioMate™ spectrophotometer from Thermo Scientific. Growth curves were recorded by taking a sample of 100 µL from a culture, dilute it with 900 µL water and transfer 1 mL to a cuvette for measurement in the BioMate™ photometer. In micro-fermentation experiments, OD₆₀₀ was measured by BioLector (M2P-labs) or TECAN (Tecan Life Sciences).

2.1.6 Strain storage conditions

All *E. coli* and *C. necator* H16 strains were stored at -80 °C. Microbank™ vials (Pro-Lab Diagnostics) were used. A preculture was grown over night (or until growth was observed) and used to inoculate three colour-coded Microbank™ vials (green, yellow and red). For strain recovery, a single bead directly streaked on an appropriate solid medium plate or dropped into 5 mL of an appropriate liquid medium (and selection antibiotics if the strain carries a plasmid). Typically, a rich medium such as LB was used, but in some cases a super-rich medium such as SOB or SOC was necessary to recover a strain.

2.2 Antibiotics

Selection antibiotics for *C. necator* H16 and *E. coli* were stored at -20 °C (powder). Stock solutions were also stored at -20°C. They were added to liquid and solid media to reach the final concentrations described in **table 2.2**.

Table 2.2 List of antibiotics that were used in this study.

Antibiotic	Stock solution	Concentration for <i>E. coli</i>	Concentration for <i>C. necator</i> H16
Tetracycline	12.5 mg mL ⁻¹ in 100% ethanol	10 µg mL ⁻¹	12.5 µg mL ⁻¹
Chloramphenicol	50 mg mL ⁻¹ in 100% ethanol	25 µg mL ⁻¹	50 µg mL ⁻¹
Ampicillin	100 mg mL ⁻¹ in H ₂ O	100 µg mL ⁻¹	100 µg mL ⁻¹

2.3 Molecular biology

2.3.1 Plasmids

Table 2.3 shows all plasmids that were used in this study. OHV indicates plasmids used for 5-hydroxyvalerate synthesis (**Chapter 3**), L indicates vectors used for 5-aminovalerate synthesis (**Chapter 4**) and BS indicates vectors used in the biosensor project (**Chapter 5**).

Table 2.3 Plasmids used in this study

Plasmid	Description	Reference/Source
pOHV0	pMTL71301-P _{phaC} - <i>empty</i> Medium to low copy-number plasmid used for constitutive heterologous expression, confers tetracycline resistance.	Unpublished, Muhammad Ehsaan, University of Nottingham
pOHV1	pMTL71301-P _{phaC} - <i>ydfg</i> _{EC} - <i>bapat</i> _{CV} - <i>pct</i> _{EC} . Used for constitutive heterologous expression of <i>ydfG</i> , <i>bapat</i> _{CV} and <i>pct</i> . Confers tetracycline resistance.	This study
pOHV2	pMTL71301-P _{phaC} - <i>ydfg</i> _{EC} - <i>bapat</i> _{CV} - <i>prpE</i> _{EC} . Used for constitutive heterologous expression of <i>ydfG</i> , <i>bapat</i> _{CV} and <i>prpE</i> . Confers tetracycline resistance.	This study
pOHV3	pMTL74311-P _{phaP} - <i>empty</i> Low copy-number plasmid used to generate pMTL74111 by replacing tetracycline resistance cassette with a chloramphenicol cassette using FseI and PmeI.	Unpublished, Alexander van Hagen, University of Nottingham
pOHV4	pMTL74111-P _{phaP} - <i>empty</i> Low copy-number plasmid used for constitutive heterologous expression, confers chloramphenicol resistance	This study
pOHV5	pMTL74111-P _{phaP} - <i>bktB</i> _{CN} - <i>phaB</i> _{CN} - <i>crt3</i> _{CN} - <i>ter</i> _{TD} Low copy-number plasmid used for heterologous expression of <i>bktB</i> , <i>phaB</i> , <i>crt3</i> and <i>ter</i> _{TD} . Confers chloramphenicol resistance.	This study
pOHV6	pMTL74111-P _{phaP} - <i>bktB</i> _{CN} - <i>phaB</i> _{CN} - <i>crt3</i> _{CN} - <i>ter</i> _{EG} Low copy-number plasmid used for heterologous expression of <i>bktB</i> , <i>phaB</i> , <i>crt3</i> and <i>ter</i> _{EG} . Confers chloramphenicol resistance.	This study
pOHV7	pMTL74111-P _{phaP} - <i>bktB</i> _{CN} - <i>hbd3</i> _{CS} - <i>crt</i> _{CA} - <i>ter</i> _{TD} Low copy-number plasmid used for heterologous expression of <i>bktB</i> , <i>hbd3</i> , <i>crt</i> and <i>ter</i> _{TD} . Confers chloramphenicol resistance.	This study
pOHV8	pMTL74111-P _{phaP} - <i>bktB</i> _{CN} - <i>hbd3</i> _{CS} - <i>crt</i> _{CA} - <i>Ter</i> _{EG} Low copy-number plasmid used for heterologous expression of <i>bktB</i> , <i>hbd3</i> , <i>crt</i> and <i>ter</i> _{TD} . Confers chloramphenicol resistance.	This study

pOHV9	pMTL74111-P _{phaP} - <i>bktB</i> _{CN} - <i>fadAB</i> _{EC} - <i>ter</i> _{TD} Low copy-number plasmid used for heterologous expression of <i>bktB</i> , <i>fadAB</i> and <i>ter</i> _{TD} . Confers chloramphenicol resistance.	This study
pOHV10	pMTL74111-P _{phaP} - <i>bktB</i> _{CN} - <i>fadAB</i> _{EC} - <i>ter</i> _{EG} Low copy-number plasmid used for heterologous expression of <i>bktB</i> , <i>fadAB</i> and <i>ter</i> _{EG} . Confers chloramphenicol resistance.	This study
pOHV11	pMTL74111-P _{phaP} - <i>paaJ</i> _{EC} - <i>phaB</i> _{CN} - <i>crt3</i> _{CN} - <i>ter</i> _{TD} Low copy-number plasmid used for heterologous expression of <i>paaJ</i> , <i>phaB</i> , <i>crt3</i> and <i>ter</i> _{TD} . Confers chloramphenicol resistance.	This study
pOHV12	pMTL74111-P _{phaP} - <i>paaJ</i> _{EC} - <i>phaB</i> _{CN} - <i>crt3</i> _{CN} - <i>ter</i> _{EG} Low copy-number plasmid used for heterologous expression of <i>paaJ</i> , <i>phaB</i> , <i>crt3</i> and <i>ter</i> _{EG} . Confers chloramphenicol resistance.	This study
pOHV13	pMTL74111-P _{phaP} - <i>paaJ</i> _{EC} - <i>hbd3</i> _{CS} - <i>crt</i> _{CA} - <i>ter</i> _{TD} Low copy-number plasmid used for heterologous expression of <i>paaJ</i> , <i>hbd3</i> , <i>crt</i> and <i>ter</i> _{TD} . Confers chloramphenicol resistance.	This study
pOHV14	pMTL74111-P _{phaP} - <i>paaJ</i> _{EC} - <i>hbd3</i> _{CS} - <i>crt</i> _{CA} - <i>ter</i> _{EG} Low copy-number plasmid used for heterologous expression of <i>paaJ</i> , <i>hbd3</i> , <i>crt</i> and <i>ter</i> _{EG} . Confers chloramphenicol resistance.	This study
pOHV15.1	pMTL71301-P _{trc} - <i>empty</i> Medium to low copy-number plasmid used for cloning, confers tetracycline resistance.	This study
pOHV15.2	pMTL71301-P _{trp} - <i>bktB</i> _{CN} - <i>phaB</i> _{CN} Medium to low copy-number plasmid used for cloning, confers tetracycline resistance.	This study
pOHV15.3	pMTL71301-P _{trp} - <i>bktB</i> _{CN} - <i>phaB</i> _{CN} - <i>crt3</i> _{CN} - <i>ter</i> _{TD} Medium to low copy-number plasmid used for cloning, confers tetracycline resistance. With synthetic RBS sites. Generated from OHV15.2	This study
pOHV15.4	pMTL71301-P _{trc} - <i>ydfg</i> _{EC} - <i>BAPAT</i> _{CV} - <i>prpE</i> _{EC} Medium to low copy-number plasmid used for cloning, confers tetracycline resistance, uses synthetic RBS sites. Generated from OHV15.1	This study
pOHV16	pMTL71301-P _{trc} - <i>ydfg</i> _{EC} - <i>BAPAT</i> _{CV} - <i>prpE</i> _{EC} -P _{trp} - <i>bktB</i> _{CN} - <i>phaB</i> _{CN} - <i>crt3</i> _{CN} - <i>ter</i> _{TD} Used for strong constitutive heterologous expression of <i>ydfG</i> , <i>bapat</i> _{CV} and <i>prpE</i> under P _{trc} control and <i>bktB</i> , <i>phaB</i> , <i>crt3</i> and <i>ter</i> _{TD} under P _{trp} control with synthetic RBS sites. Confers tetracycline resistance. Generated from OHV15.1	This study
pL0	pMTL71301-P _{BAD} - <i>empty</i> Medium to low copy-number plasmid used for cloning and as negative control, confers tetracycline resistance.	Unpublished, Giorgia Tibaldero, University of Nottingham
pL0.1	pMTL71301-P _{BAD} - <i>rfp</i> Medium to low copy-number plasmid used for cloning, confers tetracycline resistance. Conditionally expresses RFP.	Unpublished, Giorgia Tibaldero, University of Nottingham
pL1	pMTL71301-P _{BAD} - <i>davA</i> _{PP} - <i>davB</i> _{PP} Medium to low copy-number plasmid used for constitutive heterologous expression of <i>davA</i> and <i>davB</i> under P _{BAD} control, confers tetracycline resistance.	This study

pL2	pMTL71301-P _{BAD} - <i>davA</i> _{PP} - <i>davB</i> _{PP} - <i>lysC</i> _{CG} Medium to low copy-number plasmid used for constitutive heterologous expression of <i>davA</i> , <i>davB</i> and <i>lysC</i> _{CG} under P _{BAD} control, confers tetracycline resistance.	This study
pL4	pMTL71301-P _{BAD} - <i>davA</i> _{PP} - <i>davB</i> _{PP} - <i>lysC</i> _{CG} - <i>ddh</i> _{CG} Medium to low copy-number plasmid used for constitutive heterologous expression of <i>davA</i> , <i>davB</i> , <i>lysC</i> _{CG} and <i>ddh</i> _{CG} under P _{BAD} control, confers tetracycline resistance.	This study
pL8	pMTL71301-P _{BAD} - <i>lysC</i> _{CG} ^{fbr} - <i>dapA</i> _{CG} ^{fbr} - <i>ddh</i> _{CG} Medium to low copy-number plasmid used for cloning. Confers tetracycline resistance.	This study
pL9	pMTL71301-P _{BAD} - <i>lysC</i> _{CG} ^{fbr} - <i>dapA</i> _{CG} ^{fbr} - <i>ddh</i> _{CG} -P _{trp} - <i>davA</i> _{PP} - <i>davB</i> _{PP} Medium to low copy-number plasmid used for constitutive heterologous expression of <i>lysC</i> _{CG} ^{fbr} , <i>dapA</i> _{CG} ^{fbr} and <i>ddh</i> _{CG} under P _{BAD} control and <i>davA</i> and <i>davB</i> under P _{trp} control with synthetic RBS sites. Confers tetracycline resistance. Generated from L8.	This study
pBS0.1	pMTL74111-P _{BAD} - <i>empty</i> Low copy-number plasmid used for cloning, generated from OHV4 by switching the P _{Phac} promoter for the P _{BAD} promoter using the NotI and NdeI cut sites. Confers chloramphenicol resistance.	This study
pBS0.2	pMTL74111-P _{BAD} - <i>orf26</i> _{SA} - <i>chnR</i> _{RAC} Low copy-number plasmid generated from BS0.1 that was used for cloning. Confers chloramphenicol resistance. No terminator after <i>chnR</i> .	This study
pBS2	pMTL74111-P _{BAD} - <i>orf26</i> _{SA} - <i>chnR</i> _{RAC} Low copy-number plasmid generated from BS0.2 that was used as control. Confers chloramphenicol resistance. With terminator after <i>chnR</i> .	This study
pBS1	pMTL74111-P _{BAD} - <i>orf26</i> _{SA} - <i>chnR</i> _{RAC} -P _{ChnB} - <i>rfp</i> Low copy-number plasmid generated from BS2 that was used as biosensor. Confers chloramphenicol resistance.	This study
pBS3	pMTL74111-P _{BAD} - <i>caiC</i> _{EC} - <i>chnR</i> _{RAC} -P _{ChnB} - <i>rfp</i> Low copy-number plasmid generated from BS0.2 that was used as biosensor. Confers chloramphenicol resistance.	This study
pET16b	Expression vector for protein purification, ampicillin resistance	Unpublished, Jessica Locker, University of Nottingham
pCaiC_EX	Expression vector for 6xHis CaiC purification, ampicillin resistance	This study
pChnR_EX	Expression vector for 6xHis ChnR purification, ampicillin resistance	This study

If applicable, **Table 2.4** shows with which (HiFi assembly) fragments the plasmids shown in **Table 2.3** were generated.

Table 2.4 HiFi fragments used to generate plasmids described in this study. (*)

Ordered long oligonucleotides can be used in HiFi assembly if forward and reverse strands are combined to form dsDNA. Only the forward strand is given in the primer table.

Plasmid	Fragment name	Primer combination	Template	Linearisation sites
pOHV0	N/A	N/A	N/A	N/A
pOHV1	YdfG_1	1 + 2	<i>E. coli</i> (colony PCR)	NdeI + NheI
	CvBAPAT_1	3 + 4	<i>bapat_{CV}</i> cloned on plasmid (Diego Orol)	
	Pct_1	5 + 6	<i>E. coli</i> (colony PCR)	
pOHV2	YdfG_2	1 + 2	<i>E. coli</i> (colony PCR)	NdeI + NheI
	CvBAPAT_2	7 + 8	<i>bapat_{CV}</i> cloned on plasmid (Diego Orol)	
	PrpE_2	9 + 10	<i>E. coli</i> (colony PCR)	
pOHV3	N/A	N/A	N/A	N/A
pOHV4	Cm	N/A	Any pMTL7x1xx series, fragment cut out and ligated.	FseI + PmeI
pOHV5	Bktb_5	11 + 12	<i>C. necator</i> H16 (colony PCR)	NdeI + NheI
	R1_5	13 + 14	<i>C. necator</i> H16 (colony PCR)	
	R2_5	15 + 16	<i>C. necator</i> H16 (colony PCR)	
	TdTer_5	17 + 18	Synthetic gene on plasmid (Biomatik)	
pOHV6	Bktb_6	11 + 12	<i>C. necator</i> H16 (colony PCR)	NdeI + NheI
	R1_6	13 + 14	<i>C. necator</i> H16 (colony PCR)	
	R2_6	15 + 19	<i>C. necator</i> H16 (colony PCR)	
	EgTer_6	20 + 21	Synthetic gene on plasmid (Biomatik)	
pOHV7	Bktb_7	22 + 23	<i>C. necator</i> H16 (colony PCR)	NdeI + NheI
	S1_7	24 + 25	<i>C. saccharoperbutylacetonicum</i> (genomic DNA)	
	S2_7	26 + 27	<i>C. acetobutylicum</i> (colony PCR)	
	TdTer_7	28 + 18	Synthetic gene on plasmid (Biomatik)	

pOHV8	Bktb_8	22 + 23	<i>C. necator</i> H16 (colony PCR)	Ndel + Nhel
	S1_8	24 + 25	<i>C. saccharoperbutylacetonicum</i> (genomic DNA)	
	S2_8	26 + 29	<i>C. acetobutylicum</i> (colony PCR)	
	EgTer_8	30 + 21	Synthetic gene on plasmid (Biomatik)	
pOHV9	Bktb_9	22 + 31	<i>C. necator</i> H16 (colony PCR)	Ndel + Nhel
	FadAB_9	32 + 33	<i>C. necator</i> H16 (colony PCR)	
	TdTer_9	34 + 18	Synthetic gene on plasmid (Biomatik)	
pOHV10	Bktb_10	22 + 31	<i>C. necator</i> H16 (colony PCR)	Ndel + Nhel
	FadAB_10	32 + 35	<i>C. necator</i> H16 (colony PCR)	
	EgTer_10	36 + 21	Synthetic gene on plasmid (Biomatik)	
pOHV11	PaaJ_11	37 + 38	<i>E. coli</i> (colony PCR)	Ndel + Nhel
	R1_11	39 + 14	<i>C. necator</i> H16 (colony PCR)	
	R2_11	15 + 16	<i>C. necator</i> H16 (colony PCR)	
	TdTer_11	17 + 18	Synthetic gene on plasmid (Biomatik)	
pOHV12	PaaJ_12	37 + 38	<i>E. coli</i> (colony PCR)	Ndel + Nhel
	R1_12	39 + 14	<i>C. necator</i> H16 (colony PCR)	
	R2_12	15 + 19	<i>C. necator</i> H16 (colony PCR)	
	EgTer_12	20 + 21	Synthetic gene on plasmid (Biomatik)	
pOHV13	PaaJ_13	37 + 40	<i>E. coli</i> (colony PCR)	Ndel + Nhel
	S1_13	41 + 25	<i>C. necator</i> H16 (colony PCR)	
	S2_13	26 + 27	<i>C. necator</i> H16 (colony PCR)	
	TdTer_13	28 + 18	Synthetic gene on plasmid (Biomatik)	
pOHV14	PaaJ_14	37 + 40	<i>E. coli</i> (colony PCR)	Ndel + Nhel
	S1_14	41 + 25	<i>C. necator</i> H16 (colony PCR)	
	S2_14	26 + 29	<i>C. necator</i> H16 (colony PCR)	
	EgTer_14	30 + 21	Synthetic gene on plasmid (Biomatik)	

pOHV15.1	ptrc promoter with ydfg2kRBS	42	Ordered long oligonucleotide*	NotI + NdeI
pOHV15.2	Ptrp promoter Bktb_16 R1_16 2kRBS_(R2)_16	49 43 + 44 45 + 46 48	Ordered long oligonucleotides* OHV5 OHV5 Ordered long oligonucleotides*	NotI + HindIII
pOHV15.3	R2_15.3 TdTer_15.3	50 + 51 52 + 53	OHV5 OHV5	XhoI + NheI
pOHV15.4	YdfG_15.4 CvBAPAT_15.4 PrpE_15.4	54 + 55 56 + 57 58 + 59	OHV2 OHV2	NdeI + NheI
pOHV16	Ptrp->PrpE Ptrc -> TdTer	60 + 61 62 + 63	OHV15.4 OHV15.3	NotI + NheI
pL0	N/A	N/A	N/A	N/A
pL1	DavA_1 DavB_1	64 + 65 66 + 67	Synthetic gene on plasmid (Biomatik) Synthetic gene on plasmid (Biomatik)	NdeI + NheI
pL2	DavA_2 DavB_2 LysC_2	64 + 65 66 + 68 69 + 70	Synthetic gene on plasmid (Biomatik) Synthetic gene on plasmid (Biomatik) <i>C. glutamicum</i> (colony PCR)	NdeI + NheI
pL4	DavA_2 DavB_2 LysC_2 Ddh_2	64 + 65 66 + 68 69 + 71 72 + 73	Synthetic gene on plasmid (Biomatik) Synthetic gene on plasmid (Biomatik) <i>C. glutamicum</i> (colony PCR) <i>C. glutamicum</i> (colony PCR)	NdeI + NheI
pL8	lysC_A279T_A_8 lysC_A279T_B_8 DapA_fbr_8 Ddh_8	74 + 75 76 + 77 78 + 79 80 + 81	L4 L4 <i>C. glutamicum</i> (colony PCR) L4	NdeI + XhoI

pL9	ptrp_DavA5k_8	82	Ordered long oligonucleotides*	XhoI + NheI
	DavA_8	83 + 84		
	DavB_8	85 + 67		
pBS0.1	pBAD	N/A	L0, fragment cut out and ligated.	NotI + NdeI
pBS0.2	ORF26_0.2	86 + 87	Synthetic gene on plasmid (Biomatik)	NdeI + BamHI
	ChnR_0.2	88 + 89	Synthetic gene on plasmid (Biomatik)	
pBS2	repA1_Terminator_2	90 + 91	Any pMTL7xxxx series vector	BamHI + XhoI
pBS1	pChnB(r)_1	92 + 93	Synthetic gene on plasmid (Biomatik) 71301 pBAD::RFP (by Giorgia Tibaldero)	XhoI + NheI
	RFP(r)_1	94 + 95		
pBS3	CaiC_3	96 + 97	<i>E. coli</i> (colony PCR)	NdeI + HindIII
	ChnR_3	98 + 99	Synthetic gene on plasmid (Biomatik)	
	Term_pChnB(r)_RFP(r)	100 + 101	BS1	
pCaiC_EX	CaiC-EX	102 + 103	BS3	NcoI + BamHI
pChnR_EX	ChnR-EX	104 + 105	BS3	NcoI + BamHI

The correct sequence of all plasmids used in this study was verified via sequencing by Eurofins genomics.

2.3.2 Oligonucleotide primers

Table 2.5 shows the sequences of the primers used to generate the plasmids in **table 2.3**. Sequencing primers were designed to provide an appropriate coverage of 600 bp, on average, with a melting temperature T_m of ca. 58 °C. Primers were ordered from Sigma Aldrich as lyophilised DNA and diluted to appropriate concentrations for stocks and PCR. Stocks were stored at -20 °C and working dilution primers were stored at 4 °C.

Table 2.5 Sequences of primers used in this study

Primer number	Sequence	Directionality
1	AGTGACGGCAGAGAGACAATCAACATATGATGGCCGTTTTAGTAACTG	Forward
2	CGCAAGCCTCTTACTGACGGTGGTTACTGACGGTGGACATTCAGTC	Reverse
3	CCACCGTCAGTAAGAGGCTTGCGATGAACCACCCGCTCACCAC	Forward
4	TGATTCAGATGTGTCAGGCCAGCTTGGCCAG	Reverse
5	CAAGCTGGCCTGACACATCTGAATCAGGAATTAAC	Forward
6	CAAATGCAGGCTTCTTATTTTTATGCTAGCTTAATGAGCCGCTTCAGG	Reverse
7	CCACCGTCAGTAAGAGGCTTGCGATGAACCACCCGCTCACCAC	Forward
8	CTCCTGTTGAACTTCAGGCCAGCTTGGCCAG	Reverse
9	CAAGCTGGCCTGAAGTTCAACAGGAGAGCATTATG	Forward
10	CAAATGCAGGCTTCTTATTTTTATGCTAGCCTACTCTCCATCGCCTG	Reverse
11	AGTTCACCACTGGAGACCAGCACATATGATGACGCGTGAAGTGGTAG	Forward
12	ACTCCTTGATTGGTCAGATACGCTCGAAGATG	Reverse
13	CGAGCGTATCTGACCAATCAAGGAGTGGACATG	Forward
14	CGACTGGTTTGAATCAGCCCATATGCAGGC	Reverse
15	GCATATGGGCTGATTCAAACCAGTCGGGAGGC	Forward
16	CGTGGTCCTCCTTCATTGGGCCCTCCTGGA	Reverse
17	GAGGGCCCAATGAAGGAGGACCACGATGATCG	Forward
18	CAAATGCAGGCTTCTTATTTTTATGCTAGCTTAAATACGATCGAAACGTT CAAC	Reverse
19	CGTGGTCCTCCTTCATTGGGCCCTCCTGGA	Reverse
20	GAGGGCCCAATGAAGGAGGACCACGATGTCGTGCCCCGCTCG	Forward
21	CAAATGCAGGCTTCTTATTTTTATGCTAGCCTGCTGGGCAGCACTGGG	Reverse
22	AAGTTCACCACTGGAGACCAGCACATATGATGACGCGTGAAGTGGTAG	Forward
23	AAGCCTCCTTGAATTATCAGATACGCTCGAAGATG	Reverse
24	TATCTGATAATTCAAGGAGGCTTAATAAATGGCTAATTC	Forward
25	CTCCTAAAATATTTATTTATTTTTATATAGGACTTTAATTAAATAATC	Reverse

26	TATAAAAATAAATAAAATATTTTAGGAGGATTAGTCATGGAACAAAC	Forward
27	GGTCCTCCTGCGAAAACATCTATTTTTGAAGCCTTCAATTTTTTC	Reverse
28	TTTTCGCAGGAGGACCACGATGATCGTCAAG	Forward
29	GGTCCTCCTGCGAAAACATCTATTTTTGAAGCCTTCAATTTTTTC	Reverse
30	AATAGATAGTTTTCGCAGGAGGACCACGATGTCGTGC	Forward
31	CCTGGATTAGTGATCAGATACGCTCGAAGATG	Reverse
32	CGAGCGTATCTGATCACTAATCCAGGAGCGAG	Forward
33	GGTCCTCCTGCGAAAATTAGTTACGCACCGGCTTG	Reverse
34	CGTAACTAATTTTCGCAGGAGGACCACGATGATCGT	Forward
35	GGTCCTCCTGCGAAAATTAGTTACGCACCGGCTTG	Reverse
36	CGTAACTAATTTTCGCAGGAGGACCACGATGT	Forward
37	AAGTTCACCACTGGAGACCAGCACATATGATGCGTGAAGCCTTATTTG	Forward
38	CACTCCTTGATTGTCAAACACGCTCCAGAATC	Reverse
39	GGAGCGTGTGGACAATCAAGGAGTGGACATGACTC	Forward
40	AAGCCTCCTGAATTATCAAACACGCTCCAGAATC	Reverse
41	CGTGTTTGATAATTCAAGG AGG CTTAATAAATGGCTAATT	Forward
42	CAGCTATGACCGCGGCCGCTGTTGACAATTAATCATCGAACTAGTTAACT AGTACGCATTGGCATACTCTTCGACACAGGGGGCCCATATGACGCGTGA A	Forward
43	TAAAACGACGGCCAGTGCCAAGCTTGGTGGTGGTGGTCCAAAC	Forward
44	CTGCGCAACTGTTGGGAAGGGCGATCGGGTGGTGGTGGTCCAAAC	Reverse
45	GCGTCATCATATGAGGGCTTACCTTAG	Forward
46	TCAGCCCATATGCAG	Reverse
47	ACGCAAGCATCAAGGAGGACTCGAGATGAGCCAGGTCCAG	Forward
48	ACTTCTCGCTCAACGGCGGCCTGCATATGGGCTGATCGCTACGCAAGCA TCAAGGAGGACTCGAGGCCTGCAGACATGCAAGCTTGGCACTGGC	Forward
49	CAGCTATGACCGCGGCCGCTGTTGACAATTAATCATCGAACTAGTTAACT AGTACGCATTGGCATACTCTTCGACACAGGGGGCCCATATGACGCGTGA A	Forward
50	ACGCAAGCATCAAGGAGGACTCGAGGTGTACGCAGCTAAGG	Forward
51	TCATGTAATGAGCCTATAAAAGGGTTCATTGGGCCCTCC	Reverse
52	ATGAACCCTTTTATAGGCTCATTACATGATCGTCAAGCCAAT	Forward

53	GCAGGCTTCTTATTTTTATGCTAGCTTAAATACGATCGAAACGTTTC	Reverse
54	CAGCGAGGGAACAGGAGGCACTCATATGGCCGTTTTAGTAACTG	Forward
55	GAGTTATATATCTTAGTCGTTAGCTTTACTGACGGTGGACA	Reverse
56	GCTAACGACTAAGATATATAACTCTATGAACCACCCG	Forward
57	CCGTTGATCTTGTGAATGTTGAGAGGTCTTCAGGCCAGCTTG	Reverse
58	CTCTCAACATTCACAAGATCAACGGATGAAACCTGTAAAACCAC	Forward
59	GCAGGCTTCTTATTTTTATGCTAGCTTAAATGAGCCGCTTCA	Reverse
60	AGGAAACAGCTATGACCGCGGCCGAGCTGTTGACAATTAATCATCC	Forward
61	AGCTTGCATGTCTGCAGGCCTCGAGCTACTCTCCATCGCCT	Reverse
62	CCAGGCGATGGAAGAGTAGCTCGAGCTGTTGACAATTAATCATCGAACT A	Forward
63	GCAGGCTTCTTATTTTTATGCTAGCTTAAATACGATCGAAACGTTCAAC	Reverse
64	AGATCTTTTAAGAAGGAGATATACATATGCGCATCGCTCTGTACCAG	Forward
65	AATGACCTTGCCATCAGCCTTTACGCAGGTG	Reverse
66	GCGTAAAGGCTGATGGCAAGGTCATTTATGAACAAG	Forward
67	CAAATGCAGGCTTCTTATTTTTATGCTAGCTCAATCCGCCAGGGCGAT	Reverse
68	TTGTGCACCTTTCTCAATCCGCCAGGGCGAT	Reverse
69	CCTGGCGGATTGAGAAAGGTGCACAAAGGTGGC	Forward
70	CAAATGCAGGCTTCTTATTTTTATGCTAGCTTAGCGTCCGGTGCCTG	Reverse
71	GTAATCCTCCAAATTAGCGTCCGGTGCCTGC	Reverse
72	CACCGGACGCTAATTTGGAGGATTACAAGAACATGACC	Forward
73	CAAATGCAGGCTTCTTATTTTTATGCTAGCTTAGACGTGCGTGCGATC	Reverse
74	GATCTTTTAAGAAGGAGATATACATATGGCCCTGGTTCGTAC	Forward
75	CGGAAAACCTTCGCAGTCTCGCCTGGCTTATCGG	Reverse
76	AAGCCAGGCGAGACTGCGAAGGTTTTCCGTGC	Forward
77	CTTCCCTCATTTGTTAGCGTCCGGTGCCTGC	Reverse
78	CACCGGACGCTAACAAATGAGGGAAGAAGGTAAC	Forward
79	GTAATCCTCCAAATTATAGAACTCCAGCTTTTTTC	Reverse
80	TGGAGTTCTATAATTTGGAGGATTACAAGAACATGACC	Forward
81	AGCTTGCATGTCTGCAGGCCTCGAGTTAGACGTGCGTGC	Reverse
82	GATCGCACGCGACGTCTAACTCGAGCTGTTGACAATTAATCATCGAA	Forward

	CTAGTAACTAGTACGCACGTCACGCATACTGCCTAGGAGGTAAGCAT	
83	CGCATACTGCCTAGGAGGTAAGCATATGCGCATCGCTCTGTA	Forward
84	GATGGACTCCCGTACTTAATTAGTGTTACGCCTTTACGCAGGTG	Reverse
85	ACACTAATTAAGTACGGGAGTCCATCATGAACAAGAAGAACCGCCA	Forward
86	AGATCTTTTAAGAAGGAGATATACATATGCGTCCTATGACCGCAAAAAT TTTTG	Forward
87	GAGAATTGAGCTCTTATTCGGCGGCCATGCG	Reverse
88	GGCCGCCGAATAAGAGCTCAATTCTCTTTTGAC	Forward
89	TGGACGCGTGACGTCGACTCTAGAGGATCCTCAAAAAACAATAGAGGA GAC	Reverse
90	TCAGTCTCCTCTATTGTTTTTTGAGGATCCTTGCGCAGCCTGAATGGCGA ATGGC	Forward
91	GCATGTCTGCAGGCCTCGAGATCTCCATGGCGCTCCTGCGGCCGCGCCG	Reverse
92	CGCTACTCGCCATGATAATCTCCATTACGACATGTGAATTTATTC	Forward
93	TAAAACGACGGCCAGTGCCAAGCTTGGTGGTGGTGGTCCAAAC	Reverse
94	CGGCCGCAGGAGCGCCATGGAGATCTCGAGTTAAGCACCGGTGGAGTG	Forward
95	AATGGAGATTATCATGGCGAGTAGCGAAGAC	Reverse
96	CTTTTAAGAAGGAGATATACATATGGATATCATTGGCGGAC	Forward
97	TTAAAGTCAAAGAGAATTGAGCTCTTATTTAGATTCTTTCTAATTATT T C	Reverse
98	CGCCATTCAGGCTGCGCAAGGATCCTCAAAAAACAATAGAGGAGACTG	Forward
99	GAGCTCAATTCTCTTTGACTTTAAGGATGAAAGTTAAATGAGCACAGA	Reverse
100	GGATCCTTGCGCAGCCTG	Forward
101	GTAAAACGACGGCCAGTGCC	Reverse
102	CAGCGGCCATATCGAAGGTCGTCATATGCGTCCTATGACCG	Forward
103	CTTTGTTAGCAGCCGGATCCTCGAGTTATTCGGCGGCCAT	Reverse
104	CAGCGGCCATATCGAAGGTCGTCATATGAGCACAGACAAAGCA	Forward
105	CTTTGTTAGCAGCCGGATCCTCGAGTCAAAAAACAATAGAGGAGACTGA AT	Reverse

2.3.3 Plasmid DNA isolation

Plasmid DNA isolation was performed using the New England Biolabs “Monarch® Plasmid Miniprep Kit” using the manufacturer’s instructions. 3-6 mL of overnight liquid culture was used for plasmid preparation.

2.3.4 Chromosomal DNA isolation of 5-AV adapted strains

Genomic DNA from 5-AV adapted strains (**Chapter 4.2.3**) was isolated using the Sigma Aldrich “GenElute DNA Kit”, using the manufacturer’s instructions. 3 mL overnight culture of three biological replicate strains of the nitrogen adapted condition were used to purify genomic DNA. The samples were then sent to the University of Nottingham DeepSeq Next Generation Sequencing facility to perform Illumina whole genome sequencing. The obtained sequencing reads were mapped to the *C. necator* H16 wildtype genome (DSM428) [211] using Geneious R9. For the multiple alignment, a ClustalW alignment algorithm of the software was used, with the standard settings (Cost matrix = CLUSTALW, Gap open cost = 15, and Gap extend cost = 6.66). The alignment was then manually checked for point mutations.

2.3.5 Polymerase Chain Reaction (PCR)

Lyophilised oligonucleotide primers were supplied by Sigma Aldrich, purified by HPLC. The primers were resuspended in nuclease free water (Ambion) and set to a concentration of 100 pmol μL^{-1} . These primers were considered “stocks” and stored at $-20\text{ }^{\circ}\text{C}$. Working concentration primers for PCR were 1:10 dilutions with autoclaved water of stock primers, to a concentration of 10 pmol μL^{-1} . Working concentration primers were stored at $-4\text{ }^{\circ}\text{C}$.

PCR was performed using Thermo Fisher 2x DreamTaq PCR Master Mix (For diagnostic PCR and clone screening) or New England Biolabs 2x Q5® High-Fidelity Master Mix (For HiFi fragment PCR), each in accordance to the manufacturers protocol.

A reaction mix of of 25 μL volume contained 12.5 μL 2x Master Mix, 1 μL template, 1.25 μL forward and reverse working concentration primers each, and 9 μL autoclaved water.

As template, a 1:10 dilution of a colony resuspended in 10 μL autoclaved water was used for colony PCR. For templates from purified plasmids, 25 ng of plasmid DNA was used.

Gene fragments were amplified by PCR in an Eppendorf Mastercycler Nexus X2e in a two-step PCR protocol. As all primers that were used in this study are HiFi primers with significant overhang over their target sequences, 5 cycles using the annealing temperature of the overlapping part were used to generate template (30 s), followed by 25 cycles at the annealing temperature of the whole primer (typically $72\text{ }^{\circ}\text{C}$, 30 s). The denaturing temperature was set to $95\text{ }^{\circ}\text{C}$ and 30 s/kb amplified length were allowed for extension and a final extension step.

2.3.8 Agarose gel electrophoresis

DNA electrophoresis was conducted using 0.8% (w/v) agarose gels, cast with TAE buffer (PanReac AppliChem) and containing 1 $\mu\text{L}/10\text{ mL}$ SYBR Safe DNA Gel Staining dye (Thermo Fisher Scientific).

10 μL of 2-Log DNA ladder (0.1 – 10.0 kb; NEB) were used as molecular weight marker. 25-30 μL of sample was loaded. Samples were either diagnostic PCR reaction products using DreamTaq (e.g. colony screening), HiFi assembly fragments generated by PCR using Q5 or linearised plasmids. All samples were treated with an appropriate amount of SDS-free loading dye (NEB, Gel Loading Dye, Purple (6X), no SDS) before loading.

The gels were loaded into a Compact XS/S Horizontal Gel Electrophoresis Apparatus (Biometra) and run in TAE buffer at 120 V for approximately 40 minutes. Gels were then visualized using a Gel Doc™ XR+ (Bio-Rad) and bands cut for purification with the help of a UV transilluminator.

2.3.9 Purification of DNA after gel electrophoresis

Agarose gel bands were excised using a surgical scalpel and purified using the New England Biolabs “Monarch® DNA Gel Extraction Kit” in accordance with the manufacturer’s protocol. Purified fragments and plasmid DNA was eluted in water to avoid problems that the NEB elution buffer components could potentially cause during sequencing, HiFi assembly, or transformation.

2.3.10 Restriction digest of plasmid and amplified DNA

All used restriction enzymes for diagnostic digests of plasmids were purchased from New England Biolabs or as “FastDigest” enzymes from Thermo Fisher Scientific. The manufacturer’s instructions were used for all restriction digests and the storage of enzymes. 1 μg of isolated DNA was treated with 0.5 units of enzyme (several enzymes were used in one reaction, if buffer-compatible), by resuspending the DNA in a volume of 15 μL autoclaved water, adding 2 μL 10x buffer, adding enzymes and adjusting the volume of the reaction to 20 μL with water. The digests were conducted at 37 °C for 1-2 h and analysed by agarose gel electrophoresis after addition of an appropriate amount of loading dye, where necessary.

2.3.11 Ligation

Plasmid pOHV4 was generated from pOHV3 by cutting out the tetracycline resistance cassette of pOHV3 (pMTL74311- P_{PhaP} -*empty*) using a restriction digest with FseI and PmeI. The chloramphenicol resistance cassette of a pMTL7x1xx-series vector (supplied by Muhammad Ehsaan, University of Nottingham, unpublished) was equally digested with FseI and PmeI. In the same fashion, BS0.1 was generated by linearising the plasmid pOHV4 with NotI and NdeI and cutting the insert P_{BAD} /AraC promoter cassette from vector pBS0 (Giorgia Tibaldero, University of Nottingham, unpublished) using the same enzymes.

Linearised plasmid was dephosphorylated using antarctic phosphatase (NEB) in accordance with the manufacturer's instructions. Insert and plasmid were then purified from bands obtained by agarose gel electrophoresis and ligated using T4 DNA ligase (New England Biolabs) in accordance with the manufacturer's instructions with one exception: NEB recommends incubation at 16 °C overnight – instead, ligation was performed over 3 weeks at 4 °C.

2.3.12 HiFi-assembly

Plasmids containing recombinant genes were created by HiFi assembly using the fragments described in **table 2.4**. HiFi assembly was conducted using the NEBuilder® HiFi DNA Assembly Mix in accordance to the manufacturer's protocol. In all assemblies, 100 ng of linearised vector DNA and 0.03 pmol of all other fragments were used. The fragments were designed with 15-35 bp overlap sequence to each other and the plasmid backbone. The assembly reaction was carried out for 1 h at 50 °C in a volume of 10 µL using a TProfessional TRIO Thermocycler (Analytik Jena). All of the reaction mix was then subsequently used to transform super-competent *E. coli* DH5α cells (New England Biolabs).

2.3.13 DNA quantification

DNA concentrations were measured using the SimpliNano microvolume spectrophotometer (GE Healthcare Life Sciences). Purity of DNA was checked by comparing the A260/A280 ratio – values between 1.8 and 2.0 were deemed acceptable for further experimentation.

2.4 Transformation of bacterial strains

2.4.2 Preparation of chemically competent *E. coli* strains

For simple cloning applications where the New England Biolabs DH5 α supercompetent cells were not necessary, chemically competent *E. coli* DH5 α cells were prepared. A single colony of *E. coli* DH5 α , grown on LB, was used to inoculate preculture of 5 mL in LB. The cells were grown over night at 37 °C, 200 rpm. 0.5 mL of the preculture was used to inoculate 25 mL fresh LB medium and the cells were grown to an optical density OD₆₀₀ of 0.4. The cells were harvested by centrifugation in a 50 mL falcon tube for 5 minutes, 5000 xg and 4 °C and the supernatant removed. The pellets were resuspended in 8 mL transformation buffer 1 (EC-T1, detailed in section 2.1.3.8) and kept on ice for 20 minutes. They were then harvested by centrifugation for 5 minutes, 5000 xg and 4 °C, the supernatant removed, and resuspended in 4 mL of transformation buffer 2 (EC-T2, detailed in section 2.1.3.9). The cells were then aliquoted in lots of 100 μ L and stored at -80 °C.

2.4.3 Preparation of electrocompetent *C. necator* strains

C. necator H16 electrocompetent cells were prepared using the protocol of Muhammad Ehsaan (University of Nottingham, unpublished). *C. necator* H16 strains were grown on rich medium (LB) plates and single colonies used to inoculate 5 mL of SOB medium in a 50 mL falcon tube. The cells were then grown over night at 30 °C and 200 rpm. This preculture was used to inoculate a 50 mL volume of SOB to a starting OD₆₀₀ of 0.075 in 250 mL baffled shake flasks. These main cultures were then grown for 2-3 h to a final OD₆₀₀ of 0.3. Half of the culture (25 mL) was harvested by centrifugation in a 50 mL falcon tube for 10 minutes at 5000 xg and 4 °C. The supernatant was discarded and the cells were washed with 10 mL ice-cold HEPES buffer (1 mM, pH 7) and centrifuged as before. For the second wash step, 5 mL of ice-cold HEPES buffer (1 mM, pH 7) were used and centrifuged as before. Lastly, the cell pellets were resuspended in 1 mM HEPES buffer that contains 10% glycerol. The cells were then aliquoted in lots of 100 μ L and immediately used for electroporation. All *C. necator* H16 electrocompetent cells were always prepared fresh and never stored.

2.4.4 Transformation of chemically competent *E. coli* strains

For chemical transformation, either 50 μ L New England Biolabs *E. coli* DH5 α super-competent cells were used (HiFi assemblies), or prepared competent cells (according to section 2.4.2, for all other purposes). Either 5 μ g purified plasmid DNA or 10 μ L HiFi assembly Mix (after the reaction) were used for transformation. Plasmid DNA was added to 100 μ L competent cells in a 1.5 mL Eppendorf tube and kept on ice for 20 minutes. The cells were then heat-shocked in a water bath at 42 °C for 45 seconds (Super competent cells) or 1 minute 20 seconds (prepared cells). The cells were then transferred back to ice and kept to cool for 3 minutes. 900 μ L room-temperature S.O.C. medium (Thermo Fisher Scientific, Catalog #15544034) were added and the cells were incubated at 37 °C and 200 rpm for one hour. The transformed cells were then

centrifuged in a microcentrifuge at 10000 xg for 1 minute and 900 μ L supernatant removed. The cells were resuspended by brief vortexing in the remaining 100 μ L liquid, plated on LB plates containing the appropriate selection antibiotic and incubated at 37 °C over night.

2.4.5 Transformation of electrocompetent *Cupriavidus necator* H16 strains

100 μ L freshly prepared electrocompetent cells were mixed with 200 ng of plasmid DNA that was previously resuspended in water (to avoid arcing due to high salt content). The mixture was transferred to a pre-chilled (0 °C) electroporation cuvette (2 mm gap) and kept on ice for 5 minutes. After incubation, the cells were electroporated at 2.5 kV, 25 μ F and 200 Ω setting using a MicroPulser (Bio-Rad) electroporator. After electroporation, the cells were flushed with 900 μ L S.O.C. medium (Thermo Fisher Scientific, Catalog #15544034) that was pre-warmed to 30 °C. The cells were transferred into 1.5 mL Eppendorf tube and incubated for 2-3 hours at 200 rpm at 30 °C. The transformed cells were then centrifuged in a microcentrifuge at 10000 xg for 1 minute and 900 μ L supernatant removed. The cells were resuspended by brief vortexing in the remaining 100 μ L liquid, plated on LB plates containing the appropriate selection antibiotic and incubated at 30 °C for 48-72 h, until transformant colonies were grown to a size appropriate for picking and screening.

2.5 Protein expression and analysis

2.5.1 Growth conditions for recombinant protein expression

Protein production was induced in *E. coli* Lemo21 cells using isopropyl β -D-1-thiogalactopyranoside (IPTG) and rhamnose, using the concentrations detailed in **Chapter 5**. Rosetta-gami™ 2 cells were induced with IPTG. Cells were induced at the beginning of fermentation (before exponential phase) at a concentration between 50 μ M and 400 μ M. For details, see experimental results in Section 5.2.4 and 5.2.6.

Recombinant protein expression in *E. coli* DH5 α and *C. necator* H16 strains harbouring plasmids that were using the P_{BAD}/AraC promoter was induced with 0.2% arabinose, unless stated otherwise.

2.5.2 Protein extraction

Proteins were extracted using BugBuster® Protein Extraction Reagent (Merck Millipore). The mix was made using 100 μ L 10x BugBuster® master mix, 20 μ L PIC (protease inhibitor cocktail, Roche), 1 μ L lysozyme (200 g L⁻¹, Sigma) and 0.1 μ L benzonase (Sigma Aldrich) in PBS (Sigma Aldrich) for a total volume of 1 mL.

BugBuster® mix was then added to cell pellets at a volume of 112.5 μ L per OD₆₀₀ x ml of pellet. For example, a pellet generated by centrifugation of a 10 mL culture at OD₆₀₀ = 5 would require 5 x 10 x 111.2 μ L BugBuster®.

Soluble and insoluble fractions were separated by centrifugation at 20000 \times g for ten minutes at 4 °C. All steps were conducted on ice, if possible.

2.5.2 Protein purification

Soluble protein fractions containing His-tagged recombinant proteins were purified using a HisPur Ni-NTA spin purification kit (Thermo Fisher Scientific). Purification was conducted at room temperature and in accordance with the manufacturer's protocols. The columns were loaded and then washed three times with imidazole concentrations of 50 mM and then eluted from the column with three elution buffers containing 100 mM, 200 mM and 300 mM imidazole, respectively. Soluble protein fraction cell lysate, wash fractions and elution fractions were subsequently analysed by denaturing SDS-PAGE.

2.5.3 Denaturing SDS-PAGE and blotting

Precast 4-12% Bis-Tris gels (Thermo Fisher Scientific) were used for denaturing SDS-PAGE. The gels were loaded with 5 μ L PageRuler™ Prestained Protein ladder (Thermo Fisher Scientific) or Color Prestained Protein Standard, Broad Range (New England Biolabs).

5 μ L of sample were mixed with 1 μ L 10 x NuPAGE™ Sample Reducing Agent (Thermo Fisher Scientific), 2.5 μ L 4x NuPAGE™ LDS Sample Buffer, Thermo Fisher Scientific and 1.5 μ L water for a total volume of 10 μ L. The samples were then heated at 70 °C for 10 minutes and loaded on the gels. Gels were run at 120 V for 80 minutes. After electrophoresis, gels were either stained or blotted.

For staining, the gels were treated with hot Coomassie Brilliant Blue (ThermoFisher) solution (10% (v/v) acetic acid, 60 mg L⁻¹ Coomassie Blue R-250) in water for 15-20 minutes. Destaining was conducted in with a solution of 10% (v/v) acetic acid and 40% (v/v) methanol in water until destained.

2.5.4 Western blot

For blotting, proteins were transferred from the PAGE gel to a 0.2 µm PVDF membrane (BioRad) with a Trans-Blot Turbo Transfer System (Bio-Rad). Mixed MW settings were used for all blots. (suitable for 5-150 kDa, 7 minutes, 1.3 A constant, ca. 25 V).

Blotted PVDF membranes were blocked using a suspension of 5% (w/v) non-fat dried milk (Oxoid™) and 1% (w/v) bovine serum albumin (BSA) in PBS for one hour at 4 °C on a slow shaker (60 rpm).

The membranes were washed with PBS and then treated with monoclonal Anti-Poly His-HRP conjugate antibody (HISP12-HRP, 2BScientific) diluted to an appropriate concentration in accordance to the manufacturer's instructions, in PBS, containing 1% (w/v) BSA. The membranes were incubated at 4 °C for 12 h on a slow shaker (60 rpm).

The membranes were washed with 0.1% (w/v) Tween-20 (Merck) in water three times for 10 minutes at 60 rpm shaking. Antibodies were visualised using 1-Step™ TMB-Blotting Substrate Solution - a chromogenic substrate for HRP conjugates.

2.6 Chemistry

2.6.1 Synthesis and purification 5-hydroxyvaleric acid sodium salt by ring-opening polymerisation and subsequent hydrolysis of 5-valerolactam

4 mL δ -Valerolactone were added to a solution of 2.64 g NaOH in 22 mL of H₂O in a 250 mL round bottom flask on ice. δ -Valerolactone was added dropwise over the course of 15 minutes, while the solution is stirring and cooled. Once δ -Valerolactone was added, the ice could be removed and the flask was left to stir for at least 15 hours. Upon addition of δ -Valerolactone to NaOH, a ring-opening polymerisation occurred and the solution became cloudy, with flakes of polymer visible. This polymerization could not be avoided in aqueous solution, however, a 0.1 molar excess of NaOH is enough to hydrolyse the polymer overnight. Reformed or unreacted lactone was removed by extraction with dichlormethane (DCM, 2 x 10 mL). The aqueous solution was then left to dry under N₂ flow for 2 days, which led to the precipitation of sodium 5-hydroxyvalerate as a white salt. I wish to acknowledge the help of Professor of Medicinal and Biological Chemistry, Neil R. Thomas, who loaned me the glassware for this procedure and allowed me to use his laboratory for the nitrogen flow desiccation of my product.

2.6.2 ¹H-NMR analysis of synthesised 5-hydroxyvaleric acid sodium salt

¹H-NMR analysis of 5-OHV was carried out on a Bruker400 NMR system. The sample was diluted in D₂O. The spectrum was analysed using MestReNova software. The spectrum and a simulated reference spectrum can be found in the appendix (**Figure A1**).

5-hydroxyvaleric acid was measured at:

¹H NMR (400 MHz, D₂O) δ 3.51 (t, J = 6.1 Hz, 2H), 2.11 (t, J = 7.0 Hz, 2H), 1.48 (ttd, J = 12.8, 6.9, 4.0 Hz, 4H).

The first peak at δ 3.51 is a triplet peak from the 2 hydrogen atoms bound to the ω carbon atom. The second triplet peak at δ 2.11 is caused by the 2 hydrogen atoms bound to the α carbon atom. The four hydrogen atoms bound to the aliphatic β and γ carbons cause a peak splitting that is reported as triplet of triplet doublets but should be a doublet of triplets of triplets. This is due to the poor resolution of the signal from these two chemically quite similar moieties.

I also wish to acknowledge the help of Technician Manager Lee Hibett, who helped me to access and use the NMR facilities at the Centre for Biomolecular Science at the University of Nottingham.

2.7 Analytics

2.7.1 Amino acid content analysis from fermentation supernatants using HPLC

2.7.1.1 Extraction of fermentation supernatants for HPLC analysis

1 mL of bacterial culture was centrifuged in a 1.5 mL Eppendorf tube at 5000 xg for 2 minutes. The supernatant was filtered through 0.2 µm syringe filters and dispensed into a new tube. 50 µL supernatant were mixed 450 µL H₂O and 400 µL methanol. 200 µL of this mix was then transferred to HPLC vials with 300 µL inlets.

2.7.1.2 Mixing and storing of a ortho-phthalaldehyde derivatisation solution

The OPA agent consisted of 200 mg Fluoraldehyde™ crystals, that were mixed with 9 mL methanol, 1 mL 0.4 M pH 9.0 borate buffer and 160 µL β-mercaptoethanol.

2.7.1.3 In-vial derivatisation HPLC protocol

An in-vial derivatisation protocol sets the autosampler of a Dionex UltiMate 3000 HPLC system up to draw 100 µL sample and 100 µL OPA derivatisation agent. The mixture is incubated for 2 min at 4 °C and subsequently 25 µL were injected.

2.7.1.5 HPLC settings for the detection of amino acids

On a Dionex UltiMate 3000 HPLC system, the flow rate was set to 0.4 mL min⁻¹. 0-2 minutes: 100% isocratic mobile phase A (0.1 M sodium acetate in water). 2-22 minutes: to 20% mobile phase A, 80% mobile phase B (methanol). 22-24 minutes: to 100% mobile phase B. 24 – 26 minutes: 100% isocratic mobile phase B. 26 – 28 minutes: to 100% mobile phase A. 28 – 30 minutes: isocratic 100% mobile phase A. Stop run at 30 minutes. A 150 mm Kinetex (2.6u C18 100A, 00F-4462-E0, 530779-76) column was used. All amino acids could be detected as OPA derivates at 338 nm and 286 nm.

2.7.2 Gluconate and 3-HP quantification using HPLC

Samples of cultures were centrifuged at 10,000 xg for 2 minutes. The supernatant was recovered and transferred into a new tube. All samples, including analytical standards, were filtered through 0.2 µm syringe filters. 150 µL sample was mixed with 150 µL diluent solution, consisting of a 50 µM aqueous sulphuric acid solution, supplemented with 50 mM valerate as internal standard. All samples were run at 0.5 mL min⁻¹ flow rate for 55 minutes on a Dionex UltiMate 3000 HPLC system with a 300mm x 7.8 mm Aminex column with the diluent as mobile phase. 3HP and gluconate were detected in the UV channel at 210 nm.

2.7.3 5-aminovaleric acid content analysis from fermentation supernatants using GCMS

In order to quantify 5-AV levels, a modified version of James Fothergill's protocol (University of Nottingham, unpublished) that was established for the derivatisation and detection of β-alanine was used. 20 µL of standard or culture

supernatant were added to a 2 mL screwcap tube. 200 μ L of 0.5 M sodium hydroxide, 200 μ L of 4:1 propanol: pyrimidine mixture, 10 μ L of 10 mM benzoic acid and 20 μ L of propylchloroformate were added to the tube. The cap was closed, the tube shaken under the fume cupboard and reclosed. The tube was vortexed for 30 seconds, opened, 20 μ L of propyl chloroformate added, and closed. The tube was vortexed for 30 seconds, 400 μ L of chloroform added, and closed. The tube was vortexed for 10 seconds, 400 μ L of 50 mM sodium bicarbonate added, and closed. The tube was vortexed and 200 μ L of the organic solvent fraction was transferred to a 200 μ L GC glass insert in a labelled GC vial. GC-MS analysis was carried out by James Fothergill using the protocol published by Alagesan et al. [212].

2.7.4 Metabolite analysis using LC-MS

2.7.4.1 Extraction of fermentation supernatants for LC-MS analysis

15 OD x mL units of culture were centrifuged at 10,000 xg for 5 minutes and 50 μ L supernatant was transferred to a new 1.5 mL Eppendorf tube. 50 μ L of ice-cold methanol were added, then 100 μ L of ice-cold chloroform. The mixture was vortexed for 30 s. The tubes were kept on ice for 2 minutes and then centrifuged at 10000 xg and 4 °C for 5 minutes. 50 μ L of the aqueous phase was then transferred to a HPLC vial with 200 μ L inlet for further analysis.

2.7.4.2 Extraction of intracellular samples for LC-MS analysis

200 μ L of ice-cold 50% methanol was added to 15 OD x mL units of culture pellet (see **2.7.4.1**) and vortexed for 30 s. Then, 200 μ L ice-cold chloroform was added to the resuspended cells and vortexed for 1 minute. The cells were lysed by three cycles of freeze-thaw in liquid nitrogen. The lysed cells were then centrifuged at 10000 xg and 4 °C for 5 minutes. 50 μ L of the aqueous phase was transferred to a HPLC vial with 200 μ L inlet for further analysis.

2.7.4.3 LC-MS protocol

LC-MS was performed using a Dionex UHPLC system (Thermo Fisher Scientific) in conjunction with a high-resolution orbital-trap mass spectrometer (Q-Exactive, Thermo Fisher Scientific).

Chromatography was performed with a 4.6 \times 150 mm, 5 μ m particle size ZIC-pHILIC column (Merck Sequant) at 45 °C and a flow rate of 300 μ L min⁻¹. Mobile phase A (20 mM ammonium carbonate in water, pH 9.1) and mobile phase B (acetonitrile) were used in a gradient setting, starting with 20% A and increased to 95% A over 8 minutes. This was followed by equilibration to initial conditions to give a total of 15 minutes run time, excluding a 2-minute wash cycle with water to avoid precipitation of ammonium carbonate in the lines. 10 μ L sample was injected and all samples were stored and handled at 4 °C during the analysis.

MS was performed in simultaneous ESI+ and ESI- full-scan modes. Spray voltages of 4.5 kV (ESI+) and 3.5 kV (ESI-) and capillary voltages of 40 V (ESI+) and -30 V (ESI-) were used. In all modes, the sheath-, auxiliary-, and sweep-gas

flow rates were 40:5:1 arb unit, respectively. The capillary and heater temperatures were set to 275 °C and 150 °C, respectively. Data was acquired with an automatic gain control of 1×10^6 and a resolution of 140 000 from m/z 80 to 1200. The full scan data files were then analysed using TraceFinder™ and XCalibur™ software by Thermo Fisher Scientific.

Examples of the LC-MS profiles of standard reagents (β -alanine, 3-HP, 5-OHV and 5-AV) can be found in the appendix (**Figures A2-A5**). LC-MS profiles of bacterial samples that produced the compounds in **Chapter 3**, can also be found in the appendix: **Figures A6-A8** for the *E. coli* negative control strains, **Figure A9-11** for the β -alanine, 3-HP and 5-OHV traces of EC11 and EC12, shown in **Chapter 3.3.1**. **Figures A12-A14** for a *C. necator* negative control strain, **Figures A15 and A16** for the 3-HP and 5-OHV traces in the supernatants of CN1 and CN2. **Figures A17** shows the alanine signal in supplemented and unsupplemented CN11. **Figure A18** shows the alanine signal in supplemented CN11 and CN12 cultures. **Figure A19** shows the ambiguous 3-HP signal in supplemented and unsupplemented CN11 cultures. **Figure A20** shows the ambiguous 3-HP signal in supplemented CN11 and CN12 cultures. **Figure A21** shows the 5-OHV signal in supplemented CN11 and CN12 cultures. **Figure A22** shows the 5-AV signal in supplemented L7 cultures harbouring pBS2 used in **Chapter 5**. **Figure A23** shows the putative δ -valerolactam signal in supplemented L7 cultures harbouring pBS2. **Figure A25** shows the putative δ -valerolactam signal in supplemented L1 cultures without pBS2.

2.8 Assays

2.8.1 Toxicity assays with BioLector

Single *C. necator* H16 wildtype colonies grown on LB were used to inoculate 48 pre-cultures of 2 mL volume (LB) in 10 mL flacon tubes. The strains were grown to OD₆₀₀ = 1.7 and 1.5 OD mL units transferred to 1.5 mL Eppendorf tubes. The cells then centrifuged at 5000 xg for 5 minutes and washed with minimal medium without phosphate (CNMM-P). They were then used to inoculate 0.5 mL micro-fermentation wells in a BioLector to OD 1.5. Six wells were used for each fermentation condition, in which *C. necator* was challenged with either none (0 mM), 0.5 mM, 5 mM, 50 mM, 200 mM or 500 mM 5-AV. Cells were incubated at a constant temperature (30 °C), shaking (1200 rpm), humidity (85%) and O₂ (21%) values for 48 hours.

2.8.2 RFP assays with TECAN

RFP reporter function in biosensors was assayed with an Infinite® M1000 PRO microplate reader (Tecan) in a Corning® 96-well Black and Clear Bottom Polystyrene Microplate.

E. coli precultures grown in LB were used to inoculate LB containing appropriate concentrations of antibiotics and inducer (0.2% arabinose) to an OD₆₀₀ of 0.2 before being transferred to the wells in volumes of 200 µL per well. RFP excitation and emission wavelengths of 558 nm and 583 nm were used. A manual gain of 120% was set. OD₆₀₀ was measured and used to normalise fluorescence. Measurements were taken every 30 minutes. The cells were grown at 37°C with 1200 rpm shaking for 24 hours.

2.8.3 Growth assays: calculation of growth rates

The doubling times in **Chapter 3.2.3** and for the cultures shown in the growth curves in **Fig. 26A-46A (Appendix)** were calculated by using the following formula:

$$T_D = \frac{t \times \log(2)}{\log(\text{final OD}) - \log(\text{start OD})}$$

Where T_D is the doubling time and t is time of the last timepoint of exponential growth.

2.9 Bioinformatics

2.9.1 Plasmid map analysis and genome alignments

Geneious R9 was used for sequence alignments, restriction site analysis and design of constructs. Sequencing reads obtained of *C. necator* H16 isolates (**Chapter 4**) reads were assembled in Geneious R9 and mapped against the wildtype reference genome for *C. necator* H16. The latest downloadable software version can be found at <https://www.geneious.com/>

A table of genes containing SNPs in the strains analysed in **Chapter 4** in reference to the wildtype can be found in the appendix (**Table A1**).

2.9.2 Sequence databases

The NCBI (National Center for Biotechnology Information) database was used to identify and access all DNA and protein sequences of interest and can be found at <https://www.ncbi.nlm.nih.gov/>

KEGG, the Kyoto Encyclopedia of Genes and Genomes was used to identify pathways, and annotated genes and can be accessed at <https://www.genome.jp/kegg/>

2.9.3 BLAST analysis

The BLAST algorithm, available for public use on the NCBI website, was used to identify sequences and find homologous sequences to the entered query. Homologous proteins and protein subunits were identified of the blastp (protein-to-protein BLAST) function which can be accessed at <https://blast.ncbi.nlm.nih.gov/Blast.cgi?PAGE=Proteins>. Standard settings were applied.

2.9.4 Design of RBS motifs

The algorithm used to predict and design the strength of RBS sites in *C. necator* H16 is available by De Novo DNA, a spinoff of the Salis lab. [213]. It is based on calculating the interaction strength between an mRNA transcript and the 30S ribosome of the organism of interest. The latest version of the calculator can be found at:

https://salislab.net/software/design_rbs_calculator

2.9.5 Statistical analysis

Statistical analysis was conducted using GraphPad Prism software or manually, where necessary. All errors are given as standard deviation.

In **Chapter 4.1.2.2** a student t-test was manually calculated due to an uneven sample size of timepoints that required a normalisation. t was calculated by dividing the location parameter $\hat{\mu}$ by the scaling parameter $\hat{\sigma}$ of the t-distribution:

$$t = \frac{\hat{\mu}}{\hat{\sigma}} \quad (1)$$

Where $\hat{\mu}$ is the total sum all the differences between each pair of means of any timepoint value, divided by the amount of timepoints:

$$\hat{\mu} = \frac{\sum_t (\bar{V}_1 - \bar{V}_2)}{n_t} \quad (2)$$

This means that at first, a mean OD value is calculated for each timepoint from three to six measurements (wells). For instance, this may be 1.65 for timepoint 0 in the 0 mM set and 1.45 for timepoint 0 in the 500 mM set. The difference is thus 0.2 for the first timepoint. These 18 difference values are summed up and divided by n_t (18).

$$\hat{\sigma} = \sqrt{\frac{\sum_t \left(\frac{\sigma_1^2}{n_1} + \frac{\sigma_2^2}{n_2} \right)}{n_t^2}} \quad (3)$$

With σ^2 being the squared standard deviation corresponding to each of the means in (2), n the number of values used to obtain it and n_t the total amount of timepoints (18)

This gives a t-value of 0.8289 for the Student's statistic and a corresponding p-value of 0.4087 >> 0.05 assuming 137 degrees of freedom from the experiment data. This means that the dataset 0 mM and the dataset 500 mM in **Chapter 4.1.2.2** do not significantly differ from each other.

2.9.6 Quantitative and qualitative analysis of metabolites using LC-MS and XCalibur™ and TraceFinder

Metabolite concentrations were measured using data processed by XCalibur™ QualBrowser and TraceFinder™. Standard curves were first obtained and linearity established. Then, sample data was filtered to only include masses within 3 ppm mass accuracy of the monoisotopic mass of the analyte. Furthermore, quality control samples were used to monitor drift or detection problems during the run. The filtered peaks were then integrated and the total ion count compared to the reference standard curve to obtain a quantitative value.

Typical ion count per μL linear regression formulas obtained for the calculations of the analytes in **Chapter 4** and **5** are:

β -alanine	$x = y / 7275898$	at $m/z = 88.0404$	RT= 8.98
3-HP	$x = y / 239766$	at $m/z = 89.0245$	RT= 7.62
5-OHV	$x = y / 1127036$	at $m/z = 117.0558$	RT= 7.01
Aspartate	$x = y / 1072314$	at $m/z = 132.0302$	RT= 8.63
L-lysine	$x = y / 238016$	at $m/z = 145.0983$	RT= 12.27
5-AV	$x = y / 232525$	at $m/z = 116.0717$	RT= 8.91

With x equating the analyte concentration in μM , y the obtained ion count (dimensionless) and the number provided a scaling factor with the units ion

count (dimensionless) per μM . RT stands for retention time, m/z stands for mass-to-charge ratio.

These specific values were used for the calculations in **Chapter 4** and **5** and slightly adjusted depending on the ion counts obtained by quality control standard samples throughout the run, if necessary. All analytes were measured in the negative ion channel $[-\text{H}^+]$ with the exception of δ -valerolactam, which was measured in the positive ion channel $[\text{H}^+]$.

For qualitative analysis, the detection limit was set to a signal to noise ratio of 25, which roughly corresponds to $10 \mu\text{M}$ analyte in these cases. For an easier understanding of this cut-off value, the $10 \mu\text{M}$ were used in this thesis to depict the decision point between a positive sample and a negative sample in **Chapter 4**.

The latest version of TraceFinder can be found at:

<https://www.thermofisher.com/uk/en/home/industrial/mass-spectrometry/liquid-chromatography-mass-spectrometry-lc-ms/lc-ms-software/lc-ms-data-acquisition-software/tracefinder-software.html>

The latest version of XCalibur can be found at:

<https://www.thermofisher.com/order/catalog/product/OPTON-30965#/OPTON-30965>

Chapter 3

**Metabolic engineering of *Cupriavidus necator* for
5-hydroxyvaleric acid production from β -alanine**

Chapter 3 - Metabolic engineering of *Cupriavidus necator* H16 for 5-hydroxyvaleric acid production from β -alanine

3.1 Introduction

3.1.1 General introduction

Rising demand for value-added chemicals and environmental concerns associated with petrochemical synthesis routes make it necessary to develop new solutions for the production of chemicals in microorganisms [34]. This Chapter aims to add the production of 5-hydroxyvaleric acid to the portfolio of bio-based chemicals could potentially be produced in an environmentally friendly way. A new pathway towards 5-hydroxyvaleric acid production in *C. necator* H16 from β -alanine is described. β -alanine was chosen as feedstock while ongoing and future work by Alejandro Salinas et al. (University of Nottingham, unpublished) is aimed to bridge the gap between the *C. necator* H16 central metabolism and β -alanine, making the proposed biosynthetic route accessible by sole use of CO₂ as carbon source in bioreactors without relying on the addition of expensive carbon sources such as gluconate [214].

Rather than characterising each enzyme candidate of the eight-step pathway individually and choose those with the most promising kinetic characteristics to build a final pathway, this work also aimed to showcase a “top-down” workflow approach to add to the bottom-up approach of traditional synthetic biology. With increasing number of steps in the pathway, a new challenge emerges: the risk of implementing trusted individual solutions and having them fail once they are “stitched together” to form a whole, owing to the innate complexity of biological systems that interact with the designed bio-circuits on multiple levels

[215]. Unless fully bio-orthogonal, any designed biological process will be challenged by a cell in a species-unique manner [216]. For example, expression strength of any synthetic gene is codon-usage dependent [217]. The strength of a heterologous promoter may be different in a new host compared to the original host organism or suffer from the lack regulatory mechanism such as active repressor proteins [218]. mRNA stability may vary. Cells may recognise a heterologous protein as foreign and flag it for degradation, or degrade it through random proteolysis [219]. Necessary co-factors may be absent or present in lower concentrations [220]. A change in redox-balance may interfere with the new pathway or formation of disulphide bonds that are necessary for proper protein folding [221]. And, to add a last point to this non-exhaustive list of challenges that would interfere with any designed heterologous bio-circuit, intermediate compounds of a synthetic pathway may be targeted as substrate by promiscuous enzymes - a double edged sword as promiscuity can also advance synthetic biology by enabling a computationally driven search for putative enzymes capable of catalysing chemical reactions of non-natural substrates [222]. Hence, a bottom-up approach often leads to lengthy troubleshooting and optimisation if the interdependent reactions are not functioning as expected or compatibility issues arise [223]. Thus, this Chapter describes the “top-down” approach of screening multiple pathways simultaneously that are constructed in a modular manner. Each pathway combination carries a unique set of enzyme candidates for all necessary reactions.

This work aims to demonstrate that building metabolic pathways is possible by such a top-down approach, contrasting the methodology of gathering enzymatic information before undertaking the first molecular cloning steps. The newly assembled pathways were first tested in the intermediate cloning host *E. coli*, then later transferred and tested in the destination host *C. necator* H16. The assembled pathways were then tested in background hosts such as the *C. necator* H16 wildtype and engineered deletion mutant strains like $\Delta\textit{phaCAB} \Delta\textit{mmsA1} \Delta\textit{mmsA2} \Delta\textit{mmsA3}$ (henceforth referred to as “ $\Delta 4$ strain”). Once all pathways were designed, tested and chassis strains engineered, optimisations on the fermentation level were subsequently introduced to aim for improved yields. To conclude the “top-down” approach, synthetic ribosomal binding sites were introduced alongside a new set of strong constitutive promoters to the assembly, thereby investigating how effective these elements are in impacting 5-OHV yields.

3.1.2 Introduction to the pathway

Figure 3.1 shows an overview of the proposed pathways from β -alanine to 5-hydroxyvaleric acid for this study.

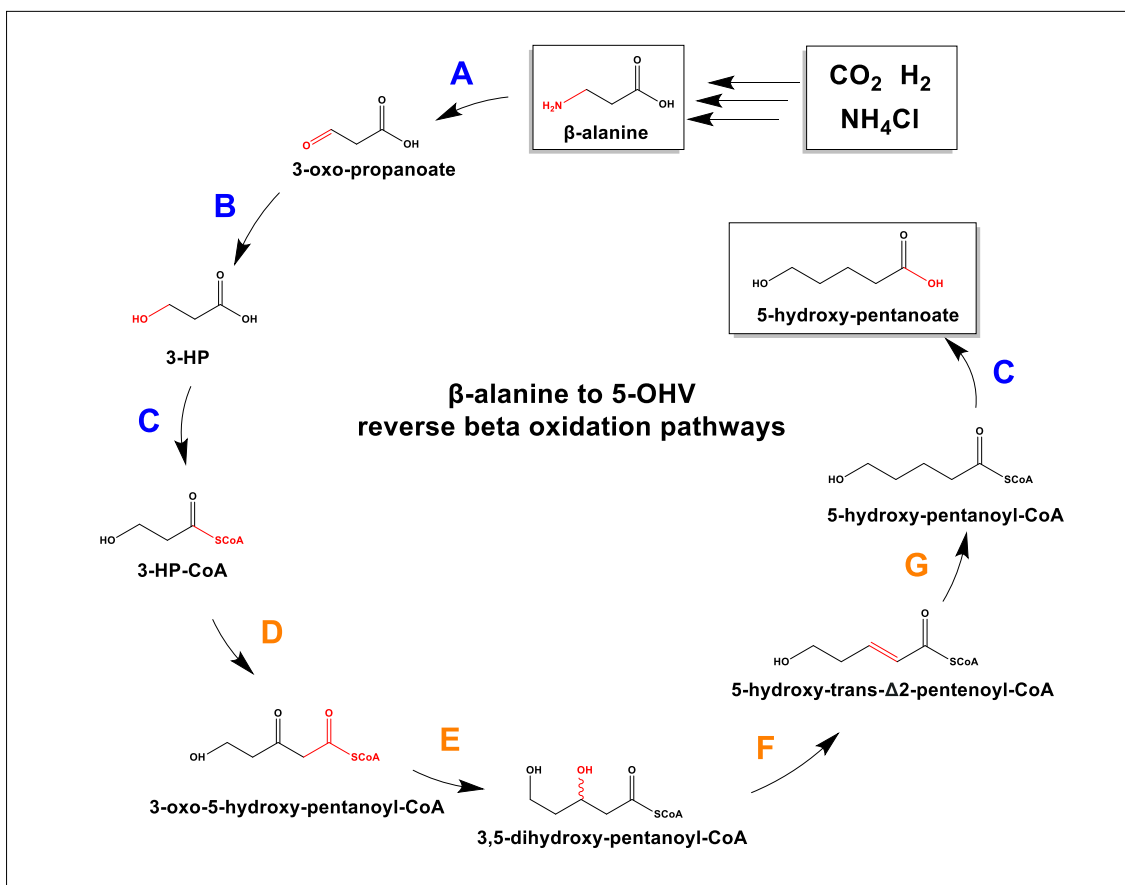


Figure 3.1 Proposed pathways for the production of 5-hydroxyvaleric acid from β -alanine. (A) Transaminase, **(B)** Oxidoreductase, **(C)** CoA Transferase or CoA Synthetase, **(D)** β -ketothiolase, **(E)** 3-hydroxybutyryl-CoA dehydrogenase, **(F)** Enoyl-CoA hydratase, **(G)** Trans-2-Enoyl-CoA reductase

β -alanine was chosen as feedstock as it is under current investigation to be produced from *C. necator* H16 central metabolism by other members of the research group. Furthermore, β -alanine was shown to be efficiently convertible to 3-HP by an established synthetic pathway from β -alanine [144] (**Fig. 3.1**, steps **A**, **B**). 3-HP is then activated by a CoA-ligase (**Fig. 3.1**, step **C**) and chain-

length elongation in a reverse beta oxidation cycle (**Fig. 3.1**, steps **D, E, F, G**) yields a C5 chain by addition of an acetyl moiety. Reverse beta-oxidation is derived from beta-oxidation, a well-known strategy for cells to break down fatty acids to acetyl-CoA moieties, particularly well-studied for mitochondrial beta-oxidation [224]. Reverse beta-oxidation describes the reversal of the metabolic flux through this pathway, but, according to Kallscheuer et al.[225]: “[the] involved enzymes are solely active on CoA-activated thioesters and do not convert the acyl-ACP thioesters of fatty acid synthesis”. This process is thermodynamically viable and existent in nature, albeit uncommon [225, 226]. Engineered reverse beta-oxidation was first demonstrated by Dellomonaco et al. [227] in *E. coli* and since then numerous research projects have established engineered reverse beta-oxidation in *E. coli* [228-230] and other organisms, such as *Saccharomyces cerevisiae* (baker’s yeast), [231] and *Co. glutamicum* [232]. This work aimed to show a novel fully metabolically-engineered reverse beta-oxidation pathway for small molecule synthesis in *C. necator* H16, although it should be noted that reverse beta-oxidation enzymes have been used in *C. necator* H16 prior to this study to boost levels of hydroxyhexanoate in PHA co-polymers [233]. Exiting the beta oxidation cycle by cleavage of the CoA moiety (**Fig. 3.1** step **C**) 5-hydroxyvaleric acid is produced.

3.1.3 3-HP synthesis from β -alanine

The first novel approach of 5-hydroxyvaleric acid synthesis in *C. necator* H16 builds on producing 3-hydroxypropanoic acid through an established synthetic pathway from β -alanine developed by Orol [144] (**Figure 3.1**).

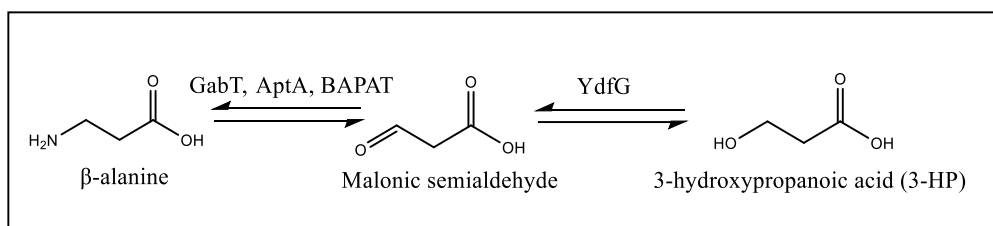


Figure 3.2 Conversion of β -alanine to 3-HP through malonic semialdehyde in *Cupriavidus necator* H16. β -alanine is converted to malonic semialdehyde by the aminotransferase BAPAT from *Chromobacterium violaceum*. GabT and AptA are native to *C. necator* H16, but likely downregulated during initial fermentation conditions and not present in the *E. coli* genome. Malonic semialdehyde is subsequently converted to 3-HP by YdfG, an oxidoreductase native to *E. coli*, which forms part of the pathway assembly.

The first step catalyses the conversion from β -alanine to malonic semialdehyde.

This transamination reaction requires the presence of an α -ketoacid, pyruvate, to be converted into the conjugated amino acid, L-alanine. PLP is a required cofactor for the transaminase BAPAT_{cv} (EC 6.2.1.18), which is introduced from the *Chromobacterium violaceum* genome [234]. Genes in *C. necator* H16 that are involved in conversion of malonic semialdehyde to β -alanine have been annotated in KEGG, such as *aptA* and *gabT*. However, *aptA* forms an operon with the methylmalonate-semialdehyde dehydrogenase coding *mmsA1* under the regulation of a putative MocR type regulator[144]. This is a logical operon structure, given that the *mmsA* genes, of which three exist in *C. necator* H16, encode malonic semialdehyde dehydrogenases. As AptA produces malonic

semialdehyde, malonic semialdehyde dehydrogenases are responsible to detoxify this intermediate. This is necessary because aldehydes in general are toxic to cells due to their high reactivity [235]. This also explains how *mmsA1*, *mmsA2* and *mmsA3* play a major role in 3-HP degradation [144].

Studies [143, 236, 237] have shown that a *Bacillus subtilis* homologue of GabT under control of a homologous regulator, GabR, is only expressed during the presence of GABA, suggesting that the MocR type regulator that controls *aptA* and *mmsA1* is equally evolved to react to - and then help degrade - C4 compounds such as 4-hydroxybutyrate rather than C3 compounds. It is thus possible that the aminotransferases native to *Cupriavidus* sp. are only upregulated by the presence of ω -hydroxy acids and inactive if only β -alanine is present, which makes either the deregulation of *gabT* and *aptA* or the addition of an exogenous, unregulated, enzyme such as BAPAT_{CV}, necessary. In *E. coli*, GabT and AptA are not present and only BAPAT can be active.

Malonic semialdehyde is subsequently reduced to 3-HP, a reaction which requires the presence of a terminal aldehyde to be converted into an alcohol by oxidoreductase YdfG (EC 1.1.1.59) from *E. coli*. As described by Fujisawa et al. [238], YdfG forms a homotetramer of 27 kDa subunit and carries out its reaction depending on NADP⁺. It has previously been successfully used to produce 3-HP, poly-3-HP and malonic semialdehyde in *E. coli* [239, 240].

3.1.4 3-HP thioester formation

The transfer of coenzyme A (CoA) to yield 3-hydroxypropanoyl-CoA (3HP-CoA) requires the presence of a CoA donor (**Figure 3.3**). The propionate CoA-transferase Pct (EC 2.8.3.1) for this reaction is already present in the *C. necator* H16 genome. This transferase encoded by *pct* shows a broad range in substrate specificity and uses acetyl-CoA as donor [241, 242]. Alternatively, expression of a synthetase from a different organism was considered.

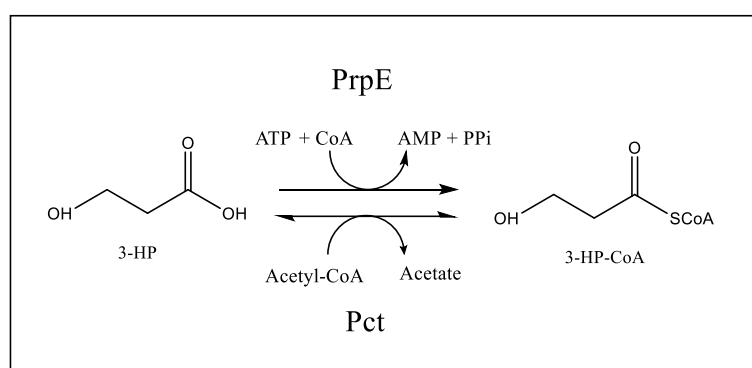


Figure 3.3 Transfer of CoA to 3-HP through either one of two proposed reactions. The propionate CoA transferase Pct, native to *C. necator* H16, uses acetyl-CoA as CoA donor, while PrpE from *Salmonella typhimurium* LT2 uses free CoA and ATP.

The propionate CoA synthetase PrpE (EC 6.2.1.17) catalyses the priming of propionic acid [243]. However, this reaction is driven by hydrolysis of ATP and thus detrimental to the overall energetic viability of the pathway. Because of the irreversible hydrolysis of ATP in this reaction, PrpE may help to drive flux through the pathway. The gene *prpE* from the *prp* operon found in *Salmonella enterica* serovar Typhimurium LT2 was chosen as a suitable test candidate that has been used for medium chain fatty acid production previously [244] and even the production of 3-HP copolymers [245, 246].

C. necator H16 has the natural capability to synthesize the polyhydroxyalkanoate (PHA) poly-3-hydroxybutyrate (PHB) as a storage compound [247-249], which makes it easier to access carbon metabolism by hijacking this storage system. Under stressful conditions (stringent response), triggered by limited availability of oxygen, bioavailable nitrogen or phosphates and the simultaneous excess of carbon, PHA synthesis is stimulated [250]. This stress response leads to the upregulation of the *phaCAB* operon, which entails the *phaA* gene and homologues such as *bktB*, coding for a β -ketothiolase which mediates the condensation of two molecules of acetyl-CoA (**Figure 3.4 B**), yielding acetoacetate-CoA, the first step towards PHA accumulation from central metabolism [251-254]. BktB, in particular, was selected as promising enzyme candidate to catalyse the condensation of acetyl-CoA with 3-hydroxypropionyl-CoA to yield of 3-oxo-5-hydroxy-pentanoyl-CoA (**Figure 3.4 A**). This enzyme was expected to perform better than the other selected candidate 3-oxoadipyl-CoA thiolase PaaJ, which had been described in the preparation of 7-hydroxyheptanoic acid and related compounds through reverse beta oxidation in a patent in 2017 [255] and also in reverse beta oxidation by Kallscheuer et al. [256, 257].

The most notable difference between BktB and PaaJ is the substrate – BktB catalyses the reverse reaction with a C4 compound (Acetoacetyl-CoA) and PaaJ with a C6 compound (3-oxoadipyl-CoA) (**Figure 3.4 B**). It is desired to achieve promiscuous activity to a C5 compound (3-oxo-5-hydroxypentanoyl-CoA).

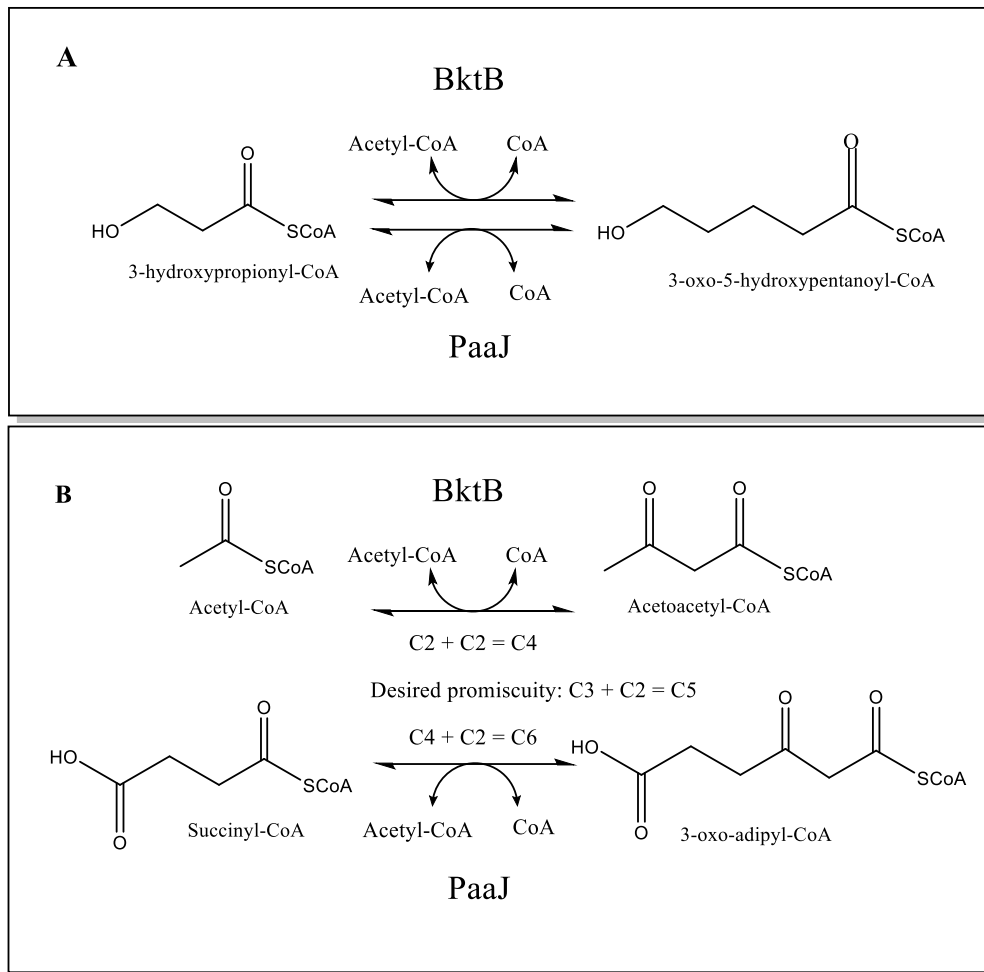


Figure 3.4 (A) Desired chain elongation by two carbon atoms mediated by β -ketothiolase BktB and 3-oxoadipyl-CoA thiolase PaaJ. (B) Native reactions catalysed by BktB and PaaJ.

The only known available route for β -alanine production that would enable the shown pathways to draw flux from central metabolism is currently under investigation in *C. necator* H16 by other members of the research group. It is achieved through decarboxylation of aspartate using PanD and its maturation factor PanM [239], hereby depleting the TCA cycle. Adding to that cataplerotic

flux by using Paaj (which depletes succinate) would make further efficient anaplerotic reactions mandatory rather than optional.

3.1.5 Reverse beta-oxidation chain lengthening

From 3-HP-CoA, reversed beta oxidation extends the chain length from C3 to C5. **(Figure 3.5)**

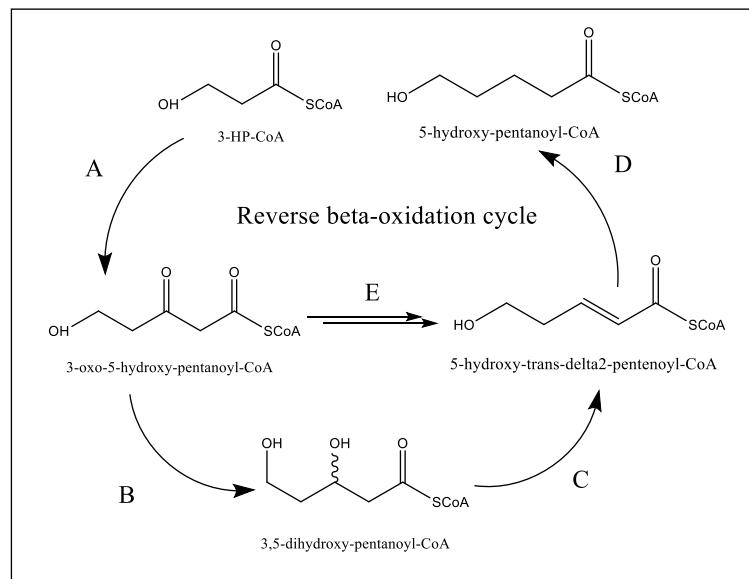


Figure 3.5 Reverse beta oxidation chain lengthening converts 3-HP-CoA to 5-hydroxyvaleryl-CoA through a series of reactions A-E. (A) Condensation of 3-HP-CoA with acetyl-CoA by Paaj or BktB. **(B)** Reduction of 3-oxo-5-hydroxy-pentanoyl-CoA to R-3,5-dihydroxy-pentanoyl-CoA by PhaB or S- R-3,5-dihydroxy-pentanoyl-CoA by Hbd3. **(C)** Dehydration of R-3,5-dihydroxy-pentanoyl-CoA by Enoyl-CoA hydratase or, S-3,5-dihydroxy-pentanoyl-CoA by S2, to 5-hydroxy-trans- Δ 2-pentenoyl-CoA. **(D)** Reduction of 5-hydroxy-trans- Δ 2-pentenoyl-CoA to 5-hydroxy-pentanoyl-CoA by either Ter_{TD} or Ter_{EG}. **(E)** Reverse beta-oxidation with the FadB complex.

The reduction of 3-oxo-5-hydroxy-pentanoyl-CoA to 3,5-dihydroxy-pentanoyl-CoA is achieved by the acetoacetyl-CoA reductase PhaB [258, 259]. Alternatives, such as *hbd3*, which is annotated to encode a hydroxybutyrate dehydrogenase from *Clostridium saccharoperbutylacetonicum*, yields the (S)-

isomer and has been used to produce hexanoic acid via reverse beta oxidation [260]. Another alternative explored is *fadAB*, which has been proposed to encode a key component of the reversed beta-oxidation pathway [133, 261]. FadB can be found as a heterotetramer in *E. coli*, composed of a homodimer of FadB and a homodimer of FadA. FadA has thiolase activity. The FadA/FadB complex showed seemingly promising simplicity to handle 3 steps with one complex [262, 263]. The reduction of 3,5-dihydroxy-pentanoyl-CoA to 5-hydroxy-trans- Δ^2 -pentenenoyl-CoA can also be catalysed by FadB, however the use of an endogenous ((R)-specific) or exogenous ((S)-specific) crotonase is also explored.

The endogenous crotonase (encoded by *crt3*), which shows substrate specificity for (R)-3,5-dihydroxy-pentanoyl-CoA, is annotated in the NCBI database as H16_RS27940, a 3-hydroxybutyryl-CoA dehydratase on chromosome 2 of *C. necator* H16 and has not been characterised to date. Two other known (R)-specific crotonases exist in *C. necator* H16, however none were characterised prior to the date of plasmid and experimental design. One, encoded by *crt*, is mentioned in a patent dating 2016 by Mizunashi et al. [264] and then López et al. [265] (H16_B1189). The other was described as the gene product of *crt2* (H16_A3307) by Segawa et al. in 2018 [266]. Hence, the used crotonase, annotated as H16_RS27940, was thus named Crt3.

The exogenous crotonase with (S)-3,5-dihydroxy-pentanoyl-CoA specificity is found in *Clostridium acetobutylicum* ATCC 824 and annotated in the NCBI database as CA_C2712. Notably, this gene appears in the same cluster as *hbd* in *C. acetobutylicum*, which makes it a promising candidate for synergistic

action. This variant has been used under the name *crt* in a reversed beta oxidation pathway in a previous study [260].

Reduction of 5-hydroxy-trans- Δ^2 -pentenenoyl-CoA to 5-hydroxy-pentanoyl-CoA is the key step to leave the reverse beta oxidation cycle and yield a C5 compound. Reductases of the Ter family from multiple organisms have been used for this step before. For example, Ter_{TD}, from *Treptonema denticola*, has been used in reversed beta oxidation pathways successfully. [267-271]. Alternatively Ter_{EG} from *Euglena gracilis* is explored, which has also been reported to function in reversed beta oxidation pathways [272].

3.1.6 Thioester hydrolysis and product formation

Finally, the hydrolysis of the thioester with Coenzyme A, from 5-hydroxy-pentanoyl-CoA to 5-hydroxyvaleric acid can be carried out by the same enzymes that catalysed the formation of the thioester previously, but in reverse direction (**Figure 3.6**).

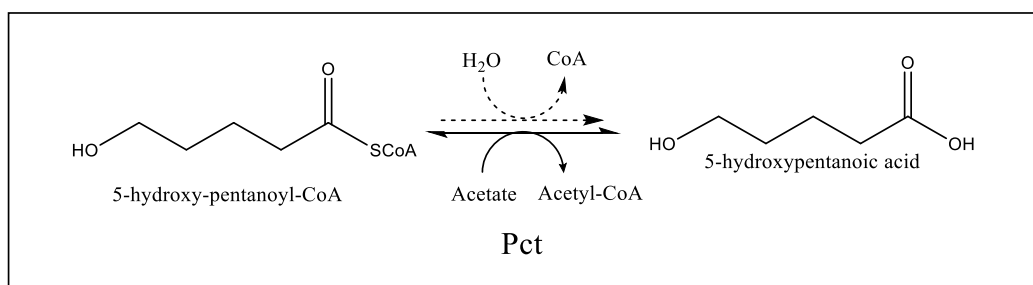


Figure 3.6 5-hydroxy-pentanoyl-CoA is hydrolysed. The reaction yields CoA if water is used as nucleophile (dashed arrow, spontaneous hydrolysis) and acetyl-CoA if Pct performs the reaction.

This reaction would recycle the cofactors used by Pct, but PrpE would not, as the released AMP is quickly converted to ATP and the cell typically maintains ATP levels 100-fold in excess of AMP levels, further pushing the chemical equilibrium of the reaction towards the educt. [273-275].

3.1.7 Results in *E. coli* may predict results in *Cupriavidus necator* H16

It may appear like the most direct approach to investigate potential pathways for the metabolic engineering of *C. necator* H16 is in the host organism itself. However, a number of obstacles exist, that favour to design and test potential pathways in *E. coli* first. Generally speaking, *E. coli* strains, especially those optimised for molecular biology applications, such as DH5 α , grow faster and benefit from easier transformation and culturing compared to *C. necator* H16.

For example, the previously used *E. coli* DH5 α strain shows a transformation efficiency of up to 1.5×10^9 cfu/ μ g pUC19 (2.7 kb) according to New England Biolabs [276]. In comparison, with the currently used protocol, an adaption of a method published 2017 by Tee et al. [277], only 3.9×10^5 cfu/ μ g pHBR1 (5.3 kb) are achievable at best. Large plasmids (>12kb) show very low transformation efficiencies by chemical methods or by electroporation in *Cupriavidus* sp. in practice [75], leaving only the option of conjugation with an *E. coli* S17-1 λ pir donor strain as a genetic tool for gene transfer. Most tested pathways in this study exceeded 10 kb length (including their vector backbone), which meant pre-selection in *E. coli* would significantly reduce the amount of time needed for screening, under the premise that the results in *E. coli* and the results in *C. necator* H16, agree. For this reason, all 20 pathway assemblies were investigated in *E. coli*, *C. necator* H16 and *C. necator* H16 Δ 4, a quadruple knockout strain that will be discussed in more detail in this introduction.

While this volume of work can be achieved in both *E. coli* and *C. necator*, future work in *C. necator* using high-throughput pathway assembly assays may

become too labour-intensive to be achievable. This raises the question, whether preliminary experimental data in “cloning strains” such as *E. coli* DH5 α is a good predictor for pathway performance in *C. necator* H16.

Once this agreement was established in my work, future research would be able to take advantage of the relative ease of handling of *E. coli* to generate reliable pathways for *C. necator* H16.

This translatability would however be confined to pathway sets that are comparable with the sets used in this study. For instance, pathways with enzymes that are membrane-bound, or that utilise a metabolite or cofactor that is not present in *E. coli*, or rely on an intracellular reaction that does not or cannot take place in *E. coli*, would still have to be investigated directly in *C. necator* H16.

3.1.9 The resting cell condition

Metabolically active, but resting (nongrowing) cell fermentation at an OD₆₀₀ of 25 or higher ensures the cells do not waste energy and carbon source for biomass growth and convert a high amount of feedstock. Such resting cells have been previously used in wide applications for the microbial production of industrially relevant products [278-280].

During resting cell conditions, growth and enzyme expression are decoupled from the production stage and it presents a natural occurrence in microbes under limited nutrient conditions [281].

The resting state in *Cupriavidus* sp. is triggered by transferring the cells in a culture in its exponential growth phase to a medium that is depleted of a nutrient that is necessary for biomass formation [282]. The element chosen for depletion is typically the nitrogen or phosphorus source [283], but depletion of elements such as sulphur [284-286] or magnesium [287] have also been explored in the current literature.

In this study, total phosphate limitation was chosen as the resting condition. Without phosphate in the medium, bacteria are unable to synthesise nucleotides necessary for DNA duplication and proliferation[283].

3.1.10 Aim of the Chapter

In summary, this Chapter aims to answer the following questions:

Which of the 20 pathway variants yields 5-OHV in *E. coli* ?

Which of the 20 pathway variants yields 5-OHV in *C. necator* H16 ?

Do the results suggest that experiments conducted in *E. coli* are transferable to *C. necator* H16 ?

Does the $\Delta 4$ deletion mutant optimise 5-OHV yields in *C. necator* H16?

Does the resting cell condition optimise 5-OHV yields in *C. necator* H16?

Does the use of synthetic biology tools, such as stronger promoters and synthetic RBS sites optimise 5-OHV yields in *C. necator* H16?

3.2 Results

3.2.1 Experimental design choices

3.2.1.1 Choosing plasmids and promoters that are compatible in both *Cupriavidus necator* H16 and *Escherichia coli*

Because the introduction of up to seven enzymes (**Chapter 3.1.2**) for the proposed pathway variants easily exceed the limit of 10-12 kb vector length for efficient transformation in *C. necator* H16, streamlining of the cloning process was necessary. Therefore, the pathway was split and cloned onto two plasmids with compatible replicons that can both be used in both *E. coli* and *C. necator* H16. The first plasmid pMTL71301 uses the Rep/mob+ replicon from pBBR1 and a Tet resistance marker. It carries the genes *ydfG*, *bapat_{CV}* and *prpE* or *pct* in this order and under control of the constitutive P_{PhaC} promoter. The second plasmid pMTL74111 uses the IncP/TraJ replicon from pCM62 and the p15A replicon from pACYC184, as well as a Chloramphenicol resistance marker. It carries the genes *bktB*; *hbd3*, *phaB* or *fadAB*; *crt* or *crt3*; and *ter_{TD}*, or *ter_{EG}*, in this order, under control of the constitutive P_{PhaP} promoter. P_{PhaC} has been shown to be a strong constitutive promoter in *C. necator* H16, P_{PhaP} was only inferred to be active in *E. coli* by previous research from López et al. (unpublished) [288-290].

3.2.1.2 Choosing the $\Delta 4$ knockout mutant that was used as a strain for 3-HP production and may be useful for 5-hydroxyvaleric acid production

The $\Delta 4$ knockout mutant was engineered by López et al. [110] to investigate 3-HP metabolism in *C. necator* H16. It lacks the $\Delta phaCAB$ operon and is thus unable to store carbon in PHB granules under stringent response, thus

removing the largest carbon-sink in the organism and helping to funnel it in into the engineered biosynthetic pathway [120, 291]. As shown by López et al. [110], the triple $\Delta mmsA1 \Delta mmsA2 \Delta mmsA3$ knockout of three putative (methyl)-malonate semialdehyde dehydrogenases prevents the degradation of malonate semialdehyde, a pathway intermediate, to acetyl-CoA and enhances 3-HP yield. (Figure 3.7).

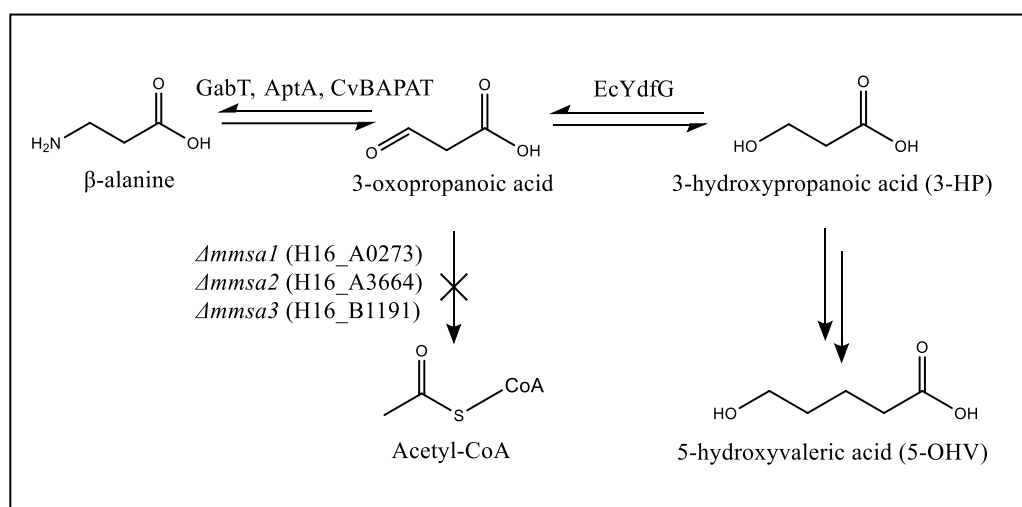


Figure 3.7 The *Cupriavidus necator* H16 $\Delta mmsA1 \Delta mmsA2 \Delta mmsA3$ deletion strain prevents the degradation of malonic semialdehyde to acetyl-CoA in the 5-OHV pathway. The reaction from malonic semialdehyde to acetyl-CoA is prevented by the triple deletion of the three malonic semialdehyde dehydrogenase encoding *mmsA* genes and removes a significant side-reaction in the 5-hydroxyvalerate pathway from β -alanine. The genes *gabT*, coding for a GABA aminotransferase and *aptA*, coding for a ω -amino acid pyruvate aminotransferase, are native to *C. necator* H16 and are complemented by *Chromobacterium violaceum* BAPAT to generate malonic semialdehyde from β -alanine. Malonic semialdehyde is then converted to 3-HP using the *E. coli* gene *ydfG*, coding for a NADP-dependent 3-hydroxy acid dehydrogenase.

In contrast to the wildtype, *C. necator* H16 $\Delta 4$ is thus unable to metabolise and degrade 3-HP, which leads to higher 3-HP production titers [144] and is hypothesized to enhance 5-hydroxyvaleric acid production. However, disruption of an important set of enzymes in an aldehyde detoxification system,

that has previously been discussed in **Chapter 3.1.3**, may result in a significant fitness cost. Aldehydes are very reactive towards proteins and impair their function, causing a bactericidal effect [292]. López et al. [110] show that a triple *mmsA* knockout results in slower growth and this work aimed to replicate these findings and answer whether the benefits of a *C. necator* H16 $\Delta 4$ strain outweigh the fitness cost disadvantages. Thus, this work aimed to investigate differences in growth between the *C. necator* H16 wildtype and the $\Delta phaCAB \Delta mmsA1 \Delta mmsA2 \Delta mmsA3$ quadruple knockout mutant strain $\Delta 4$. This work also aimed to investigate how the energy requirements for enzyme expression and the productive pathways impact growth rate in *C. necator* H16.

3.2.1.3 Using synthetic biology tools: promoter optimisation and synthetic RBS sites

In this work 20 pathways were explored in two organisms under different growth conditions. These experiments allowed to select a single pathway variant for the production of 5-OHV from β -alanine. Such a pathway was initially designed using the constitutive P_{PhaC} and P_{PhaP} promoters from *C. necator* H16.

Once a working candidate was found, optimisation work would address possible limiting factors in the expression of the reverse-beta oxidation part of the pathway in *C. necator* H16. One such limiting factor may be the use of the P_{PhaP} promoter. While active in *E. coli*, as evidenced by the successful synthesis of 5-hydroxyvaleric acid (this work), it autoregulates in *C. necator* H16 by use of the PhaR repressor, which, according to Pötter et al. [293] binds upstream of P_{PhaP} and blocks the promoter. Under PHA synthesis conditions, the PhaR

repressor detaches, as it shows a higher affinity to PHB granules, and thus allows the transcription of the operon. In the $\Delta phaCAB$ knockout strains, which include $\Delta 4$, PHB synthesis is not possible and P_{PhaP} may stay repressed.

While unproblematic in its regulation compared to P_{PhaP} in $\Delta phaCAB$ backgrounds, P_{PhaC} is far from the ideal promoter choice in *C. necator* H16. It was primarily chosen (in this and other works) because it is particularly well-characterised due to its prominent status as the promoter of the PHB biosynthesis system, which attracted most of the research attention for *C. necator* H16 with numerous studies conducted with it [294, 295]. In 2016, in a study published by Arikawa et al. [296], the constitutive promoters P_{trp} and P_{trc} were shown to be active in *C. necator* and significantly stronger than P_{PhaC} . The results of their work were summarised in Figure 4 of their publication [296].

In 2018, a study conducted by Alagesan et al. [297] tested 25 different promoters in *C. necator* H16 and found a majority of the tested candidates in their library to be significantly stronger than P_{PhaC} . The use of P_{PhaC} as a reference in the works of both Arikawa et al. [296] and Alagesan et al. [297] was indicative of how established the promoter was in the community prior to 2016. Both works then contributed to a certain relativisation and P_{PhaC} was relegated to one of many viable promoter choices for *C. necator* H16 engineering. Hence, P_{trc} and P_{trp} were considered for optimisation purposes in accordance with the prior research of Arikawa et al. [296].

The strong constitutive P_{trp} promoter is highly conserved and stems from the tryptophane biosynthesis operon in *E. coli*. It has been described as useful in

recombinant protein production applications [298]. The P_{trc} promoter drives the expression of sigma-factor $\sigma 70$ in *E. coli* and has also previously been described as strong promoter for the expression heterologous genes, both in *Cyanobacteria* sp. [299] and *C. necator* H16 [298].

To further enhance expression of a pathway, synthetic ribosomal binding sites of any desired relative strength may be introduced to an assembly, replacing the native sequences. In 2011, Salis [300] published the ribosome binding site calculator. His calculation method predicts the rate of translation initiation for any given transcript and allows to design a synthetic RBS with a chosen strength over a 1.000.000-fold range [300]. The 2011 Salis paper [300] was cited in 109 other publications to date according to the national library of medicine database, of which many employ the use of a synthetic RBS to boost translation levels. The algorithm used by Salis mainly employs a thermodynamic model that predicts RBS strength “based on the physiological 16S rRNA-binding site by identifying the rRNA–mRNA base pairings that will minimize the entire system's Gibbs free energy” [300]. When a RBS is designed using the Salis RBS calculator, the sequence of its 16S rRNA must be known, although the calculator allows for easy use with a drop-down menu in which a limited list of organisms can be found to be preselected. Furthermore, the desired length of the RBS site needs to be given and an arbitrary value (for strength) must be input for the calculator to output a suitable synthetic RBS. A typical strength value chosen may be 5,000 A.U. for strong expression without risking toxicity due to overexpression of proteins, potentially leading to protein aggregation and cell death.

Furthermore, it should be noted that the final construct for 5-OHV production shown in this work was not split on plasmids, but was instead fully assembled on one plasmid. This offers the possibility of having all genes driven by only one promoter (for example P_{trp}), causing the transcription of a single, large, polycistronic mRNA. Despite this possibility, the original pathway design was retained with two promoters (**Chapter 4.2.4**). The reason for this is that mRNA stability is a function of many factors that also include the size of the mRNA and cleavage of the transcript by endonucleases was less likely to occur with two smaller transcripts, extending the half-life of the mRNA [301, 302]. Also, the risk of unwanted intramolecular interactions that could lead to the formation of secondary structures within one large mRNA - with a negative impact on translation - should be mentioned [301].

3.2.2 2 of 20 pathways for 5-hydroxyvaleric acid production yield the final product in *Escherichia coli*

This experiment was designed to find any combination of enzymes for the seven necessary steps shown in **Figure 3.1**, that would form a complete pathway and yield 5-OHV. All tested pathway variants were designed to incorporate the following seven enzymatic functions: transaminase, oxidoreductase, CoA transferase or CoA synthetase, β -ketothiolase, 3-hydroxybutyryl-CoA dehydrogenase, enoyl-CoA hydratase and trans-2-Enoyl-CoA reductase. As explained in **Chapter 3.1.1**, a top-down approach was chosen and none of the enzyme candidates were biochemically characterized in this study prior use.

Twenty pathway variants were constructed for 5-OHV biosynthesis in *E. coli*. As explained in **Chapter 3.2.1.3**, the pathways were split on two vectors to accommodate the necessary genes on plasmids, which would, individually, not exceed a length of 12 kb, which was considered the maximum plasmid length that is transformable with reasonable efficiency by electroporation in *C. necator* H16 with the protocol shown in **Chapter 2.4.3**.

Furthermore, this experiment would show the differences in performance between PrpE and Pct, Ter_{TD} and Ter_{EG} or the stereospecific (*S*)- and (*R*)-variants of the reverse beta-oxidation pathway. Additionally, the experiment was designed to elucidate if the *fadAB* encoded complex could offer a one-size-fits-all solution to reverse-beta-oxidation in *E. coli*.

The 20 pathway combinations shown in **Figure 3.8** were constructed using HiFi-assembly in a modular manner as detailed in **Chapter 2** and chemically

transformed into super-competent NEB *E. coli* DH5 α . The resulting strains were named EC1 to EC20.

The transgenic strains and the empty vector negative control EC21 were then fermented in minimal medium supplemented with 50 mM and without β -alanine and extracellular concentrations of the carbon source β -alanine, the pathway intermediate 3-HP acid and the final product 5-OHV were measured using LC-MS according to the methods described in **Chapter 2.7.4.3** and **2.9.6**.

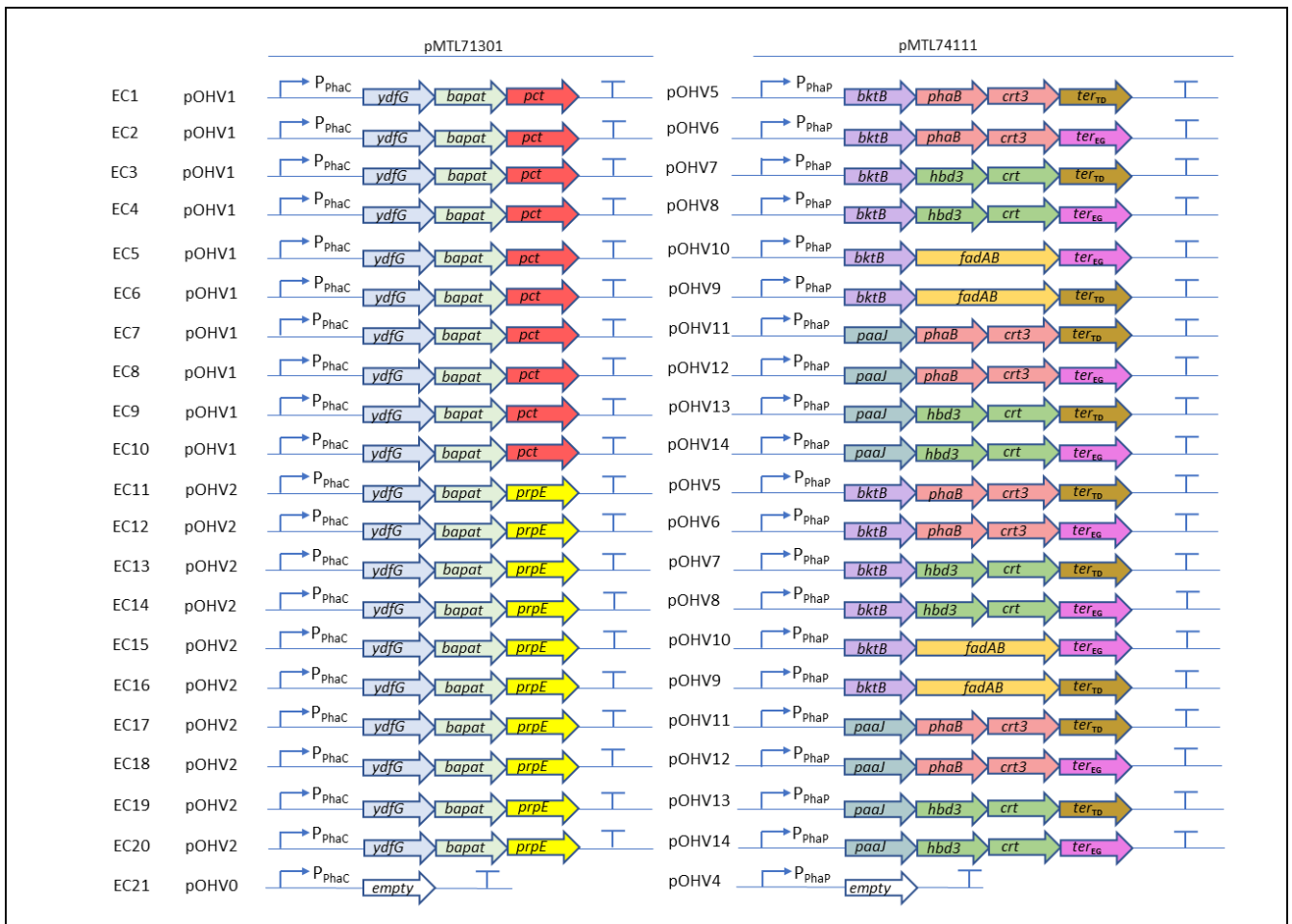


Figure 3.8 Gene combinations used for the *E. coli* DH5 α double transformant strains. Figure shows the strains (EC1-EC21) and their plasmid (OHV0 – OHC14) combinations, including promoters and gene order, used for the 48h fermentation experiment results shown in **Table 3.1**. *ydfG*_{EC} encodes a 3-HP dehydrogenase. *bapat*_{CV} encodes a β -alanine transaminase. *pct*_{CN} encodes a propionate CoA-transferase. *prpE*_{EC} encodes a propionate CoA synthetase. *bktB*_{CN} encodes a β -ketothiolase. *paal*_{EC} encodes a 3-oxoadipyl-CoA thiolase. *phaB*_{CN} encodes an acetoacetyl-CoA reductase. *hbd3*_{CS} encodes a hydroxybutyrate dehydrogenase. *fadAB*_{EC} encodes the FadA/FadB complex with thiolase, dehydrogenase and crotonase activity. *crt3*_{CN} encodes a (*R*)-3-hydroxybutyryl-CoA dehydratase. *crt*_{CA} encodes a (*S*)-3-hydroxybutyryl-CoA dehydratase. *ter*_{TD} encodes a trans-2-enoyl-CoA reductase. *ter*_{EG} encodes a trans-2-enoyl-CoA reductase.

The pMTL70301 series plasmids conferred tetracycline resistance, carried the P_{PhaC} promoter and expressed the genes *ydfG*_{EC}, *bapat*_{CV} and *pct*_{EC} or *prpE*_{EC}. The pMTL74111 vector conferred chloramphenicol resistance, carried the P_{PhaP} promoter and expressed the genes *bktB*_{CN}, *phaB*_{CN} or *hbd3*_{CS}; *crt3*_{CN} or *crt*_{CA}, *fadAB*_{EC} and *ter*_{TD} or *ter*_{EG}.

E. coli double transformants were fermented in a 25 mL EMM^{Tet, Cm} main culture in 250 mL baffled shake flasks, supplemented with 50 mM β-alanine. Two negative controls were used. Each strain was also fermented as a negative control that did not receive the supplementation with β-alanine. Furthermore, an empty-plasmid control was introduced to show that *E. coli* does not natively accumulate any of the measured metabolites. The cultures were grown as biological triplicates at 37°C for 48 hours. Starting point and end-point supernatant and intracellular samples of the cultures were analysed using LC-MS and a qualitative detection of 3-HP, 5-hydroxyvaleric acid and β-alanine conducted. Detection of the other pathway intermediates, especially the CoA-esters was attempted, but failed due to the instability of the highly activated CoA esters during extraction and a lack of commercially available analytical standards for identification. Growth curves of the strain are shown in **Appendix Figures A26 - A46**

Table 3.1 Overview of detected analytes after 48 h fermentation of transgenic *E. coli* DH5 α expressing potential metabolic pathways for 5-hydroxyvalerate production. *E. coli* DH5 α were cultivated in ECMM^{Tet,Cm} supplemented with 50 mM β -alanine for 48h. Negative controls were not supplemented. EC21 is a double empty vector control. Positive signs show a detected analyte (threshold based on signal-to-noise ratio as detailed in Chapter 2), negative signs show not detected analytes. Green highlights positive progressions in the metabolic pathway, red highlights interruption in the pathway or expected negative result. Yellow highlights possible false positive result. (*) Possible cross-detection with intracellular L-alanine. (**) Possible misidentification due to lactate (1 out of 3 replicates). No other disagreements between any of the biological triplicates were detected.

Strain/ Detected compound	Intracellular fraction						Extracellular fraction						
	Supplemented with β -alanine			Negative control			Supplemented with β -alanine			Negative control			
	β -alanine	3-HP	5-OHV	β -Alanine	3-HP	5-OHV	β -alanine	3-HP	5-OHV	β -alanine	3-HP	5-OHV	
EC1	+	+	-	+	*	-	-	+	+	-	-	-	-
EC2	+	+	-	+	*	-	-	+	+	-	-	-	-
EC3	+	+	-	-	-	-	-	+	+	-	-	-	-
EC4	+	+	-	+	*	-	-	+	+	-	-	-	-
EC5	+	+	-	+	*	-	-	+	+	-	-	-	-
EC6	+	+	-	+	*	-	-	+	+	-	-	-	-
EC7	+	+	-	-	-	-	-	+	+	-	-	-	-
EC8	+	+	-	+	*	+	**	-	+	+	-	-	-
EC9	+	+	-	+	*	-	-	+	+	-	-	-	-
EC10	+	+	-	+	*	-	-	+	+	-	-	-	-
EC11	+	+	+	+	*	-	-	+	+	+	-	-	-
EC12	+	+	+	+	*	-	-	+	+	+	-	-	-
EC13	+	+	-	+	*	-	-	+	+	-	-	-	-
EC14	+	+	-	+	*	-	-	+	+	-	-	-	-
EC15	+	+	-	+	*	-	-	+	-	-	-	-	-
EC16	+	+	-	+	*	-	-	+	+	-	-	-	-
EC17	+	+	-	-	-	-	-	+	+	-	-	-	-
EC18	+	+	-	+	*	-	-	+	+	-	-	-	-
EC19	+	+	-	+	*	-	-	+	+	-	-	-	-
EC20	+	+	-	+	*	-	-	+	+	-	-	-	-
EC21	+	-	-	+	*	-	-	+	-	-	-	-	-

Table 3.1 shows if any of the aforementioned analytes could be detected in the end-point samples in *E. coli*. As can be seen in **Table 3.1**, there are only few notable differences between the results of intracellular and extracellular fractions. All analytes could be detected in both fractions; however, some false positive results were found in intracellular fractions while all negative controls were measured as negative in extracellular fractions.

False positive results of 3-HP in pellet extractions (**) can be caused by cross-contamination with lactic acid, which is detected at the same m/z. Usually the lactic acid peak does not overlap with 3-HP, but when lactic acid accumulates due to insufficient oxygenation, (for example when a shake flask lid gas exchange membrane is covered by tape accidentally or the incubator stops shaking due to user error) the intracellular concentrations are high enough to broaden the peak and cover the 3-HP peak.

False positive results for β -alanine (*) in intracellular fractions are caused by intracellular L-alanine, which is detected at the same m/z and RT and can only be resolved from β -alanine if MS-MS is conducted. This is not an issue in extracellular samples as evidenced by **Table 3.1**, because L-alanine is not exported into the supernatant in noteworthy concentrations, and certainly not in the same order of magnitude as the supplemented concentration (50 mM). MS traces of all three analytes (standards) are shown in the appendix (**Figures A2-A4**) as well as examples of traces in positive cultures and control strains.

(Figures 6A- 11A). Growth curves of all cultures are also shown in the appendix **(Figures 26A-41A)**

Within the intracellular fractions, out of 20 pathway combinations, excluding all negative controls, all tested positive for β -alanine. Additionally, 3-HP was also detected in these samples. In two of the pathway combinations, P_{PhaC} -*ydfG-bapat-prpE* with P_{PhaP} -*bktB-phaB-crt3-ter_{TD}* (EC11) and P_{PhaC} -*ydfG-bapat-prpE* with P_{PhaP} -*bktB-phaB-crt3-ter_{EG}* (EC12), that were tested in *E. coli*, the presence of 5-hydroxyvaleric acid could be detected. The negative controls of the intracellular fractions show false detection of β -alanine in almost all samples, which is, as previously explained, due to L-alanine cross-detection. 3-HP/lactic acid cross-detection only occurred in one sample, in which 3-HP was also present in the supernatant, which points towards a problem caused by insufficient oxygenation in that particular culture.

5-hydroxyvaleric acid was not detected in any negative intracellular fraction controls. Within the extracellular fractions, and as presented in **Table 3.1**, apart from the negative controls, all samples tested positive for the presence of β -alanine. In 19 out of 20 samples, 3-HP could be detected. 5-hydroxyvaleric acid was shown to be present in two combinations. These results mirror the results from intracellular analysis, with the exception of strain EC15, where 3-HP was not detectable in the supernatant. In all negative controls, β -alanine, 3-HP and 5-hydroxyvaleric acid were not detected in the supernatant.

In summary, analysis of supernatants generally appears to result in more reliable data and 2 out of 20 pathway variants were shown to be suitable

preliminary candidates for 5-OHV production, as evidenced by the positive results in **Table 3.1**.

3.2.2 5 of 20 pathways for 5-hydroxyvaleric acid production yield the final product in *Cupriavidus necator* H16, suggesting that some results obtained in *Escherichia coli* are transferable to *Cupriavidus necator* H16.

Analogous to the experimental design shown in **Chapter 3.2.1** for *E. coli*, *C. necator* H16 wildtype and $\Delta 4$ mutant strains were transformed with two plasmid combinations to mirror the pathways tested in *E. coli*. The experiment was not only designed to test if these variants were yielding 5-OHV in *C. necator* H16, the experiment was deliberately conducted under the same conditions as before to make the data as comparable as possible to the experiments in *E. coli*.

Fourty strains were labelled CN1 to CN20 for wildtype and CN1 $\Delta 4$ to CN20 $\Delta 4$ for $\Delta 4$ mutants, accordingly. They were fermented along with their empty plasmid negative controls CN21 and CN21 $\Delta 4$ in a 25 mL CNMM^{Tet,Cm} culture in 250 mL baffled shake flasks, supplemented with 50 mM β -alanine. No-feed negative controls did not receive any β -alanine supplementation. The cultures were grown at 30°C for 48 hours. Start and end-point supernatant samples of the cultures were analysed using LC-MS and a qualitative detection of the metabolites 3-HP, 5-hydroxyvaleric acid (5-OHV) and β -alanine was conducted.

Table 3.4 shows a summary of the detected analytes β -alanine, 3-HP and 5-hydroxyvaleric acid that could be detected in the 48 h end-point supernatant samples in *Cupriavidus necator* H16 wildtype and the $\Delta 4$ strain. All 42 strains were fermented once as single screen and the experiment was repeated in triple replicates for strains 1, 2 and 11 – 14 and 17-21.

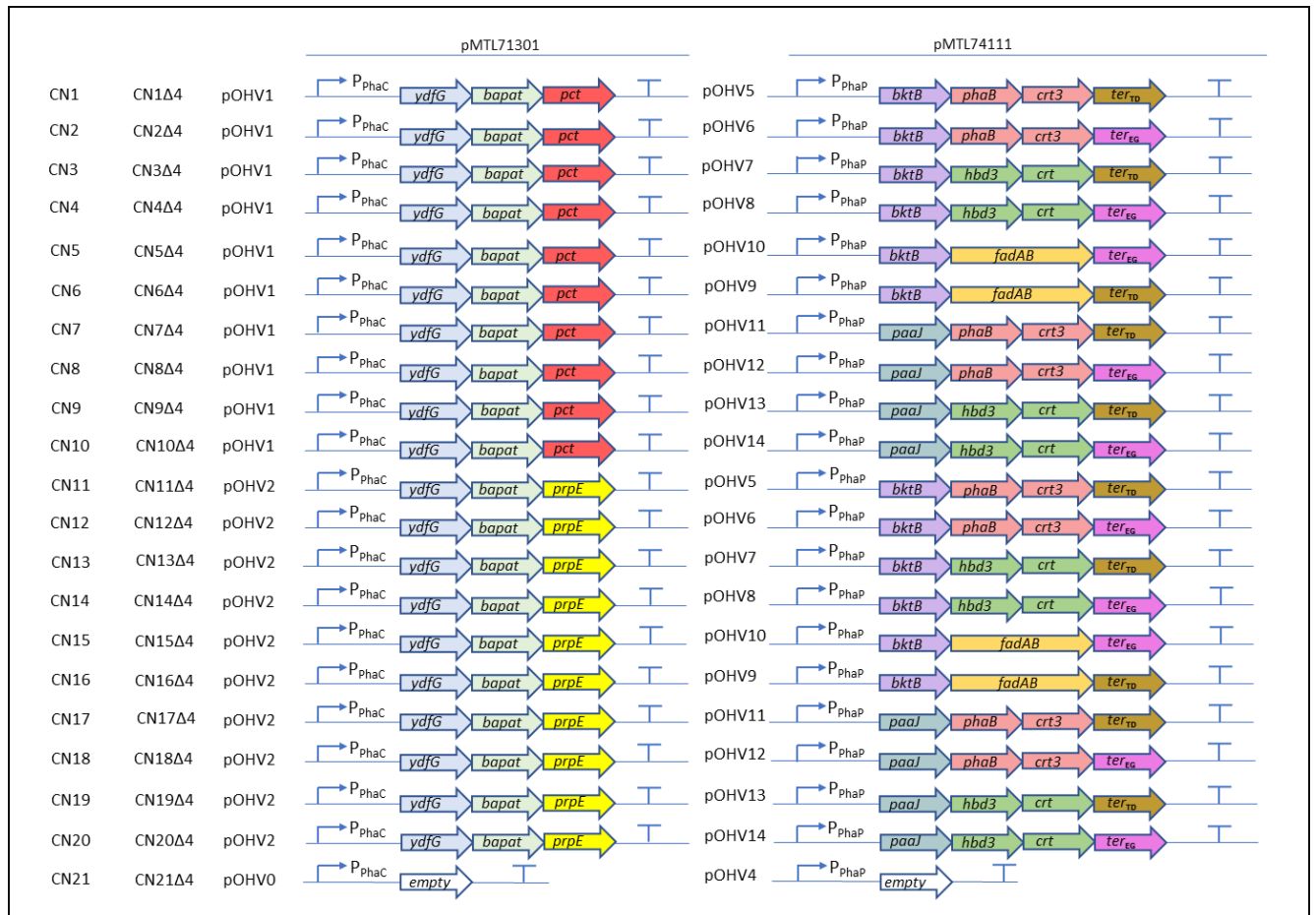


Figure 3.9 Gene combinations used for the *C. necator* H16 wildtype and $\Delta 4$ double transformant strains. Figure shows the strains (CN1-CN21 and CN1 Δ 4-CN21 Δ 4) and their plasmid (pOHV0 – pOHV14) combinations, including promoters and gene order, used for the 48 h fermentation experiment results shown in Table 3.1. *ydfG*_{EC} encodes a 3-HP dehydrogenase. *bapat*_{CV} encodes a β -alanine transaminase. *pct*_{CN} encodes a propionate CoA-transferase. *prpE*_{EC} encodes a propionate CoA synthetase. *bktB*_{CN} encodes a β -ketothiolase. *paaJ*_{EC} encodes a 3-oxoadipyl-CoA thiolase. *phaB*_{CN} encodes an acetoacetyl-CoA reductase. *hbd3*_{CS} encodes a hydroxybutyrate dehydrogenase. *fadAB*_{EC} encodes the FadA/FadB complex with thiolase, dehydrogenase and crotonase activity. *crt3*_{CN} encodes a (*R*)-3-hydroxybutyryl-CoA dehydratase. *crt*_{CA} encodes a (*S*)-3-hydroxybutyryl-CoA dehydratase. *ter*_{TD} encodes a trans-2-enoyl-CoA reductase. *ter*_{EG} encodes a trans-2-enoyl-CoA reductase.

The results obtained from β -alanine supplemented and unsupplemented fermentation of these strains are shown in **Table 3.2**.

Strain/ Detected compound	<i>Cupriavidus necator</i> H16 wildtype						<i>Cupriavidus necator</i> H16 $\Delta 4$						
	Supplemented with β -alanine			Negative control			Supplemented with β -alanine			Negative control			
	β -Ala	3-HP	5-OHV	β -Ala	3-HP	5-OHV	β -Ala	3-HP	5-OHV	β -Ala	3-HP	5-OHV	
CN1	+	+	-	-	-	-	+	+	+	-	+	-	CN1 $\Delta 4$
CN2	+	-	-	-	-	-	+	+	+	-	-	-	CN2 $\Delta 4$
CN3	+	-	-	-	-	-	+	+	-	-	-	-	CN3 $\Delta 4$
CN4	+	-	-	-	-	-	+	+	-	-	-	-	CN4 $\Delta 4$
CN5	+	-	-	-	-	-	+	+	-	-	-	-	CN5 $\Delta 4$
CN6	+	-	-	-	-	-	+	+	-	-	-	-	CN6 $\Delta 4$
CN7	+	-	-	-	-	-	+	+	-	-	-	-	CN7 $\Delta 4$
CN8	+	-	-	-	-	-	+	+	-	-	+	-	CN8 $\Delta 4$
CN9	+	-	-	-	-	-	+	+	-	-	-	-	CN9 $\Delta 4$
CN10	+	-	-	-	-	-	+	+	-	-	-	-	CN10 $\Delta 4$
CN11	+	+	-	-	-	-	+	+	+	-	-	-	CN11 $\Delta 4$
CN12	+	+	-	-	-	-	+	+	+	-	+	-	CN12 $\Delta 4$
CN13	+	-	-	-	-	-	+	+	-	-	-	-	CN13 $\Delta 4$
CN14	+	+	-	-	-	-	+	+	-	-	-	-	CN14 $\Delta 4$
CN15	+	-	-	-	-	-	+	-	-	-	-	-	CN15 $\Delta 4$
CN16	+	+	-	-	-	-	+	+	-	-	-	-	CN16 $\Delta 4$
CN17	+	+	-	-	-	-	+	+	+	-	-	-	CN17 $\Delta 4$
CN18	+	+	-	-	-	-	+	+	-	-	-	-	CN18 $\Delta 4$
CN19	+	+	-	-	-	-	+	+	-	-	-	-	CN19 $\Delta 4$
CN20	+	+	-	-	-	-	+	+	-	-	-	-	CN20 $\Delta 4$
CN21	+	-	-	-	-	-	+	-	-	-	+	-	CN21 $\Delta 4$

Table 3.2 Overview of detected analytes after 48 h fermentation of transgenic *C. necator* H16 wildtype and $\Delta 4$, expressing potential metabolic pathways for 5-hydroxyvalerate production. *C. necator* H16 wildtype and *C. necator* H16 $\Delta 4$ were cultivated in CNMM^{Tet,Cm} supplemented with 50 mM β -alanine for 48h. Negative controls were not supplemented. CN21 is a double empty vector control. Positive signs show a detected analyte (threshold based on signal-to-noise ratio as detailed in **Chapter 2**), negative signs show not detected analytes. Green highlights positive progressions in the metabolic pathway, red highlights interruption in the pathway or expected negative result. Yellow highlights possible false positive result. (*) Possible misidentification due to lactate (1 of 4 replicates). No other disagreements between any of the biological triplicates were detected.

The unproductive strains 3-10, 15 and 16 were excluded from experiment replication due to constraints with the number of samples that could be analysed by LC-MS at this time and no automated analysis method yet available.

Notable differences could be observed between the wildtype set compared to the $\Delta 4$ knock-out mutant. Growth curves of the $\Delta 4$ strain can be found in **Appendix Figures A47 - A67**. Growth curves of the wildtype can be found in **Appendix Figures A68 - A88**.

In the *C. necator* H16 wildtype, where β -alanine was supplemented, it was also detected in the end-point, while in the unsupplemented negative controls it was not. This result indicated that *C. necator* H16 did not deplete the 50 mM supplemented β -alanine after 48 h and it was not natively produced where non-supplemented. 3-HP production was detected in 9 of 20 cultures. With the exception of CN1, all other strains (CN11, CN12, CN14, CN16, CN17, CN18, CN19, CN20) carry the *prpE* gene instead of the *pct* gene and use the pMTL71301-P_{PhaC}-*ydfG-bapat_{CV}-prpE* vector, accordingly. None of the samples contained detectable 5-OHV in the supernatant, suggesting that the wildtype strain does not support sufficient flux to the end-product. The supernatant of the empty vector control CN21 contained only the supplemented β -alanine and none of the other metabolites, as expected.

In the $\Delta 4$ mutant, in line with the results of the wildtype set, where β -alanine was supplemented, it was also detected, while in the unsupplemented negative controls it was not. 3-HP was detected in the supernatant of all 20

supplemented cultures, with the exception of CN15. 5-hydroxyvaleric acid could be detected in five supernatants. Notably, those strains (CN1Δ4, CN2Δ4, CN11Δ4, CN12Δ4 and CN17Δ4) share the genes *phaB* and *crt3*, which encode the enzymes of the (*R*)-stereospecific reverse beta-oxidation chain elongation pathway. Four (CN1Δ4, CN2Δ4, CN11Δ4, CN12Δ4) of these five share *bktB*. Three out of the five constructs share *prpE* (CN11Δ4, CN12Δ4 and CN17Δ4). However, false positive signals of 3-HP were detected in four samples, CN1Δ4, CN8Δ4, CN12Δ4 and CN21Δ4. All these false positive detections were above the S/N threshold over which an analyte was considered “detected”. These false positives are likely the result of a restricted flow of oxygen into baffled flasks during fermentation. Due to the lack of oxygen, anaerobic breakdown of pyruvate to lactate can be observed at late time points. High lactate (2-hydroxypropionic acid) concentrations can cause the LC-MS peak to overlap with the 3-HP (3-hydroxypropionic acid) peak. This happens because both molecules share the same mass (and *m/z*) and their retention times (RT) are close due to their chemical similarities and hence comparable interaction strength with the used polymeric chromatography column. The false positive results that occurred during the initial high-throughput screen were confirmed to be false-positives by subsequent repeat of the experiment in triplicates in the case of CN1Δ4, CN12Δ4 and CN21Δ4 (with proper oxygenation, causing the false positive signal to disappear in those fermentation runs), while CN8Δ4 was simply excluded from any further analysis due to lacking productivity.

3.2.3 The $\Delta 4$ deletion strain grows slower than the $\Delta phaCAB$ deletion strain and the wildtype

The experiments shown in this subchapter were designed to investigate differences in growth (and in extension, fitness) between the *C. necator* H16 wildtype and its quadruple knockout mutant $\Delta 4$. Furthermore, the growth rates of the strains carrying pathway variants were comparatively investigated to further understanding of the energy requirements for enzyme expression and the potential impact a productive pathway may have on the growth rate in *C. necator* H16.

Hence, growth curves of *C. necator* H16 wildtype, as well as $\Delta phaCAB$ and $\Delta 4$ mutant strains carrying empty vectors were obtained and the metabolic burden of the pathway investigated by comparing the growth performance of a $\Delta 4$ negative control strain with $\Delta 4$ strains carrying productive pathways for 3-HP and 5-hydroxyvalerate, respectively.

The first growth experiment was designed to investigate if the $\Delta phaCAB$ and $\Delta 4$ knockouts affect growth of *C. necator* H16.

The *C. necator* H16 wildtype and the $\Delta phaCAB$ and $\Delta 4$ mutant were transformed with the two empty vector controls: pMTL71301- P_{PhaC} -*empty* and pMTL74111- P_{PhaP} -*empty*. The cells were grown on CNMM^{Tet,Cm} and single colonies used to inoculate a CNMM^{Tet,Cm} preculture which was grown to OD 0.7. During exponential growth phase, the cells were used to inoculate 25 mL CNMM^{Tet,Cm} cultures in 250 mL baffled shake flasks. The cells were then grown 60 h at 30 °C and OD₆₀₀ measured. The results of these measurements are

shown in **Figure 3.10 (A)**. Timepoints were taken and analysed for levels of gluconate in LC-MS to monitor the usage of the primary carbon source. The results can be seen in **Figure 3.10 (B)**.

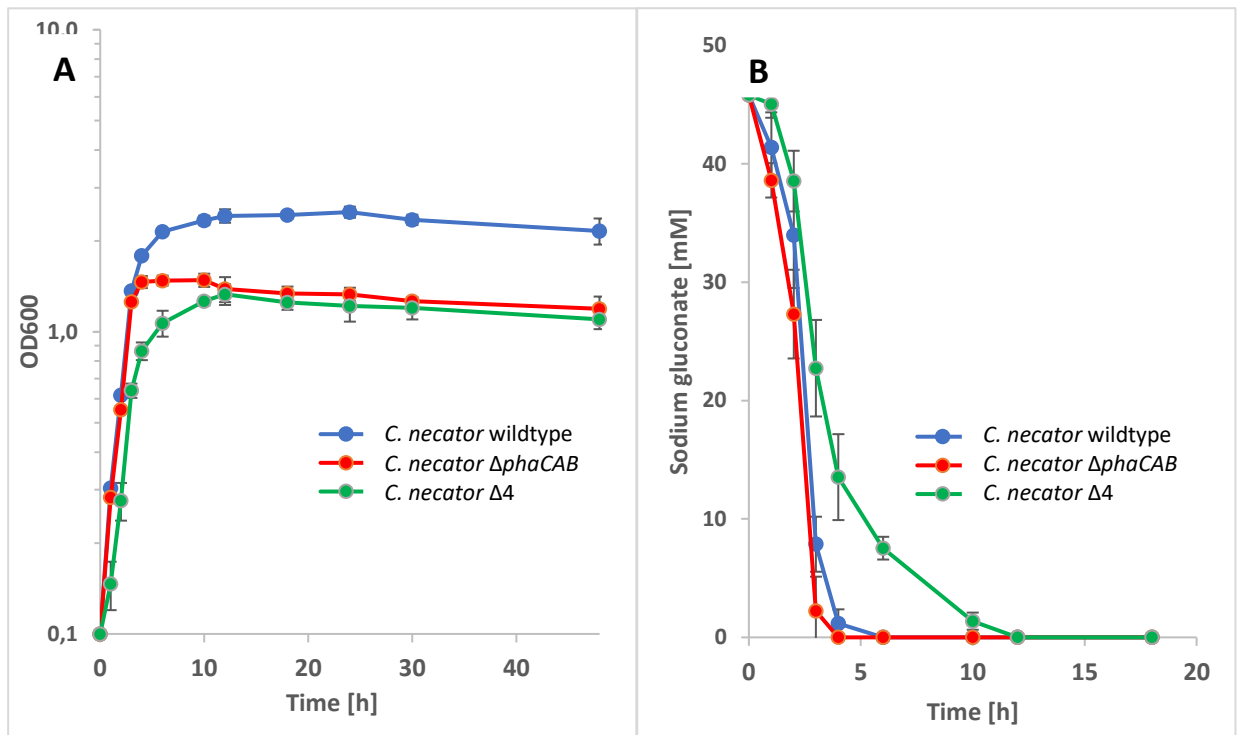


Figure 3.10 Growth profiles and gluconate consumption of the double empty vector transformed *Cupriavidus necator* wildtype and its Δ phaCAB and Δ 4 knockout mutants. The *C. necator* H16 wildtype is shown in blue, Δ phaCAB mutant in red and Δ 4 mutant in green. **(A)** OD₆₀₀ measurements over 60h growth in CNMM^{Tet,Cm} medium. **(B)** Sodium gluconate levels during growth, measured using LC-MS. Values from 18 h – 60 h were omitted due to depletion (all zero). All strains were grown as biological triplicates.

The doubling times were calculated by using the formula shown in **Chapter**

2.8.3 with the following results:

$$T_D (\text{wildtype}) = 0.79 \text{ h}; T_D (\Delta\text{phaCAB}) = 0.82 \text{ h} \text{ and } T_D (\Delta 4) = 1.286 \text{ h.}$$

Figure 3.10 (A) and the comparison of the calculated doubling times show that the wildtype (blue) and $\Delta phaCAB$ mutants (red) have a similar growth rate during exponential phase. It should be noted that OD_{600} are normally not comparable between strains that accumulate PHB granules and those that do not - due to a difference in light scattering behaviour. However, PHB accumulation occurs during stationary phase, when stringent response triggers the incorporation of carbon into granules. The wildtype reaches maximum OD_{600} values of 2.5 under the given conditions. The $\Delta phaCAB$ reaches a maximum OD_{600} of 1.5. The $\Delta 4$ mutant (green) shows a longer doubling time compared to the wildtype and $\Delta phaCAB$, but eventually reaches maximum OD_{600} values of 1.4, marginally less than the $\Delta phaCAB$ knock out mutant. **Figure 3.10 (B)** shows the consumption of carbon source (1% or 45.8 mM sodium gluconate). The wildtype and the $\Delta phaCAB$ mutants show similar carbon source depletion rates, which appears delayed in the $\Delta 4$ mutant. This result indicates that the $\Delta phaCAB$ deletion does not adversely affect growth rate compared to the wildtype, but the three $\Delta mmsA1$ $\Delta mmsA2$ and $\Delta mmsA3$ deletions of the $\Delta 4$ strain do.

The second set of growth experiments were designed to investigate how strong the energetic demand of the pathways themselves would interfere with *C. necator* H16 $\Delta 4$ growth. The reason this experiment was only conducted in $\Delta 4$ is that $\Delta 4$ is the only background in which 5-OHV production was previously seen and therefore the only background in which the burden of a functional 5-OHV pathway could be assessed.

The *C. necator* H16 strain CN21Δ4 was selected as the empty plasmid negative control. The strain CN19Δ4 was selected because it produced 3-HP but not 5-OHV (see Table 3.2). The strain CN11Δ4 was selected for carrying a fully functional pathway and producing the end-product 5-OHV. The three selected *C. necator* H16 strains were grown on CNMM^{Tet,Cm} and single colonies used to inoculate a CNMM^{Tet,Cm} preculture which was grown to OD₆₀₀ 0.8. During exponential growth phase, the cells were used to inoculate 25 mL CNMM^{Tet,Cm} cultures, supplemented with 50 mM β-alanine, in 250 mL baffled shake flasks. The cells were and grown 48 h at 30 °C and OD₆₀₀ measured. Figure 3.11 shows the slight differences in growth rate and large differences in maximum OD₆₀₀ between the three selected strains.

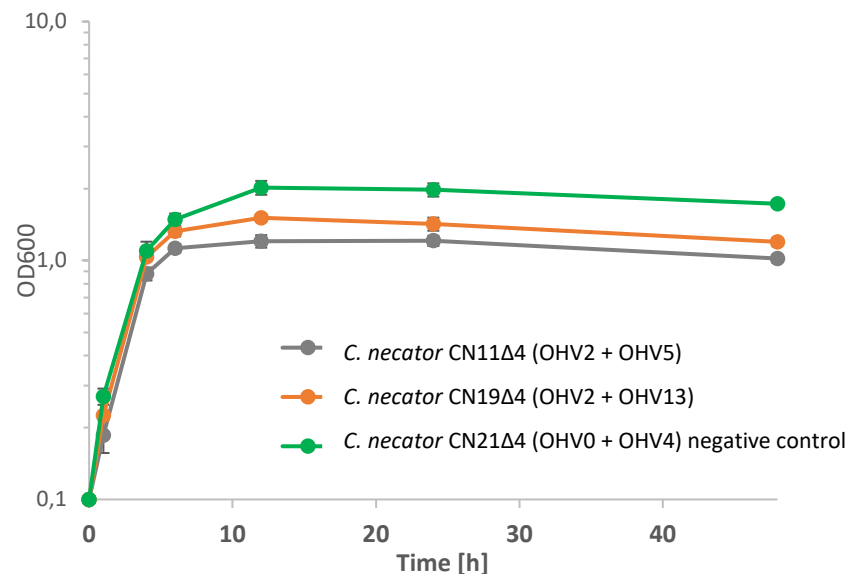


Figure 3.11 Growth profiles of the double empty vector transformed *Cupriavidus necator* Δ4 mutant (CN21Δ4), the 3-HP producing strain CN19Δ4 and the 5-hydroxyvalerate producing strain CN11Δ4. The *Cupriavidus necator* double empty vector transformed Δ4 mutant (CN21Δ4) is shown in green, the 3-HP producing strain CN19Δ4 in orange and the 5-hydroxyvalerate producing strain CN11Δ4 in grey. OD₆₀₀ measurements over 60 h growth in CNMM^{Tet,Cm} medium supplemented with 50 mM β-alanine.

The negative control strain CN21Δ4 with empty vectors (green) grows fastest and reaches a maximum OD₆₀₀ of 2.0. It should be noted here that the maximum OD₆₀₀ of CN21Δ4 is higher than in the previous experiment shown in **Figure 3.10 (A)**. This is likely due to the abundance of β-alanine, which was added in similar molarity as the favoured carbon source (sodium gluconate) and may thus contribute to extra bio-mass formation. The 3-HP producing strain CN19Δ4 (orange) reaches a maximum OD₆₀₀ of 1.5 and lastly, the 5-OHV producing strain CN11Δ4 a maximum OD₆₀₀ of 1.2.

The differences observed and shown in **Figure 3.11** between the empty vector strain (CN21Δ4, green) and the producer strains (CN19Δ4, orange and CN11Δ4, grey) can be explained by the combined effects of the energetic demand of protein expression in producers and pathway demand. The difference between CN19Δ4 and CN11Δ4, however, can be explained by the specific energetic demand that the part of the pathway, that converts 3-HP to 5-hydroxyvalerate, places on the cell. Other, less likely explanations, are toxic effects of pathway metabolites or side-products. In summary, the productive pathway seems to have no impact on growth rate, but it does cause differences in total biomass formation.

3.2.3 Resting cell fermentation conditions allow for 5-OHV formation in *Cupriavidus necator* H16 $\Delta 4$, but cause undesired accumulation of uracil

Chapter 3.2.2 showed that pathways that convert β -alanine to 3-HP using BAPAT and YdfG were efficient producers of 5-OHV in *C. necator* $\Delta 4$. From 3-HP, the best candidates for 5-OHV production were shown to be pathways containing BktB, PhaB, Crt3 and Ter_{TD}. However, without quantifiable results, some of the other pathways that have shown detectable amounts of 5-hydroxyvaleric acid could not be dismissed.

The experiments shown in this section were designed to quantify the metabolites β -alanine, 3-hydroxypropanoic acid and 5-hydroxyvaleric acid after 24 h of batch fermentation in resting *C. necator* $\Delta 4$ cells. This strain was chosen as the main chassis strain for development and optimisation of the pathway, based on the positive results shown in **Chapter 3.2.3**

The resting cell condition was chosen to test if the decoupling of the growth phase and the production phase could have beneficial effects on product formation, as explained in **Chapter 3.1.9**. This decision was taken after assessing the burden of the pathway on biomass formation in **Chapter 3.2.3**.

C. necator $\Delta 4$ cells were grown on CNMM^{Tet,Cm} minimal medium plates and single colonies used to inoculate 5 mL precultures in CNMM^{Tet,Cm} overnight. These were used to inoculate large 200 mL main cultures in 2 L flasks in CNMM^{Tet,Cm} minimal medium that were grown to an OD₆₀₀ of 0.6. 1050 mL of the grown cultures were unified and centrifuged to yield 630 OD ml units of cell pellet, which was washed twice with water and then resuspended in 25 mL non-phosphate MOPS buffered CNMM-P^{Tet,Cm} medium to yield a total optical

131

density of OD₆₀₀ of 25.2. The medium was supplemented with 20 mM β-alanine, negative controls were non-supplemented. In addition, the double empty vector control CN21Δ4 was used. The experiment was conducted in biological triplicates and the three metabolites β-alanine, 3-hydroxypropanoic acid and 5-hydroxyvaleric acid in the supernatant were quantified using LC-MS at the 24 h end-timepoint. For specific details regarding the use of LC-MS for the quantification of the analytes, see **Chapter 2.9.6**.

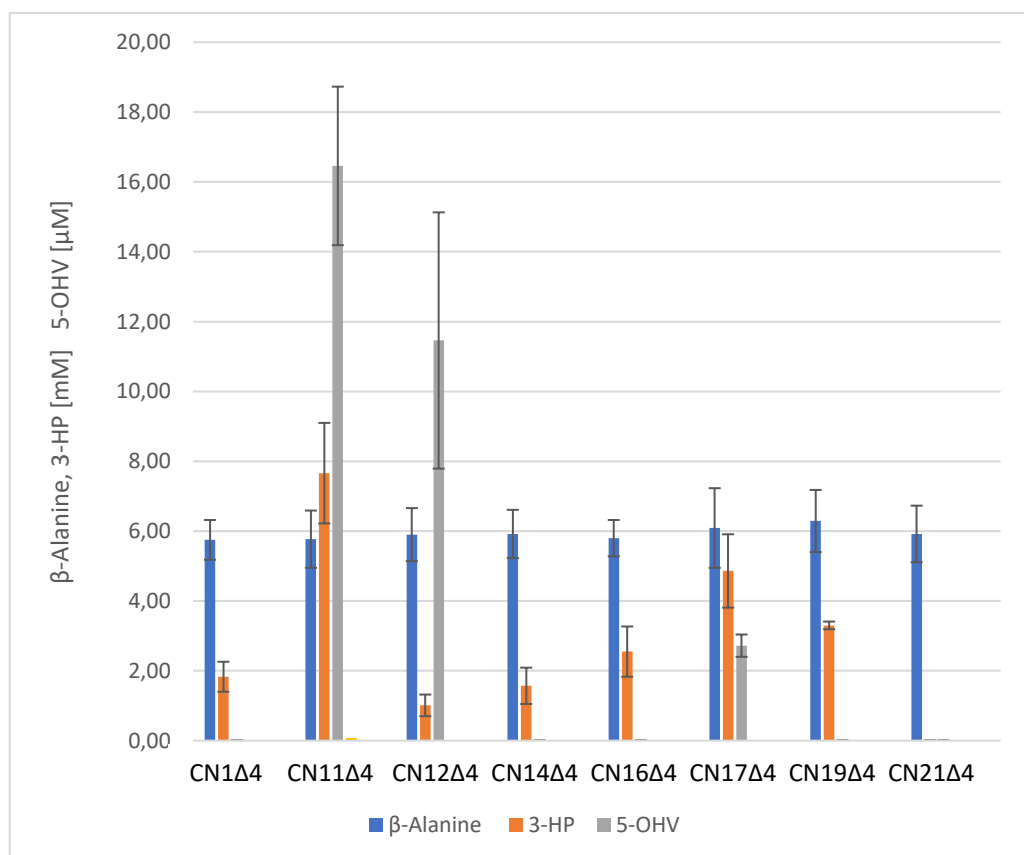


Figure 3.12 Quantified levels of β-alanine, 3-hydroxypropanoic acid and 5-hydroxyvaleric acid after 24h of resting cell fermentation in 20 mM β-alanine supplemented and non-supplemented *C. necator* H16 Δ4 cultures. Values are given in [mM] for β-alanine and 3-HP and in μM for 5-OHV. Dark blue: for β-alanine, supplemented; Orange: 3-HP, supplemented; Grey: 5-OHV, supplemented. β-alanine, non-supplemented (n.d.); 3-HP, non-supplemented (n.d.); 5-OHV, non-supplemented (n.d.). The shown values are averaged from three biological triplicates. All values were measured by LC-MS from culture supernatants.

As can be seen in **Figure 3.9**, all tested strains had between 5.8 mM and 6.2 mM β -alanine remaining in the supernatant. After 24h, 3-HP had also been produced by all tested strains in varying amounts, apart from the control. The highest 3-HP titers with 4.8 mM and 7.6 mM produced 3-HP, measured in the supernatant, were achieved by CN17 Δ 4 and CN11 Δ 4, respectively. These two strains only differed in using *bktB* or *paaJ*, respectively. Most other tested strains accumulated at least 1.0 mM of 3-HP though. 5-hydroxyvaleric acid could only be detected in strains CN11 Δ 4 (16.4 μ M), CN12 Δ 4 (11.4 μ M) and CN17 Δ 4 (2.7 μ M), of which CN17 Δ 4 is under the detection threshold.

It should be noted that the absolute amounts of consumed β -alanine are not accounted for by 3-HP production alone. Using an untargeted approach, a mass of 111,0200 m/z (within 3 ppm mass accuracy) was detected in the negative ion channel at high abundance, which was consistent with high amounts of uracil in the supernatant. Other possible molecules with the same mass are usually not found in living cells, which forms the basis of the uracil hypothesis. Unfortunately, no analytical standard was available on short notice to confirm the identity of the peak and neither could the exact concentration be determined. The standard was ordered, however only used for a similar experiment using the resting cell condition in **Chapter 4**. Retrospectively, the peak in question could be consistent with uracil, but no uracil standard was run together with the samples under the same conditions.

Because an analytical standard of 5-OHV was also not available, 5-OHV had to be chemically synthesised by conducting an alkaline catalysed ring-opening polymerisation of δ -valerolactam, followed by a slow hydrolysis of the 3-HV

polymer at low temperatures, as detailed in **Chapter 2.6.1**. The synthesised compound was analysed using NMR (see **Chapter 2.6.2**) to confirm identity and then used as analytical standard in all experiments in this Chapter, establishing confidence that the 5-OHV peaks found in this study are of the right identity.

3.2.4 Enhanced 5-hydroxyvaleric acid production using P_{trc} and P_{trp} promoters and synthetic RBS sites

20 pathway variants were investigated in the previous Chapters, of which 8 were tested under resting cell conditions (**Chapter 3.3.3**). These experiments allowed a selection of single pathway variants that produced 5-OHV from β -alanine to a titer of 16 μM (**Figure 3.12**, CN11 Δ 4). This pathway was characterised by the use of *ydfG*, *bapat* and *prpE* under the control of the constitutive P_{PhaC} promoter and *bktB*, *phaB*, *crt3* and *ter_{TD}* under control of the constitutive P_{PhaP} promoter, on two different plasmids.

The benefits and disadvantages of the Δ 4 mutant strain compared to the wildtype were investigated in **Chapter 3.2.3**, indicating that the benefits of a streamlined 3-HP production in the early pathway could potentially outweigh the disadvantages of lower biomass formation.

In the experiment described here, *C. necator* Δ 4 and the chosen pathway was optimised further to enhance the obtained yield. The pathway was united on one plasmid (pMTL71301, Tet resistant) in the configuration shown in **Figure 3.13** according to the reasons explained in **Chapter 3.2.1.1**. The pathway was transformed in a *C. necator* Δ 4 background, resulting in the formation of strain CN22 Δ 4.

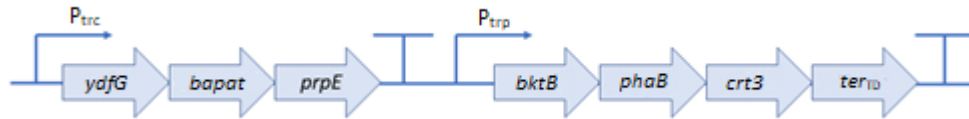


Figure 3.13 Configuration of the final 5-hydroxyvalerate producing pathway. The pathway genes were cloned into pMTL71301 plasmid and consisted of *ydfG*, *bapat* and *prpE* under the control of the constitutive P_{trc} promoter and *bktB*, *phaB*, *crt3* and *ter_{TD}* under the control of the constitutive P_{trp} promoter. The natural ribosomal binding sites of all genes in the assembly were removed and replaced by synthetic RBS sites of equal strength. The name within the arrows stand for the encoded proteins

Figure 3.13 shows the final assembly of the pathway on the pMTL71301 vector that was used in previous experiments for the expression of the genes *ydfG*, *bapat* and *prpE*. It was selected over pMTL74111 because of a higher inferred plasmid stability in growing cell fermentations that exceed 48 h. Characterisation experiments of *C. necator* H16 conducted by López [75] have shown that the bacterium is most susceptible to tetracycline, followed by chloramphenicol. In practice, *C. necator* H16 had to be grown in the presence of 50 mg/mL chloramphenicol, a concentration twice in excess of what is used in *E. coli* [75]. It was observed that in some long-term experiments that were designed to test the ability of *C. necator* H16 to metabolise different carbon or nitrogen sources, control strains inoculated at OD_{600} 0.5 without vector, would sometimes grow in the presence of chloramphenicol after 48 to 100 hours of fermentation. While seldomly occurring in practice, evolution of chloramphenicol resistance was observed, while tetracycline resistance was not. To avoid problems with plasmid loss, the vector conferring the tetracycline resistance was chosen.

C. necator CN22Δ4 were grown on CNMM^{Tet,Cm} minimal medium plates and single colonies used to inoculate precultures. The precultures were grown in 10 mL CNMM^{Tet} minimal medium at 30 °C to an OD₆₀₀ of 0.7. The cells were used to inoculate fresh 25 mL CNMM^{Tet} medium to an OD₆₀₀ of 0.1, which was supplemented by 20 mM β-alanine (or unsupplemented as negative control). In addition, an empty pMTL71301 vector control (CN23Δ4) was used. The experiment was conducted in biological triplicates and two independent technical duplicates for a total of 6 data points for each timepoint. The cells were grown in 250 mL baffled flasks at 30 °C for 60 h and timepoints of the supernatants were taken and analysed by LC-MS.

In unsupplemented controls and empty vector controls, no 3-HP or 5-OHV production could be detected (data not shown). In supplemented controls, as shown in **Figure 3.14 (A)**, gluconate was exhausted within the first 12 hours of the fermentation and was used to generate biomass.

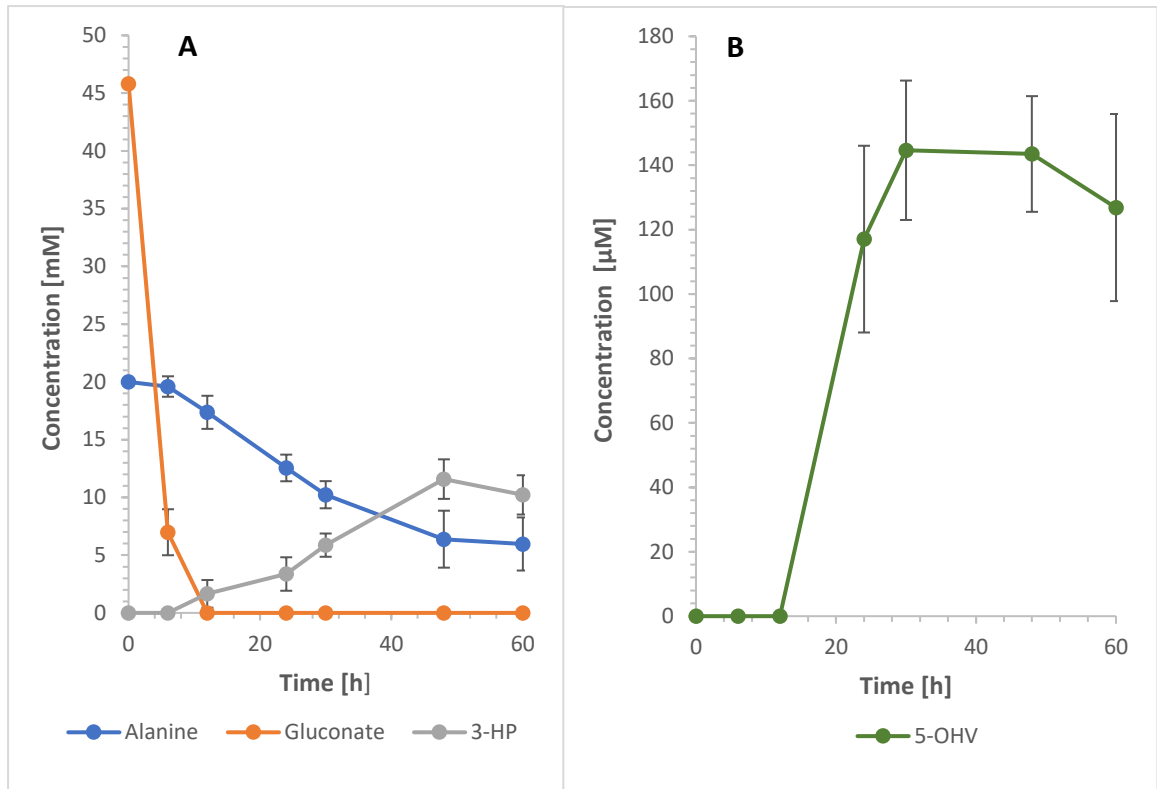


Figure 3.14 Quantified levels of pathway relevant metabolites during 60 h fermentation of 20 mM β -alanine supplemented *Cupriavidus necator* H16 strain CN22 Δ 4. (A) Detected levels of gluconate (orange), β -alanine (blue) and 3-HP (grey). (B) Detected levels of 5-Hydroxyvaleric acid (green). Biological triplicates and independent technical duplicates were used to generate this chart. All measurements were obtained by LC-MS from supernatants.

During this initial growth phase, the production of 3-HP from β -alanine is very low (2 mM at most), which could be due to a repression of β -alanine uptake which is normally not a preferred energy source for growth in *C. necator* H16. Once gluconate was depleted after 12 h, the conversion of β -alanine to 3-HP follows roughly a 1:1 molar relationship up until the 48 h timepoint. Interestingly, 3-HP production stops, which was not anticipated.

Figure 3.14 (B) shows the production of 5-hydroxyvaleric acid, which begins after 12 h and ends at the 30 h timepoint. Again, the lack of reductive power to drive flux through the reversed beta-oxidation pathway may be a possible

explanation. 5-OHV production peaked at a concentration of 145 μM . After the end of the production phase, 5-hydroxyvaleric levels remained stable for 30 h until the end of the fermentation experiment, suggesting that an adequate time window exists, during which 5-hydroxyvaleric acid is not degraded.

3.3 Discussion

3.3.1 5-OHV production in *Escherichia coli* and analytical challenges

From an analytical perspective, the results shown in **Chapter 3.2.1**, specifically **Table 3.1** and **Table 3.2** relating to pathway intermediate detection show no particular advantage of analysing intracellular fractions for the presence of the three analytes. Accidental contamination of the intracellular sample with supernatant is a frequent issue during the extraction process. Intracellularly, β -alanine cannot be distinguished from L-alanine with the used LC-MS methodology and is the most frequent false positive peak, present in all samples. Hence, its presence could not be unambiguously detected. Dietzen et al. [303] have shown that isomeric amino acids such as L-alanine and β -alanine are generally well distinguishable in mass spectrometers by fragmenting the molecules and detecting unique fragments. An implementation for such a method was attempted for the Orbitrap-type Q-Exactive mass spectrometer with the help of Salah Abdelrazig (University of Nottingham), however it was deemed unhelpful for analysis due to insufficient resolution between the peaks using bacterial sample preparations.

Two cultures stood out from the others that were tested, EC11 and EC12, as the only 5-hydroxyvalerate producing *E. coli* strains, which makes the two described biosynthetic pathways prime testing candidates for a novel 5-hydroxyvalerate production in *C. necator* H16. Apart from expressing a different *ter* gene, these two strains expressed the exact same combination of genes for all other pathway steps, singling out a most effective choice from all

proposed combinations. Conclusively, an effective pathway carried *ydfG*, *bapat* and *prpE*, excluding *pct* from further consideration. It also carried *bktB*, *phaB*, *crt3* and any *ter*, excluding *fadAB* and the proposed (*S*)-steriospecific pathway in *E. coli*. The exclusion of the *S*-specific pathway meant that the enzymes Hbd and Crt, as described previously by Cheon et al. [260] in the production of a C6 compound via reversed beta-oxidation, did not work as intended in *E. coli* in this study.

In the case of Pct, the propionate CoA-transferase native to *C. necator* H16, different reasons could be responsible for its poor performance in *E. coli*. Firstly, it may simply be a poor choice for the reaction at hand, although previous research has shown broad substrate specificity [241, 242]. Secondly, it may be poorly expressed in *E. coli* due to a number of reasons: the ribosome binding site may be weaker in *E. coli* than in its native host or the unoptimized codon usage may slow down translation of the RNA. Thirdly, the enzyme could be expressed, but inefficient in *E. coli* due to poor folding or unexpected inhibition by a metabolite that is not present in *C. necator*. While the top-down approach did not warrant an inquiry into the exact causes of the poor performance in *E. coli* in the light of a suitable alternative, further experiments with *pct* in *C. necator* will show if it performs better in its native host.

In the case of the underperforming *S*-specific pathway, the proposed enzymes were both only inferred to catalyse the chosen reactions *in-silico* and have only once been used in a study [260]. Despite the high uncertainty, the enzymes were selected for expression because they would offer a simple way of bypassing any side-reactions during the reverse-beta-oxidation cycle, because

all *S*-intermediates would have been biorthogonal and thus not recognised by promiscuous enzymes.

The allure of bio-orthogonality in synthetic biology is described well by the words of Carolyn R. Bertozzi from a time when synthetic biology itself had yet to be firmly established as its own field. As a chemist, she was interested in how “target biomolecules could be rendered chemically unique within biological settings such that probe molecules might be delivered by the selective formation of covalent bonds”, and asks: What if “the target structure was relatively simple but the environment in which the necessary reactions must proceed was so chemically complex and uncontrollable that no two functional groups could combine reliably and selectively under such conditions?” [304]. It appears that after two decades of addressing her challenges through the use of *bio-orthogonality of chemical reactions*, metabolic engineers face the same challenges in controlling *in-vivo* reactions and turn to *bio-orthogonality of pathway intermediates* to resolve theirs [305].

Unfortunately, this idea had to be discarded in view of the underperformance of the (*S*)-specific pathway. It was not possible to determine if only one, or both enzymes failed, as none of the intermediate analytes could be detected in LC-MS. All attempts failed given the short half-life of CoA derivatives and the possibility of rapid oxidation. None of the predicted masses could be detected. Methods for acyl-CoA detection have been published, for example by Yang et al. [306], but they would require a different extraction method (acetonitrile extraction) and column (C18 column). The most relevant study for acyl-CoA detection in bacteria by Zimmermann et al. relied on an untargeted MS/MS

method which described an extraction protocol that had to be carried out at -80 °C because of the instability of the compounds [307]. For this study, an extraction of acyl-CoAs and an untargeted detection approach was attempted, but failed (not shown).

Conservatively, at this point, a synthetic biologist would troubleshoot the pathway and confirm expression and solubility of the failed enzymes by SDS-PAGE. In a top-down approach these troubleshooting and optimisation steps are omitted and the failed variants are simply discarded from any further investigation to streamline the process.

In the case of *fadAB*, the complication of having to form oligomeric structures before activity sets in may have contributed to the poor performance in *E. coli*. Furthermore, as a constituent of the fatty acid biosynthesis machinery, *fadAB* may be tightly regulated both on gene and protein level and inactive under the tested fermentation conditions. Its conserved chromosomal copy is regulated by the fatty acid metabolism regulator protein FadR [308]. Long chain acyl-CoAs inhibits binding of FadR to its operator site which starts transcription of beta-oxidation related genes. Introducing a large amount of deregulated FadAB copies may confuse the regulatory network and deregulate membrane fluidity homeostasis [309]. Because of the complexity of any further troubleshooting and the existence of the working combination of PhaB and Crt3, FadAB was also discarded as a candidate for the pathway. Furthermore, a lower maximum OD₆₀₀ of the cultures harbouring a plasmid copy of *fadAB* was observed and no 3-HP could be measured in the supernatant, strengthening the case against FadAB.

In summary, for *E. coli*, β -alanine, 3-HP and 5-OHV could be detected in both supernatant and intracellularly. Quantification of the supernatant is more accurate than intracellular quantification, which is prone to cross-contamination issues during extraction. All other intermediates could not be detected with the chosen method or not targeted.

The combination of pOHV2 (pMTL71301-*P_{phaC}-ydfg_{EC}-bapat_{CV}-prp_{EEC}*) with pOHV5 (pMTL74111-*P_{phaP}-bkt_{CN}-pha_{B_{CN}}-crt3_{CN}-ter_{TD}*) or pOHV6 (pMTL74111-*P_{phaP}-bkt_{CN}-pha_{B_{CN}}-crt3_{CN}-ter_{EG}*) yielded 5-hydroxyvaleric acid. These were the only transgenic strains that produced 5-hydroxyvaleric acid in *E. coli* fermentation, narrowing down the number of potential candidate pathways in *E. coli* from 20 to 2.

In terms of the differences in performance between strains harbouring plasmids expressing *prpE* and *pct*, *ter_{TD}* and *ter_{EG}* and the stereospecific (*S*-) and (*R*-) variants of the reverse beta-oxidation pathway, only constructs with *prpE* led to successful priming 3-HP, *pct* constructs did not, under otherwise same conditions. Strains harbouring genes of both *ter_{TD}* and *ter_{EG}* yielded 5-OHV acid and it is concluded that both are equally suitable for use in the pathway. *phaB* and *crt3*, coding for integral enzymes of the engineered reverse-beta oxidation part of the pathway, outperformed the putative (*S*)-stereospecific pathway variants, which yielded no 5-hydroxyvaleric acid production. *fadAB* harbouring strains did apparently not catalyse the reverse beta-oxidation, either.

Very recently, 5-OHV production was achieved by Cen et al. [310] and Wang et al. [311] in *E. coli* using the previously (discussed L-lysine/5-AV/5-OHV

pathway. Thus, this study describes a new novel pathway for 5-OHV production in *E. coli*. Wang et al. [311] produced 690.8 mg L⁻¹ from L-lysine, levels much higher than the 1.95 mg L⁻¹ achieved in this study. Cen et al. achieved an even higher level, at 1.05 g L⁻¹ from glucose, using an L-lysine overproducing strain [310]. It should be noted though, that while the levels in this study are significantly lower than those reported in literature using other pathways in *E. coli*, the ultimate aim of this study is to further understanding of novel pathway variants, synthetic biology approaches and implementation of pathways into *C. necator* H16 for syngas utilisation, and not to compete over yields achieved through different means.

3.3.2 5-OHV production in *Cupriavidus necator* H16 and the transferability of results obtained in *Escherichia coli*

The results shown in **Table 3.2** confirm the previous findings by Orol [144] and other members of the research group. Previous research by López [75] has shown that the $\Delta 4$ mutant produces 3-HP better than the wildtype. This result could be replicated in this study and it was shown that 5-OHV was also produced more efficiently than in the *C. necator* H16 wildtype (see **Table 3.2**).

The only deletion mutant strain that failed to accumulate 3-HP was CN15 $\Delta 4$, which, analogous to previous results in *E. coli*, did not reach the same maximum OD₆₀₀ as the other strains (see appendix for growth curve). If *fadAB* indeed mediated a toxic effect, then it did not adversely affect cultures EC5 and EC6, which also carry it (**Table 3.3**). How exactly a potential toxic effect of *fadAB* could be mediated is speculation, but an interference with the fatty acid biosynthesis of *C. necator* H16 may be one explanation.

A false positive 3-HP signal possibly stemming from lactate was also detected in unsupplemented negative control cultures CN1, CN8, CN12 and CN21 during the single-flask experiment. When CN1, CN12 and CN21 were repeated in triplicates, adequate oxygenation of the culture flasks prevented a built-up of lactate which likely caused the overlapping peak for the first fermentation run and no 3-HP peak was detected anymore.

When compared to previous experiments conducted using *E. coli* the results in this work indicate that 3-HP production is feasible with YdfG and BAPAT in both organisms. As shown by López et al. ,the triple *C. necator* H16 $\Delta mmsA1$

$\Delta mmsA2 \Delta mmsA3$ deletion strain is unable to degrade 3-HP and performs better in terms of 3-HP production, while the wildtype strain performs poorly [110]. Previous research by López et al. [110] also showed the benefits of the $\Delta phaCAB$ knock-out strain on overall yields concerning the carbon metabolism in *C. necator*, which is due to the disruption of the carbon storage mechanism of the bacteria, which enables more flux towards a desired product. When the benefits of the *C. necator* H16 $\Delta mmsA1 \Delta mmsA2 \Delta mmsA3$ mutant are put in addition to the benefits of the $\Delta phaCAB$ knockout, it becomes evident that the $\Delta 4$ strain that was tested in this Chapter is the best option for the engineering of a pathway that builds on 3-HP production in *C. necator* H16.

Analogous to the previous results in *E. coli*, 5-hydroxyvaleric acid production was only observed in cultures carrying the transgenic (*R*)-specific reverse beta-oxidation chain elongation mediated through PhaB and Crt3, but not the (*S*-) enantiomeric pathway. The (*S*-) specific crotonase Crt, which was used successfully in reverse beta-oxidation before [260], is as likely the culprit for this result as to assume that the (*S*-) specific pathway stopped because of the use of Hbd3, which was described for use in the production of n-butanol from syngas in *C. ljungdahlii* [312, 313].

Similarly, to *E. coli*, there is no observable preference between Ter_{EG} and Ter_{TD} . Both enzymes remain valid candidates for their role, however, Tucci et al. [314] reported a lower Ter_{TD} K_M -value for crotonyl-CoA compared to the values reported for Ter_{EG} at 30 °C, indicating that the enzyme gains affinity to its substrate at the ideal growth temperature for *C. necator* H16. The difference in K_M for crotonyl-CoA, with 68 μM reported for Ter_{EG} by Hoffemeister et al. [315]

at 37 °C to 2.5 μM of Ter_{TD}, at 30 °C is large enough to consider Ter_{TD} over Ter_{EG}, even if no data for Ter_{EG} at 30°C is available.

The original hypothesis, that Pct may outperform PrpE in *C. necator* H16 because it is a native enzyme, had to be rejected. While some strains with *pct* (CN1, CN2) produced 5-OHV, most producer strains carried *prpE*. This is a surprising result, given that in a previous study on the production of acrylic acid via 3-HP-CoA, Pct outperformed all 13 other candidates from multiple sources for the reaction in *C. necator* H16 [316]. This strengthens a new hypothesis that the addition of coenzyme A may be a rate-limiting step in the pathway and the priming through use of ATP by PrpE significantly improves the kinetics of the reaction at the expense of the overall energetic demand that the pathway puts on the cell for the synthesis of the desired end-product.

In line with previous results in *E. coli*, *bktB* was overrepresented in cultures where 5-hydroxyvaleric acid could be detected. Bktb normally functions in the synthesis of poly(beta-hydroxybutyrate-co-beta-hydroxyvalerate), a component of the PHB storage system under stringent response. It is likely that under fermentation conditions that trigger stringent response [317], such as nutrient limitation, the chromosomal copy of *bktB* and possibly *bktC* is upregulated and helps to produce 5-OHV in this context [251]. This could explain why *C. necator* H16 is generally more capable at performing this pathway than *E. coli* is. In comparison to PaaJ, BktB is also likely to be less specific for its main substrate than PaaJ is, as to allow a larger range of ω-hydroxy acids to be stored as copolymer in PHB granules. PaaJ on the other

hand is likely to be more specialised, even though it had been described to successfully drive reverse beta-oxidation cycles by Kallscheuer et al. [257].

Put together, the similarities of results between the *E. coli* experiments in shown in **Chapter 3.2.1** and the *C. necator* H16 experiments in **Chapter 3.2.2**, allow the conclusion that in case of this pathway set, the results between the two organisms are transferable. Namely, the performance differences of the (*R*-) pathway and the (*S*-) pathway; Ter_{TD} and Ter_{EG}; PrpE and Pct; and BktB and PaaJ.

It should also be noted that, relatively speaking, more *C. necator* H16 $\Delta 4$ cultures produced 5-OHV than *E. coli*. It is therefore advisable to continue the testing of a narrowed range of pathways directly in *C. necator* H16 $\Delta 4$ despite the more difficult handling. *E. coli* is well suited for high-throughput techniques, but *C. necator* H16 appears to be the better host for these biosynthetic pathways. However, it was observed during the fermentation experiments that the *C. necator* H16 $\Delta 4$ cultures reached their maximum OD₆₀₀ considerably slower than the wildtype (**Figure 3.10 (A)**) in an investigation conducted to measure its growth performance compared to the wildtype and the Δ *phaCAB* mutant. The benefits of a streamlined pathway in $\Delta 4$ mutants may thus be offset by a slow growth rate. However, given the current trend towards fast growing strains in industry [318], such a debilitating fitness disadvantage, if large, may also lead to the future exclusion of the $\Delta 4$ strain.

The pathway variant introduced in *C. necator* H16 is novel and the results shown in **Chapter 3.3.2** are the first example of successful production of 5-OHV

in *C. necator* H16. Previous successful attempts of 5-OHV production in bacterial hosts include the previously discussed works of Cen et al. and [310] and Wang et al. [311] in *E. coli* and a recently developed *C. glutamicum* strain by Sohn et al. [115].

In summary, the previous results in *E. coli* from **Chapter 3.2.1** have been shown to be translatable to *C. necator* H16. The previous selection of plasmids that yielded 5-OHV in *E. coli* also yielded the metabolite in *C. necator* H16. Furthermore, *C. necator* H16 an effective host for the novel biosynthetic pathway and outperforms *E. coli*. In the quadruple knockout mutant $\Delta 4$, up to five strains out of 20 produced 5-OHV, compared to only two *E. coli* strains, under the same conditions, but growth defects in $\Delta 4$ must be assessed in comparison to the $\Delta phaCAB$ and wildtype stains before a verdict can be made to select $\Delta 4$ as the main chassis strain for these pathways. Due to the qualitative nature of the results, a quantitative experiment was necessary to elucidate which pathway from this range of five candidate strains (CN1 $\Delta 4$, CN2 $\Delta 4$, CN11 $\Delta 4$, CN12 $\Delta 4$, CN17 $\Delta 4$) could yield the highest titer.

3.3.3 The fitness costs of synthetic pathways and *mmsA* knockouts in *Cupriavidus necator* H16

As shown by the previous investigation by López [75], and replicated in this study, the $\Delta 4$ knock-out mutant grows slower than the wildtype strain, and, akin to the $\Delta phaCAB$ mutant, to a lower final OD₆₀₀ after consumption of the limiting carbon source, as was shown in **Figure 3.10 (A)**. This effect is due to a change in optical properties due to the lack of light scattering PHB granules in the $\Delta phaCAB$ and $\Delta 4$ mutant strains. The consumption of gluconate shown in **Figure 3.10 (B)** also reflects the lower growth rate of the $\Delta 4$ strain in comparison to the other strains. While gluconate consumption was quantified by LC-MS, prior pilot experiments were showing agreement of values obtained by HPLC and LC-MS.

By knocking out *mmsA1*, *mmsA2* and *mmsA3*, the cells lose ability to consume 3-HP, making $\Delta 4$ an ideal chassis for 5-OHV production. However, this loss-of-function also applies to the original biological role of the three *mmsA* genes. According to research by López et al. [110] MmsA1 and MmsA2 act primarily on malonic semialdehyde, whereas MmsA3 acts on methylmalonyl semialdehyde and $\Delta mmsA3$ mutants were unable to grow on either valine or isobutyrate anymore. This suggests that the disruption of branched amino acid catabolism might be partially responsible for the growth defects observed. In the same study, MmsA3 was reported to have broad enough substrate specificity to degrade malonic semialdehyde, suggesting that $\Delta mmsA1$ and $\Delta mmsA2$ are not sufficient to stop 3-HP degradation.

Figure 3.11 showed that the growth defects and total biomass accumulation were reduced in productive pathways in comparison to the empty vector. This is to be expected, due to the energy demand of enzyme expression, plasmid fitness costs [319], metabolic burden of the pathways [320] or toxic effects of pathway intermediates or off-target products due to enzyme promiscuity, even at low concentration [321]. It comes as no surprise that the 5-OHV producing strain that was used grew slower and to lower OD₆₀₀ than the 3-HP producing strain due to these effects, as it carries a higher metabolic burden. Correlations between growth rate and production rate of compounds are a common problem in industrial applications of engineered strains [322]. On the other hand, plasmid fitness costs are unlikely to explain the difference given the relative similarity of the plasmids used for these two stains. It cannot be ruled out that toxic effects played a role, either.

One solution to this problem is to decouple growth and production by the use of resting cell culture as explained in the introductory **Chapter 3.1.9**.

In summary, the observed growth defects in *C. necator* $\Delta 4$ were investigated and compared to the wildtype and the $\Delta phaCAB$ mutant. While a noticeably slower growth occurred, the total biomass of *Cupriavidus* $\Delta 4$ was not significantly affected compared to the $\Delta phaCAB$ mutant. The slower growth is likely to be caused by disruption of branched amino acid catabolism. Furthermore, the impact of the pathway energy demand on the $\Delta 4$ mutant was investigated and showed a negative correlation between achieved total biomass and productivity of strains.

3.3.4 The resting cell condition for 5-OHV production in *Cupriavidus necator* H16 is unsuitable

The results shown in **Figure 3.12** show that β -alanine is converted to 3-HP. Even where 3-HP accumulation is low (CN12 Δ 4, CN14 Δ 4), β -alanine uptake remains equally fast as in strains in which it is consumed (CN11 Δ 4, CN17 Δ 4). This suggests that β -alanine uptake is a possible bottleneck for this pathway that could be addressed, despite considerable variation between different strains investigated. On the other hand, the β -alanine route may become accessible from central metabolism by ongoing research in *C. necator* H16 (Salinas et al., University of Nottingham, unpublished), therefore β -alanine uptake will not be an issue as 5-OHV would be produced from glycerol, sugars or syngas fermentation.

In the context of a fully working biosynthetic pathway, accumulation of intermediates such as 3-HP in the supernatant is undesirable, as it suggests the formation of a bottleneck or a rate-limiting step of the pathway, in which 3-HP consumption towards the final product does not occur as fast as the production of new 3-HP. This can potentially lead to leakage through side-reactions, as rising intracellular concentrations of 3-HP become a target for an equally rising number of promiscuous enzymes with otherwise negligible affinity for 3-HP. A possible solution to this problem could be the overexpression of *bktB* using either a bespoke promoter or a stronger, possibly synthetic, RBS sequence.

Figure 3.12 also shows that the previously qualitatively selected strains EC11 and EC12 were not only successful in *E. coli*, the identified gene combination also helped drive production of 5-hydroxyvaleric acid in *C. necator* H16 $\Delta 4$.

Quantitative analysis also alerts us to a new problem in this fermentation: 3-HP and 5-OHV cannot account for all the carbon in form of β -alanine that was initially provided to the cells. The bacteria are metabolically active but unable to reproduce. OD_{600} measurements throughout the experiment showed no measurable change in biomass, nor are the cells able to store excess carbon as PHB granules due to the $\Delta phaCAB$ knock out. This leaves only one logical explanation for the missing carbon: It was either fully oxidised to CO_2 or it was converted into a side-product of the fermentation. Further analysis of the highest detectable mass peaks (see appendix) could be caused by the accumulation of uracil. Because *C. necator* H16 has no direct pathway from β -alanine to uracil and also cannot significant use β -alanine as its sole nitrogen source as evidenced by the extremely slow uptake and metabolisation without a functional ongoing pathway by Orol [144], it would be unwise to dismiss the phenomenon as a side-reaction. Instead, it appears more likely that uracil is being synthesised using the pyrimidine biosynthesis pathway, allowing the resting cells to “vent” ATP and excess nitrogen in the process, as carbamoylphosphate synthesis, a prerequisite for the uracil synthesis pathway, requires ATP investment. However, to confirm this hypothesis, labelling experiments would have to be undertaken. Because uracil accumulation is only observed in *C. necator* H16 under the specific phosphate limited resting cell

conditions, it will remain unaddressed as an artifact of the fermentation conditions, as it should not pose a problem in continuous-fed reactors.

The previous qualitative results in *C. necator* H16 have suggested a specific metabolic pathway combination to efficient in 5-OHV production compared to other combinations. In line with this result, the quantitative results showed that this pathway yielded up to 16.5 μM 5-OHV in the supernatant after 24 h. The pathway with the highest titer was $P_{\text{phaC}}\text{-}ydfg_{\text{EC}}\text{-}bapat_{\text{CV}}\text{-}prp_{\text{EC}}$ in combination with $P_{\text{phaP}}\text{-}bkt_{\text{CN}}\text{-}pha_{\text{CN}}\text{-}crt3_{\text{CN}}\text{-}ter_{\text{TD}}$. Further engineering will focus on this particular pathway variant.

The fermentation of resting cells comes with positive and negative sides. On the positive, up to half (10 mM) of all available β -alanine (20 mM) could be converted to 3-HP and other metabolites within 24 hours. However, possible accumulation of uracil in the supernatant due to the fermentation conditions prevents stoichiometric conversion.

3.3.4 Stronger promoters and synthetic RBS sites boost 5-OHV production

The current literature describes the *in vitro* production of 4-hydroxyvaleric acid from levulinic acid using an engineered mouse succinic semialdehyde reductase [323]. In another study, phosphate-limitation was used to produce higher levels of the naturally occurring 3-hydroxyvaleric acid in a 3-HB copolymer in *C. necator* H16 [324]. In a third study published in 1972, Griffin and Trudgill [325] described the production of 5-OHV from valerolactone in an *in-vitro* assay using a cell extract of *Pseudomonas* sp. *NCIB 9872*, showing that 5-OHV is an intermediate of the cyclopentanol degradation pathway in their organism of interest. Very recently, advances towards microbial fermentation of 5-OHV were made by the previously mentioned works of by Sohn et al. [115], Cen et al. [310] and Wang et al. [311]. However, to date, this study shows the first microbial production of 5-OHV in an engineered *C. necator* H16 strain.

The *C. necator* H16 $\Delta 4$ strain CN22 $\Delta 4$ shown in **Chapter 3.2.4** accumulated 11.6 mM 3-HP and 145 μ M 5-hydroxyvaleric acid after 48 h of growing-cell fermentation from a total of 20 mM supplemented β -alanine, of which only 14.1 mM were metabolised. In comparison, the phosphate-limited resting cells with the unoptimized construct (**Chapter 3.2.3**) in *C. necator* H16 $\Delta 4$ strain CN11 $\Delta 4$, achieved a titer of only 16.5 μ M 5-OHV. This marks an 8.8 fold increase in yield due to all optimisations and a more suitable fermentation condition.

Interestingly, the experiment with CN11 $\Delta 4$, has also shown incomplete metabolisation of the supplemented 20 mM β -alanine, using 14.2 mM after 24h. This value is very close to the 14.1 mM in the growing cell experiment

shown in **Chapter 3.2.3**, suggesting a common limiting factor on β -alanine metabolisation. It also suggests that this unknown limitation is independent on the growth phase of the bacteria, as it occurred in both resting cells as well as growing cells, ruling out carbon source demand for growth as the limitation. Additionally, in experiments conducted by Orol [144], 50 mM β -alanine is fully converted to 3-HP in *C. necator* H16 $\Delta 4$ harbouring a construct for the expression of *ydfG* and *bapat* over the course of 48 h. This full conversion was achieved with 20 mM sodium gluconate in the medium, which is less than half of the amount used in this study (45.8 mM).

If a major nutrient limitation leading to limited reductive power can be ruled out as probable cause for the incomplete conversion, another possible explanation may be a toxic effect with a detrimental impact on either β -alanine uptake or conversion. Further investigation has to be conducted to find the cause of the incomplete conversion, which may emerge as an unwanted toxic product of a side-reaction, a problem with the growth medium (e.g. a depletion of micronutrients) or could be found in the previous studies, in which 3-HP quantification relied on a HPLC peak that possibly overlapped with lactate, leading to the report of higher values.

In summary, we have shown the first successful production of 5-OHV in an engineered *C. necator* strain. To achieve this, we tested pathway variants in *E. coli* (**Chapter 3.2.1**), validated the results in *C. necator* (**Chapter 3.2.2**), tested knock-out mutants for viability and selected a chassis (**Chapter 3.3.3**), resulting in the first quantifiable 5-OHV synthesis in *C. necator* H16 (**Chapter 3.3.5**) of 17,1 mg L⁻¹.

Building on this foundation, a number of synthetic biology techniques were employed for increasing the yield by a factor of 8.8. These techniques included the use of stronger promoters, synthetic RBS sites and a unified pathway design that relies on only a single plasmid, rather than two, using the better selective marker.

Chapter 4

**Metabolic engineering of *Cupriavidus necator* H16
for 5-aminovaleric acid production**

Chapter 4 - Metabolic engineering of *Cupriavidus necator* H16 for 5-aminovaleric acid production

4.1 Introduction

4.1.1 5-AV toxicity and degradation in *Cupriavidus necator* H16

5-AV is a platform chemical and has industrial applications in the synthesis of nylon-5 [130]. This work aimed to present a sustainable synthesis route to 5-AV in *C. necator* H16, that would allow the nylon monomer to be produced through central metabolism.

In a similar top-down approach as shown in **Chapter 3**, this work aimed to investigate if *C. necator* H16 was a suitable host for 5-AV production by means of a toxicity test. Toxicity of a desired product compound can be a major hurdle for the production process and require considerable efforts to address, especially during down-stream processing, where the toxic product has to be removed from the medium as efficient as possible to keep concentrations during continuous fermentation below the toxic threshold. For example, *S. cerevisiae* strains used for sugarcane-based production of bioethanol need to be adapted either through breeding or genetic engineering to cope with stressors such as high ethanol concentrations [326]. As no data on 5-AV toxicity towards *C. necator* H16 or other related bacteria were described in the current literature, a toxicity test appeared necessary.

Furthermore, this work aimed to investigate if *C. necator* H16 possesses the ability to use 5-AV as carbon and nitrogen source for growth. 5-AV uptake and degradation would have to be addressed in the final production strain and the

knockout of potential product degradation pathways had been pointed in the literature [327]. A relevant 5-AV degradation pathway in *P. putida*, the AMV pathway [137-139], involves the 5-AV aminotransferase DavT and has been discussed in **Chapter 1.6.1**. A homologue, GabT, exists *C. necator* H16, which was investigated by Orol [110]. Therefore, 5-AV degradation was considered a possible outcome in *C. necator* H16 and required investigation.

4.1.2 Deregulation and optimisation of the *Cupriavidus necator* H16 L-lysine biosynthesis pathway

The biosynthetic pathway routes for L-lysine were described in **Chapter 1.6.2**.

L-lysine overproducing bacterial strains that were described in the literature were developed in *E. coli*, *Co. glutamicum*, *Brevibacterium flavum*, *Brevibacterium lactofermentum*, *Corynebacterium lilium* and *Brevibacterium divaricatum* but not for *C. necator* H16 [328].

Typical strategies for L-lysine overproduction were aimed towards overexpressing relevant genes of L-lysine synthesis pathway from aspartate and this work intended to follow a similar strategy for *C. necator* H16.

A second typical strategy described for overproducing strains was the incorporation of the bypass route for L-lysine production using the enzyme DAPDH (see **Figure 1.9**, pathway IV) [329]. The corresponding gene encoding DAPDH, *ddh_{CG}* was derived from *Co. glutamicum*, a microorganism that is used in industrial production of L-lysine [330-334].

A third strategy for L-lysine overproduction shown in the literature aimed towards the optimisation of the pathway by introducing mutations to key enzymes with negative feedback inhibition for a fully deregulated pathway [335].

A last strategy that will be employed in this work was to attempt to enhance the 5-AV yields by using synthetic promoters and RBS sites, a technique that had resulted in a significant increase in yield for 5-OHV acid, shown in **Chapter 3**.

4.1.3 Antimicrobial activity of 5-AV and 5-AV degradation

To investigate if *C. necator* H16 is a suitable host for 5-AV production, it had to be shown whether the presence of 5-AV has a toxic effect on cell growth. Ideally 5-AV should not affect bacterial growth at concentrations expected to be achieved in bioreactors. The MIC (minimal inhibitory concentration) methodology for toxicity tests is based on growth curves and of such historical importance, that it is established as by far the most common approach to measure antimicrobial activity of a compound [336]. An alternative approach is based on the so-called “kill-curve” and, for example, plots optical density over time to a constant antibiotic concentration in grown cells. This dose-response experiment is aimed to determine the minimal concentration of a substance that is needed to kill all (or a predefined percentage) of bacteria over a period of time [337].

To test if a compound shows bactericidal or bacteriostatic properties, micro-fermentation platforms can be used to measure the change in optical density over a period of time. Toxicity tests based on bacterial growth were usually designed as micro bioassays [338] but can be also be used to simply measure an antimicrobial effect in general. Typically, lysis due to an antimicrobial effect results in a decrease of optical density or growth attenuation and can thus be tracked by OD₆₀₀. Even if shown non-toxic to *C. necator* H16, it had to be established if *C. necator* H16 readily metabolises 5-AV. The easiest way to test uptake and metabolisation of any compound was to supplement the chemical as the sole carbon or nitrogen source in a minimal medium and observe if growth occurs.

4.1.4 *Cupriavidus necator* H16 quorum sensing

To help understand and interpret results of planned experiments involving 5-AV uptake and metabolism, the *C. necator* H16 quorum sensing system must be introduced. A general introduction to bacterial quorum sensing was given in **Chapter 1.7**. This introductory subchapter is meant to detail the topic of quorum sensing in *C. necator* H16 specifically. It may seem at first glance unrelated to metabolic engineering, but plays an important role in how bacteria behave in fermentation cultures.

Quorum sensing enables bacterial cells to intercommunicate and is mediated through the exchange and perception of signalling molecules, which lets them act as a collective rather than as individuals [339]. Coordination and synchronisation then enable the bacteria to achieve collective tasks, such as biofilm formation and bioluminescence [340], producing secondary metabolites as a community [341], or modulate virulence [342], to name some examples.

Typically, in gram-negative bacteria (such as *C. necator* H16), the responsible signalling molecules (autoinducers) are small molecules and are sensed through either cytoplasmatic transcription factors or transmembrane histidine kinases to which they can bind [343]. The resulting complex then drives the expression of genes under quorum sensing control [343]. Garg et al. [344] have shown that *C. necator* H16 possesses a functional Phc cell density sensing system with orthologs of the PhcB enzyme that produces the autoinducer 3-hydroxypalmitic acid methyl ester and the corresponding sensor kinase PhcS. However, they

note that some functions that are under control of the Phc system in *Ralstonia solanacearum* (a relatively close relative of *C. necator* H16) are not affected in *C. necator* H16, such as siderophore upregulation, suggesting a different physiological function in *C. necator* H16 [344]. It is also known that *C. necator* N-1 (an even closer relative) possesses predicted orthologs of CqsA, the biosynthesis enzyme for the production of the autoinducer (S)-3-hydroxytridecan-4-one (often referred to as CAI-1) and the corresponding sensor kinase CqsS. Additionally, an ortholog of the *E. coli* GABA transporter GabP is present at H16_B1890. GABA is known to be a modulator of quorum sensing in *Agrobacterium tumefaciens* [345] and, to a lesser degree, in *Pseudomonas aeruginosa* [346].

Preliminary work by López [75] and Salinas (University of Nottingham, unpublished) have demonstrated that *C. necator* H16 shows preference in uptake of different carbon sources. It remains to date unknown if these nutrient source preferences are influenced by quorum sensing or not.

4.1.5 5-AV biosynthesis pathways

L-lysine biosynthesis and degradation have been discussed in **Chapter 1.6**. By combining the biosynthesis pathway of L-lysine and the AMV degradation pathway found in *P. putida*, 5-AV biosynthesis from central metabolism can be achieved. Several successful 5-AV producing bacteria strains have been reported in literature.

Liu et al. [129] described the *in-vitro* production of 5-AV using purified DavA and DavB from L-lysine. Li et al. [347] described the production of 5-AV using the same reactions *in vivo*, using *E. coli* cells expressing a GABA transporter (for 5-AV export) and a L-lysine permease (for L-lysine import). Rohles et al. [348] described the introduction of the DavA/DavB mediated 5-AV biosynthesis pathway into *Co. glutamicum*, a natural L-lysine overproducer with a yield of 28.5 g L⁻¹ 5-AV. Park et al. [123] used a high-density resting cell culture of a recombinant *E. coli* L-lysine producer strain at OD₆₀₀ of 60 to fully convert 60 g L⁻¹ L-lysine to 5-AV in 24h. Previously, Park et al. [124] had shown direct production of 5-AV from glucose in OD₆₀₀ = 12 growing batch cultures to a titer of 2.3 mM with *E. coli* strain XQ56, another L-lysine producer strain. In parallel, research by Adkins et al. [349] achieved a titer of 7.3 mM from 25 g/L glucose using engineered *E. coli* GW25113 cells (optimised for cadaverine production through L-lysine). These were expressing the “naturally lysine insensitive” (e.g. feedback-resistant) dihydrodipicolinate synthase DapA from *Co. glutamicum* and carried the T352I aspartate kinase III (*lysC*) mutation to eliminate feedback resistance [349] (**Figure 4.1**). In the same work, *E. coli* BW25113(DE3) was used under resting cell conditions to produce 5-AV from L-lysine, suggesting that

higher yields were possible using a resting cell condition. Notably, they did not use the resting cell assays for the production of 5-AV from glucose in *E. coli* BW25113(DE3) $\Delta cadA \Delta ldcC$ pCDF-lysC^{fbr}-dapA^{fbr} but instead opted for a growing cell assay [349].

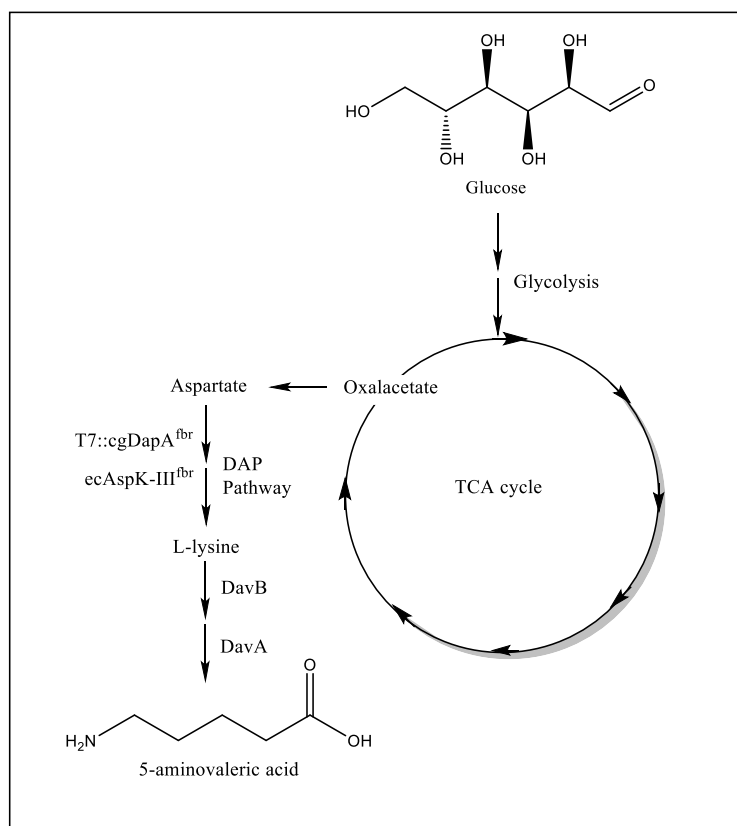


Figure 4.1 Metabolic pathway for the production of 5-AV from glucose in *E. coli* as used by Adkins et al. [349] Glucose is metabolised through glycolysis and enters the TCA cycle. Anaplerotic reactions must refill the TCA cycle as oxalacetate is converted to aspartic acid. A feedback-resistant mutation in the Aspartate Kinase III results in efficient priming to aspartylphosphate, the committing step into the DAP pathway for L-lysine synthesis. A feedback resistant dihydrodipicolinate synthase gene is expressed under the control of a T7 promoter from a vector. The Dav-pathway yields 5-AV from L-lysine. Adkins et al. used *E. coli* BW25113(DE3) $\Delta cadA \Delta ldcC$ pCDF-lysC^{fbr}-dapA^{fbr} for 5-AV production.

In their study, Atkins et al. [349] describe their preparation of the resting cells.

The cells are harvested after induction and growth and then resuspended at

high OD in PBS (phosphate-buffered saline), with the addition of “appropriate substances and Co-factors” [349]. In the case of L-lysine to 5-AV conversion these resting cell conditions equal a carbon-starvation resting cell format, because *E. coli* can utilise L-lysine as sole nitrogen source for growth, but not as sole carbon source [350]. Unfortunately, when using aspartate as feedstock, aspartate is readily used by *C. necator* H16. and *E. coli* as both nitrogen and carbon source (Salinas, University of Nottingham, unpublished) . For example, in *E. coli*, aspartate can re-enter the TCA cycle through fumarate. This can happen either by function of aspartate ammonia lyase encoded by *aspA* [351, 352] or by action of the enzymes encoded by *aspG and aspH* [353], which are part of the arginine biosynthesis pathway, or by PurA and PurB, which act in the purine nucleosynthesis pathway [354]. Thus, at the exclusion of carbon and nitrogen limiting conditions in aspartate-fed cultures, this work focused on phosphate-limiting conditions analogous to **Chapter 3.2.3** to investigate if the 5-AV titer in aspartate-fed cultures of *C. necator* H16 Δ *phaCAB* resting cells can be increased over the titer observed in growing cells - by decoupling the growth phase from the production phase.

4.1.6 The $\Delta gabT$ knockout may reduce 5-AV degradation *Cupriavidus necator* H16 $\Delta phaCAB$

A degradation pathway for 5-AV has been studied in *P. putida* and forms part of the Dav degradation pathway of L-lysine (**Figure 4.2**) [128, 141].

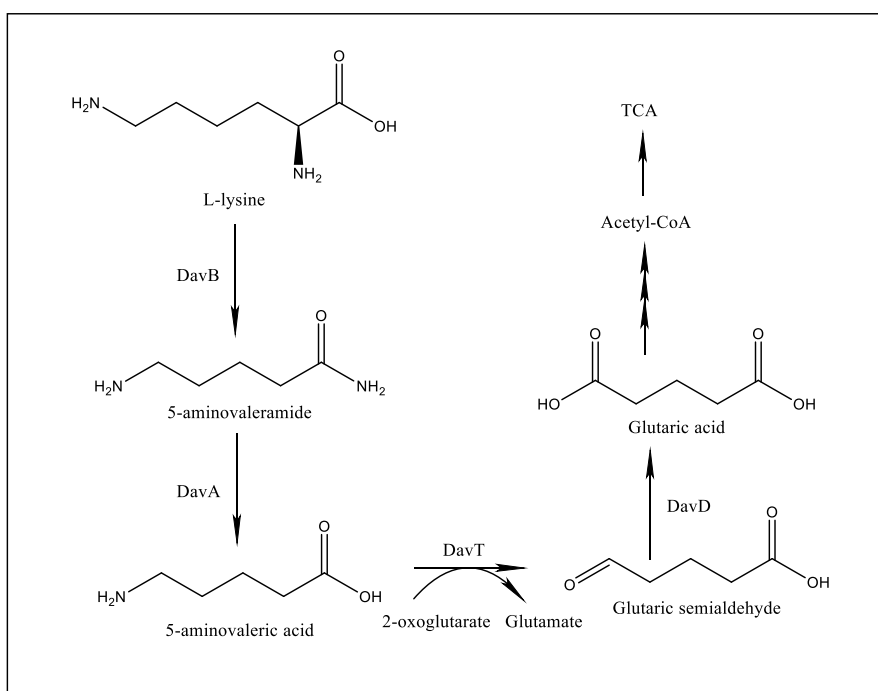


Figure 4.2 The Dav degradation pathway of L-lysine in *P. putida*. L-lysine is degraded to 5-AV by the catalysis of DavB (L-lysine 2-monooxygenase) and DavA (5-aminovaleramidase). 5-AV can be converted to glutaric semialdehyde by DavT (δ -aminovalerate aminotransferase; *C. necator* H16 homologue: GabT). The reactive semialdehyde is then converted to glutaric acid by davD (glutarate-semialdehyde dehydrogenase) and subsequently a degradation to acetyl-CoA leads into the TCA cycle.

The *davTD* operon in *P. putida* and the homologue *gabTD* in *Bacillus subtilis* are under control of the *gabR* regulator, which responds to GABA [124, 142, 143].

In *C. necator* H16, a *gabT* homologue was identified by Orol and knocked out in

the *C. necator* H16 $\Delta phaCAB$ strain, yielding the engineered *C. necator* H16 $\Delta phaCAB \Delta gabT$ strain, which was investigated in the context of a possible β -alanine degradation pathway but showed no affinity to β -alanine [144]. Research by Mayer et al. [355] on the *gabT* and *gabD* homologues in *C. necator* H16 revealed that they are active in the context of homotaurine degradation and *gabT* recognised homotaurine as a substrate. Homotaurine, GABA and 5-AV all share a common terminal amino group that is recognised as target for transamination by GabT, followed by an aliphatic chain of 3 (Homotaurine, GABA) or 4 (5-AV) carbon atom length and a terminal, negatively charged acidic moiety - sulfonic acid in case of homotaurine and a carboxyl group in case of GABA and 5-AV.

This may indicate the presence of a putative 5-AV degradation pathway in *C. necator* H16 to glutaric acid. Therefore, a knock-out mutant of the GabT homologue in *C. necator* H16 $\Delta phaCAB$ may yield higher 5-AV titers and stop the degradation pathway of 5-AV.

4.1.7 Engineering the *Cupriavidus necator* H16 L-lysine biosynthesis pathway

Given the premise that 5-AV is non-toxic in *C. necator* H16 and that the expression of the *P. putida* genes *davA* and *davB* lead to full conversion of L-lysine to 5-AV, and that product degradation can be prevented by use of the $\Delta gabT$ knockout mutant, a higher flux towards 5-AV production may be achieved by engineering the L-lysine biosynthesis pathway (see **Chapter 1**). This could supply higher intracellular concentrations of L-lysine for the Dav-pathway and form a link to central metabolism, which is a prerequisite for sustainable 5-AV production.

Such engineering efforts usually involve:

- (a) The introduction of non-native enzymatic reactions towards L-lysine
- (b) The overexpression of native and non-native enzymes of the established succinylating pathway
- (c) Knock-out of genes that drive side-reactions

The introduction of non-native enzymes includes some choices that have been discussed previously in the context of alternative biosynthetic L-lysine pathways in **Chapter 1**. The enzymes of the acetylating pathway are in theory suited to confer an additional flux towards L-lysine, but the pathway is too long to be easily cloned and introduced. The aminotransferase DAP-AT is also not suited for introduction because of its adverse kinetics. The introduction of the DAPDH dehydrogenase gene *ddh_{CG}* from *Co. glutamicum*, however, is an interesting target that can be introduced to *C. necator* H16.

In terms of overexpressing enzymes of the current native pathway, the aspartate kinase appears to be the ideal target. It catalyses the committing step towards L-lysine biosynthesis and the overexpression of it has been used a common metabolic engineering practice for L-lysine overproducing strains in various hosts [356-360].

Knock-outs in the context of L-lysine biosynthesis did not form part of further efforts to engineer *C. necator*, as the L-lysine biosynthesis pathway had no known major side-reactions that would redirect flux away from L-lysine biosynthesis that could be engineered. One side-reaction is the biosynthesis pathways for threonine and methionine, which are essential in *Cupriavidus sp.* The other side-reaction that occurs is the peptidoglycan biosynthesis pathway from *m*-DAP. It is an essential pathway for the formation of the bacterial cell wall and thus not a knock-out target either.

Apart from overexpressing a copy of the *Co. glutamicum* aspartate kinase and DHDPS, this work aimed to investigate if the introduction of feedback-resistant mutants of DHDPS and AK have an effect on L-lysine biosynthesis.

4.1.8 Engineering of L-lysine biosynthesis pathway regulation

L-lysine biosynthesis is regulated at key reactions. As the entry point of the L-lysine, methionine and threonine biosynthesis pathways, the aspartate kinase (AK) is negatively regulated by all three amino acids. Some bacteria have evolved separate copies of aspartate kinases which are feedback inhibited by only one end-product [361]. In a study published by Dong et al. [362], several aspartate kinase mutants from *Co. glutamicum* strain IWJ001 were investigated. *Co. glutamicum* is known to be one of the best overproducers in industry for L-lysine [363]. The strain IWJ001 was created by through mutagenesis and selection [364] for L-isoleucine production, which builds on overproduction of the L-threonine pathway. Aspartate kinase mutants were isolated and characterised, of which one, the AK (A279T) mutant, was found to be completely feedback resistant to L-lysine and L-threonine [362]. In this study, the native AK and the completely feedback-resistant mutant A279T from *Co. glutamicum* was introduced to *C. necator* H16 as a tool to funnel flux towards the L-lysine synthesis pathway.

A second key regulatory point is the formation of dihydropicolinate from aspartate semialdehyde, which is unique to the L-lysine biosynthesis pathway only. The dihydrodipicolinate synthase DHDPS encoded by *dapA* is feedback resistant to L-lysine and has been investigated especially in plants and bacteria. Studies in plants [365-368] have shown that DHDPS is very strongly inhibited by L-lysine at an IC₅₀ of ca. 0.05 mM. In *E. coli* and other gram-negative bacteria, DHDPS is much less feedback resistant compared to plants – by a factor of up to 100 [369-371]. In Gram-positive bacteria, such a *Co. glutamicum*, feedback

inhibition by L-lysine is even less pronounced or absent [372-375]. In a study published by Geng et al. [335], the allosteric inhibition of L-lysine on the *Co. glutamicum* DHDPS was investigated. It was shown that the mutation E84T into the *E. coli* DHDPS disrupted the allosteric binding of L-lysine to this residue on the protein, thereby disrupting feedback-inhibition without altering the kinetic parameters of the enzyme [335]. In a study by Motoyama et al. [376], introduction of a feedback-resistant DHDPS elevated DHDPS activity by a factor of 20 and resulted in higher lysine yields: 0.4 g/L obtained in wildtype *Methylobacillus glycogenes*, compared to 1.1 g/L with a feedback resistant DHDPS.

The earlier described DHDPS E84T variant confers L-lysine feedback resistance and is thus similarly deregulated as the the feedback resistant *Co. glutamicum* *dapA*. The amino acid change corresponds to residue T96 in the native *Co. glutamicum* DHDPS [377]. **Figure 4.3** shows a pairwise alignment of the native *E. coli* and *Co. glutamicum* DHDPS sequence using the standard settings of the EMBOSS Needle algorithm based on a Needleman-Wunsch pairwise alignment method [378].

```

1 MFTGSI-----VAIVTPMDEKGNVCRASLKKLIDYHVASG TSA    38
|.||..          ||:||||..|:|...|:|...|..|...|...|
1 MSTGLTAKTGVHEFGTVGVAMVTPFTESGDIIDIAAGREVAAYLV DKG L DS    50
                                     E84
39 IVSVGTTGESATLNHDEHADVMMTLDLADGRIPVIAGTGANATAE A IS L    88
:|..|...|...|...|...|...|...|...|...|...|...|...|...|
51 LVLAGTTGESPTTAAEKLELLKAVREEVGDRAKLIAGVGTNNTRTS V EL    100
                                     T96
89 TQRFNDSGIVGCLTVTPYYNRPSQEGLYQHFKAIAEHTDLPQIL Y NVPSR    138
:.....|..|..|..|..|..|..|..|..|..|..|..|..|..|..|..|..|
101 AEAAASAGADGLLVVTPYYSKPSQEGLLAHFGAIAAATEVPICL Y DIPGR    150

139 TGC DLLPETVGR LAKVKNIIGI KEATGNL TRV NQ- I K E L V S D D F V L L S G D    187
:|...|...|...|...|...|...|...|...|...|...|...|...|...|...|
151 SGIPIESDTRRRLSELPTILAVKDAKGD LVAATSLIKE---TGLAWYSGD    197

188 DASALDFMQLGGHGVISVTANVAARDMAQMCKLAAEGHFAEARVINQR LM    237
|...|...|...|...|...|...|...|...|...|...|...|...|...|...|
198 DPLNLVNLALGGSGFISVIGHAAPTALRELYTSFEEGDLVRAREINAKLS    247

238 PL---HNKLFVEPNPIPVKWACKELGLVATDTLRLPMTPTITDSGRET V RA    284
|| ..:| ..:..|...|...|...|...|...|...|...|...|...|...|
248 PLVAAQGRL---GGVSLAKAALRLQGINVGDPR LPI MAPNEQLEALRE    293

285 ALKHAGLL    292
.:|..|:|
294 DMKKAGVL    301

```

Figure 4.3 Pairwise alignment of native *Escherichia coli* DHDPS and *Corynebacterium glutamicum* DHDPS. Top row: *E. coli* DHDPS sequence, bottom row: *Co. glutamicum* DHDPS sequence. Alignment algorithm: Needleman-Wunsch. The T96 residue of the *Co. glutamicum* DHDPS maps to the E84 residue in *E. coli*. A E84T mutation of the *E. coli* DHDPS has been shown to confer L-lysine feedback resistance [377].

This shows that DHDPS variants with deregulated feedback inhibition, such as the *Co. glutamicum* DHDPS are attractive targets for inclusion in a deregulated *C. necator* H16 L-lysine biosynthesis pathway.

4.1.9 Aim of this Chapter

In summary, this Chapter aims to answer the following questions:

1. Does 5-AV exhibit a bacteriocidal or bacteriostatic effect towards *C. necator* H16?
2. Does *C. necator* H16 readily metabolise 5-AV as carbon or nitrogen source?
3. Does the Dav-pathway convert L-lysine to 5-AV in *C. necator* H16?
4. Does the resting cell condition optimise 5-AV yields in *C. necator* H16?
5. Does the $\Delta gabT$ knockout improve yields in *C. necator* H16?
6. Does the use of synthetic biology tools, such as stronger promoters and synthetic RBS sites optimise 5-AV yields in *C. necator* H16 $\Delta gabT$ $\Delta phaCAB$?

4.2 Results

4.2.1 5-AV has no significant bactericidal or bacteriostatic effect on *Cupriavidus necator* H16 wildtype

The work in this Chapter was carried out in shared contribution between myself and my undergraduate student Christopher Shave. While the design of the biosensor was my own work, he carried out cloning, culturing and protein purification under my direct supervision, while I supplied all analytical data for the project.

For the toxicity tests, *C. necator* H16 wildtype was grown to $OD_{600} = 1.5$ in rich (LB) medium, washed with minimal medium without phosphate (CNMM-P) and used to inoculate 0.5 mL micro-fermentation wells in a BioLector micro fermenter to a starting OD_{600} of approximately 1.5. Six wells were used for each fermentation condition, in which *C. necator* H16 was challenged with varying concentrations of 5-AV during resting cell fermentation. The concentrations used were 0 mM (control), 0.5 mM, 5 mM, 50 mM, 200 mM or 500 mM 5-AV. Due to the phosphate limitation, the cells would enter a resting state (as discussed in **Chapter 3**), while staying metabolically active due to the abundance of carbon and nitrogen in the medium. Toxicity can be measured as a decrease of optical density (OD) at 600 nm due to cell lysis. The cells were incubated at a constant temperature (30 °C), shaking (1200 rpm), humidity (85%) and O_2 (21%) values.

At the beginning and at the end of the experiment, samples were taken to measure colony forming units (CFU) after pooling of samples taken from the six

wells – essentially serving as second method to measure viability and to validate the results from the toxicity test.

Figure 4.4 shows OD_{600} over time of phosphate-starved resting cells of *C. necator* H16 that were inoculated at $OD_{600} = 1.5$ in CNMM-P and that were challenged with varying amounts of 5-AV to observe bactericidal effects.

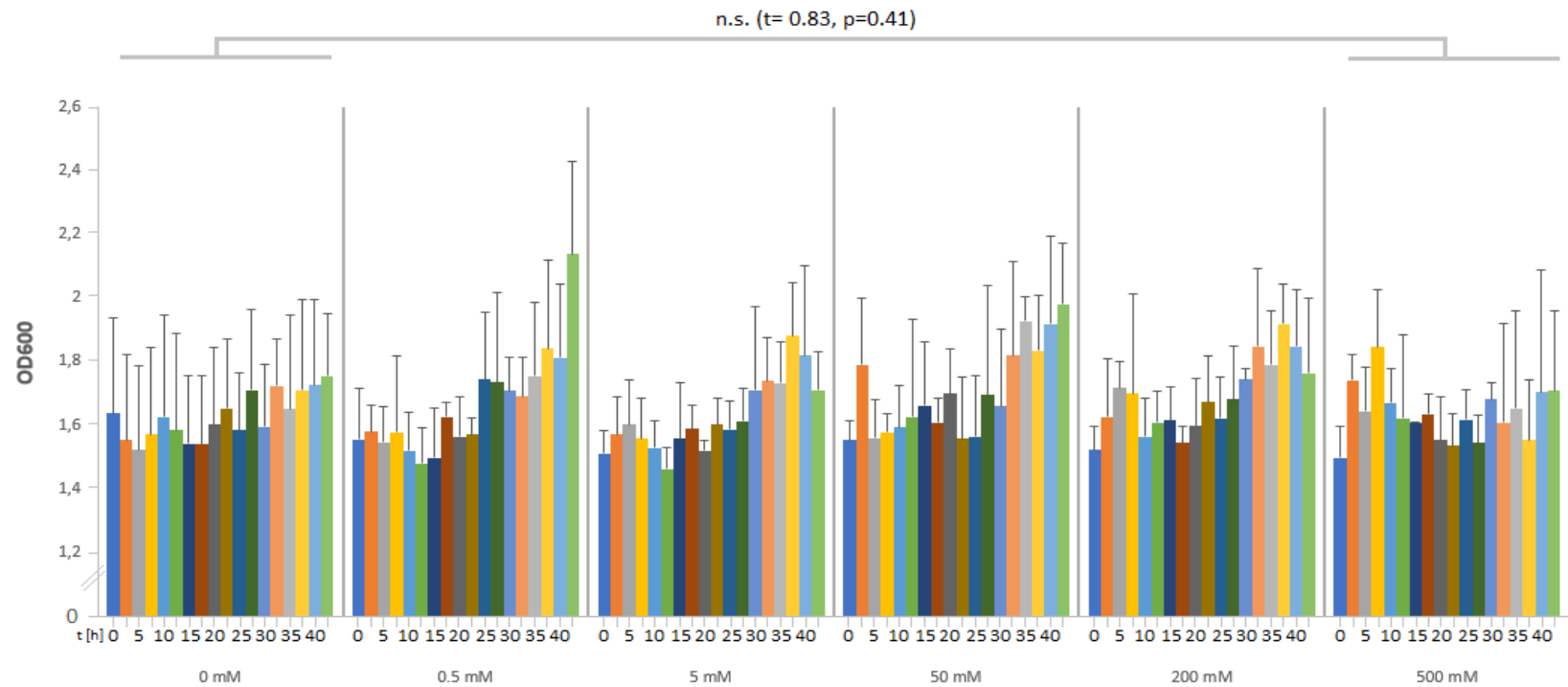


Figure 4.4 Optical density of resting cell *Cupriavidus necator* H16 micro fermentation cultures over 40 h in the presence of 5-AV in CNMM-P medium. Coloured bars: Timepoints taken every 2.5 h. Every bar represents the mean of OD₆₀₀ values from three to six fermentation wells. 6 sets of 5-AV concentration conditions were tested (left to right); 0 mM, 0.5 mM, 5 mM, 50 mM, 200 mM and 500 mM.

The results shown in **Figure 4.4** showed that the OD_{600} does not decrease under 1.4 in any experimentation condition, irrespective of the amount of 5-AV that was added. To quantify the results, a paired t-test weighted for varying sample sizes per condition was conducted between the extreme condition dataset with 0.5 M 5-AV and the unsupplemented control (0 mM) to test if the datasets show a significant difference from each other (for details on the calculation, see **Chapter 2.9.5**).

A t-value of 0.8289 was obtained for the Student's statistic and a corresponding p-value of 0.4087 \gg 0.05 assuming 137 degrees of freedom from the experiment data. This meant that the dataset 0 mM and the dataset 500 mM did not significantly differ from each other.

A detail that can be observed in **Figure 4.4**, is, that while optical density does not *decrease* over time, it appears to *increase*, sometimes to values up to 2.0. The cells do not divide in phosphate-free medium and while it cannot be completely ruled out that some phosphate was carried over despite the washes with CNMM-P, it is unlikely to result in such an increase of OD. Examination of the fermentation wells after the run revealed, that despite the use of sealing foils, some evaporation caused the total volume of medium in the well to decrease, leading to a higher optical density.

To test if the OD_{600} measurements correlate with the amount of colony forming units (cfu), samples of 5 μ L were taken before and after the fermentation and pooled for each condition, and additionally adjusted for the loss of liquid by evaporation. These samples were diluted, plated out and total amount of cfu

was measured. The ratios between the 0 h and 40 h cfu counts were calculated to be 0.91 (0 mM set) and 0.95 (500 mM set). This means that only a small number of cells (between 5% and 9%) died during the fermentation, with the number in the 500 mM sample set actually being lower than the control, meaning that, within margins of error, the conclusion from the experiments is that 5-AV is not significantly bactericidal.

4.2.2 5-AV shows no bacteriostatic effect on *Cupriavidus necator* H16 wildtype

To test if 5-AV might have a bacteriostatic effect, growth curves of *C. necator* H16 in the presence of 5-AV were obtained. *C. necator* H16 cultures were grown in 50 mL CNMM in shakeflasks from OD₆₀₀ of 0.1 to maximum OD₆₀₀ for 40 hours in the presence of 0 mM (control) and 500 mM 5-AV (very high concentration).

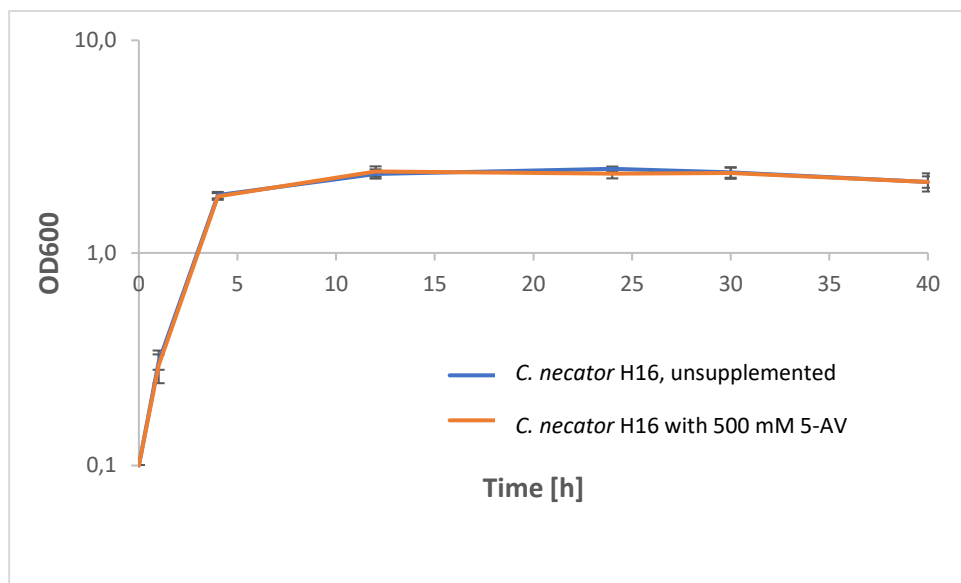


Figure 4.5 Growth curves of *Cupriavidus necator* H16 wildtype in CNMM medium with and without 5-AV supplementation over 40 h. *C. necator* H16 wildtype was used to inoculate CNMM medium at 0.1 OD₆₀₀ and grown for 40 hours. Blue curve, OD₆₀₀ of the unsupplemented cultures. Orange curve: OD₆₀₀ of cultures supplemented with 0.5 M 5-AV. All cultures were grown in biological triplicates and pH adjusted.

Figure 4.5 shows that the addition of 500 mM 5-AV (orange curve) does not change the growth kinetics of *C. necator* H16 in comparison to the unsupplemented control (blue curve). This allows to conclude that 5-AV has no bacteriostatic effect. Interestingly, despite the large amounts of nitrogen and carbon added to the supplemented cultures in form of 5-AV, no differences in

the reached final OD_{600} can be seen, meaning that 5-AV was not used to generate extra biomass.

4.2.3 *Cupriavidus necator* H16 adapts in 7 days to 5-AV as a nitrogen source and 10 days as a carbon source.

A long-term experiment was conducted, designed to test for 5-AV uptake and metabolisation. Here, *C. necator* H16 cultures were grown in 50 mL CNMM, CNMM-N and CNMM-C medium supplemented with 50 mM 5-AV and growth was observed over a long period of time. The use of nitrogen and carbon depleted media would facilitate the use of 5-AV as a nutrient source.

The *C. necator* H16 wildtype strain was grown in CNMM, pelleted, washed with water and transferred to 50 mL shake flasks containing three media conditions.

CNMM-N is a nitrogen depleted medium and 50 mM 5-AV were added as the only available nitrogen source. CNMM-C is a carbon depleted medium and was supplemented with 50 mM 5-AV as the only available carbon source. CNMM was used as a positive control condition (which is carbon limited at 45.8 mM C or 10 g L⁻¹ sodium gluconate). As a negative control the cells were added to PBS, a buffer without carbon or nitrogen source.

These media were inoculated with *C. necator* H16 in triplicates at a starting OD₆₀₀ of 0.2 and growth was observed and recorded for 14 days. In all cases (except the negative control), growth would not be observed gradually over the course of several days. The OD₆₀₀ would remain at 0.2 for several days after which cell growth was observed and measurements would stop.

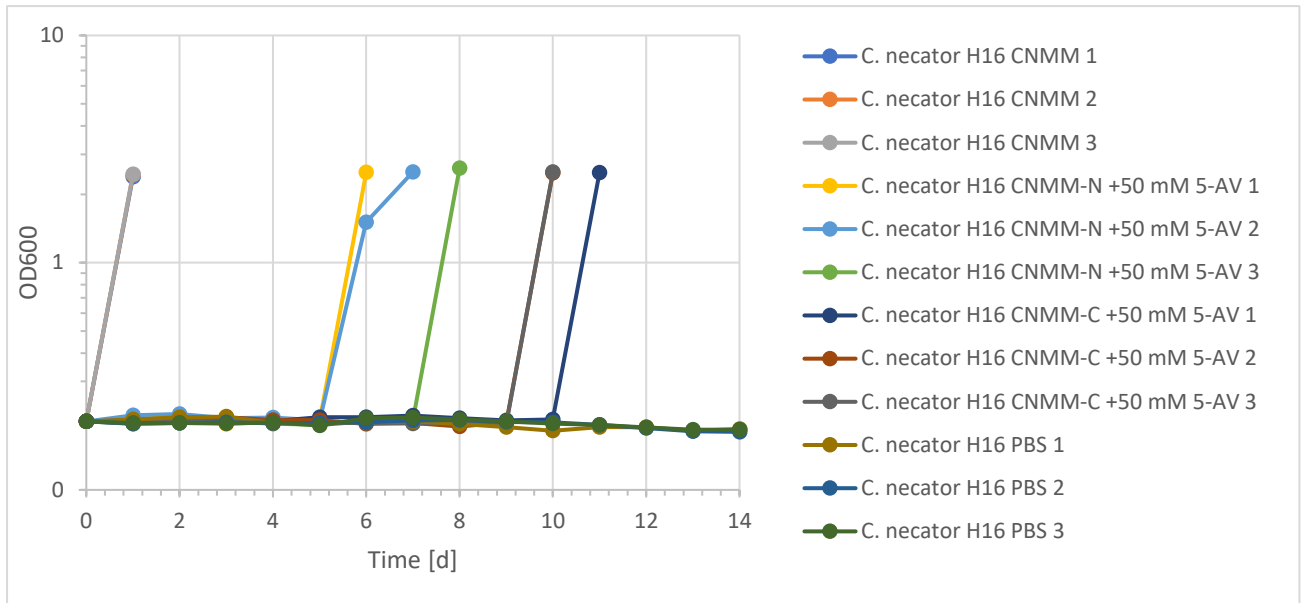


Figure 4.6 Growth curves of *Cupriavidus necator* H16 wildtype in limiting media conditions and 5-AV supplementation. Triplicate stains were aerobically grown in CNMM (positive control), CNMM-N +50 mM 5-AV (5-AV as sole nitrogen source), CNMM-C +50 mM 5-AV (5-AV as sole carbon source) and PBS (negative control)

Figure 4.6 shows that all three positive control strains grew on the first day of fermentation (orange, grey, blue). For the nitrogen-depleted cultures, (yellow, light blue and light green) the mean observed was 7.0 days for full growth and for the carbon-depleted cultures (dark blue, burgundy and brown) it was 10.3 days. None of the cells in the PBS negative control showed growth.

Interestingly, when these “adapted” strains were harvested, washed and used as inoculum for their adapted condition (e.g. grown in fresh medium), they would not immediately grow. Instead, they would need a roughly equal amount of time to re-adapt to the condition. Based on this observation, it was concluded that *C. necator* H16 has the ability of metabolising 5-AV as both sole

nitrogen and carbon source, but does so after an extensive period of adaption that spans between 7 and 10 days, which would not pose a problem for 5-AV production in batch fermentation. Chromosomal DNA was harvested from nitrogen adapted cultures and the adapted strains were attempted to be sequenced to find possible mutations that could have an impact in 5-AV uptake or metabolisation (see **Chapter 2.3.4** for details). A list of polymorphisms can be found in the appendix (**Appendix, Table A1**). Due to a lack of coverage, not all polymorphisms could be recovered. Furthermore, only the affected genes and the type of polymorphism were recorded, not the position of the SNPs (single nucleotide polymorphisms) or INDELS (insertions and deletions). This means that the sequencing data can only be regarded as a tentative, preliminary result. Only one potentially relevant SNP was detected, a Q626L mutant of a putative branched-chain amino acid transporter encoded on chromosome 2 (H16_RS28925).

4.2.4 DavA and DavB convert L-lysine to 5-aminovaleric acid in *Escherichia coli* and *Cupriavidus necator* H16

To test conversion of L-lysine to 5-AV, DavA and DavB from *P. putida* were cloned under control of the arabinose inducible P_{BAD} promoter in pMTL71301, a vector backbone that was previously used in **Chapter 3**. The vector replicates in both *E. coli* and *C. necator* H16 and confers tetracycline-resistance (**Figure 4.7**).

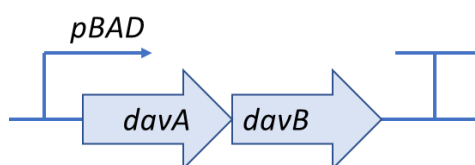


Figure 4.7 Vector pL1: Pathway for the production of 5-AV from L-lysine. *P. putida* *davA* and *davB* with native RBS sites are expressed under control of the IPTG-inducible P_{BAD} promoter on the pMTL71301 vector backbone. The names in the arrows stand for the genes encoding the enzymes of the pathway.

The resulting vector pL1 was transformed into *E. coli* and *C. necator* H16 Δ *phaCAB*. The knockout mutant was chosen to economise on carbon source and avoid PHB accumulation. The strains were grown in ECMM^{Tet} and CNMM^{Tet}, respectively and supplemented with either 20 mM L-lysine or 20 mM L-aspartate. Additionally, an empty vector control was used (data not shown). The P_{BAD} promoter was induced at 0 h by addition of 0.2% arabinose.

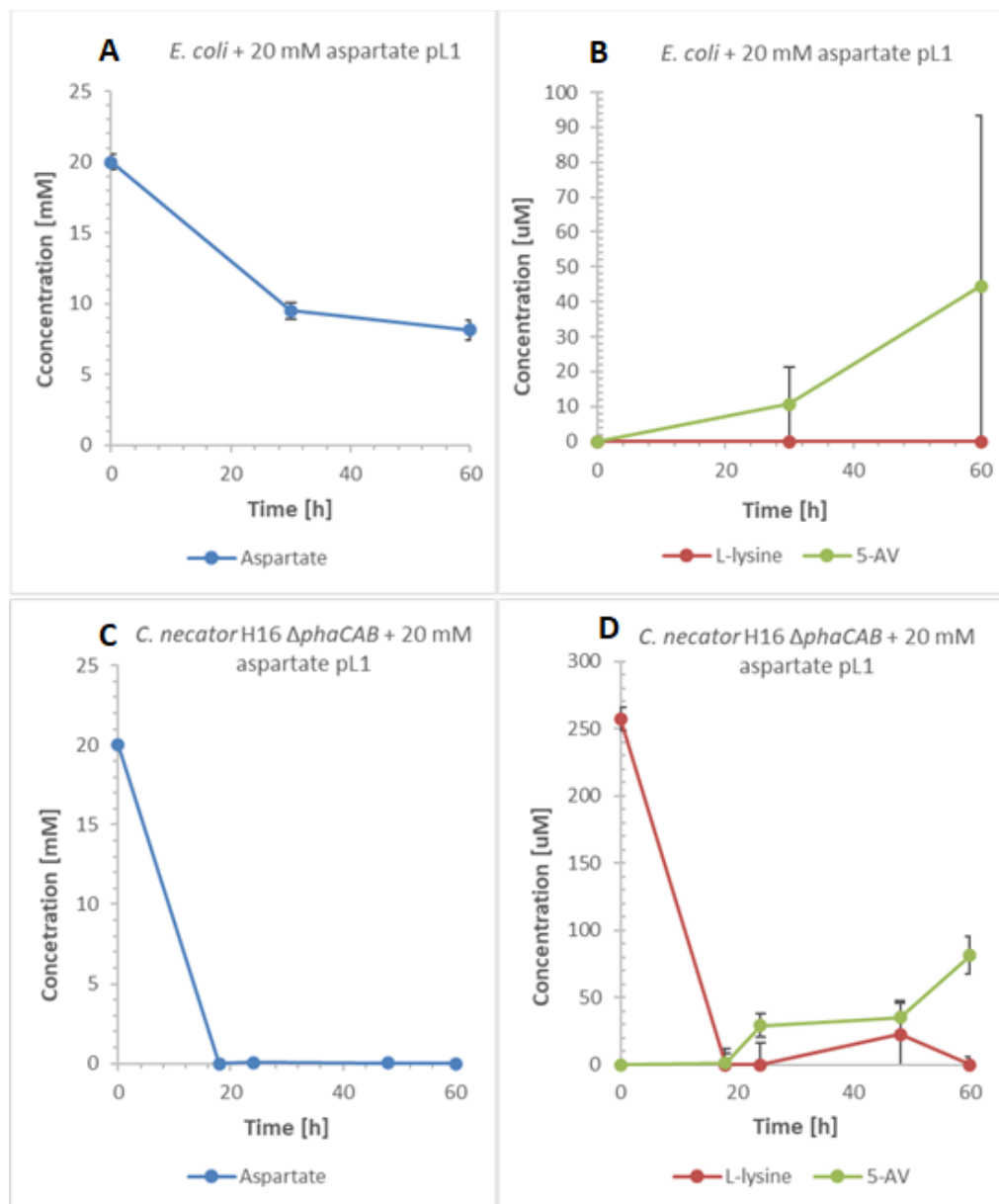


Figure 4.8 Aspartate, L-lysine and 5-AV levels in aspartate-fed *Escherichia coli* and *Cupriavidus necator* H16 cultures harbouring the pL1 plasmid. Blue: Aspartate; Red: L-lysine; Green: 5-AV; 60 h aerobic fermentation runs. (A, B) *E. coli* cells were grown in ECMM^{Tet} supplemented with 20 mM aspartate. (C, D) *C. necator* H16 Δ phaCAB cells were grown in CNMM^{Tet} and supplemented with 20 mM aspartate. Biological triplicates, values obtained by LC-MS. Cultures induced at 0 h with 0.2% arabinose.

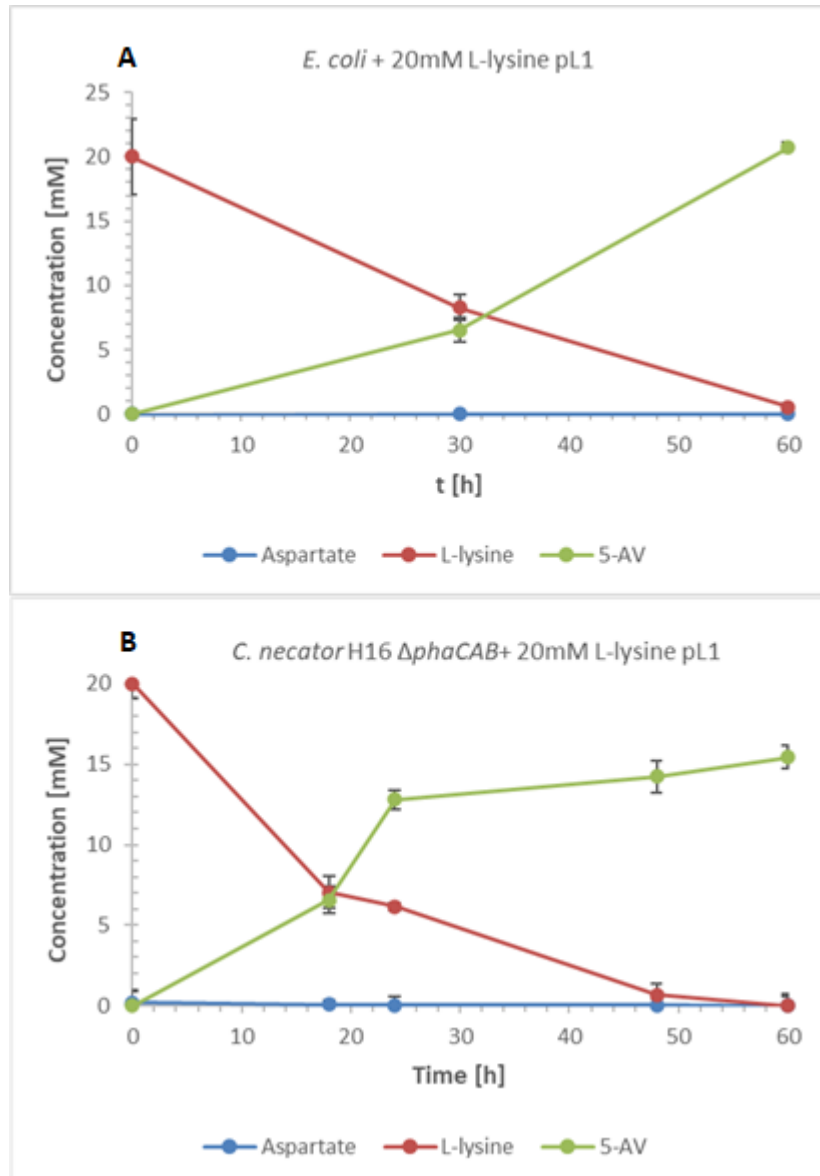


Figure 4.9 Aspartate, L-lysine and 5-AV levels in L-lysine-fed *Escherichia coli* and *Cupriavidus necator* H16 cultures harbouring the pL1 plasmid. Blue: Aspartate; Red: L-lysine; Green: 5-AV; 60 h aerobic fermentation runs. (A) *E. coli* cells were grown in ECMM^{Tet} supplemented with 20 mM L-lysine. (B) *C. necator* H16 $\Delta phaCAB$ cells were grown in CNMM^{Tet} and supplemented with 20 mM L-lysine. Biological triplicates, values obtained by LC-MS. Cultures induced at 0 h with 0.2% arabinose.

Figure 4.8 (A) shows that *E. coli* DH5 α cultures that expressed *davA* and *davB* metabolised 20 mM aspartate only partially, as 8.16 mM remained in the supernatant without being metabolised after 60 hours of cultivation. This result shows that aspartate is not used a preferred carbon source in *E. coli* DH5 α when glucose is present in the medium. **Figure 4.8 (B)** shows that *E. coli* reached a titer of 44.5 μ M 5-aminovaleric acid from 20 mM supplemented aspartate. L-lysine was not detected in the supernatant at any timepoint. Also, once the growth phase halted due to the depletion of a critical nutrient, aspartic acid was only slowly converted to 5-AV through L-lysine at a rate of 1.15 μ M h⁻¹.

Figure 4.8 (C) shows that *C. necator* H16 Δ *phaCAB* cultures expressing *davA* and *davB* depleted the carbon source aspartate by the 20 hour timepoint, indicating that aspartate is a preferred carbon source in *C. necator*. If aspartate was preferentially used for biomass generation, it would be a suboptimal feedstock to test the 5-AV pathway in *C. necator* H16. **Figure 4.8 (D)** shows that the cultures reached a concentration of 81.4 μ M 5-AV from 20 mM aspartate, roughly double the value observed in *E. coli* (**Figure 4.8 B**) and at a slow rate of 1.92 μ M h⁻¹. L-lysine was detected in the supernatant at the zero timepoint (250 μ M), indicating a possible carry-over from a preculture in rich medium. After 18 h fermentation, the contaminant could not be detected in the supernatant anymore and 5-AV was not yet detectable either. It cannot be ruled out however, that the L-lysine contamination contributed to higher intracellular 5-AV levels which would have led to a higher supernatant titer in the later stages of the fermentation.

In the empty vector controls, 5-AV was not detected in any of the culture supernatants.

Figure 4.9 (A) shows that *E. coli* DH5 α cultures expressing *davA* and *davB* reach a titer of 20.72 mM 5-AV from 20 mM L-lysine. Aspartate was not detected in the supernatant at any timepoint. From 20 mM L-lysine, 0.59 mM remained in the supernatant after 60 h. This result shows that L-lysine to 5-AV conversion with DavA and DavB in *E. coli* follows a 1:1 molar ratio, starting at the beginning of the exponential growth phase until complete conversion is reached after 60 h at an average rate of 330 $\mu\text{M h}^{-1}$, which appears to be higher as more biomass is present (peak: 470 $\mu\text{M h}^{-1}$ after full growth).

Figure 4.9 (B) shows that *C. necator* H16 ΔphaCAB cultures expressing *davA* and *davB* reach a titer of 15.42 mM 5-AV from 20 mM supplemented L-lysine. L-lysine levels reached zero after 60 h of fermentation, indicating a conversion ratio of 0.77 mol/mol, which is lower than the full conversion observed in *E. coli*. Aspartate could not be detected in the supernatant at any timepoint. It is possible that roughly 5-8 mM L-lysine was used for biomass generation in the initial growth phase. After 18 h, 13 mM L-lysine were metabolised, but only 6.5 mM 5-AV were generated. After the exponential growth phase, the remaining 7 mM L-lysine yielded an additional 9 mM 5-AV in the supernatant at a rate of 210 $\mu\text{M h}^{-1}$. The results shown in **Figure 4.9 (A)** and **(B)** hint towards a more pronounced amino acid utilisation for biomass in *C. necator* H16 ΔphaCAB cultures compared to *E. coli*.

In the empty vector controls, 5-AV was not detected and aspartate was metabolised at similar rates as in cultures harbouring the pathway. L-lysine metabolisation was observed to be very low (2 mM after 60 h) in *C. necator* H16 $\Delta phaCAB$ and was not observed in *E. coli*.

4.2.5 Aerobic resting cell 5-AV production in minimal supplemented medium using phosphate limitation in *Cupriavidus necator* Δ phaCAB

As discussed in **Chapter 1**, the *C. necator* H16 resting cell condition may allow to decouple growth phase (and therefore, biomass formation) from the production phase. Aspartate is a sub-optimal feedstock when producing in *C. necator* H16, as data shown in this work (**Chapter 4.2.4**) and data from Salinas (University of Nottingham, unpublished) suggest that aspartate is a preferred carbon source for biomass formation and will be used for growth before flux can be directed towards product formation. For this reason, the resting cell condition was tested, to ferment aspartate under non-growing conditions.

C. necator H16 Δ phaCAB was transformed with pL1 (pMTL71301-P_{BAD}-*davA*-*davB*), expressing *davA* and *davB* under the control of the arabinose-inducible P_{BAD} promoter. The cells were grown on CNMM^{Tet} minimal medium plates and single colonies used to inoculate 5 mL precultures in CNMM^{Tet} overnight. These were used to inoculate large 200 mL main cultures in 2 L flasks in CNMM^{Tet} minimal medium that were grown to an OD₆₀₀ of 0.6. 1050 mL of the grown cultures were unified and centrifuged to yield 630 OD ml units of cell pellet, which was washed twice with water and then resuspended in 25 mL non-phosphate MOPS buffered CNMM-P^{Tet} medium to yield a total optical density of OD₆₀₀ of 25.2. The medium was supplemented with 20 mM aspartate, negative controls were non-supplemented. The experiment was conducted in biological triplicates for 60 h and the four metabolites aspartate, 5-AV, glutaric acid in the supernatant were quantified using LC-MS. Additionally, uracil was attempted to be quantified using a published standard curve for uracil [379] as

it was not available as a standard at the time of the experiment and only analysed retrospectively. It is important to note that the used published standard curve had a linearity range only shown to 1.4 μM and the extraction protocol and instrument settings were different [379]. This means that the extrapolated estimated values and identification for uracil given in this work are tentative and can only be interpreted as a rough indication.

The results from the resting cell experiment shown in **Figure 4.10 (A)** show that aspartic acid and gluconate (not shown) are mainly converted to uracil under resting cell conditions. A similar result has been shown in the previous chapter, where significant amounts of uracil were converted from β -alanine under resting cell conditions. Again, it has to be stressed that the quantified molarities of uracil was estimated as no uracil standard was available and uracil was identified by mass and by ruling out other metabolites of similar mass that are not stable over longer timeframes. **Figure 4.10 (B)** shows that under resting cell conditions, 711 μM 5-AV were produced alongside 726 μM glutaric acid. While this result presents a 8.7-fold improvement over the 81 μM 5-AV under growing cell conditions over a similar time frame, the OD_{600} of the resting cell cultures was also denser by a factor of 10. The OD-adjusted productivity was therefore not higher than in the previous experiments. Interestingly, the accumulation of glutaric acid as a major by-product of 5-AV formation could be shown.

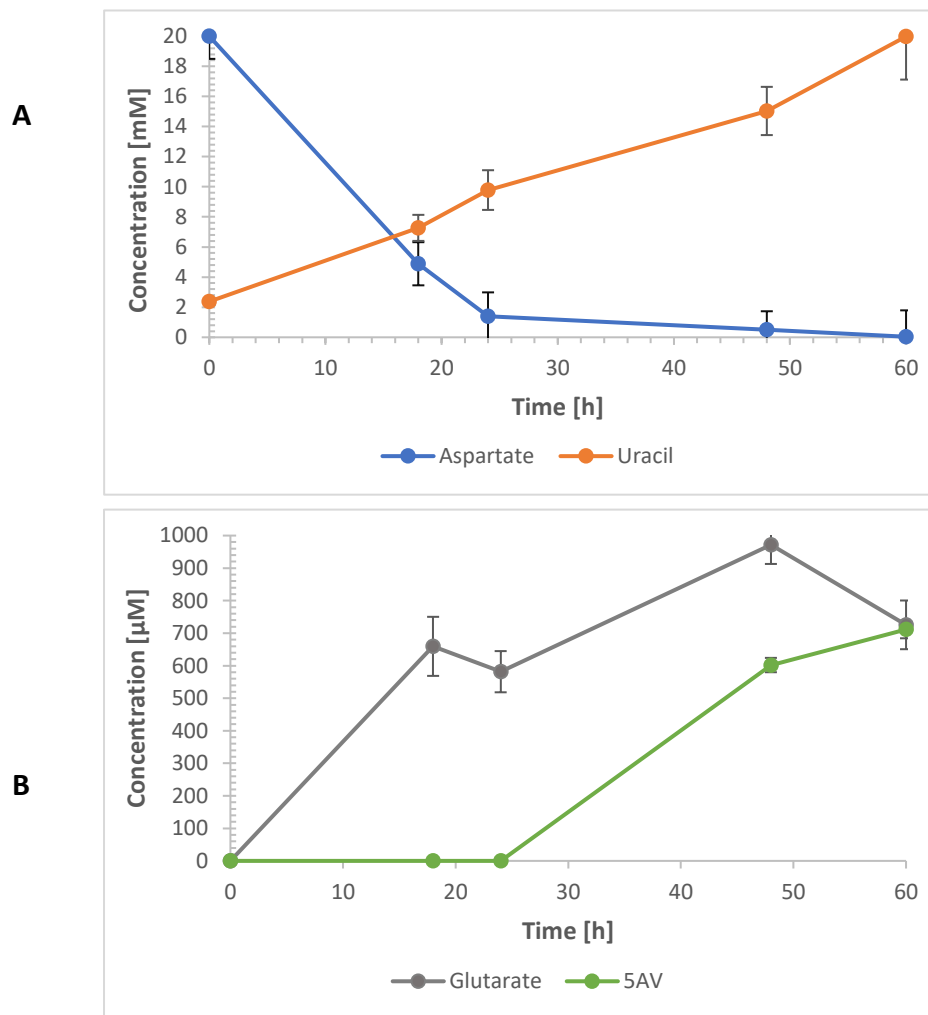


Figure 4.10 Aerobic resting cell fermentation in minimal 20 mM aspartate supplemented medium using phosphate limitation in *Cupriavidus necator* H16 Δ phaCAB. (A) Aspartate (blue) and (tentative) uracil (orange) levels are shown in mM. (B) 5-AV (green) and glutaric acid (grey) levels are shown in μ M. Resting cell fermentation over 60 hours in CNMM-P^{Tet} at OD25. Experiment was conducted in biological triplicates.

The titers of similar magnitude suggest that a knockout of the 5-AV degradation pathway via glutaric acid could potentially increase 5-AV yields by a factor of 2. It should also be noted that glutaric acid formation precedes 5-AV accumulation in the supernatant.

In unsupplemented negative controls, 5-AV and glutaric acid could not be detected and uracil levels were found to be generally considerably lower (0.5 - 1 mM).

4.2.6 The $\Delta gabT$ knockout in *Cupriavidus necator* H16 $\Delta phaCAB$ improves 5-AV yield in aerobic fermentation using aspartate supplemented minimal medium

As discussed in **Chapter 4.1.6**, the DavT homologue of *C. necator* H16, GabT, was a prime candidate for investigation, as 5-AV degradation would lower yields. Additionally, results shown in **Chapter 4.2.4** suggested that glutaric acid, the product of 5-AV catabolism, was present in *C. necator* H16 $\Delta phaCAB$ producer strains. Therefore it was necessary to investigate if a $\Delta gabT$ knockout strain would lower the rate of 5-AV degradation in *C. necator* H16 $\Delta phaCAB$.

To test this, *C. necator* H16 $\Delta phaCAB$ and *C. necator* H16 $\Delta phaCAB \Delta gabT$ were transformed with vector pL1 (pMTL71301- P_{BAD} -*davA-davB*). The strains were grown in CNMM^{Tet} and supplemented with 20 mM aspartate. Negative controls were unsupplemented and additionally, an empty vector control was used. The strains were fermented for 60 h at 30 °C and timepoints analysed for the metabolites glutaric acid and 5-AV.

As can be seen in **Figure 4.11 (A)**, the *C. necator* H16 $\Delta phaCAB$ strain produces a maximum of 42.8 μ M 5-AV from 20 mM aspartate. This value is lower than the previous reported value of 81 μ M in **Chapter 4.2** and nearly identical to titers found in *E. coli* - without any changes of conditions. However, previously, a contamination of L-lysine led to higher conversion values. In this experiment, no L-lysine could be detected in any of the fermentation samples. It can be observed that 5-AV production takes place after growth. Glutaric acid titers in the *C. necator* H16 $\Delta phaCAB$ strain reached up to 26 μ M.

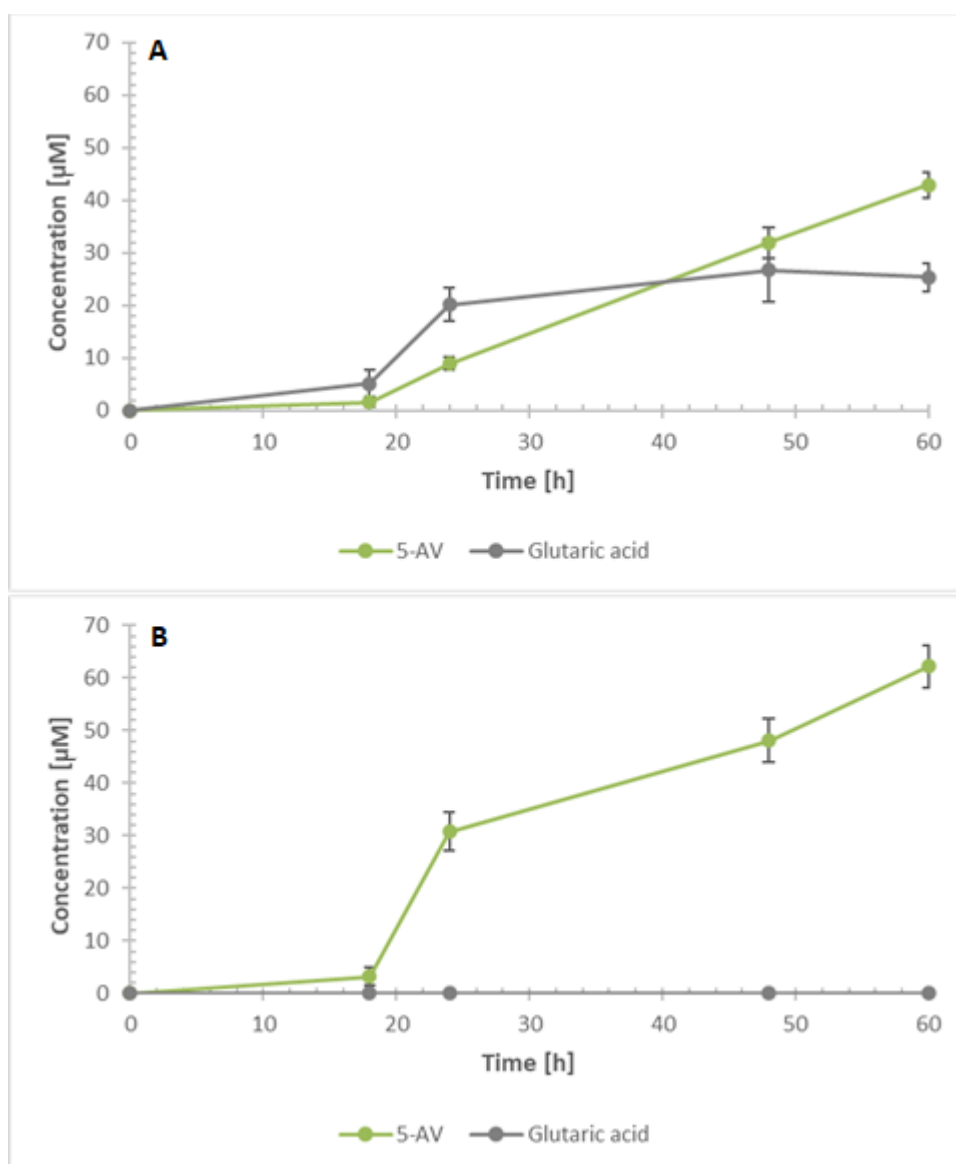


Figure 4.11 *Cupriavidus necator* H16 $\Delta phaCAB$ and $\Delta phaCAB \Delta gabT$ carrying pL1 in aerobic fermentations with 20 mM aspartate supplemented minimal medium. (A) $\Delta phaCAB$ strain. Grey: Glutaric acid levels; Green: 5-AV levels. (B) $\Delta phaCAB \Delta gabT$ strain. Grey: Glutaric acid levels; Green: 5-AV levels. All data obtained from biological triplicates. Quantification by LC-MS.

However, previously, a contamination of L-lysine lead to higher conversion values. In this experiment, no L-lysine could be detected in any of the fermentation samples. It can be observed that 5-AV production takes place

after growth. Glutaric acid titers in the *C. necator* H16 $\Delta phaCAB$ strain reach up to 26 μM .

Figure 4.10 (B) shows titers in the *C. necator* H16 $\Delta phaCAB \Delta gabT$ strain under identical fermentation conditions. No glutaric acid could be detected in any of the supernatant samples, suggesting that the conversion of 5-AV to glutarate was successfully stopped using the $\Delta gabT$ knockout, ruling out the presence of any other aminotransferases in *C. necator* H16 that could also catalyse the reaction in meaningful quantities. 5-AV titers reach 62.3 μM , which is a 45% increase over the *C. necator* H16 $\Delta phaCAB$ strain.

Neither glutaric acid nor 5-AV were detected in unsupplemented controls and empty vector controls (data not shown).

4.2.7 Enhancing 5-AV production from *Cupriavidus necator* H16 Δ *phaCAB* Δ *gabT* central metabolism by using feedback-resistant enzyme variants, P_{trc} and P_{trp} promoters and synthetic RBS sites

The use of synthetic biology tools such as stronger, constitutive promoters and synthetic RBS sites has already been successfully explored in **Chapter 3** for the production of 5-OHV in *C. necator* H16. Additionally, to these tools, this study shows the implementation of feedback resistant enzyme variants of the L-lysine biosynthesis pathway to boost 5-AV levels in *C. necator* H16. The used enzymes variants, a feedback resistant *Co. glutamicum* *dapA* and the native and feedback-resistant enzyme variants of *lysC* from *Co. glutamicum* have been discussed in more detail in **Chapter 4.1.8**.

A number of plasmids were introduced to test 5-AV production in *C. necator* H16. The L0 strain expressed an empty pL0 vector control. The L1 strain tested 5-AV production from L-lysine using *davA* and *davB* under P_{BAD} control. P_{BAD} is a well-characterised strong inducible promoter and derived from the *araBAD* operon in *E. coli* [380]. It is inducible by AraC, a protein that binds as a positive regulator in the presence of L-arabinose [380]. Therefore, when AraC is constitutively expressed, expression levels of other proteins under P_{BAD} control can be tuned with differing L-arabinose concentrations [380].

The L2 strain tested if 5-AV is accessible from central metabolism (glucose / aspartate) by expressing the Dav pathway and an extra copy of native aspartate kinase (*lysC_{CN}*) under pBAD control.

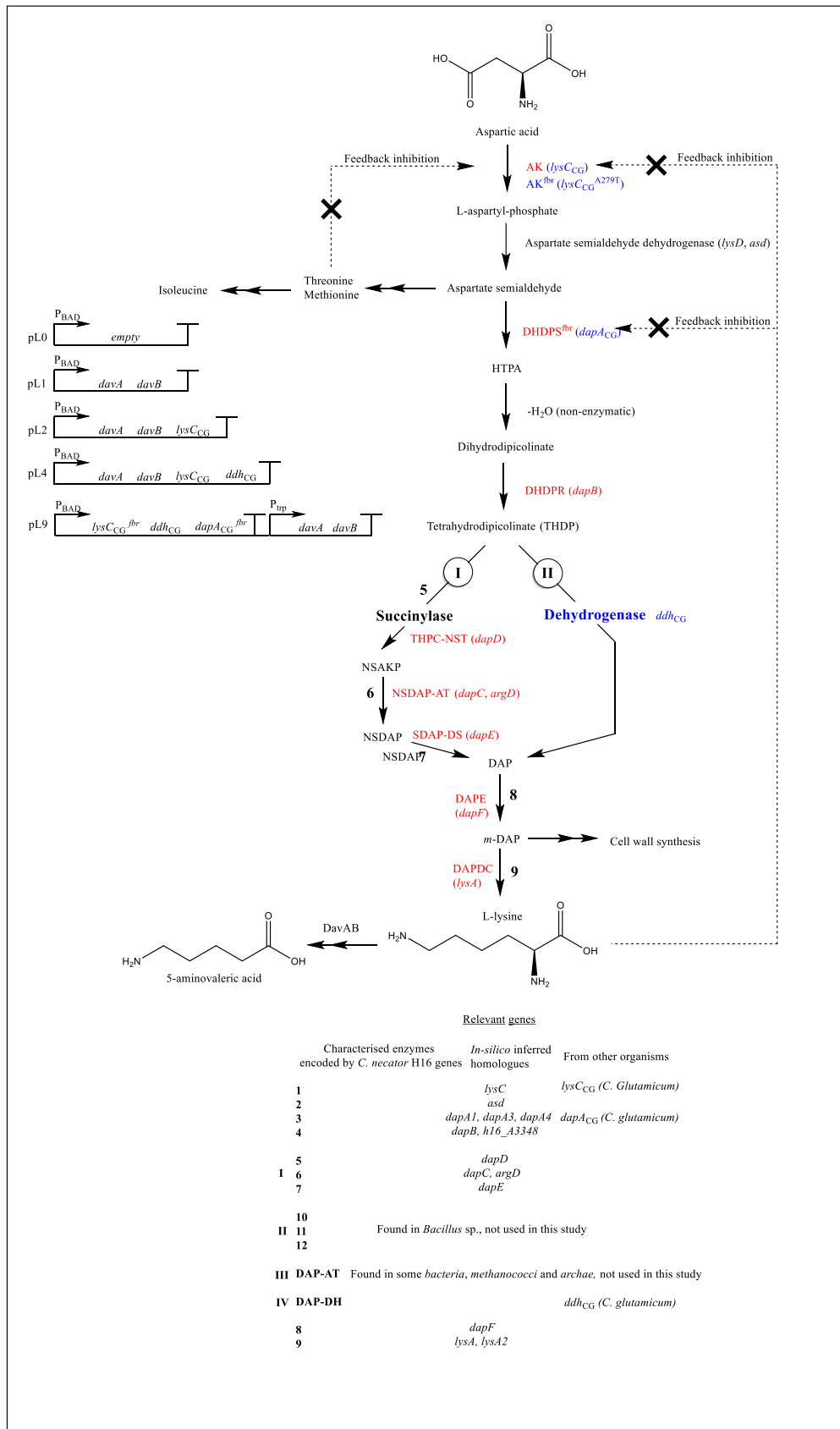


Figure 4.12 Proposed 5-AV biosynthesis pathway in *Cupriavidus necator* H16 Δ phaCAB Δ gabT.

(legend continued)(Figure adapted from Scapin et al.: *Enzymology of bacterial lysine biosynthesis* [156]) (I) Succinylase pathway (II) Dehydrogenase pathway. Dashed lines indicate negative feedback relationship which was deregulated (crosses). Homologs for enzymes in red are found in *C. necator* H16 but have not been experimentally verified. They are assumed to be functional as the strain is an L-lysine prototroph. Enzymes in blue are not found in *C. necator* H16, but in other bacterial species. The feedback-resistant mutant of *Co. glutamicum* AK (A279T) and the natively feedback-resistant *Co. glutamicum* DHDPS are introduced with the dehydrogenase bypass to overproduce L-lysine in *C. necator* H16 Δ *phaCAB* Δ *gabT*. DavA and DavB convert lysine to 5-AV. AK – aspartate kinase. HTPA - 4-hydroxy-2,3,4,5-tetrahydrodipicolinate. DHDPS - dihydrodipicolinate synthase. DHDPR - dihydrodipicolinate reductase. THDP – tetrahydrodipicolinate. THPC-NST - 2,3,4,5-tetrahydropyridine-2-carboxylate *N*-succinyltransferase. NS-AKP - *N*-succinyl-L-2-amino-ketopimelate. NSDAP-AT - *N*-succinyldiaminopimelate aminotransferase. NSDAP - *N*-succinyl-L,L-2,6,-diaminopimelate. SDAP-DS - succinyldiaminopimelate desuccinylase. DAPE - diaminopimelate epimerase. *m*-DAP – *meso*-diaminopimelate. DAPDC - diaminopimelate decarboxylase. DavA - δ -aminovaleramidase. DavB - lysine monooxygenase.

The L4 strain tested if an additional implementation of a bypass pathway using the *ddh*_{CG} encoded DAPDH under P_{BAD} control improved yields. Finally, the L9 pathway tested if deregulation of the overexpressed enzymes (feedback-resistant versions) could improve yields, carrying the pL9 construct: pMTL71301-P_{BAD}-*lysC*_{CG}^{fbr}-*dapA*_{CG}^{fbr}-*ddh*_{CG}-P_{trp}-*davA*_{pp}-*davB*_{pp}. In pL9, additionally to deregulated enzymes, synthetic RBS sites of 5000 AU strength (analogous to those used in **Chapter 3**) were used for the Dav pathway, which was cloned under P_{trp} control, a strong constitutive promoter that does not require induction. An overview of the pathway introduced by pL9 is shown in **Figure 4.12**.

C. necator H16 $\Delta phaCAB \Delta gabT$ was transformed with vectors pL0, pL1, pL2, pL4 and pL9, yielding the strains L0, L1, L2, L4 and L9, respectively. The pathways conferred by these plasmids are shown in **Figure 4.13**.

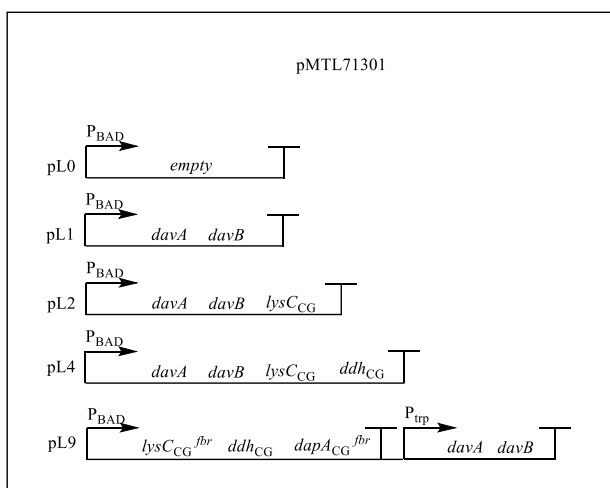


Figure 4.13 Synthetic pathways for the production of 5-AV in *Cupriavidus necator* H16 $\Delta phaCAB \Delta gabT$. P_{BAD} is an arabinose inducible promoter. P_{trp} is a strong constitutive promoter. *davA* encodes δ -aminovaleramidase. *davB* encodes lysine monooxygenase. *lysC* encodes aspartate kinase. *ddh* encodes DAPDH. *dapA* encodes DHDPS. ^{fbr} indicates feedback-resistance.

The strains were grown in CNMM and supplemented with 10 mM aspartate.

Negative controls were unsupplemented and additionally, the empty vector control pL0 was used. The strains were fermented in shake flasks for 60 h at 30 °C and the supernatants at the end-timepoints of the fermentation analysed for 5-aminovaleric acid titers using LC-MS. The results are shown in **Figure 4.15**.

The unsupplemented cultures of L0, L1 and L4 did not accumulate any 5-aminovaleric acid. In the unsupplemented culture L9, however, 5-AV could be detected. CNMM contains 10 g L⁻¹ gluconate. In the cultures with 10 mM aspartic acid supplementation, 5-AV was not detected in the L0 empty vector control strain.

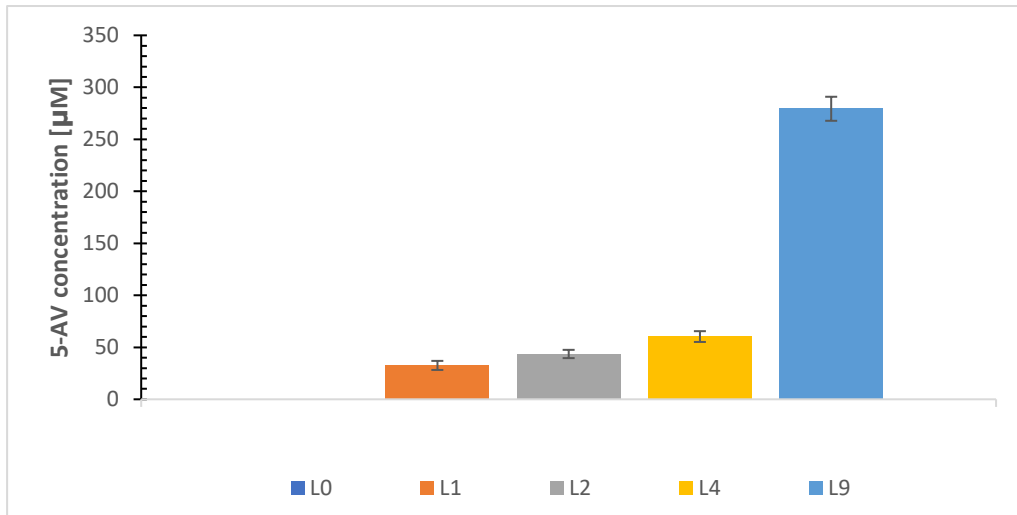


Figure 4.14 5-aminovaleric acid levels in *Cupriavidus necator* H16 Δ *phaCAB* Δ *gabT* growing cell fermentations using CNMM^{Tet} supplemented with 10 mM aspartic acid. Data shows levels of 5-AV in the supernatant of the 60 h endpoint samples. 0.2% arabinose was added at the 0 h timepoint. All fermentations were carried out as biological triplicates. 5-AV levels were quantified by LC-MS.

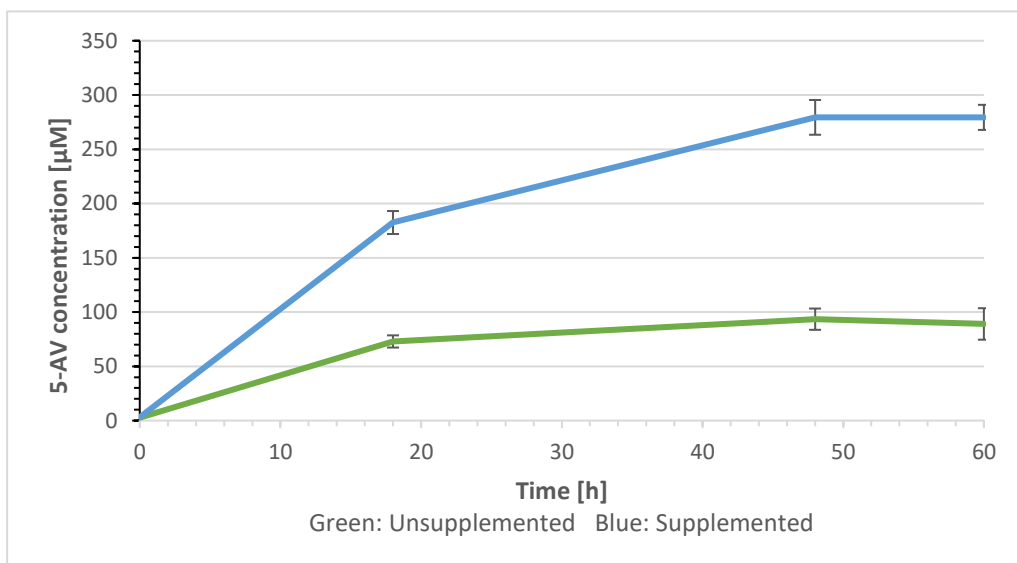


Figure 4.15 5-aminovaleric acid levels in *Cupriavidus necator* H16 Δ *phaCAB* Δ *gabT* growing cell L9 fermentations: Unsupplemented CNMM^{Tet} medium and supplemented CNMM^{Tet} medium with 10 mM aspartic acid. Green curve: Unsupplemented (1% sodium gluconate). Blue curve: Supplemented (1% sodium gluconate and 10 mM aspartic acid). Data shows levels of 5-AV in the supernatant. 0.2% arabinose were added at the 0 h timepoint. All fermentations were carried out as biological triplicates. 5-AV levels were quantified by LC-MS.

L1 accumulated 32.5 μM 5-AV. L2, expressing the native aspartate kinase from *Co. glutamicum* yielded 43.5 μM 5-AV from 10 mM aspartate, an increase of 33% over the strain without AK on the plasmid. L4, adding the *ddh* bypass, yielded 60.3 μM 5-AV, a 38% increase over L2. L9, expressing the feedback resistant AK mutant, *ddh*, and the feedback resistant *dapA_{CG}^{fbr}*, yielded 279.4 μM . The use of feedback resistant AK and *DapA_{CG}^{fbr}* marked an increase of 4.6-fold over strain L4.

L9 was also the only stain with measurable 5-AV levels in the unsupplemented culture, which contains 10 g L⁻¹ sodium gluconate (45.8 mM). **Figure 4.16** shows the production of 5-AV over time in L9 cultures that were either unsupplemented (green curve) or supplemented (blue curve).

L9 yielded 279.4 μM 5-AV after 60 h when supplemented and 89.05 μM 5-AV unsupplemented. This result marks the first instance of 5-AV production in an engineered *C. necator* H16 strain from central metabolism alone, with a productivity of 1.56 $\mu\text{M h}^{-1}$ in the first 50 h.

4.3 Discussion

4.3.1 5-AV toxicity and degradation in *Cupriavidus necator* H16

Unsurprisingly, the data suggests that 5-AV is not toxic to *C. necator* H16 as related compounds such as 4-aminobutyric acid (GABA) are consumed and produced by many bacteria species [381]. This result is in line with current literature on 5-AV toxicity for bacteria. Adkins et al. [349] have shown in their research that *E. coli* was not impacted in growth by exogenous 5-AV addition up to a concentration of 20 g L⁻¹.

However, several hypotheses concerning the regulation of 5-AV uptake and metabolism were formed. The strains were adapted for growth on gluconate before they were transferred to the 5-AV medium, meaning that 5-AV transporters may not have been expressed and the metabolism was adapted for using sugars for growth. However, after adapted strains were sub-cultured, the same lag-phase appeared. This means that expression of transporters and adaption of the general metabolism is not the mechanism that mediates the lag-phase, neither is an adaption through mutation, which would have been inherited by the daughter culture from the parent culture and was tentatively ruled out by sequencing of the adapted strain, which did not appear to carry significant mutations compared to the wildtype. Only one potentially relevant SNP was detected, a Q626L mutant of a putative branched-chain amino acid transporter encoded on chromosome 2 (H16_RS28925), which may or may not play a role in 5-AV uptake. Unfortunately, a mutation would be expected to

carry the effect over to a new culture, which it had not, making this SNP an unlikely candidate to explain the effect.

A quorum-sensing based explanation may explain why the sub-culture experienced a similarly long lag-phase. It is possible that 5-AV transporters or key-enzymes of the 5-AV degradation pathway are expressed under control of a quorum-sensing mechanism, which has been discussed in **Chapter 4.1.4**. Once reset to low OD and with quorum sensing signal molecules removed by a wash step, the bacteria could have lost their ability to metabolise 5-AV and only regained it slowly.

The data also allows for a number of tentative statements about the degradation pathway of 5-AV. Literature has confirmed that the 4-aminobutyrate (GABA) aminotransferase GabT is present in *C. necator* H16 [110], which is a homologue of the *B. subtilis* GabT that was shown to accept 5-AV as substrate [382]. The fact that nitrogen-limitation is overcome first hints towards the first enzymatic step being the removal of the terminal amino group by GabT, before the carbon chain is degraded by beta-oxidation in fatty acid catabolism. As mentioned in **Chapter 3**, studies [143, 236, 237] have shown that a *Bacillus subtilis* homologue of GabT is under control of a regulator that senses GABA (the same *B. subtilis* that is prey to *C. necator* H16 [383]). Studies in *Agrobacterium tumefaciens* [345] and *Pseudomonas aeruginosa* [346] have shown that GABA can act as a quorum-sensing modulation molecule. It is thus possible that also in *C. necator* H16, GABA could act as a quorum sensing modulator and GabT is only upregulated once a minimum GABA level is sensed. This would make GabT expression, and, in expansion, 5-AV degradation,

207

dependent on a signal molecule that has been shown to be involved in quorum sensing in other species. Whether this hypothesis is true or not, cannot be concluded from our preliminary data and more experiments need to be conducted to elucidate the role of GABA in *C. necator* H16 quorum sensing and its effects on the regulator that controls GabT expression. Another explanation could be that GABA is transported into the cell and degraded as nutrient source (which may involve upregulation of GABA degradation genes) or in a role that could involve *C. necator* H16 as a quorum quencher of other species, a strategy that would allow *C. necator* H16 to disrupt their GABA-dependent quorum modulation [384]. This may be evolutionary advantageous, given that *C. necator* H16 is a predatory bacterium [383].

4.3.2 DavA and DavB convert L-lysine to 5-aminovaleric acid in *Escherichia coli* and *Cupriavidus necator* H16

5-AV production in *E. coli* through DavA and DavB is a well-established pathway in synthetic biology. Liu et al. [129] reported conversion of 40.7 mM 5-AV from 47.9 mM L-lysine, a 84.9 mol/mol conversion ratio using purified DavA and DavB in an in-vitro experiment.

Park et al. [124] expressed DavA and DavB in wild-type *E. coli*. with a conversion yield of 64 mol/mol 5-AV from L-lysine. In *E. coli* WL3110, a strain that had previously been used to produce cadaverine from glucose [385], the pathway failed to yield 5-AV from glucose. In resting cells ($OD_{600} = 60$), however, 40.93 mM 5-AVA were converted from 41 mM L-lysine in 24 h, showing that nearly a 1:1 molar conversion yield is possible [123]. In a third study, Adkins et al. published a yield conversion ratio of 88% [349].

In this study, we have shown that *E. coli* DH5 α can achieve a similar full conversion yield using DavA and DavB under the control of the strong, arabinose-inducible P_{BAD} promoter. Full conversion was reached in 60 hours at a peak OD_{600} of 1.6. We conclude that the results shown in the literature are replicable and DavA and DavB are promising candidates for efficient L-lysine to 5-AV.

Atkins et al. [349] reported a concentration-dependent conversion rate to 5-AV that would yield 1.5 mM 5-AV from 22 mM glucose (22.2 mM are used in ECMM) in *E. coli*. BW25113 (DE3). In the experiments shown in this subchapter, this 5-AV conversion from glucose cannot be replicated. However, the strain used by Atkins et al. [349] had been engineered for high L-lysine production.

To date, 5-AV production has not been shown in *Cupriavidus* sp. as a host in the literature and the results shown in **Figure 4.8 (D)** and **Figure 4.9 (B)** indicate that *C. necator* H16 Δ *phaCAB* is a suitable host for a biosynthetic pathway for 5-AV. Due to the presumed consumption of amino acids during the growth phase, conversion rates from L-lysine reached 77% and aspartate was shown to be a poor feedstock for the pathway in *C. necator* H16 due to the high uptake and metabolisation rate (**Figure 4.8 (C)**), which was also observed in feed-experiments with aspartate conducted by Salinas (University of Nottingham, unpublished).

In summary previous results from the literature in *E. coli* were replicated and it was shown that DavA and DavB can mediate full conversion of L-lysine to 5-AV. Also, this study has shown the first example of 5-AV production in *Cupriavidus* sp. In order to engineer the pathway leading to L-lysine formation from the central metabolism, aspartate may seem an attractive feedstock. However, it was revealed that it is used as a preferred carbon source for growth in *C. necator* H16 Δ *phaCAB*. Resting-cell conditions may overcome this problem. Non-growing, but metabolically active cells should not use aspartate for biomass formation, which might help to debottleneck future pathway designs.

4.3.3 Aerobic resting cell fermentation in minimal supplemented medium using phosphate limitation in *Cupriavidus necator* Δ *phaCAB* is not a suitable condition for 5-AV production

Under resting cell conditions, only 711 μ M 5-AV were formed and aspartic acid, while not contributing to biomass formation, was fully converted to other side products alongside the present carbon source in CNMM-P (sodium gluconate). Aspartate and 5-AV were chosen for targeted LC-MS quantification as the feedstock and desired product of the fermentation. Glutaric acid was chosen for targeted analysis as well, as it may be a major side-product and most important possible catabolite of 5-AV. Uracil was only analysed retrospectively in the samples, because of an unusually high ion count at the corresponding m/z value (111.0200, negative ion channel). In order to track more possible side-reactions, an untargeted approach, ideally using ^{13}C or ^{15}N labelled aspartate would have been necessary, which had not been reliably developed.

A relevant side product was shown to be glutaric acid, which was measured using LC-MS and formed at a titer of 726 μ M. Glutaric acid is a known product of 5-AV degradation in *P. putida* and forms part of the Dav-pathway for L-lysine degradation. The corresponding genes *davT* and *davD* (also: *gabT*, *gabD*) are annotated in KEGG as encoding 5-aminovalerate aminotransferase and glutarate semialdehyde dehydrogenase [386, 387]. They have been employed for the production of glutaric acid in *E. coli* and *Co. glutamicum* in several studies [124, 132, 348, 349, 382, 388-391]. A homologue in *C. necator* H16 was identified as putative GABA aminotransferase by Orol [144] and knocked out in the *C. necator* Δ *phaCAB* background. The resulting strain *C. necator* Δ *phaCAB*

$\Delta gabT$ thus presented itself as an attractive chassis to test if glutaric acid production from 5-AV can be prevented.

In a study published by Shin et al. [392], the *gabT* homologue in *Co. glutamicum* was targeted as a knockout for 5-AV production from L-lysine, reducing the amount of glutaric acid byproduct in their fed-batch fermentation from 13.4 g L⁻¹ to 2 g L⁻¹. In light of the availability of the GabT-deficient *C. necator* H16 strain, it was tested if the $\Delta gabT$ knockout mutant improves 5-AV yields from aspartate in growing cultures.

Because of the suspected strong accumulation of uracil in phosphate-limited resting cell fermentations, this format will be discontinued as it offers little tangible advantages and does not solve the problem of aspartate utilisation. Metabolically, aspartate is relatively close to the pyrimidine biosynthesis pathway that leads to uracil. *N*-carbamoyl-aspartic acid is formed through action of the aspartate carbamoyl transferase. **Figure 4.9** illustrates the Pyrimidine biosynthesis pathway in *C. necator* H16 as annotated by KEGG.

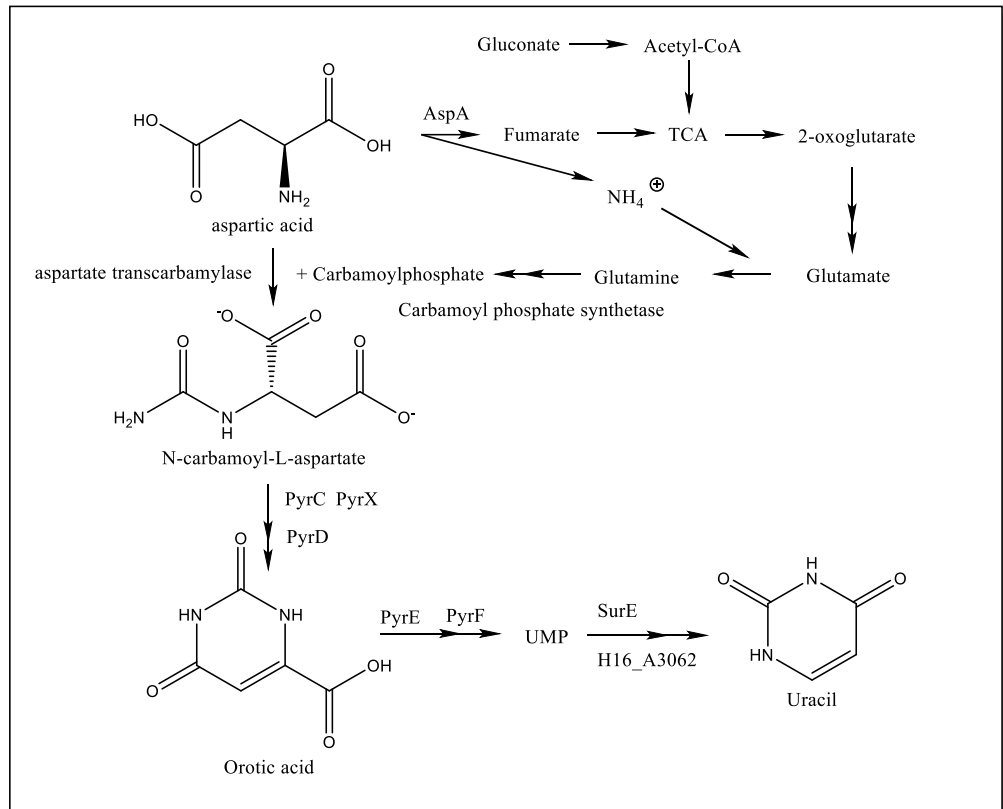


Figure 4.16 Proposed uracil synthesis route in *Cupriavidus necator* H16 resting cells from aspartate and gluconate. AspA - fumarate lyase, TCA – tricarboxylic acid cycle, PyrC – dihydroorotase, PyrX - orotate phosphoribosyltransferase, PyrD – dihydroorotate dehydrogenase, PyrE - orotate phosphoribosyltransferase, UMP – uracil monophosphate - PyrF - orotidine 5'-phosphate decarboxylase, SurE - nucleotidase

The carbamoylphosphate that is necessary for the committing step into pyrimidine biosynthesis is conveniently synthesised by the carbamoyl phosphate synthase which accepts Glutamine as nitrogen donor [353]. Glutamine biosynthesis is a cataplerotic pathway from 2-oxoglutarate and requires ammonia to be added to form glutamate. This ammonia group can be sourced from aspartate degradation by AspA to fumaric acid, an anaplerotic reaction, or by transamination to oxaloacetate. The necessary acetyl-CoA units that drive the TCA cycle to form 2-oxoglutarate from fumarate or oxaloacetate

stem from metabolisation of gluconate, which was added to the medium. Combining an anaplerotic flux (AspA) with a cataplerotic flux (carbamoylphosphate synthesis) and recycling of the amino group allows for a net positive energy balance for the formation of *N*-carbamoyl-L-aspartate. From here, the necessary pathway for uracil synthesis is present in *C. necator* H16 (*pyrC*, *pyrD*, *pyrE*, *pyrF*, *surE*, *H16_A3064*). In total, 3 ATP are expended for this, assuming the aspartate degradation through fumarate rather than oxaloacetate, which could help resting cells to “vent” ATP, while keeping the TCA cycle active.

However, there is a lack of data to confirm this hypothesis, which would have to be further investigated by a labelling experiment to confirm the synthesis of uracil and an accompanying RNA-sequencing experiment to probe if any genes of the *pyr* family are upregulated.

In summary, using resting cell conditions with phosphate limitation, a titer of 0.7 mM from 20 mM aspartic acid and 10 g L⁻¹ sodium gluconate was achieved. However, uracil and glutaric acid were found to be major by-products of the fermentation. The putative uracil formation was likely an artifact of the resting cell condition and will not pose a problem in growing cells and fed-batched cultures. In order to reduce glutaric acid formation, the next logical step towards 5-AV production would be to test the Δ *gabT* knockout strain *C. necator* Δ *phaCAB* Δ *gabT* under growing cell conditions and compare its performance with the *C. necator* Δ *phaCAB* strain.

4.3.4 The $\Delta gabT$ knockout in *Cupriavidus necator* H16 $\Delta phaCAB$ improves 5-AV yield in aerobic fermentation using aspartate supplemented minimal medium

In a study by Shin et al. [122], *Co. glutamicum* was engineered for 5-AV production and the formation of the by-product glutaric acid could be significantly reduced by the knock-out of the *gabT* homologue in the organism. In this study, a similar change on by-product suppression in *C. necator* H16 was reported, where a knockout of the *gabT* homologue resulted in complete eradication of glutaric acid production and a 45% increase of 5-AV titers in aerobic, aspartate-supplemented fermentation.

Shin et al. [122] report an increase from 19.7 to 33.1 g L⁻¹ 5-AV due to the *gabT* deletion, which marks a 68% increase. Glutaric acid titers were greatly reduced from 13.4 g L⁻¹ to 2 g L⁻¹. It is therefore possible that *Co. glutamicum* contains other promiscuous transaminases that show some activity towards 5-AV. In *C. necator* H16, glutaric acid could not be detected at all after the knock-out (**Figure 4.11 (B)**), which was strong evidence towards the absence of any putative promiscuous transaminases.

For future experiments in engineering the 5-AV production pathway shown in this work therefore made future use the *C. necator* H16 $\Delta phaCAB \Delta gabT$ strain, which had resulted in less by-product formation and higher 5-AV titers.

In summary, a $\Delta gabT$ mutant strain was therefore tested to reduce the accumulation of glutaric acid. Due to the knock-out, glutaric acid production was completely avoided and 5-AV production titers from aspartic acid rose by 45% compared to the strain with a functional *GabT* aminotransferase. The

strain *C. necator* H16 $\Delta phaCAB \Delta gabT$ was shown to be a superior host organism for 5-AV production and it solved the problem of glutaric acid accumulation. For future experiments, the pathway leading to L-lysine overproduction had to be engineered to yield higher titers of 5-AV from gluconate and ammonia as carbon and nitrogen sources. To probe the performance of suggested pathway variants, aspartate could then remain an important experimental feedstock despite rapid metabolisation to biomass.

4.3.5 Enhancing 5-AV production from *Cupriavidus necator* H16 Δ *phaCAB* Δ *gabT* central metabolism by using feedback-resistant enzyme variants, P_{trc} and P_{trp} promoters and synthetic RBS sites

As expected, the L1 control vector, which exemplified native conditions of 5-AV accumulation via the lysine pathway, yielded the lowest titer of all tested strains. The yield of 32.5 μ M from 10 mM aspartic acid is roughly half of the yield obtained previously with 20 mM aspartic acid supplementation. The main reason why the concentration was reduced for this experiment was most likely the relatively poor solubility of aspartic acid in CNMM (4.5 g L⁻¹ at a molecular weight of 130.1 g mol⁻¹ gives a maximum theoretical solubility of 33.8 mM) [393]. It was observed that at higher concentrations in stock solutions, some of the aspartic acid would not fully dissolve, resulting in cloudy media, which was considered an error-source for obtaining accurate values.

The addition of a *lysC_{CG}* copy in L2 increased 5-AV yields by 33%. It is known that the native *AK_{CG}* is not completely feed-back resistant to lysine [394]. However, the additional copy with lower inhibition than the *C. necator* H16 enzyme helped to increase 5-AV values noticeably.

When the dehydrogenase bypass from *Co. glutamicum* was added to the pathway, another increase of 38% was observed. When a thermostable *ddh* was introduced to *E. coli* for L-lysine production, the authors of the study reported an increase of 66% in their final titer [395]. In comparison, the effect that this study reported is lower.

The largest increase in yield from aspartic acid was observed with the pL9 construct. The combined effects of complete feedback-inhibition of *AK_{CG}^{fbr}* and

DHDPS_{CG}^{fbr} in conjunction with the dehydrogenase pathway is becoming an increasingly popular combination to achieve high L-lysine titers, as exemplified by a study from Kwak et al. [396], in which *E. coli* was engineered to produce cadaverine using this combination. Unfortunately, no comparative figure to a wildtype was shown, but a 9-fold increase in titer was achieved here using this method. Additionally, the engineered *C. necator* H16 strain L9 yielded 89 μ M 5-AV from a medium containing 45.8 mM sodium gluconate in growing cell fermentation. This yield is higher than the achieved 5-AV yield from the *C. necator* H16 Δ *phaCAB* Δ *gabT* mutant using pL1 and 20 mM aspartate supplementation, showing how powerfully the deregulation of the lysine biosynthesis pathway impacted 5-AV yields. Additionally, *davA* and *davB* expression was moved under control of a constitutive promoter to allow the L-lysine-pathway related genes to be situated closer downstream of the P_{BAD} promoter, which may have contributed a positive influence on expression levels.

In future experiments, the 5-AV synthesis pathway could be expressed under the control of a constitutive promoter and integrated in the *C. necator* Δ *phaCAB* Δ *gabT* genome. This strain would then be a potential candidate to produce 5-AV from central metabolism in fermentation from CO₂ and hydrogen.

In summary, several biosynthetic pathways were constructed and tested in *C. necator* H16 Δ *phaCAB* Δ *gabT*. A moderate (30-35%) increase in yield of 5-AV from aspartic acid was observed when expressing the *Co. glutamicum* genes *lys*_{CG} and *ddh*_{CG}, respectively. When using feedback-resistant Lys_{CG}^{fbr} and DapA_{CG}^{fbr} in conjunction with Ddh_{CG}, a dramatic increase in 5-AV titers from

aspartic acid by over 9-fold was observed. Additionally, the engineering of *C. necator* H16 by deregulation of L-lysine biosynthesis pathways allowed for the production of 5-AV from gluconate. This result marks the first example of a *Cupriavidus* sp. strain capable of 5-AV production from central metabolism and marks an important step towards 5-AV production from syngas.

Chapter 5

Development of a 5-aminovalerate biosensor

Chapter 5 - Development of a 5-aminovalerate biosensor

5.1 Introduction

5-aminovaleric acid (5-AV) is a platform chemical with applications for nylon 5,5 and nylon 5,6- synthesis [123] as well as potential uses in other textiles and plastics. Such monomers for polymer production are usually reliant on fossil resources for their production. More sustainable, non-petrochemical based approaches to 5-AV production to date have been engineered enzymatically *in-vitro* [129, 397], in *Co. glutamicum* [122, 131, 398] and in *E. coli* [123, 124, 130, 349]. In this study, the first example of sustainable 5-AV production from the *C. necator* H16 central metabolism is shown, offering the opportunity for 5-AV production from CO₂ or, in a CO-resistant strain, from syngas, which can be sustainably sourced from steel-work off-gases [78] or from municipal solid waste biomass [79].

Unfortunately, the number of strains, pathways and conditions that can be tested for the metabolic engineering for 5-AV production is limited due to the lack of high-throughput screening methods. 5-AV quantification to date is heavily dependent on HPLC and LC-MS. The current standard for 5-AV quantification on HPLC involves the derivatisation of 5-AV along with other amino acids in the sample with a fluorescent dye marker (such as *ortho*-phthalaldehyde) and subsequent photometric detection [122]. In LC-MS, the 5-AV titers could be accurately measured using a HPLC-based chromatography, with a polymeric HILIC column for polar metabolites, in conjunction with a high-resolution Orbitrap mass spectrometer (this study). However, either method

requires a minimal chromatographic separation time of 10 minutes, which causes a bottleneck by the analytical procedures once hundreds or thousands of samples have to be analysed [399].

To expedite the high-throughput development of improved 5-AV production strains, a robust, cheap and fast quantification of 5-AV titers was necessary. Plasmid-based biosensors can enable such high-throughput strain development by exploiting specific interactions between the molecule of interest and a transcription factor that induces the expression of a reporter gene, such as an antibiotic resistance gene or a fluorescent protein gene [400-402]. If a fluorescent reporter gene is used, intracellular concentrations of the molecule of interest can be translated to an optical output, which is easily monitored by photometric measurements (e.g. fluorescence assays). Sub-populations of cells with mixed reporter gene expression can be identified [402] and also potentially separated by flow cytometric cell sorting (FACS) [403]. One successful example of such a transcription-factor based biosensor design was the itaconic acid biosensor described by Hanko et al. [402]. This biosensor employs an itaconate-inducible promoter and a corresponding LysR-type transcriptional regulators from *Yersinia pseudotuberculosis* and *Pseudomonas aeruginosa* [402]. This YpltcR/Pccl itaconate inducible system was shown to be active in both in *E. coli* and *C. necator* H16 [402].

As described in **Chapter 1.8**, a transcription-factor based biosensor relies on a sensor/transcription factor pair. No such sensor protein was described in the literature for 5-AV. However, the *chnR*/P_{ChnB} inducible expression system was shown to be sensitive for the ring-closed form of 5-AV, δ -valerolactam. The

enzymes ORF26 [404-406] and CaiC [407] have been shown to catalyse ring-closure of 5-AV to δ -valerolactam, theoretically enabling a biosensor to extend its specificity spectrum to 5-AV.

ORF26 is an acyl-CoA ligase from *Streptomyces aizunensis* and has been previously described in the literature as 4-aminobutyryl-CoA ligase or a 4-guanidinobutyryl-CoA ligase [404-406]. In a publication by Zhang et al. [407], ORF26 was expressed and purified in *E. coli* and subsequent characterisation of the enzyme demonstrated its function as a lactam synthase – enabling the formation of butyrolactam, δ -valerolactam and caprolactam [406]. The study concluded that ORF26 can act on ω -amino acids with a wide substrate specificity and catalyses their ring closure to their respective lactams. In a co-expression experiment using DavA and DavB, L-lysine was converted to δ -valerolactam through 5-AV. In total, the biosynthetic pathway yielded 5.0 mM δ -VL from 68.4 mM L-lysine after 48 h fermentation [407].

In a second publication by Zhang et al. [408], the *chnR/P_{ChnB}* inducible expression system is used to demonstrate a lactam biosensor, in conjunction with an mCherry reporter, that can sense ϵ -caprolactam, δ -valerolactam and butyrolactam in a dose-dependent manner [408]. The *chnR/P_{ChnB}* pair had previously been investigated as part of a cyclohexanol degradation pathway in *Acinetobacter* sp., activating the expression of a cyclohexanone 1,2-monoxidase ChnB and the cyclohexanone dehydrogenase ChnA [409, 410]. In another study, the regulator of this degradation pathway, ChnR, was shown to be activated by broad range of inducers in a luciferase assay, including δ -valerolactone and other cyclic compounds [411]. Zhang et al. conclude that the

chnR/ P_{ChnB} pair can enable high-throughput screening of lactam titers that is selective for C4-C6 lactams such as δ -valerolactam [408]. However, to date, none of the authors of the study have demonstrated that the lactam biosensor can be expanded as a 5-AV biosensor by expressing ORF26, which is investigated in this study.

This study therefore investigated the 5-AV biosensor design shown in **Figure 5.1**, in which ORF26 and ChnR are expressed under control of the arabinose-inducible $P_{\text{BAD}}/araC$ system. ORF26 then converts 5-AV to δ -valerolactam, which is bound by ChnR and induces the expression of RFP via the P_{ChnB} promoter.

5.2 Results

5.2.1 BS1 can sense extracellular levels of δ -VL, but not 5-AV.

In this study, a bimodular biosensor design was developed that enabled an optical RFP-based output dependent on intracellular 5-AV concentrations.

(Figure 5.1)

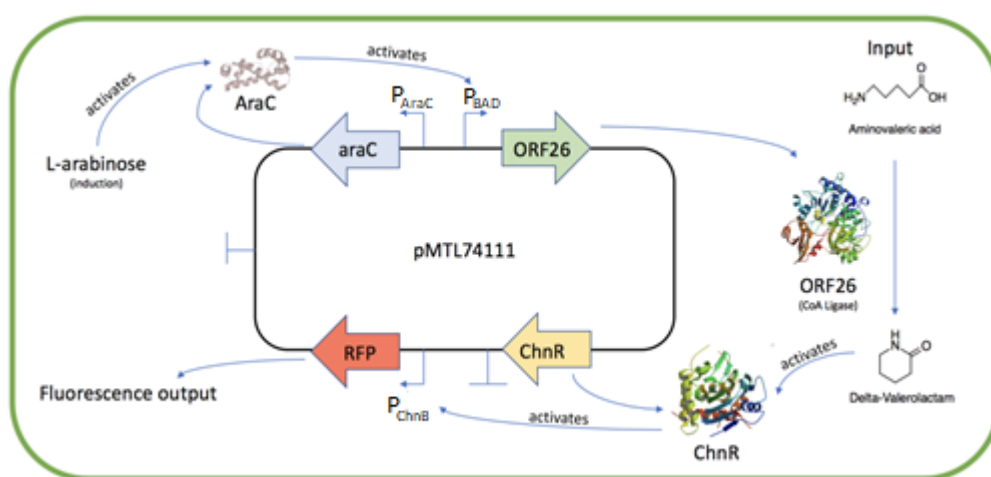


Figure 5.1 A plasmid-based 5-AV biosensor. $P_{BAD}/araC$ is an arabinose inducible expression system and drives the expression of ORF26 and ChnR. ORF26 is a CoA-ligase that converts 5-AV into its ring-closed form δ -valerolactam (δ VL). δ -valerolactam is specifically bound by ChnR, a positive regulator of the P_{ChnB} promoter, which induces RFP expression.

The plasmid containing the biosensor was designed on the basis of pMTL74111.

The plasmid contains a chloramphenicol resistance cassette and is compatible with pMTL71301-series plasmids that were used in **Chapter 4** for the production of 5-AV, enabling the co-expression of the 5-AV synthesis pathway enzymes and biosensor proteins. The $P_{BAD}/araC$ promoter system allowed for an arabinose inducible production [380] of two downstream proteins: ORF26

and ChnR. RFP is expressed under control of P_{ChnB} , which can be activated by ChnR, under the condition that a lactam is present.

E. coli DH5 α cells were transformed with the 5-AV biosensor pBS1 (Figure 5.2).

Details for the construction of this biosensor can be found in Chapter 2.3.1 and

2.3.2

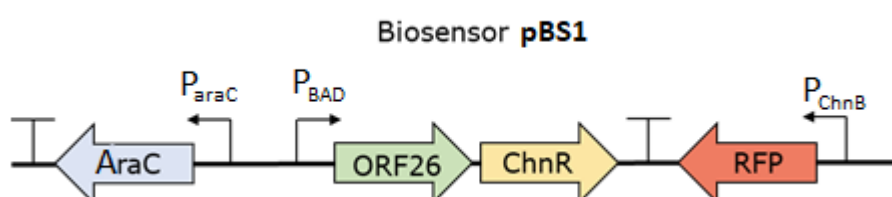


Figure 5.2 Biosensor pBS1 assembly design. The biosensor was assembled by HiFi-assembly (see Chapter 2) and was based on the pMTL74111 vector. *araC* – arabinose operon regulatory protein. P_{AraC} – constitutive promoter of *araC*. P_{BAD} – arabinose inducible promoter. ORF26 - acyl-CoA ligase. ChnR - positive regulator of the P_{ChnB} promoter. P_{ChnB} – δ -valerolactam inducible promoter. RFP – red fluorescent protein. The name within the arrows stand for the encoded proteins.

The transformed cells were grown on LB^{Cm}, harvested by centrifugation and resuspended in water. The cells were then spotted on ECMM^{Cm} plates supplemented with 0-50 mM δ -valerolactam or 5-AV and containing 0.2% arabinose inducer. The cells were incubated for 48 h at 37 °C.

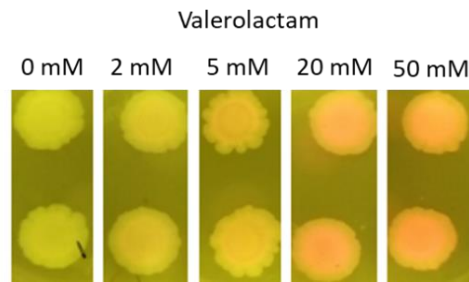


Figure 5.3 *E. coli* DH5 α cells expressing the BS1 biosensor in the presence of δ -valerolactam. Left to right: 0, 2, 5, 20 and 50 mM δ -valerolactam. Cells were spotted on LB^{Cm} medium containing 0.2% arabinose and grown for 48 h.

As can be seen in **Figure 5.3**, the expression of the biosensor BS1 results in a strong visible red colouring of *E. coli* colonies that were supplemented with 20 mM and 50 mM δ -valerolactam and a faint colouring of colonies supplemented with 5 mM. No colouring could be detected on plates that were supplemented with 5-AV by eye (not shown).

5.2.2 Extracellular 5-AV is not converted to δ -valerolactam in *E. coli* harbouring BS2

To test if conversion from 5-AV to δ -valerolactam was catalysed by ORF26, the lactam biosensor construct pBS2 (**Figure 5.4**) was transformed in *E. coli* cells which were then induced with 0.01-0.05% arabinose concentrations. The cells were grown in rich medium (LB^{Cm}) and analysed by LC-MS for δ -valerolactam formation.

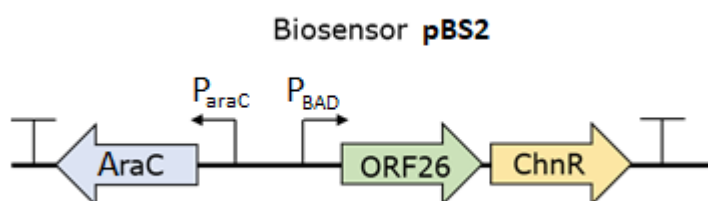


Figure 5.4 Biosensor BS2 assembly design. The biosensor is assembled by HiFi-assembly and based on the pMTL74111 vector. *araC* – arabinose operon regulatory protein. P_{AraC} – constitutive promoter of *araC*. P_{BAD} – arabinose inducible promoter. ORF26 - acyl-CoA ligase. ChnR - positive regulator of the P_{ChnB} promoter. The name within the arrows stand for the encoded proteins.

The LC-MS analysis of these samples, fermented in biological triplicates, yielded no δ -valerolactam formation as no molecule with the mass of δ -VL could be detected. This result was interpreted in the context of the 5-AV toxicity tests that was discussed in **Chapter 4.3.1** In *C. necator* H16, 5-AV is non-toxic and metabolisation as a nitrogen source occurs only after 7 days of fermentation. The possibility of poor 5-AV uptake from the medium was a probable cause for poor 5-AV conversion in *E. coli*, as it could be equally struggling with poor uptake - rather than a failure of ORF26 to catalyse the reaction.

5.2.3 Intracellularly produced 5-AV is slowly converted to δ -valerolactam in *E. coli* harbouring BS2 and L1.

To test the “no-uptake” hypothesis, *E. coli* cells that were transformed with BS2 and the 5-AV biosynthesis plasmid L1 (introduced in **Chapter 4**) were fermented. As both plasmids carry arabinose-inducible elements, the cells were fermented in LB^{Cm} containing 0.1% arabinose and supplemented with 20 mM L-lysine. Negative control strains were grown without L-lysine supplementation or did not contain L1. Another control strain was harbouring only L1, supplemented with L-lysine and another only BS2, supplemented with L-lysine.

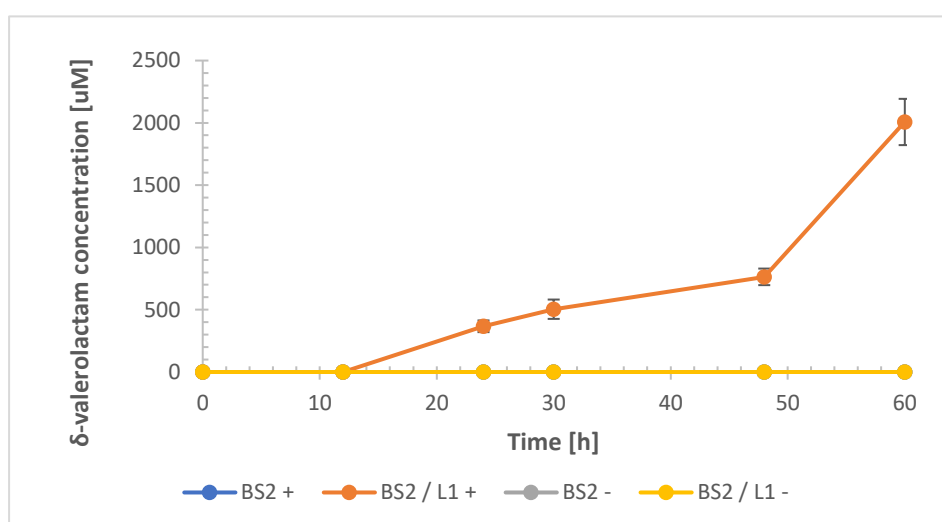


Figure 5.5 Quantified levels of δ -valerolactam in aerobic *E. coli* cells harbouring pBS2 and pL1 in LB^{Cm} supplemented with 20 mM L-lysine. Orange curve: pBS1 and pL1, supplemented. Yellow curve: pBS1 and pL1, unsupplemented. Blue curve: pBS2 only, supplemented. Grey curve: pBS2 only, unsupplemented.

As can be seen in **Figure 5.5**, *E. coli* cells that were expressing pBS1 and pL1 in L-lysine supplemented cultures, were able to accumulate 2006 μ M δ -valerolactam in the supernatant. All control strains without L1 or without L-lysine supplementation could not accumulate δ -valerolactam, because 5-AV

was not produced. However, it should be noted that 5-AV was not quantified in this experiment, as a 1:1 molar conversion from L-lysine to 5-AV had already been established under identical media and fermentation conditions in **Chapter 4.2.4**. A qualitative MS trace of the 5-AV production using L7 instead of L1 (but still feeding L-lysine) can be found in the Appendix (**Figure A20**). Interestingly, low levels (<50 μ M) of δ -valerolactam were measured in the supplemented control strains with pL1 but without pBS2 (**Appendix Fig. A22**), hinting towards the presence of an enzyme native to *E. coli* that can catalyse the ring-closing reaction to δ -valerolactam. The results also show that ORF26 is generally capable of catalysing the desired reaction, but the kinetics of the enzyme are too poor to yield the δ -valerolactam titer that is required for a visible RFP induction. In this study, ORF26 in conjunction with DavA and DavB yielded 2.01 mM δ -valerolactam from 20 mM L-lysine after 60 hours fermentation. Previous results, shown in **Figure 5.3**, have indicated that this level, albeit extracellular, is not high enough to induce a visible RFP response.

5.2.4 ORF26 could not be characterised due to poor solubility

The slow kinetics of ORF26 prompted us to investigate under which conditions ORF26 could be optimised *in vitro*. Characterisation of enzyme kinetics to find a solution that may lead to a faster turnaround of 5-AV to δ -VL was planned. For this purpose, it was attempted to purify ORF26. *orf26* was cloned into a pET-16b vector, resulting in a T7-driven expression cassette for a N-terminal polyhistidine tagged ORF26 (IPTG-inducible). This expression vector was transformed into *E. coli* Lemo21 cells, which carry a helper plasmid that allows for tunable T7 expression by allowing variation of lysozyme levels, which is a natural inhibitor of T7 RNA polymerase. This is an approach that allows for optimisation of expression of “difficult” proteins, such as insoluble membrane proteins [412]. The expression level of lysozyme is controlled by adding rhamnose. For the purification of ORF26, a level of 400 μ M IPTG was chosen and the rhamnose levels were modulated between 0 (strongest expression) and 2000 μ M (weakest expression). The expression of ORF26 was tested at cooler temperatures after induction (30°C) to avoid aggregation [413] and limit degradation by heat-shock proteases [414].

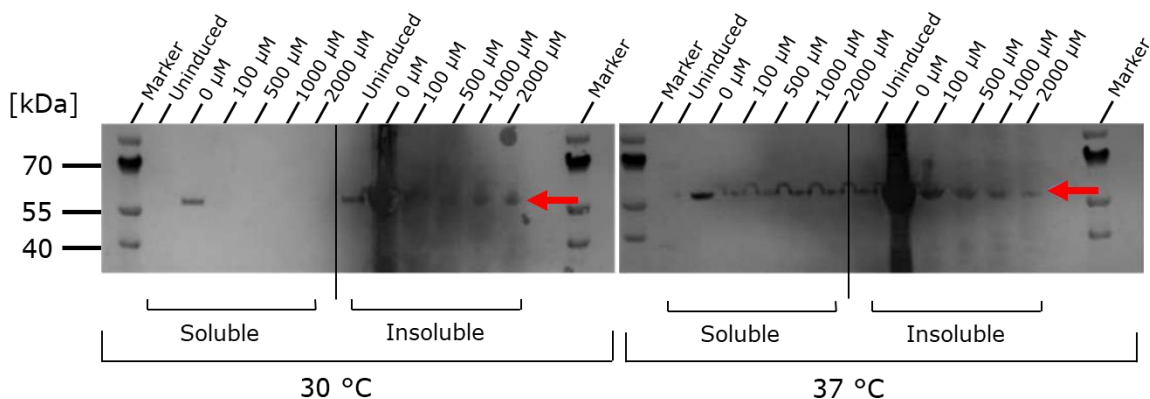


Figure 5.6 Western-blot of His-tagged ORF26 in soluble and insoluble fractions of Lemo21 cells. Protein expression was induced with 400 μ M IPTG and the indicated concentrations of rhamnose. Protein expression was conducted at 30 $^{\circ}$ C (left) and 37 $^{\circ}$ C (right). The expected band height of the ORF26 protein is indicated by arrows.

Lemo21 cells were lysed using BugBuster™ post expression and SDS-PAGE conducted using 4-12% precast Bis-Tris gels (Invitrogen). The proteins were transferred to a PVDF membrane for western blotting and incubated with peroxidase conjugated α -His antibodies. The bands were then visualised with a TMB blotting solution.

As shown in **Figure 5.6**, expressed ORF26 was found mainly in the insoluble fractions on the western blot, regardless of used rhamnose concentrations. Uninduced (no IPTG) fractions showed no band. The strongest expression was found when 0 mM rhamnose was used, which led to no repression of T7 and the highest protein expression. The bands appeared overloaded in the insoluble fractions; however, this condition is the only one that yielded a clear band in the soluble fraction at 30 $^{\circ}$ C. For all rhamnose concentrations over 0 mM, no band in the soluble fractions could be observed at 30 $^{\circ}$ C, but at 37 $^{\circ}$ C faint bands were visible. Generally, most of the expressed ORF26 protein was insoluble.

Attempts to purify soluble His-tagged ORF26 for an enzymatic assay were made using a Nickel column, but failed.

5.2.5 Characterisation of a redesigned biosensor using CaiC

It was concluded that due to the insufficient activity of ORF26, the biosensor would require a redesign if it were to be used as 5-AV sensor. The native *E. coli* CaiC enzyme was hypothesised to be the ideal candidate to drive the reaction from 5-AV to δ -VL in lieu of ORF26, following its overexpression. CaiC is a crotonobetaine/carnitine CoA ligase and catalyses the biotransformation from crotonobetaine to L-carnitine in *E. coli* [415, 416]. It was also shown to catalyse the ring-closure of 4-aminobutyric acid to butyrolactam [417].

For the purpose of replacing ORF26, the new biosensor design BS3 was introduced (**Figure 5.7**)

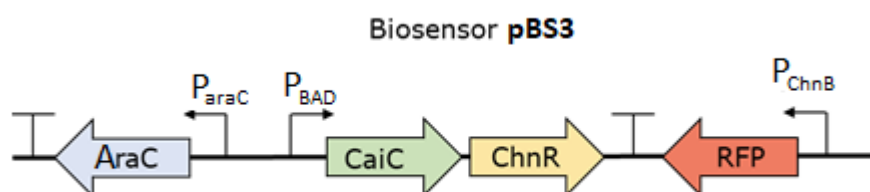


Figure 5.7 Biosensor BS3 assembly design. The biosensor is assembled by HiFi-assembly and based on the pMTL74111 vector. *araC* – arabinose operon regulatory protein. P_{AraC} – constitutive promoter of *araC*. P_{BAD} – arabinose inducible promoter. CaiC - crotonobetaine/carnitine CoA ligase. ChnR - positive regulator of the P_{ChnB} promoter. P_{ChnB} – δ -valerolactam inducible promoter. RFP – red fluorescent protein. The name within the arrows stand for the encoded proteins.

The biosensor plasmid pBS3 was assembled and introduced in *E. coli* DH5 α . The temperature stability of RFP expression from the δ -valerolactam sensor module *ChnR*/ P_{ChnB} -RFP was investigated with colony-spot tests at different temperatures (20 °C, 30 °C and 37°C).

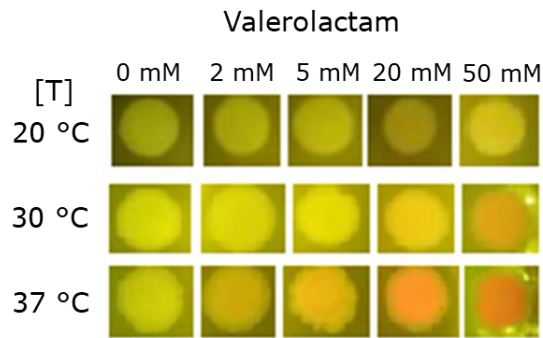


Figure 5.8 *E. coli* DH5 α cells expressing the pBS3 biosensor in the presence of δ -valerolactam at different temperatures. Left to right: 0, 2, 5, 20 and 50 mM δ -valerolactam. Cells were spotted on LB^{Cm} medium containing 0.2% arabinose and grown for 48 h.

Figure 5.8 shows that *E. coli* cells harbouring the biosensor BS3, incubated for 48 h on ECMM^{Cm} plates, in the presence of varying levels of δ -valerolactam and 0.2% arabinose, showed the best results at higher temperatures. The sensor module *ChnR*/*P_{ChnB}-RFP* was most efficient at 37 °C, where slight colouring of colonies could be observed at 2-5 mM δ -VL. At 30 °C, efficiency decreased and 20-50 mM δ -VL were necessary for colouring. At 20 °C, the sensor did not show any visible colouration. This effect was hypothesised to be mainly caused by a slowdown of *E. coli* metabolism at lower temperatures and poorer expression of the sensor module. This result also highlighted an important caveat in biosensor development: While the sensor module profited from high expression levels and higher temperatures, recombinant proteins usually profit from expression at lower temperatures to avoid aggregation [418, 419].

5.2.6 Characterisation of the *ChnR*/ P_{ChnB} -RFP sensor module was not possible due to poor solubility of ChnR.

In order to investigate if the temperature dependency of *ChnR*/ P_{ChnB} -RFP is caused by lower expression levels or a change in the δ -VL/ChnR binding mode, it was desirable to perform a mobility shift assay (EMSA) using purified ChnR in a gel of containing P_{ChnB} DNA and δ -VL at different temperatures and concentrations.

While it is possible to perform EMSA with unpurified crude extracts [420], it would be necessary to show that any observed mobility shift is due to the protein that is being overexpressed, requiring a comparison between induced and uninduced extracts, which could be difficult to interpret if background binding occurs. Furthermore, *E. coli* cells contain DNases, which could further complicate the assay. Also, ChnR would have to have been present in sufficient abundance in the extract to determine a shift and. Therefore, a crude extract EMSA was not attempted.

In order to perform the assay in a controlled manner, it was attempted to express and purify N-terminally His-tagged ChnR using Rosetta-gami™ cells and the pET16(b) vector as described in the material and methods section and analogous to previous attempts to purify ORF26.

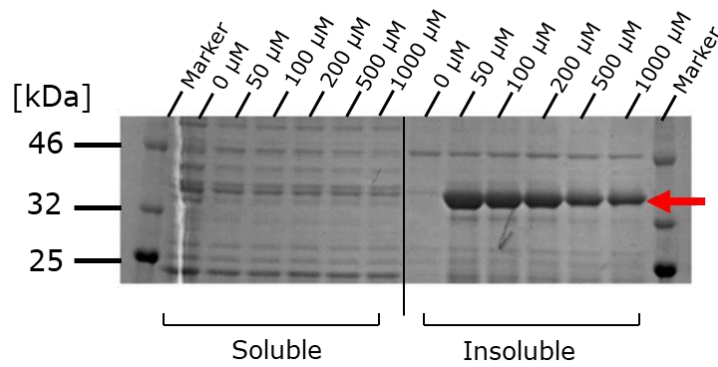


Figure 5.8 SDS-PAGE of His-tagged ChnR in soluble and insoluble fractions of Rosetta-gami™ cells. Protein expression was induced with the indicated levels of IPTG. Protein expression was conducted at 37°C. The expected band height of the ORF26 protein is indicated by arrows.

As can be seen in **Figure 5.8**, ChnR was found to be fully insoluble under all tested IPTG induction conditions. Interestingly, the expression of ChnR was stronger at lower induction levels (50 μM) compared to higher IPTG levels (1000 μM). During fermentation, cells with lower concentrations of arabinos also showed more vivid colouration. It was then attempted to purify ChnR using a nickel affinity column from a culture induced with 400 mM IPTG with no positive result.

5.2.7 Characterisation of ChnR specificity reveals a broad substrate spectrum

To investigate the response of BS3 in the presence of other lactams, including δ -valerolactam, the substrate specificity of the sensor module was tested using the δ -valerolactam analogues 2-pyrrolidone, ϵ -Caprolactam and N-methyl-2-piperidone (**Figure 5.9**).

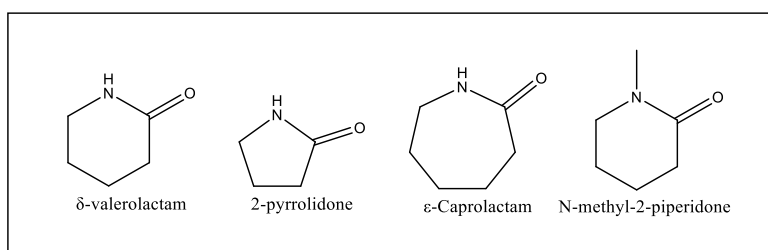


Figure 5.9 δ -valerolactam and its analogues. δ -valerolactam and its analogues 2-pyrrolidone, ϵ -Caprolactam and N-methyl-2-piperidone are supplemented to cells carrying the BC3 biosensor to test ChnR specificity.

2-pyrrolidone is the cyclised form of GABA and tests how a change in ring size affects binding to ChnR together with ϵ -Caprolactam, the cyclised form of 6-aminocaproic acid. N-methyl-2-piperidone is the N-methylated analogue of δ -valerolactam and tests if the presence of a secondary amine in the heterocycle is necessary for ChnR binding. Varying concentrations of δ -valerolactam and its analogues ranging from 0 mM to 50 mM were used to supplement micro-fermentation cultures (200 μ l), induced at $OD_{600} = 0.2$ with 0.2% arabinose. Fluorescence was periodically measured using at the optimal wavelengths for RFP detection ($\lambda_{exc} = 558$ nm and $\lambda_{emm} = 583$ nm).

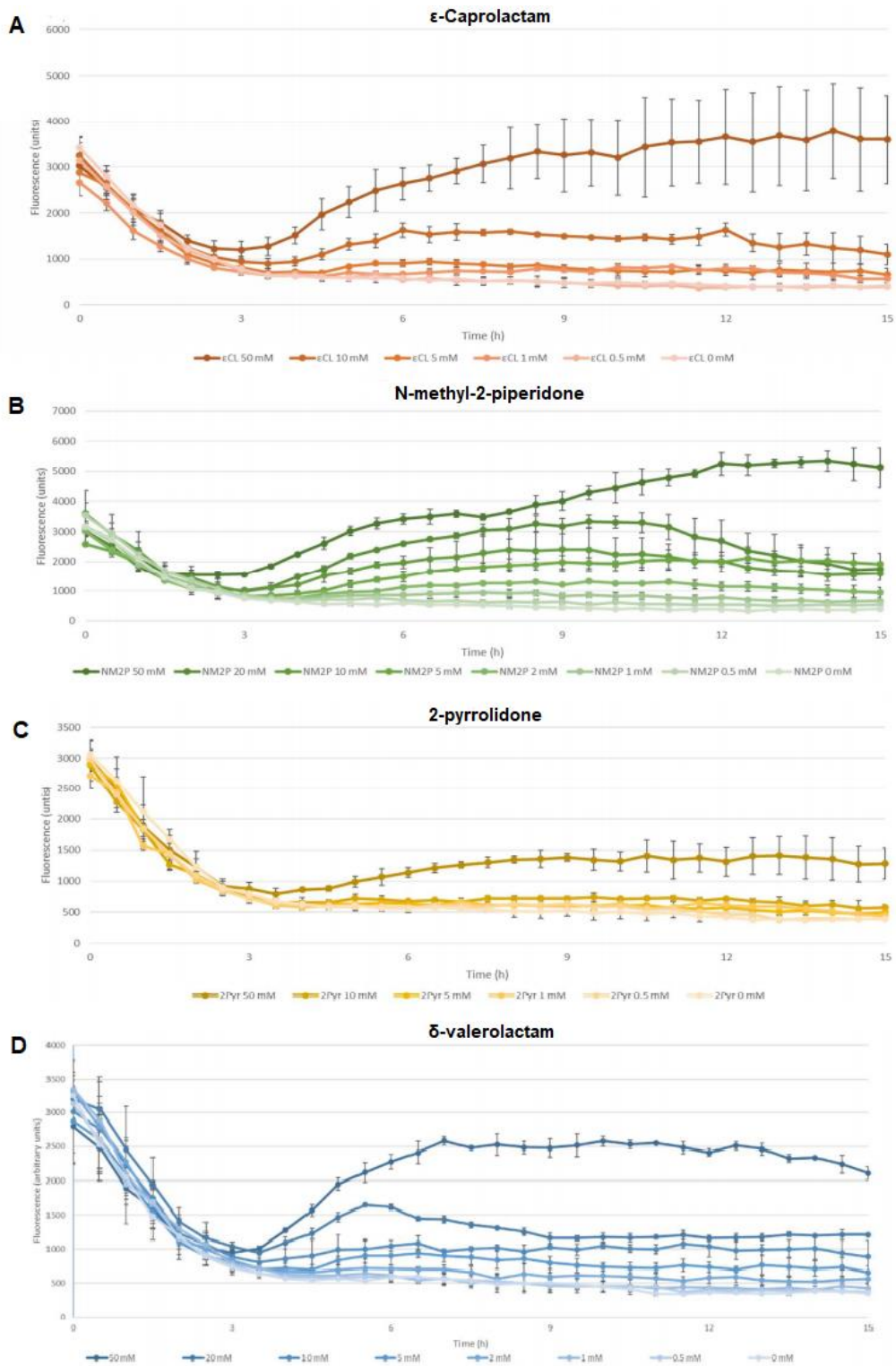


Figure 5.10 Fluorescence of DH5α cells (OD normalised) expressing biosensor pBS3 in microfermentation using ECMM^{Cm}, supplemented with δ-valerolactam and its analogues. (A) ε-Caprolactam (B) N-methyl-2-piperidone (C) 2-pyrrolidone (D) δ-valerolactam. Colour shades correspond to varying supplementation. Fluorescence was measured in A.U. and is directly comparable. Biological triplicates were used.

Figure 5.10 shows that the strongest inducer of ChnR was N-methy-2-piperidone (**B**) with a maximum fluorescence intensity of 5300 A.U. at 50 mM. Followed by ϵ -Caprolactam (**A**) at 3900 A.U., δ -valerolactam (**D**) at 2500 A.U. and lastly 2-pyrrolidone at 1500 A.U. This result indicated that a loss of polarity by N-methylation of the lactam amine is beneficial to the binding mode towards ChnR and that binding occurs more efficiently with larger ring size.

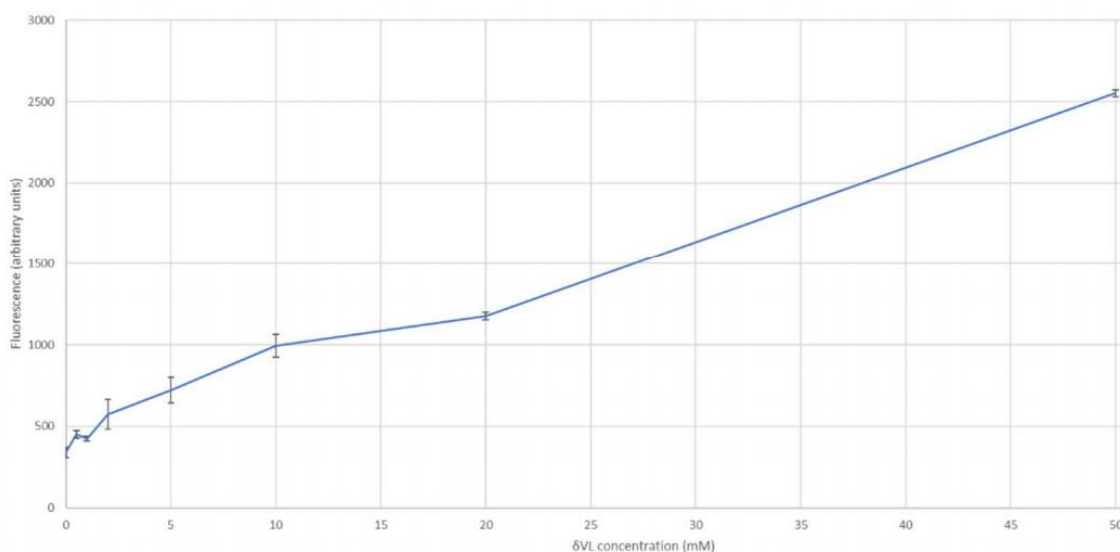


Figure 5.11 Relationship between δ -valerolactam concentration and fluorescence.

The results shown in **Figure 5.10 (D)** allowed to calculate a fluorescence-based standard curve for δ -valerolactam with the maximum A.U. that was caused by each concentration. This standard curve shows a linear relationship between δ -valerolactam titer and fluorescence output. Unfortunately, this linear relationship becomes less pronounced for lower concentrations. Also, measurements between 0 and 4 mM are situated only 10-20% over noise level, leading to a poor signal-to-noise ratio for the obtained values.

5.3 Discussion

This study has shown that the biosensor design pBS1 was capable of detecting δ -valerolactam in a graded manner. The results have shown that 5 mM δ -valerolactam were the minimum threshold for a visibly discernible RFP production. pBS1, was, however, not able to act as a biosensor for 5-AV.

Causes were troubleshooted and it was found that the underlying problem is likely poor 5-AV uptake by *E. coli*. In a strain containing the 5-AV biosynthesis vector pL1 with the biosensor, that produces 5-AV from L-lysine (see **Chapter 4.2.4**), 2.01 mM δ -valerolactam were produced from 20 mM L-lysine after 60 hours fermentation. This level is too low for the detection threshold of 5 mM and thus does not produce visibly red cells.

A similar test, under comparable conditions, was conducted by Zhang et al. [407] and yielded 2.5 mM δ -valerolactam from 6.8 mM L-lysine. In comparison, the yield in this study was lower, but Zhang et al. [407] used a maltose binding protein (MBP) tagged ORF26 and expressed the protein in the BL-21 strain that is optimised for protein expression and purification, without explanation of why the assay was carried out using a purification construct rather than the native ORF26. The used MBP affinity tag is known to also act as a solubility tag and the authors lowered the temperature after induction to 25 °C. These circumstances possibly alleviate aggregation and were likely responsible for a higher yield than reported in this study [407]. Interestingly, the authors also observed a production of low δ -VL titers in cultures without ORF26 and this could be reproduced in this study. In their discussion, the authors hypothesise that a

native enzyme in *E. coli* must be capable of performing the ring-closing reaction to δ -VL to some degree and postulate that the CoA ligase CaiC is responsible [407]. CaiC is a known betaine:CoA ligase [415] that was shown to catalyse the ring-closure of 4-aminobutyric acid to butyrolactam [417] and its performance in regard to catalysing the ring-closing catalysis of 5-AV was then shown to be comparably strong to ORF26 by Zhang et al.[407].

In order to perform an enzymatic characterisation of ORF26 under our conditions, it was attempted to purify ORF26 using a N-terminal 6xHis-tag but problems with insolubility thwarted the attempt. In comparison, Zhang et al. [407] successfully purified N-terminal 6xHis-tagged ORF26 using the pET28b expression vector and BL21 Star (DE3) cells. The strain used in this study, Lemo21 and their strain, BL21 Star, are both pLysS containing strains and T7-based. BL21 Star expresses T7 lysozyme, whereas Lemo21 offers a tunable expression. Both strains also contain the DE3 lysogen and are deficient in OmpT and Lon proteases. BL21 star offers a higher basal expression of mRNA due to a mutation in the RNAaseE gene *rne131*. This leads to the conclusion that the strains are sufficiently similar so that their difference should not significantly impact the expression of ORF26.

Characterisation of a redesigned biosensor, BS3, showed that the sensor module profits from high expression levels and higher temperatures. Unfortunately, the cyclising enzymes generally profit from colder temperatures for expression to avoid aggregation [418, 419].

In order to further investigate the P_{ChnB} /ChnR module, which has to date not been characterised fully, it was attempted to purify ChnR but the attempt failed again due to poor solubility of the protein. ChnR is predicted *in-silico* as helix-turn-helix (HTH) transcriptional regulator. While most proteins with HTH DNA binding motifs are soluble, some examples in *E. coli*, such as the transmembrane DNA-binding protein CadC, are not [421].

Binding of ChnR to various δ -VL analogues was then investigated and it was found that binding and activation were more efficient with N-methylation and larger lactam ring sizes. This result may suggest the existence of a hydrophobic pocket for lactam binding, which evolved for the role of ChnR in cyclohexanone degradation. Larger rings showed more hydrophobic surface and methylation reduces the polarity of the N-residue. Our result also replicated previous investigations by Zhang et al. [407], where ϵ -Caprolactam and 2-pyrrolidone were tested alongside δ -valerolactam. In their study, Zhang et al. [407] performed a fluorescence assay and also reported a similar result.

The relationship between fluorescence and δ -valerolactam concentration was found to be linear for concentrations greater than 2-5 mM. Currently, δ -valerolactam titers from 20 mM L-lysine only reach the lower threshold and pBS3 could not be used as a reliable biosensor. Assuming the full conversion of L-lysine to 5AV within 60 h, which was not measured, this would mean that the conversion of 5AV to δ -valerolactam was catalysed at a maximum productivity of $33.3 \mu\text{M h}^{-1}$. However, once strain development allows for 5-AV production in titers in excess of 50 mM, the biosensors BS1 and BS3 would be able to detect it.

5.4 Key outcomes of the biosensor development

A design of a bimodular biosensor for 5-AV based on CoA ligase ORF26 with substrate specificity for 5-AV and the ChnR/P_{ChnB} regulator/promoter pair with sensitivity towards δ -valerolactam was proposed.

The biosensor pBS1 was shown to detect δ -valerolactam in a graded manner, but not 5-AV, when added to medium or plates. The δ -valerolactam biosensor module pBS2 was then used to troubleshoot. Poor uptake of 5-AV was hypothesised as the main reason for the outcome.

To circumvent the uptake problem, the Dav-biosynthetic pathway was used to produce 5-AV intracellularly from L-lysine and δ -valerolactam was detected in the supernatant of cultures co-expressing BS2. However, the kinetics of ORF26 were too slow to convert 5-AV in necessary concentrations for a visible colour change of *E. coli* colonies.

As a result, a redesign of the biosensor was proposed to incorporate the CoA-ligase CaiC from *E. coli* instead of ORF26. However, the new CoA ligase performed similarly to ORF26 in spot tests. It was attempted to purify CaiC for assaying but poor solubility of the protein thwarted the experiment.

In order to characterise the sensor module, it was attempted to purify ChnR, but the protein was found to be insoluble. Future experiment could attempt to use crude extracts for EMSA assays instead.

The binding of ChnR to activating molecules was investigated by measuring fluorescence output in presence of δ -valerolactam and its analogues, resulting

in a hypothesis of the existence of a hydrophobic binding pocket. The TECAN data also allowed to calculate a standard curve for δ -valerolactam quantification using fluorescence, which was found to be linear above concentrations of 5 mM. While the current biosensors pBS1 and pBS3 suffered from a high lower detection limit of 5 mM, they could be useful in applications where 5-AV is produced in quantities in excess of 50 mM.

Chapter 6

**General discussion
and future work**

Chapter 6: General discussion and future work

6.1 General outcomes of this study

The overall aim of this study was to engineer a strain of *C. necator* H16 for the production of the two platform chemicals 5-aminovaleric acid and 5-hydroxyvaleric acid. No previous studies had attempted to produce these compounds in *C. necator* H16, although the compounds were previously shown to be producible in other hosts such as *Co. glutamicum* in a high titer. It is, however, the unique ability of *C. necator* H16 to grow lithoautotrophically from CO₂, hydrogen and a nitrogen source, that allows these compounds to be made through a synthetic pathway that utilises sustainable feedstocks, as opposed to the feedstocks that were used in the previous studies, such as glucose or L-lysine.

This study shows the production of 5-OHV from β -alanine (**Chapter 3**) in *C. necator* H16, which marks an important step towards sustainable polyester production depending on the closure of the gap from aspartate (central metabolism) to β -alanine, which is under current investigation (Salinas, University of Nottingham, unpublished). This study also investigated the production of 5-AV from gluconate (**Chapter 4**) in *C. necator* H16, showing 5-AV production from central metabolism and marking a significant step towards future sustainable nylon-5 production using this host and syngas as feedstock. Another aim of this study was to design and test a transcription-factor based 5-AV biosensor for high-throughput screening. A novel biosensor design was tested (**Chapter 5**) and showed potential for screening of high-yielding

synthetic 5-AV pathways in excess of 50 mM. **Figure 6.1** shows the pathways that were implemented for the three engineering projects.

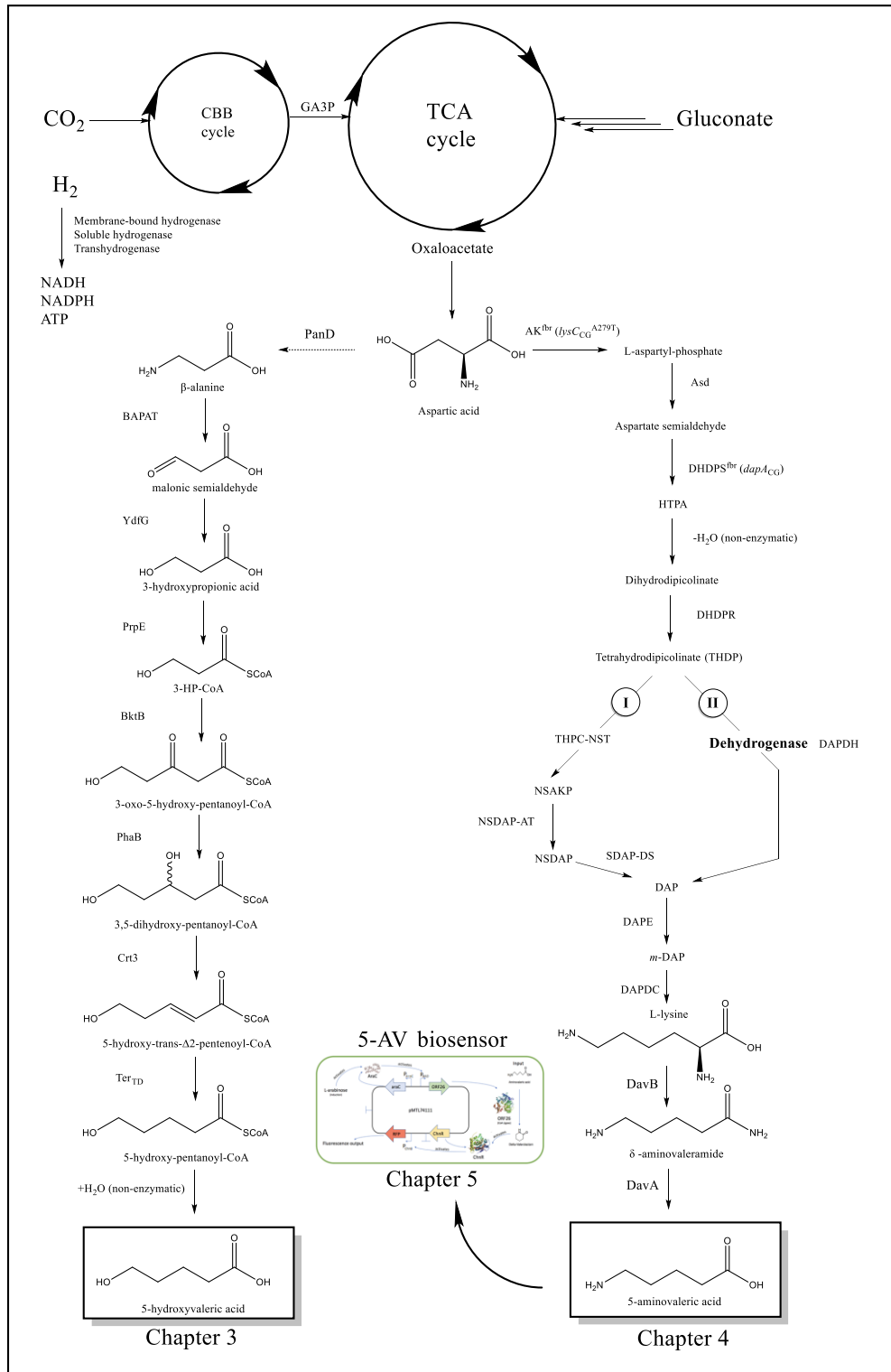


Figure 6.1 Main outcomes of this study: Engineered pathways for the production of 5-AV, 5-OHV and a 5-AV biosensor.

(legend continued) (I) Succinylase pathway (II) Dehydrogenase pathway. Dashed arrow indicates missing pathway component. The feedback-resistant mutant of *Co. glutamicum* AK (A279T) and the natively feedback-resistant *Co. glutamicum* DHDPS were introduced with the dehydrogenase bypass to overproduce L-lysine in *C. necator* H16 $\Delta phaCAB \Delta gabT$. DavA and DavB convert lysine to 5-AV. AK – aspartate kinase. HTPA - 4-hydroxy-2,3,4,5-tetrahydrodipicolinate. DHDPS - dihydrodipicolinate synthase. DHDPR - dihydrodipicolinate reductase. THDP – tetrahydrodipicolinate. THPC-NST - 2,3,4,5-tetrahydropyridine-2-carboxylate *N*-succinyltransferase. NS-AKP - *N*-succinyl-L-2-amino-ketopimelate. NSDAP-AT - *N*-succinyldiaminopimelate aminotransferase. NSDAP - *N*-succinyl-L,L-2,6,-diaminopimelate. SDAP-DS - succinyldiaminopimelate desuccinylase. DAPE - diaminopimelate epimerase. *m*-DAP – *meso*-diaminopimelate. DAPDC - diaminopimelate decarboxylase. DavA - δ -aminovaleramidase. DavB – lysine monooxygenase. A reverse beta-oxidation pathway was introduced to produce 5-OHV in *C. necator* H16 $\Delta 4$, introducing transaminase BAPAT, oxidoreductase YdfG, CoA synthetase PrpE, β -ketothiolase BktB, 3-hydroxybutyryl-CoA dehydrogenase PhaB, crotonase Crt3 and trans-2-enoyl-CoA reductase Ter_{TD}. GA3P – glyceraldehyde 3-phosphate. A transcription-factor based biosensor was introduced to measure intracellular 5-AV levels using a fluorescent output.

6.2 5-OHV production in *C. necator* H16

This work showed the production of up to 17.1 mg L⁻¹ 5-hydroxyvaleric acid from β -alanine in the supernatants of shake flask cultures of *C. necator* H16, making this precursor for biodegradable polyesters more easily accessible from central metabolism in *C. necator* H16. A novel reverse beta-oxidation pathway was constructed for this purpose and is shown in **Figure 6.1**. Reverse beta-oxidation reactions were shown in this study to successfully convert a C3 feedstock to a C5 value-added product – a synthesis route with a slowly growing popularity among synthetic biologists [228, 422, 423].

The knockout mutant strain *C. necator* Δ *phaCAB* Δ *mmsA1* Δ *mmsA2* Δ *mmsA3* was engineered as suitable host strain, minimising 3-HP degradation and maximising product yields through disruption of the PHA synthesis machinery, which can act as a carbon sink. The Δ *mmsA1* Δ *mmsA2* Δ *mmsA3* disruptions have been shown as effective for 3-HP production by López et al. [424] and this study replicated the result.

A main goal of this thesis was to investigate if a top-down screening approach would be suitable to identify pathways for 5-OHV production. In this study, twenty tested combinations were tested and two yielded the desired product. This shows that future biological engineering design strategies can also likely employ top-down strategies successfully, provided that there is an abundance of putative enzymes to test.

Future designs for synthetic pathways using the top-down strategy can improve on the example shown in this work and employ a broader range of synthetic

biology tools to search for relevant pathway enzymes. In this work, selection of putative enzymes was based on prior biochemical characterisation, or a shown functionality in other synthetic pathways. In future, *in-silico* analysis of the genomes of many species could predict a wealth of to-date uncharacterised putative enzymes, of which some may have scientifically interesting properties or surprising functionalities, depending on the ecological niche in which they developed.

As a result of the top-down screening approach, a novel pathway design was established. This pathway, shown in **Figure 6.1**, entailed the transaminase BAPAT from *C. violaceum* that had previously been characterised for 3-HP production by López et al. [210], replicating their result. Equally, the *E. coli* oxidoreductase YdfG proved to be effective, also previously shown by López et al. [210] and replicated in this study. Then, the CoA synthetase PrpE was shown as more effective in catalysing thioester formation than the CoA ligase Pct, likely because the expense of ATP during the reaction shifts the chemical equilibrium of the reaction towards the side of the products. Chen et al. [425]. suggest that Pct may be more effective if the medium contains acetate as carbon source, elevating the acetyl-CoA levels that are needed to drive the thioester formation with Pct. *C. necator* H16 would be tolerant towards acetate, as evidenced by metabolic engineering efforts to produce ethanol from acetate in it [426]. This however would also defeat the original aim of this work to provide a foundation for C5 production from sustainable sources. The beta-ketothiolase BktB showed a better performance over PaaJ, which has been shown to catalyse the condensation of acetyl-CoA with succinyl-CoA.

Succinyl-CoA is a C₄ acceptor in these reactions and it is possible that PaaJ may struggle with C₃ acceptors, such as 3-HP-CoA. The substrate spectrum of PaaJ is therefore an interesting topic for further biochemical investigation. The (*R*)-stereospecific pathway variant of the reverse beta-oxidation step was found to be favoured over the (*S*)- variant. This may be due to the endogenous nature of the used enzyme PhaB and Crt3, which guarantees compatible codon-usage, folding and cofactor usage. The introduction of the FadAB complex on the other hand led to lower cell densities during fermentation and impaired fitness, likely due to a disruption of lipid homeostasis. More research must be conducted in future to elucidate the role of the FadAB complex and its impact on membrane composition. In regards to trans-2-enoyl-CoA reductases, both Ter_{TD} and Ter_{EG} catalysed the reaction, replicating the results of successful prior use in cyanobacteria [269], *E. coli* [271] and *Methylobacterium extorquens* AM1 [427].

Further pathway optimisation was conducted using synthetic RBS sites and strong constitutive promoters. Such a strategy is well-known in the synthetic biology community and builds on the foundation of known strong endogenous promoters [294, 428]. In future work, the promoters could be further finetuned by employing promoter engineering, an approach that seeks to control gene expression more precisely by rationally designing bespoke promoter sequences for a given synthetic pathway [429].

In this study, the resting cell culturing condition of *C. necator* H16 was investigated using phosphate limitation. Decoupling the production phase from the growth phase produced higher titers, but unfortunately *C. necator* H16

displayed a surprising accumulation of uracil under this condition. Further research should be conducted on the cause of this phenomenon, ideally by tracking the metabolisation of the used carbon and nitrogen source by radiolabelling and untargeted LCMS analysis [430].

Future work on the 5-hydroxyvalerate biosynthesis pathway should aim to integrate it into the chromosome of the *C. necator* H16 Δ 4 strain and introduce recombinant enzymes such as PanD and PanM that bridge the gap from oxaloacetate to β -alanine (**Figure 6.1**, dotted arrow), which would make 5-OHV producible in CO₂/H₂ fermentation.

6.3 5-AV production in *C. necator* H16

In this work, we have also shown the production of 5-AV titers of up to 10.5 mg L⁻¹ directly from central metabolism of *C. necator* H16 $\Delta gabT$, putting 5-AV production in CO₂/H₂ in feasible reach.

It was shown that the product 5-AV can be produced in high concentrations without a toxic effect in *C. necator* H16 and replicated results from the current literature in other organisms, which show that 5-AV is easily producible from L-lysine when the *P. putida* enzymes DavA and DavB are expressed.

The $\Delta gabT$ deletion was hypothesised to be beneficial for 5-AV production due to a disruption of a 5-AV degradation pathway that was inferred due to homology of GabT to DavT. The hypothesis was not rejected, as a $\Delta gabT$ deletion strain could not degrade 5-AV to glutaric acid, a side-product that had previously lowered yields.

It was then investigated if the L-lysine producing capabilities of *Co. glutamicum* could be transferred to *C. necator* H16 by expressing the native *Co. glutamicum* genes for the aspartate kinase and the dehydrogenase bypass (**Figure 6.1**). It was shown that this resulted in moderate improvements in yield, leading to another attempt to further optimise the 5-AV biosynthesis pathway using a constitutive promoter, synthetic RBS sites and a new expression construct with feedback-resistant variants of aspartate kinase and DHDPS, alongside the dehydrogenase bypass. These optimisations resulted in a steep 4-fold increase of 5-AV titers. This successful use of a deregulated pathway replicates previous findings in *E. coli* [431] *Co. glutamicum* [432].

Future work on the 5-AV biosynthesis pathway should aim to engineer the mutations that lead to L-lysine pathway deregulation directly into the respective copies of the enzymes that are already present (inferred by homology) in *C. necator* H16 $\Delta gabT$. The Dav pathway may also be introduced into the chromosome. As it is dependent on flux through the TCA cycle, the introduction of anaplerotic reactions may become necessary to replenish it. A study about anaplerotic reactions in *C. necator* H16 detected the enzyme activities of the malic enzyme Mae and phosphoenolpyruvate carboxykinase Pck, but not pyruvate carboxylase Pyc and phosphoenolpyruvate carboxylase Ppc [433], suggesting plenty potential for heterologous expression of anaplerotic enzymes in *C. necator* H16.

Future work should also aim to investigate if 5-AV is producible in CO₂/H₂ fermentation, which would result in a bio-based nylon-5 production.

6.4 A novel 5-AV biosensor

This work also shows a novel biosensor design for 5-AV detection based on the specific cyclisation of 5-AV to δ -valerolactam and subsequent sensing through ChnR as well as a downstream RFP reporter. This investigation has shown that while the general principle of the transcription-factor based biosensor works, the concentration range in which it was active and linear does not match the concentrations at which 5-AV is currently produced through the *C. necator* H16 pathway shown in **Figure 6.1**. However, the biosensor may either become more useful in the future with improved yields or could be used in high-yield 5-AV production applications in other organisms. The enzymes that convert 5AV to δ -valerolactam may have to be rationally engineered or mutagenised for faster kinetics. The use of robot-assisted high-throughput screening of randomly mutagenised CaiC, for example, may aid in engineering a faster enzyme. Such an enzyme would also be highly useful in a pathway that produces δ -valerolactam instead of 5-AV, making nylon-5 even easier to synthesise industrially by simple ring-opening polymerisation, rather than from its amino acid monomer. To help making all the described progress possible, this work established analytical protocols for the detection of amino acids via HPLC that were shared collaboratively within the research group and recently used in paper published by Hanko et al. [434]. Furthermore, as outcome of this thesis, robust analytical procedures were developed to detect pathway intermediates in LC-MS from *C. necator* H16 as well as chemical synthesis route for 5-OHV, which is not commercially available.

Acknowledgements

I want to acknowledge the help of Dr. Salah Abdelrazig and Dr. Catherine Otori at the University of Nottingham for training and helpful discussions surrounding LCMS analysis of my samples. In particular, Dr. Salah Abdelrazig trained me to use the LCMS to full user status and supported my research with valuable experience and the following protocols for extraction and analysis of my samples. I would also like to thank Nigel Minton and Kati Kovacs for encouraging me to take a metabolomics course at the Phenome Centre at the University of Birmingham as a start to my training with the Q-Exactive MS.

I also would like to thank Dr. Klaus Winzer, who co-supervised Christopher with me and Dr. Katalin Kovacs, for their fantastic advice throughout the biosensor development. As a result of his great efforts and admirable work-ethic, Christopher graduated from the University of Nottingham with a Masters degree and I could not be prouder of him for his achievements and wish him all the best for his future in science.

References

1. El Karoui, M., M. Hoyos-Flight, and L. Fletcher, *Future Trends in Synthetic Biology—A Report*. Frontiers in Bioengineering and Biotechnology, 2019. **7**(175).
2. Philp, J.C., R.J. Ritchie, and J.E. Allan, *Synthetic biology, the bioeconomy, and a societal quandary*. Trends Biotechnol, 2013. **31**(5): p. 269-72.
3. Claire Bailey, H.M., Brian Crook *Synthetic biology: A review of the technology, and current and future needs from the regulatory framework in Great Britain*. Health and Safety Executive, 2012. **Research Report**(RR944).
4. Verma, A.S., et al., *Biotechnology in the realm of history*. Journal of pharmacy & bioallied sciences, 2011. **3**(3): p. 321-323.
5. Fairbanks, D.J., *Mendel and Darwin: untangling a persistent enigma*. Heredity, 2020. **124**(2): p. 263-273.
6. Pederson, T., *The nucleus introduced*. Cold Spring Harbor perspectives in biology, 2011. **3**(5): p. a000521.
7. Dahm, R., *Friedrich Miescher and the discovery of DNA*. Developmental Biology, 2005. **278**(2): p. 274-288.
8. Scheuerlein, H., F. Henschke, and F. Köckerling, *Wilhelm von Waldeyer-Hartz- A Great Forefather: His Contributions to Anatomy with Particular Attention to "His" Fascia*. Frontiers in surgery, 2017. **4**: p. 74-74.
9. Watson, J.D. and F.H.C. Crick, *Molecular Structure of Nucleic Acids: A Structure for Deoxyribose Nucleic Acid*. Nature, 1953. **171**(4356): p. 737-738.
10. Tobin, M.J., *April 25, 1953: three papers, three lessons*. Am J Respir Crit Care Med, 2003. **167**(8): p. 1047-9.
11. Holm, S., *Is synthetic biology mechanical biology? History and Philosophy of the Life Sciences*, 2015. **37**(4): p. 413-429.
12. Xie, M., V. Haellman, and M. Fussenegger, *Synthetic biology—application-oriented cell engineering*. Current Opinion in Biotechnology, 2016. **40**: p. 139-148.
13. Opgenorth, P., et al., *Lessons from Two Design–Build–Test–Learn Cycles of Dodecanol Production in Escherichia coli Aided by Machine Learning*. ACS Synthetic Biology, 2019. **8**(6): p. 1337-1351.
14. Petzold, C., et al., *Analytics for Metabolic Engineering*. Frontiers in bioengineering and biotechnology, 2015. **3**: p. 135.
15. Morange, M., *A new revolution?* EMBO reports, 2009. **10**(S1): p. S50-S53.
16. Eisenstein, M., *How to build a genome*. Nature, 2020. **578**: p. 633-635.
17. Müller, K. and K. Arndt, *Standardization in Synthetic Biology*. Methods in molecular biology (Clifton, N.J.), 2012. **813**: p. 23-43.
18. Sedlmayer, F., D. Aubel, and M. Fussenegger, *Synthetic gene circuits for the detection, elimination and prevention of disease*. Nature Biomedical Engineering, 2018. **2**(6): p. 399-415.
19. Breuer, M., et al., *Essential metabolism for a minimal cell*. Elife, 2019. **8**.
20. Hutchison, C.A., et al., *Design and synthesis of a minimal bacterial genome*. Science, 2016. **351**(6280): p. aad6253.
21. Clarke, L. and R. Kitney, *Developing synthetic biology for industrial biotechnology applications*. Biochemical Society transactions, 2020. **48**(1): p. 113-122.
22. Cameron, D.E., C.J. Bashor, and J.J. Collins, *A brief history of synthetic biology*. Nat Rev Microbiol, 2014. **12**(5): p. 381-90.

23. Alexandra Daisy, G., et al., *Synthetic Biology: What It Is and Why It Matters*, in *Synthetic Aesthetics: Investigating Synthetic Biology's Designs on Nature*. 2014, MIT Press. p. 2-25.
24. Anderson, T.R., E. Hawkins, and P.D. Jones, *CO₂, the greenhouse effect and global warming: from the pioneering work of Arrhenius and Callendar to today's Earth System Models*. Endeavour, 2016. **40**(3): p. 178-187.
25. Maddah, H., *Comprehensive Review on C5, C6 and C9 Chemicals – Production Processes, Applications and Market Analyses*. International Journal of Scientific and Engineering Research, 2015. **6**.
26. Mohammadi, M., et al., *Anionic copolymerization of nylon 6/12: A comprehensive review*. Polymer Engineering & Science, 2019. **59**(8): p. 1529-1543.
27. Shimizu, A., et al., *An Industrial Process for Adipic Acid Production by the Liquid-Phase Oxidation of Cyclohexanone with Molecular Oxygen*. Bulletin of the Chemical Society of Japan, 2003. **76**(10): p. 1993-2001.
28. Bellussi, G. and C. Perego, *Industrial Catalytic Aspects of the Synthesis of Monomers for Nylon Production*. CATTECH, 2000. **4**(1): p. 4-16.
29. Gordillo Sierra, A.R. and H.S. Alper, *Progress in the metabolic engineering of bio-based lactams and their omega-amino acids precursors*. Biotechnol Adv, 2020. **43**: p. 107587.
30. Porta, M., *One hundred years ago: the dawning of the insulin era*. Acta Diabetologica, 2021. **58**(1): p. 1-4.
31. Stylianou, C. and C. Kelnar, *The introduction of successful treatment of diabetes mellitus with insulin*. Journal of the Royal Society of Medicine, 2009. **102**(7): p. 298-303.
32. Zahn, H. *Struktur und Synthese von Insulin*. in *Zweiundsiebzigster Kongress*. 1967. Munich: J.F. Bergmann-Verlag.
33. Quianzon, C.C. and I. Cheikh, *History of insulin*. Journal of community hospital internal medicine perspectives, 2012. **2**(2): p. 10.3402/jchimp.v2i2.18701.
34. Becker, J. and C. Wittmann, *Advanced biotechnology: metabolically engineered cells for the bio-based production of chemicals and fuels, materials, and health-care products*. Angew Chem Int Ed Engl, 2015. **54**(11): p. 3328-50.
35. Buschke, N., et al., *Metabolic engineering of industrial platform microorganisms for biorefinery applications--optimization of substrate spectrum and process robustness by rational and evolutive strategies*. Bioresour Technol, 2013. **135**: p. 544-54.
36. Kind, S., et al., *From zero to hero - production of bio-based nylon from renewable resources using engineered Corynebacterium glutamicum*. Metab Eng, 2014. **25**: p. 113-23.
37. Atsumi, S. and J.C. Liao, *Metabolic engineering for advanced biofuels production from Escherichia coli*. Curr Opin Biotechnol, 2008. **19**(5): p. 414-9.
38. Casini, A., et al., *A Pressure Test to Make 10 Molecules in 90 Days: External Evaluation of Methods to Engineer Biology*. Journal of the American Chemical Society, 2018. **140**(12): p. 4302-4316.
39. Gruber, K., *Biohackers: A growing number of amateurs join the do-it-yourself molecular biology movement outside academic laboratories*. EMBO Rep, 2019. **20**(6).
40. Wendisch, V.F., *Microbial production of amino acids and derived chemicals: Synthetic biology approaches to strain development*. Current Opinion in Biotechnology, 2014. **30**: p. 51-58.

41. Schneider, J., K. Niermann, and V.F. Wendisch, *Production of the amino acids L-glutamate, L-lysine, L-ornithine and L-arginine from arabinose by recombinant Corynebacterium glutamicum*. J Biotechnol, 2011. **154**(2-3): p. 191-8.
42. Perez-Garcia, F., P. Peters-Wendisch, and V.F. Wendisch, *Engineering Corynebacterium glutamicum for fast production of L-lysine and L-pipecolic acid*. Appl Microbiol Biotechnol, 2016. **100**(18): p. 8075-90.
43. Singh, S. and B.S. Tiwari, *Chapter 11 - Biosynthesis of High-Value Amino Acids by Synthetic Biology*, in *Current Developments in Biotechnology and Bioengineering*, S.P. Singh, et al., Editors. 2019, Elsevier. p. 257-294.
44. Lee, K.H., et al., *Systems metabolic engineering of Escherichia coli for L-threonine production*. Molecular systems biology, 2007. **3**: p. 149-149.
45. Zhang, Y., et al., *Determination of key enzymes for threonine synthesis through in vitro metabolic pathway analysis*. Microb Cell Fact, 2015. **14**: p. 86.
46. Wendisch, V.F., *Microbial production of amino acids and derived chemicals: synthetic biology approaches to strain development*. Curr Opin Biotechnol, 2014. **30**: p. 51-8.
47. Khan, N., et al., *Modeling the growth of Corynebacterium glutamicum under product inhibition in L-glutamic acid fermentation*. Biochemical Engineering Journal, 2005. **25**: p. 173-178.
48. Becker, J. and C. Wittmann, *Bio-based production of chemicals, materials and fuels -Corynebacterium glutamicum as versatile cell factory*. Curr Opin Biotechnol, 2012. **23**(4): p. 631-40.
49. Kim, J.Y., et al., *Production of non-proteinogenic amino acids from alpha-keto acid precursors with recombinant Corynebacterium glutamicum*. Biotechnol Bioeng, 2013. **110**(11): p. 2846-55.
50. Kinoshita, S., *Amino-acid production by the fermentation process*. Nature, 1972. **240**(5378): p. 211.
51. Bušić, A., et al., *Bioethanol Production from Renewable Raw Materials and Its Separation and Purification: A Review*. Food technology and biotechnology, 2018. **56**(3): p. 289-311.
52. Mohd Azhar, S.H., et al., *Yeasts in sustainable bioethanol production: A review*. Biochemistry and Biophysics Reports, 2017. **10**: p. 52-61.
53. Tang, T., et al., *Recent developments in the microbial production of 1,3-propanediol*. Biofuels, 2013. **4**(6): p. 651-667.
54. Oh, B.-R., et al., *Efficient production of 1,3-propanediol from crude glycerol by repeated fed-batch fermentation strategy of a lactate and 2,3-butanediol deficient mutant of Klebsiella pneumoniae*. Microbial Cell Factories, 2018. **17**(1): p. 92.
55. Saxena, R.K., et al., *Microbial production and applications of 1,2-propanediol*. Indian journal of microbiology, 2010. **50**(1): p. 2-11.
56. Song, C.W., et al., *Microbial production of 2,3-butanediol for industrial applications*. Journal of Industrial Microbiology & Biotechnology, 2019. **46**(11): p. 1583-1601.
57. Fu, C., et al., *Recent advances on bio-based isobutanol separation*. Energy Conversion and Management: X, 2021. **10**: p. 100059.
58. Stichnothe, H., et al., *Bio-Based Chemicals A 2020 Update Bio-Based Chemicals A 2020 Update With input from: (pdf version) Published by IEA Bioenergy*. 2020.
59. Saltzberg, M.A., et al., *DuPont: Biorenewables at E.I. DU Pont DE Nemours & Co*, in *Industrial Biorenewables*. 2016. p. 175-217.

60. Chung, H., et al., *Bio-based production of monomers and polymers by metabolically engineered microorganisms*. *Curr Opin Biotechnol*, 2015. **36**: p. 73-84.
61. Niimi, S., et al., *Metabolic engineering of 1,2-propanediol pathways in Corynebacterium glutamicum*. *Appl Microbiol Biotechnol*, 2011. **90**(5): p. 1721-9.
62. Lee, S.H., et al., *Biomass, strain engineering, and fermentation processes for butanol production by solventogenic clostridia*. *Appl Microbiol Biotechnol*, 2016. **100**(19): p. 8255-71.
63. Papoutsakis, E.T., *Engineering solventogenic clostridia*. *Curr Opin Biotechnol*, 2008. **19**(5): p. 420-9.
64. Zhao, M., et al., *Metabolic engineering of Escherichia coli for producing adipic acid through the reverse adipate-degradation pathway*. *Metab Eng*, 2018. **47**: p. 254-262.
65. Choi, S., et al., *Biorefineries for the production of top building block chemicals and their derivatives*. *Metab Eng*, 2015. **28**: p. 223-39.
66. Salvachua, D., et al., *Succinic acid production from lignocellulosic hydrolysate by Basfia succiniciproducens*. *Bioresour Technol*, 2016. **214**: p. 558-66.
67. Cimini, D., et al., *Production of succinic acid from Basfia succiniciproducens up to the pilot scale from Arundo donax hydrolysate*. *Bioresour Technol*, 2016. **222**: p. 355-360.
68. Scholten, E., T. Renz, and J. Thomas, *Continuous cultivation approach for fermentative succinic acid production from crude glycerol by Basfia succiniciproducens DD1*. *Biotechnol Lett*, 2009. **31**(12): p. 1947-51.
69. Papagianni, M., *Advances in citric acid fermentation by Aspergillus niger: biochemical aspects, membrane transport and modeling*. *Biotechnol Adv*, 2007. **25**(3): p. 244-63.
70. Wang, L., et al., *The opposite roles of agdA and glaA on citric acid production in Aspergillus niger*. *Appl Microbiol Biotechnol*, 2016. **100**(13): p. 5791-803.
71. Hu, W., et al., *A mutation of Aspergillus niger for hyper-production of citric acid from corn meal hydrolysate in a bioreactor*. *J Zhejiang Univ Sci B*, 2014. **15**(11): p. 1006-10.
72. Saha, B.C., *Emerging biotechnologies for production of itaconic acid and its applications as a platform chemical*. *J Ind Microbiol Biotechnol*, 2017. **44**(2): p. 303-315.
73. Shin, W.S., et al., *Enhanced Production of Itaconic Acid through Development of Transformed Fungal Strains of Aspergillus terreus*. *J Microbiol Biotechnol*, 2017. **27**(2): p. 306-315.
74. Yang, Z., et al., *Enhanced itaconic acid production by self-assembly of two biosynthetic enzymes in Escherichia coli*. *Biotechnol Bioeng*, 2017. **114**(2): p. 457-462.
75. Lopez, C.A., *The genetic basis of 3-hydroxypropanoate metabolism in Cupriavidus necator H16*. Thesis submitted to the University of Nottingham, 2017.
76. Straathof, A.J., et al., *Feasibility of acrylic acid production by fermentation*. *Appl Microbiol Biotechnol*, 2005. **67**(6): p. 727-34.
77. Papoutsakis, E.T. and C.L. Meyer, *Fermentation equations for propionic-acid bacteria and production of assorted oxychemicals from various sugars*. *Biotechnol Bioeng*, 1985. **27**(1): p. 67-80.
78. Lundgren, J., et al., *Methanol production from steel-work off-gases and biomass based synthesis gas*. *Applied Energy*, 2013. **112**: p. 431-439.

79. Veses, A., et al., *A combined two-stage process of pyrolysis and catalytic cracking of municipal solid waste for the production of syngas and solid refuse-derived fuels*. Waste Manag, 2020. **101**: p. 171-179.
80. Ragauskas, A.J., et al., *The path forward for biofuels and biomaterials*. Science, 2006. **311**(5760): p. 484-9.
81. Cui, X., et al., *Room-temperature electrochemical water-gas shift reaction for high purity hydrogen production*. Nat Commun, 2019. **10**(1): p. 86.
82. Saleh, A.R., et al., *Syngas production from municipal solid waste with a reduced tar yield by three-stages of air inlet to a downdraft gasifier*. Fuel, 2020. **263**: p. 116509.
83. Wainaina, S., I.S. Horváth, and M.J. Taherzadeh, *Biochemicals from food waste and recalcitrant biomass via syngas fermentation: A review*. Bioresour Technol, 2018. **248**(Pt A): p. 113-121.
84. Aftab, A., et al., *PRODUCTION OF SYNTHETIC GAS FROM AGRICULTURE AND FOREST WASTES USING FIXED BED GASIFIER*. PAKISTAN JOURNAL OF AGRICULTURE AGRICULTURAL ENGINEERING AND VETERINARY SCIENCES, 2016. **32**: p. 229-236.
85. Heinrich, D., M. Raberg, and A. Steinbüchel, *Studies on the aerobic utilization of synthesis gas (syngas) by wild type and recombinant strains of Ralstonia eutropha H16*. Microb Biotechnol, 2018. **11**(4): p. 647-656.
86. Pohlmann, A., et al., *Genome sequence of the bioplastic-producing "Knallgas" bacterium Ralstonia eutropha H16*. Nat Biotechnol, 2006. **24**(10): p. 1257-62.
87. Fritsch, J., O. Lenz, and B. Friedrich, *The maturation factors HoxR and HoxT contribute to oxygen tolerance of membrane-bound [NiFe] hydrogenase in Ralstonia eutropha H16*. J Bacteriol, 2011. **193**(10): p. 2487-97.
88. *Taxonomy Browser*. National Center for Biotechnology Information.
89. Fukui, T., et al., *Enhancement of glycerol utilization ability of Ralstonia eutropha H16 for production of polyhydroxyalkanoates*. Appl Microbiol Biotechnol, 2014. **98**(17): p. 7559-68.
90. Hyeon, J.E., et al., *Efficient biological conversion of carbon monoxide (CO) to carbon dioxide (CO₂) and for utilization in bioplastic production by Ralstonia eutropha through the display of an enzyme complex on the cell surface*. Chem Commun (Camb), 2015. **51**(50): p. 10202-5.
91. Volova, T., et al., *A glucose-utilizing strain, Cupriavidus eutrophus B-10646: growth kinetics, characterization and synthesis of multicomponent PHAs*. PloS one, 2014. **9**(2): p. e87551-e87551.
92. Heinrich, D., et al., *Synthesis Gas (Syngas)-Derived Medium-Chain-Length Polyhydroxyalkanoate Synthesis in Engineered Rhodospirillum rubrum*. Appl Environ Microbiol, 2016. **82**(20): p. 6132-6140.
93. Schwartz, E. and B. Friedrich, *A physical map of the megaplasmid pHG1, one of three genomic replicons in Ralstonia eutropha H16*. FEMS Microbiol Lett, 2001. **201**(2): p. 213-9.
94. Lenz, O. and B. Friedrich, *A novel multicomponent regulatory system mediates H₂ sensing in Alcaligenes eutrophus*. Proceedings of the National Academy of Sciences of the United States of America, 1998. **95**(21): p. 12474-12479.
95. Friedrich, B., et al., *A hydrogen-sensing multiprotein complex controls aerobic hydrogen metabolism in Ralstonia eutropha*. Biochemical Society Transactions, 2005. **33**(1): p. 97-101.
96. Bernhard, M., et al., *Functional and Structural Role of the Cytochrome b Subunit of the Membrane-Bound Hydrogenase Complex of Alcaligenes Eutrophus H16*. European Journal of Biochemistry, 1997. **248**(1): p. 179-186.

97. Schneider, K., et al., *The iron-sulphur centres of soluble hydrogenase from Alcaligenes eutrophus*. Biochimica et Biophysica Acta (BBA) - Protein Structure, 1979. **578**(2): p. 445-461.
98. Schneider, K. and H.G. Schlegel, *Purification and properties of soluble hydrogenase from Alcaligenes eutrophus H 16*. Biochimica et Biophysica Acta (BBA) - Enzymology, 1976. **452**(1): p. 66-80.
99. Burgdorf, T., et al., *[NiFe]-Hydrogenases of *Ralstonia eutropha* H16: Modular Enzymes for Oxygen-Tolerant Biological Hydrogen Oxidation*. Microbial Physiology, 2005. **10**(2-4): p. 181-196.
100. Kohlmann, Y., et al., *Analyses of soluble and membrane proteomes of Ralstonia eutropha H16 reveal major changes in the protein complement in adaptation to lithoautotrophy*. J Proteome Res, 2011. **10**(6): p. 2767-76.
101. Bowien, B. and B. Kusian, *Genetics and control of CO₂ assimilation in the chemoautotroph Ralstonia eutropha*. Arch Microbiol, 2002. **178**(2): p. 85-93.
102. Soo Youn Lee, Y.S.K., Woo-Ri Shin, Jaeyoung Yu, b and S.L. Jiye Lee, Yang-Hoon Kim, Jiho Min *b, *Non-photosynthetic CO₂ bio-mitigation by Escherichia coli harbouring CBB genes*. Green Chemistry, 2020. **22**: p. 6889 - 6896.
103. Md. Salatul Islam Mozumder, L.G.-G., Heleen De Wever, Eveline I.P. Volcke, *Poly(3-hydroxybutyrate) (PHB) production from CO₂: Model development and process optimization*. Biochemical Engineering Journal, 2015. **98**: p. 107-116.
104. Andreessen, B., N. Taylor, and A. Steinbuchel, *Poly(3-hydroxypropionate): a promising alternative to fossil fuel-based materials*. Appl Environ Microbiol, 2014. **80**(21): p. 6574-82.
105. Kozhevnikov, I.V., et al., *Cloning and molecular organization of the polyhydroxyalkanoic acid synthase gene (phaC) of Ralstonia eutropha strain B5786*. Prikl Biokhim Mikrobiol, 2010. **46**(2): p. 153-60.
106. Horng, Y.T., et al., *Enhanced polyhydroxybutyrate (PHB) production via the coexpressed phaCAB and vgb genes controlled by arabinose P promoter in Escherichia coli*. Lett Appl Microbiol, 2010. **50**(2): p. 158-67.
107. Mravec, F., et al., *Accumulation of PHA granules in Cupriavidus necator as seen by confocal fluorescence microscopy*. FEMS Microbiology Letters, 2016. **363**(10).
108. Horng, Y.T., et al., *Functional cis-expression of phaCAB genes for poly(3-hydroxybutyrate) production by Escherichia coli*. Lett Appl Microbiol, 2011. **52**(5): p. 475-83.
109. Yee, L.N., et al., *Molecular characterisation of phaCAB from Comamonas sp. EB172 for functional expression in Escherichia coli JM109*. Microbiol Res, 2012. **167**(9): p. 550-7.
110. Arenas-Lopez, C., et al., *The genetic basis of 3-hydroxypropanoate metabolism in Cupriavidus necator H16*. Biotechnol Biofuels, 2019. **12**: p. 150.
111. Eikmanns, U. and W. Buckel, *Properties of 5-hydroxyvalerate CoA-transferase from Clostridium aminovalericum*. Biol Chem Hoppe Seyler, 1990. **371**(11): p. 1077-82.
112. Myung, J., et al., *Expanding the range of polyhydroxyalkanoates synthesized by methanotrophic bacteria through the utilization of omega-hydroxyalkanoate co-substrates*. AMB Express, 2017. **7**(1): p. 118.
113. Papadopoulos, L., et al., *Synthesis and characterization of novel poly(ethylene furanoate-co-adipate) random copolyesters with enhanced biodegradability*. Polymer Degradation and Stability, 2018. **156**: p. 32-42.
114. Tokiwa, Y. and T. Suzuki, *Hydrolysis of polyesters by lipases*. Nature, 1977. **270**(5632): p. 76-78.

115. Sohn, Y.J., et al., *Fermentative High-Level Production of 5-Hydroxyvaleric Acid by Metabolically Engineered Corynebacterium glutamicum*. ACS Sustainable Chemistry & Engineering, 2021. **9**(6): p. 2523-2533.
116. Voss, I. and A. Steinbuchel, *Application of a KDPG-aldolase gene-dependent addiction system for enhanced production of cyanophycin in Ralstonia eutropha strain H16*. Metab Eng, 2006. **8**(1): p. 66-78.
117. Ewering, C., et al., *Metabolic engineering of strains of Ralstonia eutropha and Pseudomonas putida for biotechnological production of 2-methylcitric acid*. Metab Eng, 2006. **8**(6): p. 587-602.
118. Lu, J., et al., *Studies on the production of branched-chain alcohols in engineered Ralstonia eutropha*. Appl Microbiol Biotechnol, 2012. **96**(1): p. 283-97.
119. Muller, J., et al., *Engineering of Ralstonia eutropha H16 for autotrophic and heterotrophic production of methyl ketones*. Appl Environ Microbiol, 2013. **79**(14): p. 4433-9.
120. Grousseau, E., et al., *Isopropanol production with engineered Cupriavidus necator as bioproduction platform*. Appl Microbiol Biotechnol, 2014. **98**(9): p. 4277-90.
121. Brigham, C.J., et al., *Engineering Ralstonia eutropha for Production of Isobutanol from CO₂, H₂, and O₂*, in *Advanced Biofuels and Bioproducts*, J.W. Lee, Editor. 2013, Springer New York: New York, NY. p. 1065-1090.
122. Shin, J.H., et al., *Metabolic engineering of Corynebacterium glutamicum for enhanced production of 5-aminovaleric acid*. Microb Cell Fact, 2016. **15**(1): p. 174.
123. Park, S.J., et al., *High-level conversion of L-lysine into 5-aminovalerate that can be used for nylon 6,5 synthesis*. Biotechnol J, 2014. **9**(10): p. 1322-8.
124. Park, S.J., et al., *Metabolic engineering of Escherichia coli for the production of 5-aminovalerate and glutarate as C5 platform chemicals*. Metab Eng, 2013. **16**: p. 42-7.
125. SEKIGUCHI, F.J.C.a.H., *Thermal properties of amino acid type polyamides*. Chem. zvesti, 1976. **30**(3): p. 281-291.
126. Greco, T. and M. Wegener, *Piezo- and/or pyroelectric polymer composition, useful e.g. as imaging material in piezo- and/or pyroelectric component, comprises a matrix containing piezo- and/or pyroelectric (co)polymer and a nanoparticle comprising e.g. metal*. German Patent DE102009016209, 2010.
127. Zhongbo Zhang, M.H.L., and Lei Zhu, *Unified Understanding of Ferroelectricity in n-Nylons: Is the Polar Crystalline Structure a Prerequisite?* Macromolecules, 2016. **49**(8): p. 3070 - 3982.
128. Revelles, O., et al., *Multiple and interconnected pathways for L-lysine catabolism in Pseudomonas putida KT2440*. J Bacteriol, 2005. **187**(21): p. 7500-10.
129. Liu, P., et al., *Enzymatic production of 5-aminovalerate from L-lysine using L-lysine monooxygenase and 5-aminovaleramidase amidohydrolase*. Sci Rep, 2014. **4**: p. 5657.
130. Li, Z., et al., *Overexpression of transport proteins improves the production of 5-aminovalerate from L-lysine in Escherichia coli*. Sci Rep, 2016. **6**: p. 30884.
131. Rohles, C.M., et al., *Systems metabolic engineering of Corynebacterium glutamicum for the production of the carbon-5 platform chemicals 5-aminovalerate and glutarate*. Microb Cell Fact, 2016. **15**(1): p. 154.
132. Kim, H.T., et al., *Metabolic engineering of Corynebacterium glutamicum for the production of glutaric acid, a C5 dicarboxylic acid platform chemical*. Metab Eng, 2019. **51**: p. 99-109.

133. Botes, A.L. and A.V.E. Conradie, *Methods, Reagents and cells for biosynthesising compounds*. US Patent Application 20150361459, 2015.
134. Jorge, J.M., et al., *Improved fermentative production of gamma-aminobutyric acid via the putrescine route: Systems metabolic engineering for production from glucose, amino sugars, and xylose*. *Biotechnol Bioeng*, 2017. **114**(4): p. 862-873.
135. Cheng, J., et al., *Production of nonnatural straight-chain amino acid 6-aminocaproate via an artificial iterative carbon-chain-extension cycle*. *Metabolic Engineering*, 2019. **55**: p. 23-32.
136. Arruda, P. and P. Barreto, *Lysine Catabolism Through the Saccharopine Pathway: Enzymes and Intermediates Involved in Plant Responses to Abiotic and Biotic Stress*. *Frontiers in Plant Science*, 2020. **11**(587).
137. Espinosa-Urgel, M. and J.L. Ramos, *Expression of a Pseudomonas putida aminotransferase involved in lysine catabolism is induced in the rhizosphere*. *Appl Environ Microbiol*, 2001. **67**(11): p. 5219-24.
138. Cao, X., et al., *The OCT plasmid encodes D-lysine membrane transport and catabolic enzymes in Pseudomonas putida*. *Plasmid*, 1993. **30**(2): p. 83-9.
139. Chang, Y.F. and E. Adams, *Glutarate semialdehyde dehydrogenase of Pseudomonas. Purification, properties, and relation to L-lysine catabolism*. *J Biol Chem*, 1977. **252**(22): p. 7979-86.
140. Matsui, D., et al., *Mutational and crystallographic analysis of l-amino acid oxidase/monooxygenase from Pseudomonas sp. AIU 813: Interconversion between oxidase and monooxygenase activities*. *FEBS Open Bio*, 2014. **4**: p. 220-8.
141. Revelles, O., et al., *The davDT operon of Pseudomonas putida, involved in lysine catabolism, is induced in response to the pathway intermediate delta-aminovaleric acid*. *J Bacteriol*, 2004. **186**(11): p. 3439-46.
142. Edayathumangalam, R., et al., *Crystal structure of Bacillus subtilis GabR, an autorepressor and transcriptional activator of gabT*. *Proc Natl Acad Sci U S A*, 2013. **110**(44): p. 17820-5.
143. Belitsky, B.R., *Bacillus subtilis GabR, a protein with DNA-binding and aminotransferase domains, is a PLP-dependent transcriptional regulator*. *J Mol Biol*, 2004. **340**(4): p. 655-64.
144. Orol Gómez, D., *Characterisation of the native beta-alanine pathway in Cupriavidus necator H16*. Thesis submitted to The University of Nottingham, 2019. <http://eprints.nottingham.ac.uk/id/eprint/60481>.
145. Brautaset, T. and T.E. Ellingsen, *3.47 - Lysine: Industrial Uses and Production*, in *Comprehensive Biotechnology (Second Edition)*, M. Moo-Young, Editor. 2011, Academic Press: Burlington. p. 541-554.
146. Blickling, S., et al., *Reaction mechanism of Escherichia coli dihydrodipicolinate synthase investigated by X-ray crystallography and NMR spectroscopy*. *Biochemistry*, 1997. **36**(1): p. 24-33.
147. Blickling, S. and J. Knäblein, *Feedback inhibition of dihydrodipicolinate synthase enzymes by L-lysine*. *Biol Chem*, 1997. **378**(3-4): p. 207-10.
148. Christensen, J.B., et al., *Structure and Function of Cyanobacterial DHDPS and DHDPR*. *Sci Rep*, 2016. **6**: p. 37111.
149. Cremer, J., et al., *Regulation of enzymes of lysine biosynthesis in Corynebacterium glutamicum*. *J Gen Microbiol*, 1988. **134**(12): p. 3221-9.
150. Blickling, S. and J. Knäblein, *Feedback inhibition of dihydrodipicolinate synthase enzymes by L-lysine*. *Biol Chem*, 1997. **378**(3-4): p. 207-10.

151. Dommaraju, S.R., et al., *Catalytic mechanism and cofactor preference of dihydrodipicolinate reductase from methicillin-resistant Staphylococcus aureus*. Arch Biochem Biophys, 2011. **512**(2): p. 167-74.
152. Girish, T.S., V. Navratna, and B. Gopal, *Structure and nucleotide specificity of Staphylococcus aureus dihydrodipicolinate reductase (DapB)*. FEBS Lett, 2011. **585**(16): p. 2561-7.
153. Reddy, S.G., J.C. Sacchettini, and J.S. Blanchard, *Expression, purification, and characterization of Escherichia coli dihydrodipicolinate reductase*. Biochemistry, 1995. **34**(11): p. 3492-501.
154. Gillner, D.M., D.P. Becker, and R.C. Holz, *Lysine biosynthesis in bacteria: a metallodesuccinylase as a potential antimicrobial target*. J Biol Inorg Chem, 2013. **18**(2): p. 155-63.
155. Hutton, C.A., M.A. Perugini, and J.A. Gerrard, *Inhibition of lysine biosynthesis: an evolving antibiotic strategy*. Mol Biosyst, 2007. **3**(7): p. 458-65.
156. Scapin, G. and J.S. Blanchard, *Enzymology of bacterial lysine biosynthesis*. Adv Enzymol Relat Areas Mol Biol, 1998. **72**: p. 279-324.
157. Simms, S.A., W.H. Voige, and C. Gilvarg, *Purification and characterization of succinyl-CoA: tetrahydrodipicolinate N-succinyltransferase from Escherichia coli*. J Biol Chem, 1984. **259**(5): p. 2734-41.
158. Beaman, T.W., et al., *Three-dimensional structure of tetrahydrodipicolinate N-succinyltransferase*. Biochemistry, 1997. **36**(3): p. 489-94.
159. Schnell, R., et al., *Tetrahydrodipicolinate N-succinyltransferase and dihydrodipicolinate synthase from Pseudomonas aeruginosa: structure analysis and gene deletion*. PLoS One, 2012. **7**(2): p. e31133.
160. Weyand, S., G. Kefala, and M.S. Weiss, *The three-dimensional structure of N-succinyldiaminopimelate aminotransferase from Mycobacterium tuberculosis*. J Mol Biol, 2007. **367**(3): p. 825-38.
161. Ledwidge, R. and J.S. Blanchard, *The dual biosynthetic capability of N-acetylornithine aminotransferase in arginine and lysine biosynthesis*. Biochemistry, 1999. **38**(10): p. 3019-24.
162. Boyen, A., et al., *Acetylornithine deacetylase, succinyldiaminopimelate desuccinylase and carboxypeptidase G2 are evolutionarily related*. Gene, 1992. **116**(1): p. 1-6.
163. Ray, S.S., et al., *Cocrystal structures of diaminopimelate decarboxylase: mechanism, evolution, and inhibition of an antibiotic resistance accessory factor*. Structure, 2002. **10**(11): p. 1499-508.
164. White, P.J. and B. Kelly, *Purification and Properties of Diaminopimelate Decarboxylase from Escherichia Coli*. Biochem J, 1965. **96**: p. 75-84.
165. Cheraghi, S., et al., *Improved production of L-lysine by over-expression of Meso-diaminopimelate decarboxylase enzyme of Corynebacterium glutamicum in Escherichia coli*. Pak J Biol Sci, 2010. **13**(10): p. 504-8.
166. Chatterjee, S. and A.K. Banerjee, *Production of extracellular lysine by a strain of Bacillus coagulans. Identification and requirements for growth and lysine accumulation*. Folia Microbiol (Praha), 1975. **20**(1): p. 46-51.
167. Peterkofsky, B. and C. Gilvarg, *N-Succinyl-L-diaminopimelic-glutamic transaminase*. J Biol Chem, 1961. **236**: p. 1432-8.
168. Hudson, A.O., et al., *An LL-diaminopimelate aminotransferase defines a novel variant of the lysine biosynthesis pathway in plants*. Plant Physiol, 2006. **140**(1): p. 292-301.
169. Liu, Y., R.H. White, and W.B. Whitman, *Methanococci use the diaminopimelate aminotransferase (DapL) pathway for lysine biosynthesis*. Journal of bacteriology, 2010. **192**(13): p. 3304-3310.

170. Triassi, A.J., et al., *L,L-diaminopimelate aminotransferase (DapL): a putative target for the development of narrow-spectrum antibacterial compounds*. Front Microbiol, 2014. **5**: p. 509.
171. Hudson, A.O., et al., *Biosynthesis of lysine in plants: evidence for a variant of the known bacterial pathways*. Biochimica et Biophysica Acta (BBA) - General Subjects, 2005. **1721**(1): p. 27-36.
172. Hudson, A.O., et al., *An Diaminopimelate Aminotransferase Defines a Novel Variant of the Lysine Biosynthesis Pathway in Plants*. Plant Physiology, 2006. **140**(1): p. 292-301.
173. Misono, H., et al., *Occurrence of meso-alpha, epsilon-diaminopimelate dehydrogenase in Bacillus sphaericus*. Biochem Biophys Res Commun, 1976. **72**(1): p. 89-93.
174. Dong, X., et al., *Attenuating l-lysine production by deletion of ddh and lysE and their effect on l-threonine and l-isoleucine production in Corynebacterium glutamicum*. Enzyme Microb Technol, 2016. **93-94**: p. 70-78.
175. Scapin, G., S.G. Reddy, and J.S. Blanchard, *Three-dimensional structure of meso-diaminopimelic acid dehydrogenase from Corynebacterium glutamicum*. Biochemistry, 1996. **35**(42): p. 13540-51.
176. Scapin, G., et al., *Substrate and inhibitor binding sites in Corynebacterium glutamicum diaminopimelate dehydrogenase*. Biochemistry, 1998. **37**(10): p. 3278-85.
177. Xu, J.Z., et al., *Overexpression of thermostable meso-diaminopimelate dehydrogenase to redirect diaminopimelate pathway for increasing L-lysine production in Escherichia coli*. Sci Rep, 2019. **9**(1): p. 2423.
178. Misono, H., et al., *Meso-alpha,epsilon-diaminopimelate D-dehydrogenase: distribution and the reaction product*. Journal of bacteriology, 1979. **137**(1): p. 22-27.
179. Schruppf, B., et al., *A functionally split pathway for lysine synthesis in Corynebacterium glutamicum*. J Bacteriol, 1991. **173**(14): p. 4510-6.
180. Hudson, A.O., et al., *Dual diaminopimelate biosynthesis pathways in Bacteroides fragilis and Clostridium thermocellum*. Biochim Biophys Acta, 2011. **1814**(9): p. 1162-8.
181. Miller, M.B. and B.L. Bassler, *Quorum sensing in bacteria*. Annu Rev Microbiol, 2001. **55**: p. 165-99.
182. Subramaniam, R., *High-density Cultivation in the Production of Microbial Products*. Chemical and Biochemical Engineering Quarterly, 2019. **32**: p. 451-464.
183. Monnet, V. and R. Gardan, *Quorum-sensing regulators in Gram-positive bacteria: 'cherchez le peptide'*. Mol Microbiol, 2015. **97**(2): p. 181-4.
184. Verbeke, F., et al., *Peptides as Quorum Sensing Molecules: Measurement Techniques and Obtained Levels In vitro and In vivo*. Front Neurosci, 2017. **11**: p. 183.
185. Papenfort, K. and B.L. Bassler, *Quorum sensing signal-response systems in Gram-negative bacteria*. Nature reviews. Microbiology, 2016. **14**(9): p. 576-588.
186. Dunlap, P.V., *Quorum regulation of luminescence in Vibrio fischeri*. J Mol Microbiol Biotechnol, 1999. **1**(1): p. 5-12.
187. Ruby, E.G. and K.H. Lee, *The Vibrio fischeri-Euprymna scolopes Light Organ Association: Current Ecological Paradigms*. Applied and environmental microbiology, 1998. **64**(3): p. 805-812.
188. Nyholm, S.V. and M.J. McFall-Ngai, *Sampling the light-organ microenvironment of Euprymna scolopes: description of a population of host*

- cells in association with the bacterial symbiont Vibrio fischeri*. Biol Bull, 1998. **195**(2): p. 89-97.
189. Steindler, L., et al., *LasI/R and RhII/R quorum sensing in a strain of Pseudomonas aeruginosa beneficial to plants*. Applied and environmental microbiology, 2009. **75**(15): p. 5131-5140.
 190. Pesci, E.C., et al., *Quinolone signaling in the cell-to-cell communication system of Pseudomonas aeruginosa*. Proceedings of the National Academy of Sciences of the United States of America, 1999. **96**(20): p. 11229-11234.
 191. Mehrotra, P., *Biosensors and their applications - A review*. Journal of oral biology and craniofacial research, 2016. **6**(2): p. 153-159.
 192. Bhalla, N., et al., *Introduction to biosensors*. Essays in biochemistry, 2016. **60**(1): p. 1-8.
 193. Thakur, M.S. and K.V. Ragavan, *Biosensors in food processing*. Journal of food science and technology, 2013. **50**(4): p. 625-641.
 194. Ory, J., F. Jacques, and Y. Boudey. *A biosensor for water quality monitoring*. in *Quality Measurement: The Indispensable Bridge between Theory and Reality (No Measurements? No Science! Joint Conference - 1996: IEEE Instrumentation and Measurement Technology Conference and IMEKO Tec*. 1996.
 195. Prante, M., et al., *A Portable Biosensor for 2,4-Dinitrotoluene Vapors*. Sensors, 2018. **18**(12).
 196. Carpenter, A.C., I.T. Paulsen, and T.C. Williams, *Blueprints for Biosensors: Design, Limitations, and Applications*. Genes, 2018. **9**(8): p. 375.
 197. Updike, S.J. and G.P. Hicks, *The Enzyme Electrode*. Nature, 1967. **214**(5092): p. 986-988.
 198. Diviés, C., [*Remarks on ethanol oxidation by an "Acetobacter xylinum" microbial electrode (author's transl)*]. Ann Microbiol (Paris), 1975. **126**(2): p. 175-86.
 199. Shi, S., E.L. Ang, and H. Zhao, *In vivo biosensors: mechanisms, development, and applications*. Journal of Industrial Microbiology and Biotechnology, 2018. **45**(7): p. 491-516.
 200. Rechnitz, G., *Biochemical electrodes uses tissues slice*. Chem Eng News, 1978. **56**: p. 16-21.
 201. Greenwald, E.C., S. Mehta, and J. Zhang, *Genetically Encoded Fluorescent Biosensors Illuminate the Spatiotemporal Regulation of Signaling Networks*. Chemical Reviews, 2018. **118**(24): p. 11707-11794.
 202. Zhang, J., M.K. Jensen, and J.D. Keasling, *Development of biosensors and their application in metabolic engineering*. Curr Opin Chem Biol, 2015. **28**: p. 1-8.
 203. Ellington, A.D. and J.W. Szostak, *In vitro selection of RNA molecules that bind specific ligands*. Nature, 1990. **346**(6287): p. 818-22.
 204. Ellington, A.D. and J.W. Szostak, *Selection in vitro of single-stranded DNA molecules that fold into specific ligand-binding structures*. Nature, 1992. **355**(6363): p. 850-2.
 205. Chai, C., Z. Xie, and E. Grotewold, *SELEX (Systematic Evolution of Ligands by EXponential Enrichment), as a powerful tool for deciphering the protein-DNA interaction space*. Methods Mol Biol, 2011. **754**: p. 249-58.
 206. Kalinowski, J., et al., *The complete Corynebacterium glutamicum ATCC 13032 genome sequence and its impact on the production of L-aspartate-derived amino acids and vitamins*. J Biotechnol, 2003. **104**(1-3): p. 5-25.
 207. Willson, B.J., et al., *Production of a functional cell wall-anchored minicellulosome by recombinant Clostridium acetobutylicum ATCC 824*. Biotechnol Biofuels, 2016. **9**: p. 109.

208. *1129. Phototrophic medium*. DSMZ Microorganisms.
209. Lenz, O., et al., *The Alcaligenes eutrophus H16 hoxX gene participates in hydrogenase regulation*. J Bacteriol, 1994. **176**(14): p. 4385-93.
210. Arenas-López, C., et al., *The genetic basis of 3-hydroxypropanoate metabolism in Cupriavidus necator H16*. Biotechnol Biofuels, 2019. **12**: p. 150.
211. Little Gareth, T., et al., *Complete Genome Sequence of Cupriavidus necator H16 (DSM 428)*. Microbiology Resource Announcements. **8**(37): p. e00814-19.
212. Alagesan, S., N.P. Minton, and N. Malys, *13C-assisted metabolic flux analysis to investigate heterotrophic and mixotrophic metabolism in Cupriavidus necator H16*. Metabolomics, 2017. **14**(1): p. 9.
213. Salis, H.M., E.A. Mirsky, and C.A. Voigt, *Automated design of synthetic ribosome binding sites to control protein expression*. Nature Biotechnology, 2009. **27**(10): p. 946-950.
214. Heinrich, D., M. Raberg, and A. Steinbuchel, *Studies on the aerobic utilization of synthesis gas (syngas) by wild type and recombinant strains of Ralstonia eutropha H16*. Microb Biotechnol, 2018. **11**(4): p. 647-656.
215. Greco, F.V., et al., *Harnessing the central dogma for stringent multi-level control of gene expression*. Nature Communications, 2021. **12**(1): p. 1738.
216. Bölker, M., *Complexity in Synthetic Biology: Unnecessary or Essential?* 2015. p. 59-69.
217. Nakamura, Y., T. Gojobori, and T. Ikemura, *Codon usage tabulated from international DNA sequence databases: status for the year 2000*. Nucleic Acids Res, 2000. **28**(1): p. 292.
218. Arpino, J.A.J., et al., *Tuning the dials of Synthetic Biology*. Microbiology (Reading), 2013. **159**(Pt 7): p. 1236-1253.
219. Maurizi, M.R., *Proteases and protein degradation in Escherichia coli*. Experientia, 1992. **48**(2): p. 178-201.
220. Cravens, A., J. Payne, and C.D. Smolke, *Synthetic biology strategies for microbial biosynthesis of plant natural products*. Nature Communications, 2019. **10**(1): p. 2142.
221. Kadokura, H. and J. Beckwith, *Mechanisms of oxidative protein folding in the bacterial cell envelope*. Antioxidants & redox signaling, 2010. **13**(8): p. 1231-1246.
222. Copley, S.D., *Shining a light on enzyme promiscuity*. Curr Opin Struct Biol, 2017. **47**: p. 167-175.
223. Fu, P., *Grand Challenges in Synthetic Biology to be Accomplished*. Frontiers in Bioengineering and Biotechnology, 2013. **1**(2).
224. Houten, S.M., et al., *The Biochemistry and Physiology of Mitochondrial Fatty Acid β -Oxidation and Its Genetic Disorders*. Annual Review of Physiology, 2016. **78**(1): p. 23-44.
225. Kallscheuer, N., et al., *Reversal of β -oxidative pathways for the microbial production of chemicals and polymer building blocks*. Metabolic Engineering, 2017. **42**: p. 33-42.
226. Angenent, L.T., et al., *Chain Elongation with Reactor Microbiomes: Open-Culture Biotechnology To Produce Biochemicals*. Environmental Science & Technology, 2016. **50**(6): p. 2796-2810.
227. Dellomonaco, C., et al., *Engineered reversal of the β -oxidation cycle for the synthesis of fuels and chemicals*. Nature, 2011. **476**(7360): p. 355-359.
228. Wu, J., et al., *A systematic optimization of medium chain fatty acid biosynthesis via the reverse beta-oxidation cycle in Escherichia coli*. Metab Eng, 2017. **41**: p. 115-124.

229. Zhuang, Q. and Q. Qi, *Engineering the pathway in Escherichia coli for the synthesis of medium-chain-length polyhydroxyalkanoates consisting of both even- and odd-chain monomers*. *Microbial Cell Factories*, 2019. **18**(1): p. 135.
230. Babu, T., et al., *Engineering Escherichia coli for the production of adipic acid through the reversed β -oxidation pathway*. *Process Biochemistry*, 2015. **50**(12): p. 2066-2071.
231. Lian, J. and H. Zhao, *Reversal of the β -oxidation cycle in Saccharomyces cerevisiae for production of fuels and chemicals*. *ACS Synth Biol*, 2015. **4**(3): p. 332-41.
232. Shin, J.H., *Engineering synthetic pathways for adipic acid biosynthesis*. Doktorsavhandlingar vid Chalmers tekniska högskola, Chalmers University of Technology, SE-412 96 Gothenburg, Sweden, 2021. **4886**.
233. Zhang, M., et al., *Modification of acetoacetyl-CoA reduction step in Ralstonia eutropha for biosynthesis of poly(3-hydroxybutyrate-co-3-hydroxyhexanoate) from structurally unrelated compounds*. *Microb Cell Fact*, 2019. **18**(1): p. 147.
234. Sayer, C., M.N. Isupov, and J.A. Littlechild, *Crystallization and preliminary X-ray diffraction analysis of omega-amino acid:pyruvate transaminase from Chromobacterium violaceum*. *Acta Crystallogr Sect F Struct Biol Cryst Commun*, 2007. **63**(Pt 2): p. 117-9.
235. Bisignano, G., et al., *In vitro antibacterial activity of some aliphatic aldehydes from Olea europaea L.* *FEMS Microbiology Letters*, 2001. **198**(1): p. 9-13.
236. Wu, R., et al., *PLP and GABA trigger GabR-mediated transcription regulation in Bacillus subtilis via external aldimine formation*. *Proc Natl Acad Sci U S A*, 2017. **114**(15): p. 3891-3896.
237. Belitsky, B.R. and A.L. Sonenshein, *GabR, a member of a novel protein family, regulates the utilization of gamma-aminobutyrate in Bacillus subtilis*. *Mol Microbiol*, 2002. **45**(2): p. 569-83.
238. Fujisawa, H., S. Nagata, and H. Misono, *Characterization of short-chain dehydrogenase/reductase homologues of Escherichia coli (YdfG) and Saccharomyces cerevisiae (YMR226C)*. *Biochim Biophys Acta*, 2003. **1645**(1): p. 89-94.
239. Wang, Q., et al., *Metabolic engineering of Escherichia coli for poly(3-hydroxypropionate) production from glycerol and glucose*. *Biotechnol Lett*, 2014. **36**(11): p. 2257-62.
240. Song, C.W., et al., *Metabolic Engineering of Escherichia coli for the Production of 3-Hydroxypropionic Acid and Malonic Acid through beta-Alanine Route*. *ACS Synth Biol*, 2016. **5**(11): p. 1256-1263.
241. Volodina, E., et al., *Characterization of propionate CoA-transferase from Ralstonia eutropha H16*. *Appl Microbiol Biotechnol*, 2014. **98**(8): p. 3579-89.
242. Lindenkamp, N., M. Schurmann, and A. Steinbuchel, *A propionate CoA-transferase of Ralstonia eutropha H16 with broad substrate specificity catalyzing the CoA thioester formation of various carboxylic acids*. *Appl Microbiol Biotechnol*, 2013. **97**(17): p. 7699-709.
243. Horswill, A.R. and J.C. Escalante-Semerena, *The prpE gene of Salmonella typhimurium LT2 encodes propionyl-CoA synthetase*. *Microbiology (Reading)*, 1999. **145** (Pt 6): p. 1381-1388.
244. Wu, H. and K.Y. San, *Engineering Escherichia coli for odd straight medium chain free fatty acid production*. *Appl Microbiol Biotechnol*, 2014. **98**(19): p. 8145-54.
245. Aldor, I. and J.D. Keasling, *Metabolic engineering of poly(3-hydroxybutyrate-co-3-hydroxyvalerate) composition in recombinant Salmonella enterica serovar typhimurium*. *Biotechnol Bioeng*, 2001. **76**(2): p. 108-14.

246. Valentin, H.E., et al., *Application of a propionyl coenzyme A synthetase for poly(3-hydroxypropionate-co-3-hydroxybutyrate) accumulation in recombinant Escherichia coli*. Appl Environ Microbiol, 2000. **66**(12): p. 5253-8.
247. Anderson, A.J. and E.A. Dawes, *Occurrence, metabolism, metabolic role, and industrial uses of bacterial polyhydroxyalkanoates*. Microbiol Rev, 1990. **54**(4): p. 450-72.
248. Handrick, R., S. Reinhardt, and D. Jendrossek, *Mobilization of poly(3-hydroxybutyrate) in Ralstonia eutropha*. J Bacteriol, 2000. **182**(20): p. 5916-8.
249. Dennis, D., et al., *Formation of poly(3-hydroxybutyrate-co-3-hydroxyhexanoate) by PHA synthase from Ralstonia eutropha*. J Biotechnol, 1998. **64**(2-3): p. 177-86.
250. Karstens, K., et al., *Phosphotransferase protein EllANtr interacts with SpoT, a key enzyme of the stringent response, in Ralstonia eutropha H16*. Microbiology (Reading), 2014. **160**(Pt 4): p. 711-722.
251. Slater, S., et al., *Multiple beta-ketothiolases mediate poly(beta-hydroxyalkanoate) copolymer synthesis in Ralstonia eutropha*. J Bacteriol, 1998. **180**(8): p. 1979-87.
252. Tseng, H.C., et al., *Metabolic engineering of Escherichia coli for enhanced production of (R)- and (S)-3-hydroxybutyrate*. Appl Environ Microbiol, 2009. **75**(10): p. 3137-45.
253. Valencia, L.E., et al., *Seven-enzyme in vitro cascade to (3R)-3-hydroxybutyryl-CoA*. Org Biomol Chem, 2019. **17**(6): p. 1375-1378.
254. Wang, Q., et al., *Engineering of Escherichia coli for the biosynthesis of poly(3-hydroxybutyrate-co-3-hydroxyhexanoate) from glucose*. Appl Microbiol Biotechnol, 2015. **99**(6): p. 2593-602.
255. Alex Van Eck Conradie, A.L.B., Jonathan Kennedy, Nadia Fatma Kadi, *Methods and materials for producing 7-carbon monomers*. WO 2017/096260 A8, 2017.
256. Kallscheuer, N., et al., *Improved production of adipate with Escherichia coli by reversal of beta-oxidation*. Appl Microbiol Biotechnol, 2017. **101**(6): p. 2371-2382.
257. Kallscheuer, N., et al., *Reversal of beta-oxidative pathways for the microbial production of chemicals and polymer building blocks*. Metab Eng, 2017. **42**: p. 33-42.
258. Lawrence, A.G., et al., *Transcriptional analysis of Ralstonia eutropha genes related to poly-(R)-3-hydroxybutyrate homeostasis during batch fermentation*. Appl Microbiol Biotechnol, 2005. **68**(5): p. 663-72.
259. Segawa, M., et al., *Two NADH-dependent (S)-3-hydroxyacyl-CoA dehydrogenases from polyhydroxyalkanoate-producing Ralstonia eutropha*. J Biosci Bioeng, 2019. **127**(3): p. 294-300.
260. Cheon, Y., et al., *A biosynthetic pathway for hexanoic acid production in Kluyveromyces marxianus*. J Biotechnol, 2014. **182-183**: p. 30-6.
261. Park, S.J. and S. Yup Lee, *New FadB homologous enzymes and their use in enhanced biosynthesis of medium-chain-length polyhydroxyalkanoates in FadB mutant Escherichia coli*. Biotechnol Bioeng, 2004. **86**(6): p. 681-6.
262. Menendez-Bravo, S., et al., *Identification of FadAB Complexes Involved in Fatty Acid beta-Oxidation in Streptomyces coelicolor and Construction of a Triacylglycerol Overproducing strain*. Front Microbiol, 2017. **8**: p. 1428.
263. Yang, S.Y., et al., *Evidence that the fadB gene of the fadAB operon of Escherichia coli encodes 3-hydroxyacyl-coenzyme A (CoA) epimerase, delta 3-cis-delta 2-trans-enoyl-CoA isomerase, and enoyl-CoA hydratase in addition to 3-hydroxyacyl-CoA dehydrogenase*. J Bacteriol, 1988. **170**(6): p. 2543-8.

264. O'Malley, M.S., Kevin; Mizunashi, Wataru; Yu, Fujio, *Biological production of methyl methacrylate*. AU 2016340470 B2, 2016. **Australian patent office**.
265. Arenas-López, C., et al., *The genetic basis of 3-hydroxypropanoate metabolism in Cupriavidus necator H16*. *Biotechnology for Biofuels*, 2019. **12**(1): p. 150.
266. Segawa, M., et al., *Two NADH-dependent (S)-3-hydroxyacyl-CoA dehydrogenases from polyhydroxyalkanoate-producing Ralstonia eutropha*. *Journal of Bioscience and Bioengineering*, 2019. **127**(3): p. 294-300.
267. Hu, K., et al., *Structures of trans-2-enoyl-CoA reductases from Clostridium acetobutylicum and Treponema denticola: insights into the substrate specificity and the catalytic mechanism*. *Biochem J*, 2013. **449**(1): p. 79-89.
268. Bond-Watts, B.B., A.M. Weeks, and M.C. Chang, *Biochemical and structural characterization of the trans-enoyl-CoA reductase from Treponema denticola*. *Biochemistry*, 2012. **51**(34): p. 6827-37.
269. Lan, E.I. and J.C. Liao, *Metabolic engineering of cyanobacteria for 1-butanol production from carbon dioxide*. *Metab Eng*, 2011. **13**(4): p. 353-63.
270. Kataoka, N., et al., *Construction of CoA-dependent 1-butanol synthetic pathway functions under aerobic conditions in Escherichia coli*. *J Biotechnol*, 2015. **204**: p. 25-32.
271. Kataoka, N., et al., *Butyrate production under aerobic growth conditions by engineered Escherichia coli*. *J Biosci Bioeng*, 2017. **123**(5): p. 562-568.
272. Vick, J.E., et al., *Escherichia coli enoyl-acyl carrier protein reductase (FabI) supports efficient operation of a functional reversal of beta-oxidation cycle*. *Appl Environ Microbiol*, 2015. **81**(4): p. 1406-16.
273. Hardie, D.G., *AMP-activated protein kinase: an energy sensor that regulates all aspects of cell function*. *Genes Dev*, 2011. **25**(18): p. 1895-908.
274. Hardie, D.G., *Keeping the home fires burning: AMP-activated protein kinase*. *J R Soc Interface*, 2018. **15**(138).
275. Meyrat, A. and C. von Ballmoos, *ATP synthesis at physiological nucleotide concentrations*. *Sci Rep*, 2019. **9**(1): p. 3070.
276. Biolabs, N.E., *NEB 5-alpha Competent E.coli (High Efficiency) C2987H Datasheet*. 2020.
277. Tee, K.L., et al., *An Efficient Transformation Method for the Bioplastic-Producing "Knallgas" Bacterium Ralstonia eutropha H16*. *Biotechnol J*, 2017. **12**(11).
278. Julsing, M.K., et al., *Resting cells of recombinant E. coli show high epoxidation yields on energy source and high sensitivity to product inhibition*. *Biotechnol Bioeng*, 2012. **109**(5): p. 1109-19.
279. Jackson, E., M. Ripoll, and L. Betancor, *Efficient glycerol transformation by resting Gluconobacter cells*. *Microbiologyopen*, 2019. **8**(12): p. e926.
280. Lang, Y.J., et al., *Production of ectoine through a combined process that uses both growing and resting cells of Halomonas salina DSM 5928T*. *Extremophiles*, 2011. **15**(2): p. 303-10.
281. Orsi, E., et al., *Growth-uncoupled isoprenoid synthesis in Rhodobacter sphaeroides*. *Biotechnol Biofuels*, 2020. **13**: p. 123.
282. Kang, D.J., et al., *Bioconversion of vitamin D3 to calcifediol by using resting cells of Pseudonocardia sp.* *Biotechnol Lett*, 2015. **37**(9): p. 1895-904.
283. Kim, J.S., et al., *Microbial glycolipid production under nitrogen limitation and resting cell conditions*. *J Biotechnol*, 1990. **13**(4): p. 257-66.
284. Mao, J., et al., *A high-throughput method for screening of L-tyrosine high-yield strains by Saccharomyces cerevisiae*. *J Gen Appl Microbiol*, 2018. **64**(4): p. 198-201.

285. SongyuanLi, C.B., Jendresen, Prof.Alex Toftgaard Nielsen, *Increasing production yield of tyrosine and mevalonate through inhibition of biomass formation*. *Process Biochemistry*, 2016. **51**(12): p. 1992-2000.
286. Masuda, A., Y. Toya, and H. Shimizu, *Metabolic impact of nutrient starvation in mevalonate-producing Escherichia coli*. *Bioresour Technol*, 2017. **245**(Pt B): p. 1634-1640.
287. Willrodt, C., et al., *Decoupling production from growth by magnesium sulfate limitation boosts de novo limonene production*. *Biotechnol Bioeng*, 2016. **113**(6): p. 1305-14.
288. Li, H. and J.C. Liao, *A synthetic anhydrotetracycline-controllable gene expression system in Ralstonia eutropha H16*. *ACS Synth Biol*, 2015. **4**(2): p. 101-6.
289. Arikawa, H. and K. Matsumoto, *Evaluation of gene expression cassettes and production of poly(3-hydroxybutyrate-co-3-hydroxyhexanoate) with a fine modulated monomer composition by using it in Cupriavidus necator*. *Microb Cell Fact*, 2016. **15**(1): p. 184.
290. Johnson, A.O., et al., *An Engineered Constitutive Promoter Set with Broad Activity Range for Cupriavidus necator H16*. *ACS Synth Biol*, 2018. **7**(8): p. 1918-1928.
291. Crepin, L., E. Lombard, and S.E. Guillouet, *Metabolic engineering of Cupriavidus necator for heterotrophic and autotrophic alka(e)ne production*. *Metab Eng*, 2016. **37**: p. 92-101.
292. Zaldivar, J., A. Martinez, and L.O. Ingram, *Effect of selected aldehydes on the growth and fermentation of ethanologenic Escherichia coli*. *Biotechnol Bioeng*, 1999. **65**(1): p. 24-33.
293. Potter, M., H. Muller, and A. Steinbuchel, *Influence of homologous phasins (PhaP) on PHA accumulation and regulation of their expression by the transcriptional repressor PhaR in Ralstonia eutropha H16*. *Microbiology (Reading)*, 2005. **151**(Pt 3): p. 825-833.
294. Fukui, T., et al., *Evaluation of promoters for gene expression in polyhydroxyalkanoate-producing Cupriavidus necator H16*. *Appl Microbiol Biotechnol*, 2011. **89**(5): p. 1527-36.
295. Delamarre, S.C. and C.A. Batt, *Comparative study of promoters for the production of polyhydroxyalkanoates in recombinant strains of Wautersia eutropha*. *Applied Microbiology and Biotechnology*, 2006. **71**(5): p. 668-679.
296. Arikawa, H. and K. Matsumoto, *Evaluation of gene expression cassettes and production of poly(3-hydroxybutyrate-co-3-hydroxyhexanoate) with a fine modulated monomer composition by using it in Cupriavidus necator*. *Microbial Cell Factories*, 2016. **15**(1): p. 184.
297. Alagesan, S., et al., *Functional Genetic Elements for Controlling Gene Expression in Cupriavidus necator H16*. *Applied and environmental microbiology*, 2018. **84**(19): p. e00878-18.
298. Chevalet, L., et al., *Recombinant protein production driven by the tryptophan promoter is tightly controlled in ICONE 200, a new genetically engineered E. coli mutant*. *Biotechnol Bioeng*, 2000. **69**(4): p. 351-8.
299. Wang, B., et al., *A Genetic Toolbox for Modulating the Expression of Heterologous Genes in the Cyanobacterium Synechocystis sp. PCC 6803*. *ACS Synth Biol*, 2018. **7**(1): p. 276-286.
300. Salis, H.M., *The ribosome binding site calculator*. *Methods Enzymol*, 2011. **498**: p. 19-42.
301. Rauhut, R. and G. Klug, *mRNA degradation in bacteria*. *FEMS Microbiology Reviews*, 1999. **23**(3): p. 353-370.

302. Kozak, M., *Comparison of initiation of protein synthesis in procaryotes, eucaryotes, and organelles*. Microbiological reviews, 1983. **47**(1): p. 1-45.
303. Dietzen, D.J., et al., *Rapid comprehensive amino acid analysis by liquid chromatography/tandem mass spectrometry: comparison to cation exchange with post-column ninhydrin detection*. Rapid Commun Mass Spectrom, 2008. **22**(22): p. 3481-8.
304. Bertozzi, C.R., *A decade of bioorthogonal chemistry*. Acc Chem Res, 2011. **44**(9): p. 651-3.
305. Pandit, A.V., S. Srinivasan, and R. Mahadevan, *Redesigning metabolism based on orthogonality principles*. Nature Communications, 2017. **8**(1): p. 15188.
306. Yang, X., et al., *Development of a Method for the Determination of Acyl-CoA Compounds by Liquid Chromatography Mass Spectrometry to Probe the Metabolism of Fatty Acids*. Analytical chemistry, 2017. **89**(1): p. 813-821.
307. Zimmermann, M., et al., *Nontargeted profiling of coenzyme A thioesters in biological samples by tandem mass spectrometry*. Anal Chem, 2013. **85**(17): p. 8284-90.
308. Clark, D., *Regulation of fatty acid degradation in Escherichia coli: analysis by operon fusion*. J Bacteriol, 1981. **148**(2): p. 521-6.
309. Zhang, Y.-M. and C.O. Rock, *Membrane lipid homeostasis in bacteria*. Nature Reviews Microbiology, 2008. **6**(3): p. 222-233.
310. Cen, X., et al., *Metabolic Engineering of Escherichia coli for De Novo Production of 1,5-Pentanediol from Glucose*. ACS Synthetic Biology, 2021. **10**(1): p. 192-203.
311. Wang, J., et al., *Bacterial synthesis of C3-C5 diols via extending amino acid catabolism*. Proceedings of the National Academy of Sciences of the United States of America, 2020. **117**(32): p. 19159-19167.
312. De Tissera, S., et al., *Syngas Biorefinery and Syngas Utilization*. Adv Biochem Eng Biotechnol, 2019. **166**: p. 247-280.
313. Köpke, M., et al., *Clostridium ljungdahlii represents a microbial production platform based on syngas*. Proceedings of the National Academy of Sciences of the United States of America, 2010. **107**(29): p. 13087-13092.
314. Tucci, S. and W. Martin, *A novel prokaryotic trans-2-enoyl-CoA reductase from the spirochete Treponema denticola*. FEBS Lett, 2007. **581**(8): p. 1561-6.
315. Hoffmeister, M., et al., *Mitochondrial trans-2-enoyl-CoA reductase of wax ester fermentation from Euglena gracilis defines a new family of enzymes involved in lipid synthesis*. J Biol Chem, 2005. **280**(6): p. 4329-38.
316. Chu, H.S., et al., *Direct fermentation route for the production of acrylic acid*. Metab Eng, 2015. **32**: p. 23-29.
317. K.Muniasamy, G. and F. Pérez-Guevara, *Genome characteristics dictate poly-R-(3)-hydroxyalkanoate production in Cupriavidus necator H16*. World Journal of Microbiology and Biotechnology, 2018. **34**.
318. Pei, L. and M. Schmidt, *Fast-Growing Engineered Microbes: New Concerns for Gain-of-Function Research?* Front Genet, 2018. **9**: p. 207.
319. Hall, J.P.J., et al., *Plasmid fitness costs are caused by specific genetic conflicts*. bioRxiv, 2021: p. 2021.04.10.439128.
320. Wu, G., et al., *Metabolic Burden: Cornerstones in Synthetic Biology and Metabolic Engineering Applications*. Trends Biotechnol, 2016. **34**(8): p. 652-664.
321. Ewald, J., et al., *Optimality principles reveal a complex interplay of intermediate toxicity and kinetic efficiency in the regulation of prokaryotic metabolism*. PLoS computational biology, 2017. **13**(2): p. e1005371-e1005371.

322. Vos, T., et al., *Growth-rate dependency of de novo resveratrol production in chemostat cultures of an engineered Saccharomyces cerevisiae strain*. Microb Cell Fact, 2015. **14**: p. 133.
323. Yeon, Y.J., H.Y. Park, and Y.J. Yoo, *Engineering substrate specificity of succinic semialdehyde reductase (AKR7A5) for efficient conversion of levulinic acid to 4-hydroxyvaleric acid*. J Biotechnol, 2015. **210**: p. 38-43.
324. Grousseau, E., et al., *Phosphorus limitation strategy to increase propionic acid flux towards 3-hydroxyvaleric acid monomers in Cupriavidus necator*. Bioresource technology, 2013. **153C**: p. 206-215.
325. Griffin, M. and P.W. Trudgill, *The metabolism of cyclopentanol by Pseudomonas N.C.I.B. 9872*. Biochem J, 1972. **129**(3): p. 595-603.
326. Abreu-Cavalheiro, A. and G. Monteiro, *Solving ethanol production problems with genetically modified yeast strains*. Braz J Microbiol, 2013. **44**(3): p. 665-71.
327. Pickens, L.B., Y. Tang, and Y.H. Chooi, *Metabolic engineering for the production of natural products*. Annu Rev Chem Biomol Eng, 2011. **2**: p. 211-36.
328. Pandey, A.K., K. Pandey, and L.K. Singh, *Microbial Production and Applications of L-lysine*, in *Innovations in Food Technology: Current Perspectives and Future Goals*, P. Mishra, R.R. Mishra, and C.O. Adetunji, Editors. 2020, Springer Singapore: Singapore. p. 211-229.
329. Xu, J.Z., H.K. Yang, and W.G. Zhang, *NADPH metabolism: a survey of its theoretical characteristics and manipulation strategies in amino acid biosynthesis*. Crit Rev Biotechnol, 2018. **38**(7): p. 1061-1076.
330. Hermann, T., *Industrial production of amino acids by coryneform bacteria*. J Biotechnol, 2003. **104**(1-3): p. 155-72.
331. Tateno, T., H. Fukuda, and A. Kondo, *Direct production of L-lysine from raw corn starch by Corynebacterium glutamicum secreting Streptococcus bovis alpha-amylase using cspB promoter and signal sequence*. Appl Microbiol Biotechnol, 2007. **77**(3): p. 533-41.
332. Schneider, J. and V.F. Wendisch, *Biotechnological production of polyamines by bacteria: recent achievements and future perspectives*. Appl Microbiol Biotechnol, 2011. **91**(1): p. 17-30.
333. Becker, J., et al., *From zero to hero--design-based systems metabolic engineering of Corynebacterium glutamicum for L-lysine production*. Metab Eng, 2011. **13**(2): p. 159-68.
334. Becker, J., et al., *Corynebacterium glutamicum for Sustainable Bioproduction: From Metabolic Physiology to Systems Metabolic Engineering*. Adv Biochem Eng Biotechnol, 2018. **162**: p. 217-263.
335. Geng, F., et al., *Exploring the allosteric mechanism of dihydrodipicolinate synthase by reverse engineering of the allosteric inhibitor binding sites and its application for lysine production*. Applied Microbiology and Biotechnology, 2013. **97**(5): p. 1963-1971.
336. Mueller, M., A. de la Peña, and H. Derendorf, *Issues in pharmacokinetics and pharmacodynamics of anti-infective agents: kill curves versus MIC*. Antimicrobial agents and chemotherapy, 2004. **48**(2): p. 369-377.
337. Yourassowsky, E., et al., *Correlation between growth curve and killing curve of Escherichia coli after a brief exposure to suprainhibitory concentrations of ampicillin and piperacillin*. Antimicrob Agents Chemother, 1985. **28**(6): p. 756-60.
338. Ibanez, J., et al., *Toxicity Assay Using Bacterial Growth*. 2008.
339. Bassler, B.L. and R. Losick, *Bacterially speaking*. Cell, 2006. **125**(2): p. 237-46.

340. Hammer, B.K. and B.L. Bassler, *Quorum sensing controls biofilm formation in Vibrio cholerae*. Mol Microbiol, 2003. **50**(1): p. 101-4.
341. Barnard, A.M.L., et al., *Quorum sensing, virulence and secondary metabolite production in plant soft-rotting bacteria*. Philosophical Transactions of the Royal Society B: Biological Sciences, 2007. **362**(1483): p. 1165-1183.
342. Rutherford, S.T. and B.L. Bassler, *Bacterial quorum sensing: its role in virulence and possibilities for its control*. Cold Spring Harbor perspectives in medicine, 2012. **2**(11): p. a012427.
343. Mukherjee, S. and B.L. Bassler, *Bacterial quorum sensing in complex and dynamically changing environments*. Nature Reviews Microbiology, 2019. **17**(6): p. 371-382.
344. Garg, R.P., et al., *Evidence that Ralstonia eutropha (Alcaligenes eutrophus) contains a functional homologue of the Ralstonia solanacearum Phc cell density sensing system*. Mol Microbiol, 2000. **38**(2): p. 359-67.
345. Chevrot, R., et al., *GABA controls the level of quorum-sensing signal in Agrobacterium tumefaciens*. Proc Natl Acad Sci U S A, 2006. **103**(19): p. 7460-4.
346. Dagorn, A., et al., *Gamma-aminobutyric acid acts as a specific virulence regulator in Pseudomonas aeruginosa*. Microbiology (Reading), 2013. **159**(Pt 2): p. 339-351.
347. Li, Z., et al., *Overexpression of transport proteins improves the production of 5-aminovalerate from L-lysine in Escherichia coli*. Scientific Reports, 2016. **6**(1): p. 30884.
348. Rohles, C.M., et al., *Systems metabolic engineering of Corynebacterium glutamicum for the production of the carbon-5 platform chemicals 5-aminovalerate and glutarate*. Microb Cell Fact, 2016. **15**(1): p. 154.
349. Adkins, J., J. Jordan, and D.R. Nielsen, *Engineering Escherichia coli for renewable production of the 5-carbon polyamide building-blocks 5-aminovalerate and glutarate*. Biotechnol Bioeng, 2013. **110**(6): p. 1726-34.
350. Knorr, S., et al., *Widespread bacterial lysine degradation proceeding via glutarate and L-2-hydroxyglutarate*. Nat Commun, 2018. **9**(1): p. 5071.
351. Zampieri, M., et al., *Regulatory mechanisms underlying coordination of amino acid and glucose catabolism in Escherichia coli*. Nature Communications, 2019. **10**(1): p. 3354.
352. Shi, W., et al., *The Structure of L-Aspartate Ammonia-Lyase from Escherichia coli*. Biochemistry, 1997. **36**(30): p. 9136-9144.
353. Charlier, D., P. Nguyen Le Minh, and M. Roovers, *Regulation of carbamoylphosphate synthesis in Escherichia coli: an amazing metabolite at the crossroad of arginine and pyrimidine biosynthesis*. Amino acids, 2018. **50**(12): p. 1647-1661.
354. Wolfe, S.A. and J.M. Smith, *Separate regulation of purA and purB loci of Escherichia coli K-12*. Journal of bacteriology, 1985. **162**(2): p. 822-825.
355. Mayer, J. and A.M. Cook, *Homotaurine metabolized to 3-sulfopropanoate in Cupriavidus necator H16: enzymes and genes in a patchwork pathway*. Journal of bacteriology, 2009. **191**(19): p. 6052-6058.
356. Schendzielorz, G., et al., *Taking control over control: use of product sensing in single cells to remove flux control at key enzymes in biosynthesis pathways*. ACS Synth Biol, 2014. **3**(1): p. 21-9.
357. Contador, C.A., et al., *Ensemble modeling for strain development of L-lysine-producing Escherichia coli*. Metab Eng, 2009. **11**(4-5): p. 221-33.

358. Jakobsen, O.M., et al., *Overexpression of wild-type aspartokinase increases L-lysine production in the thermotolerant methylotrophic bacterium Bacillus methanolicus*. Appl Environ Microbiol, 2009. **75**(3): p. 652-61.
359. Zhao, Z., et al., [*Expression of feedback-resistant aspartate kinase gene in Corynebacterium crenatum*]. Wei Sheng Wu Xue Bao, 2005. **45**(4): p. 530-3.
360. Koffas, M.A., G.Y. Jung, and G. Stephanopoulos, *Engineering metabolism and product formation in Corynebacterium glutamicum by coordinated gene overexpression*. Metab Eng, 2003. **5**(1): p. 32-41.
361. Rodionov, D.A., et al., *Regulation of lysine biosynthesis and transport genes in bacteria: yet another RNA riboswitch?* Nucleic acids research, 2003. **31**(23): p. 6748-6757.
362. Dong, X., et al., *Characterization of aspartate kinase and homoserine dehydrogenase from Corynebacterium glutamicum IWJ001 and systematic investigation of L-isoleucine biosynthesis*. J Ind Microbiol Biotechnol, 2016. **43**(6): p. 873-85.
363. Eggeling, L. and M. Bott, *A giant market and a powerful metabolism: L-lysine provided by Corynebacterium glutamicum*. Appl Microbiol Biotechnol, 2015. **99**(8): p. 3387-94.
364. Zhao, J., et al., *Overexpression of ribosome elongation factor G and recycling factor increases L-isoleucine production in Corynebacterium glutamicum*. Applied microbiology and biotechnology, 2015. **99**(11): p. 4795-4805.
365. Matthews, B.F. and J.M. Widholm, *Expression of aspartokinase, dihydrodipicolinic acid synthase and homoserine dehydrogenase during growth of carrot cell suspension cultures on lysine- and threonine-supplemented media*. Z Naturforsch C Biosci, 1979. **34**(12): p. 1177-85.
366. Dereppe, C., et al., *Purification and characterization of dihydrodipicolinate synthase from pea*. Plant Physiol, 1992. **98**(3): p. 813-21.
367. Frisch, D.A., et al., *Isolation and Characterization of Dihydrodipicolinate Synthase from Maize*. Plant Physiology, 1991. **96**(2): p. 444.
368. Kumpaisal, R., T. Hashimoto, and Y. Yamada, *Purification and Characterization of Dihydrodipicolinate Synthase from Wheat Suspension Cultures*. Plant Physiology, 1987. **85**(1): p. 145.
369. Dobson, R.C., et al., *The crystal structures of native and (S)-lysine-bound dihydrodipicolinate synthase from Escherichia coli with improved resolution show new features of biological significance*. Acta Crystallogr D Biol Crystallogr, 2005. **61**(Pt 8): p. 1116-24.
370. Yugari, Y. and C. Gilvarg, *The condensation step in diaminopimelate synthesis*. J Biol Chem, 1965. **240**(12): p. 4710-6.
371. Devenish, S.R.A., et al., *Cloning and characterisation of dihydrodipicolinate synthase from the pathogen Neisseria meningitidis*. Biochimica et Biophysica Acta (BBA) - Proteins and Proteomics, 2009. **1794**(8): p. 1168-1174.
372. Domigan, L.J., et al., *Characterisation of dihydrodipicolinate synthase (DHDPS) from Bacillus anthracis*. Biochimica et Biophysica Acta (BBA) - Proteins and Proteomics, 2009. **1794**(10): p. 1510-1516.
373. Cremer, J., et al., *Regulation of Enzymes of Lysine Biosynthesis in Corynebacterium glutamicum*. Microbiology, 1988. **134**(12): p. 3221-3229.
374. Hoganson, D.A. and D.P. Stahly, *Regulation of dihydrodipicolinate synthase during growth and sporulation of Bacillus cereus*. Journal of bacteriology, 1975. **124**(3): p. 1344-1350.
375. Burgess, B.R., et al., *Structure and evolution of a novel dimeric enzyme from a clinically important bacterial pathogen*. J Biol Chem, 2008. **283**(41): p. 27598-603.

376. Motoyama, H., et al., *Overproduction of L-Lysine from methanol by Methylobacillus glycogenes derivatives carrying a plasmid with a mutated dapA gene*. Applied and environmental microbiology, 2001. **67**(7): p. 3064-3070.
377. Wang, Y., et al., *Evolving the L-lysine high-producing strain of Escherichia coli using a newly developed high-throughput screening method*. Journal of industrial microbiology & biotechnology, 2016. **43**(9): p. 1227-1235.
378. EMBL, *EMBOSS Needle Pairwise Sequence Alignment Tool*.
379. Coudoré, F., et al., *Validation of an Ultra-High Performance Liquid Chromatography Tandem Mass Spectrometric Method for Quantifying Uracil and 5,6-Dihydrouracil in Human Plasma*. Journal of Chromatographic Science, 2012. **50**(10): p. 877-884.
380. Guzman, L.M., et al., *Tight regulation, modulation, and high-level expression by vectors containing the arabinose PBAD promoter*. J Bacteriol, 1995. **177**(14): p. 4121-30.
381. Strandwitz, P., *Neurotransmitter modulation by the gut microbiota*. Brain research, 2018. **1693**(Pt B): p. 128-133.
382. Hong, Y.G., et al., *Production of glutaric acid from 5-aminovaleric acid using Escherichia coli whole cell bio-catalyst overexpressing GabTD from Bacillus subtilis*. Enzyme Microb Technol, 2018. **118**: p. 57-65.
383. Seccareccia, I., et al., *Unraveling the predator-prey relationship of Cupriavidus necator and Bacillus subtilis*. Microbiological Research, 2016. **192**: p. 231-238.
384. Grandclément, C., et al., *Quorum quenching: role in nature and applied developments*. FEMS Microbiol Rev, 2016. **40**(1): p. 86-116.
385. Qian, Z.G., X.X. Xia, and S.Y. Lee, *Metabolic engineering of Escherichia coli for the production of cadaverine: a five carbon diamine*. Biotechnol Bioeng, 2011. **108**(1): p. 93-103.
386. Revelles, O., et al., *Multiple and Interconnected Pathways for Lysine Catabolism in Pseudomonas putida KT2440*. Journal of Bacteriology, 2005. **187**(21): p. 7500.
387. Revelles, O., R.-M. Wittich, and J.L. Ramos, *Identification of the Initial Steps in Lysine Catabolism in Pseudomonas putida*. Journal of Bacteriology, 2007. **189**(7): p. 2787.
388. Li, W., et al., *Targeting metabolic driving and intermediate influx in lysine catabolism for high-level glutarate production*. Nat Commun, 2019. **10**(1): p. 3337.
389. Hong, Y.G., et al., *Enhanced production of glutaric acid by NADH oxidase and GabD-reinforced bioconversion from l-lysine*. Biotechnol Bioeng, 2019. **116**(2): p. 333-341.
390. Yang, S.Y., et al., *Production of glutaric acid from 5-aminovaleric acid by robust whole-cell immobilized with polyvinyl alcohol and polyethylene glycol*. Enzyme Microb Technol, 2019. **128**: p. 72-78.
391. Yang, S.Y., et al., *Development of glutaric acid production consortium system with α -ketoglutaric acid regeneration by glutamate oxidase in Escherichia coli*. Enzyme Microb Technol, 2020. **133**: p. 109446.
392. Shin, J.H., et al., *Metabolic engineering of Corynebacterium glutamicum for enhanced production of 5-aminovaleric acid*. Microbial cell factories, 2016. **15**(1): p. 174-174.

393. (2021), N.C.f.B.I., *PubChem Compound Summary for CID 5960, Aspartic acid*. Retrieved June 16, 2021 from <https://pubchem.ncbi.nlm.nih.gov/compound/Aspartic-acid>.
394. Min, W., et al., *Characterization of Aspartate Kinase from Corynebacterium pekinense and the Critical Site of Arg169*. International journal of molecular sciences, 2015. **16**(12): p. 28270-28284.
395. Xu, J.-Z., et al., *Overexpression of thermostable meso-diaminopimelate dehydrogenase to redirect diaminopimelate pathway for increasing L-lysine production in Escherichia coli*. Scientific Reports, 2019. **9**(1): p. 2423.
396. Kwak, D.H., et al., *Synthetic redesign of Escherichia coli for cadaverine production from galactose*. Biotechnology for biofuels, 2017. **10**: p. 20-20.
397. Aliaksei V. Pukina, C.G.B., d, Elinor L. Scott c, and M.C.R.F. Johan P.M. Sanders c, *An efficient enzymatic synthesis of 5-aminovaleric acid*. Journal of Molecular Catalysis B: Enzymatic, 2009. **65**: p. 58-62.
398. Joo, J.C., et al., *Production of 5-aminovaleric acid in recombinant Corynebacterium glutamicum strains from a Miscanthus hydrolysate solution prepared by a newly developed Miscanthus hydrolysis process*. Bioresour Technol, 2017.
399. Rogers, J.K., N.D. Taylor, and G.M. Church, *Biosensor-based engineering of biosynthetic pathways*. Curr Opin Biotechnol, 2016. **42**: p. 84-91.
400. Rogers, J.K., et al., *Synthetic biosensors for precise gene control and real-time monitoring of metabolites*. Nucleic Acids Res, 2015. **43**(15): p. 7648-60.
401. Raman, S., et al., *Evolution-guided optimization of biosynthetic pathways*. Proc Natl Acad Sci U S A, 2014. **111**(50): p. 17803-8.
402. Hanko, E.K.R., N.P. Minton, and N. Malys, *A Transcription Factor-Based Biosensor for Detection of Itaconic Acid*. ACS Synthetic Biology, 2018. **7**(5): p. 1436-1446.
403. Wang, Y., et al., *Evolving the L-lysine high-producing strain of Escherichia coli using a newly developed high-throughput screening method*. J Ind Microbiol Biotechnol, 2016. **43**(9): p. 1227-35.
404. Hong, H., T. Fill, and P.F. Leadlay, *A Common Origin for Guanidinobutanoate Starter Units in Antifungal Natural Products*. Angewandte Chemie International Edition, 2013. **52**(49): p. 13096-13099.
405. Zhang, W., et al., *A Three Enzyme Pathway for 2-Amino-3-hydroxycyclopent-2-enone Formation and Incorporation in Natural Product Biosynthesis*. Journal of the American Chemical Society, 2010. **132**(18): p. 6402-6411.
406. Zhang, J., et al., *Application of an Acyl-CoA Ligase from Streptomyces aizunensis for Lactam Biosynthesis*. ACS Synthetic Biology, 2017. **6**(5): p. 884-890.
407. Zhang, J., et al., *Application of an Acyl-CoA Ligase from Streptomyces aizunensis for Lactam Biosynthesis*. ACS Synth Biol, 2017. **6**(5): p. 884-890.
408. Zhang, J., et al., *Development of a Transcription Factor-Based Lactam Biosensor*. ACS Synthetic Biology, 2017. **6**(3): p. 439-445.
409. Iwaki, H., et al., *Identification of a Transcriptional Activator (ChnR) and a 6-Oxohexanoate Dehydrogenase (ChnE) in the Cyclohexanol Catabolic Pathway in <i>Acinetobacter</i> sp. Strain NCIMB 9871 and Localization of the Genes That Encode Them*. Applied and Environmental Microbiology, 1999. **65**(11): p. 5158.
410. Cheng, Q., et al., *Genetic analysis of a gene cluster for cyclohexanol oxidation in Acinetobacter sp. Strain SE19 by in vitro transposition*. J Bacteriol, 2000. **182**(17): p. 4744-51.

411. Steigedal, M. and S. Valla, *The Acinetobacter sp. chnB promoter together with its cognate positive regulator ChnR is an attractive new candidate for metabolic engineering applications in bacteria*. *Metab Eng*, 2008. **10**(2): p. 121-9.
412. Schlegel, S., et al., *Optimizing membrane protein overexpression in the Escherichia coli strain Lemo21(DE3)*. *J Mol Biol*, 2012. **423**(4): p. 648-59.
413. Schein, C.H., *Production of Soluble Recombinant Proteins in Bacteria*. *Bio/Technology*, 1989. **7**(11): p. 1141-1149.
414. Meyer, A.S. and T.A. Baker, *Proteolysis in the Escherichia coli heat shock response: a player at many levels*. *Current opinion in microbiology*, 2011. **14**(2): p. 194-199.
415. Bernal, V., et al., *Role of betaine:CoA ligase (CaiC) in the activation of betaines and the transfer of coenzyme A in Escherichia coli*. *J Appl Microbiol*, 2008. **105**(1): p. 42-50.
416. Eichler, K., et al., *Molecular characterization of the cai operon necessary for carnitine metabolism in Escherichia coli*. *Mol Microbiol*, 1994. **13**(5): p. 775-86.
417. Zhang, J., et al., *Metabolic engineering of Escherichia coli for the biosynthesis of 2-pyrrolidone*. *Metabolic Engineering Communications*, 2016. **3**: p. 1-7.
418. Rosano, G.L. and E.A. Ceccarelli, *Recombinant protein expression in Escherichia coli: advances and challenges*. *Frontiers in Microbiology*, 2014. **5**(172).
419. Vasina, J.A. and F. Baneyx, *Expression of aggregation-prone recombinant proteins at low temperatures: a comparative study of the Escherichia coli cspA and tac promoter systems*. *Protein Expr Purif*, 1997. **9**(2): p. 211-8.
420. Hellman, L.M. and M.G. Fried, *Electrophoretic mobility shift assay (EMSA) for detecting protein-nucleic acid interactions*. *Nature protocols*, 2007. **2**(8): p. 1849-1861.
421. Schlundt, A., et al., *Structure-function analysis of the DNA-binding domain of a transmembrane transcriptional activator*. *Scientific Reports*, 2017. **7**(1): p. 1051.
422. Wu, J., et al., *Improving metabolic efficiency of the reverse beta-oxidation cycle by balancing redox cofactor requirement*. *Metab Eng*, 2017. **44**: p. 313-324.
423. Liu, L., S. Zhou, and Y. Deng, *The 3-ketoacyl-CoA thiolase: an engineered enzyme for carbon chain elongation of chemical compounds*. *Appl Microbiol Biotechnol*, 2020. **104**(19): p. 8117-8129.
424. Arenas-López, C., et al. *The genetic basis of 3-hydroxypropanoate metabolism in Cupriavidus necator H16*. *Biotechnology for biofuels*, 2019. **12**, 150 DOI: 10.1186/s13068-019-1489-5.
425. Chen, J., et al., *Metabolic engineering of Escherichia coli for the synthesis of polyhydroxyalkanoates using acetate as a main carbon source*. *Microbial Cell Factories*, 2018. **17**(1): p. 102.
426. Lee, H.-M., B.-Y. Jeon, and M.-K. Oh, *Microbial production of ethanol from acetate by engineered Ralstonia eutropha*. *Biotechnology and Bioprocess Engineering*, 2016. **21**(3): p. 402-407.
427. Hu, B. and M.E. Lidstrom, *Metabolic engineering of Methylobacterium extorquens AM1 for 1-butanol production*. *Biotechnology for Biofuels*, 2014. **7**(1): p. 156.
428. Ho, S.C. and Y. Yang, *Identifying and engineering promoters for high level and sustainable therapeutic recombinant protein production in cultured mammalian cells*. *Biotechnol Lett*, 2014. **36**(8): p. 1569-79.

429. Xu, N., L. Wei, and J. Liu, *Recent advances in the applications of promoter engineering for the optimization of metabolite biosynthesis*. World Journal of Microbiology and Biotechnology, 2019. **35**(2): p. 33.
430. Chokkathukalam, A., et al., *Stable isotope-labeling studies in metabolomics: new insights into structure and dynamics of metabolic networks*. Bioanalysis, 2014. **6**(4): p. 511-524.
431. Korosh, T.C., et al., *Engineering photosynthetic production of L-lysine*. Metabolic engineering, 2017. **44**: p. 273-283.
432. Viswanath, B., et al., *Enhancing the Activity of Aspartate Kinase for an Overproduction of L-lysine by Corynebacterium glutamicum*. American Journal of Biochemistry and Molecular biology, 2016. **6**: p. 33-44.
433. Bruland, N., et al., *Unravelling the C3/C4 carbon metabolism in Ralstonia eutropha H16*. Journal of Applied Microbiology, 2010. **109**(1): p. 79-90.
434. Hanco, E.K.R., et al., *A genome-wide approach for identification and characterisation of metabolite-inducible systems*. Nature communications, 2020. **11**(1): p. 1213-1213.
435. Ayres, E.K., et al., *Precise deletions in large bacterial genomes by vector-mediated excision (VEX). The trfA gene of promiscuous plasmid RK2 is essential for replication in several gram-negative hosts*. J Mol Biol, 1993. **230**(1): p. 174-85.

Appendix

Figures and tables

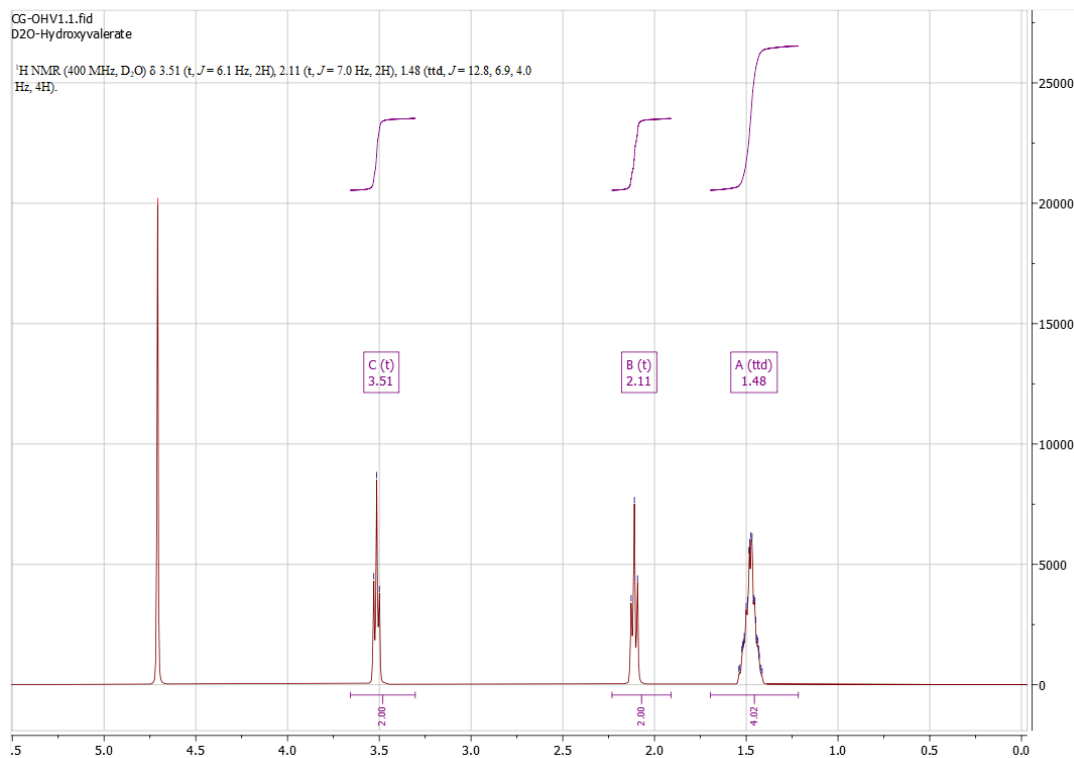


Figure A1 H¹-NMR spectrum of chemically synthesised 5-OHV

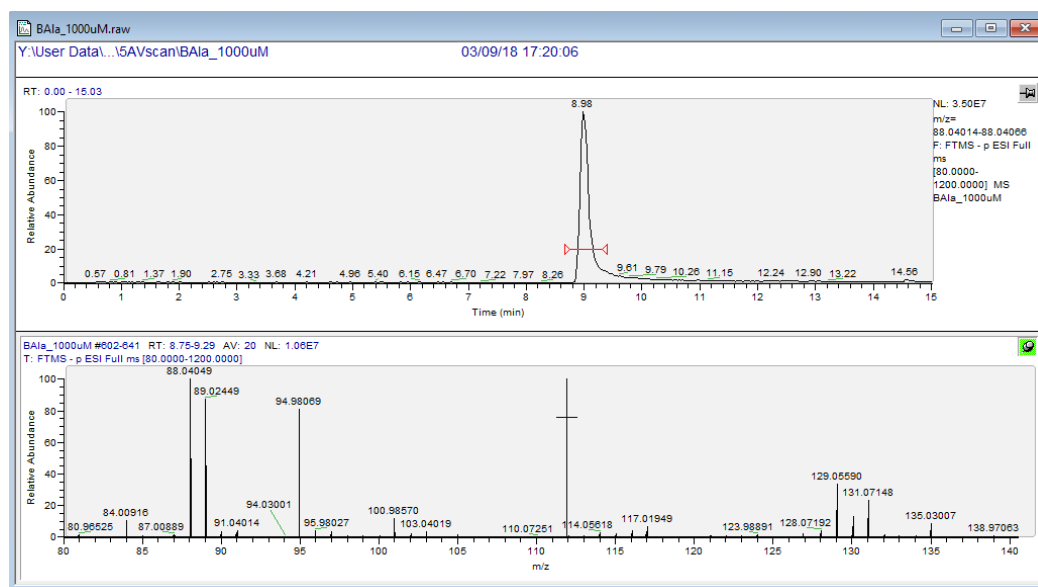


Figure A2 Mass spectrum of 1 mM β -alanine standard reagent

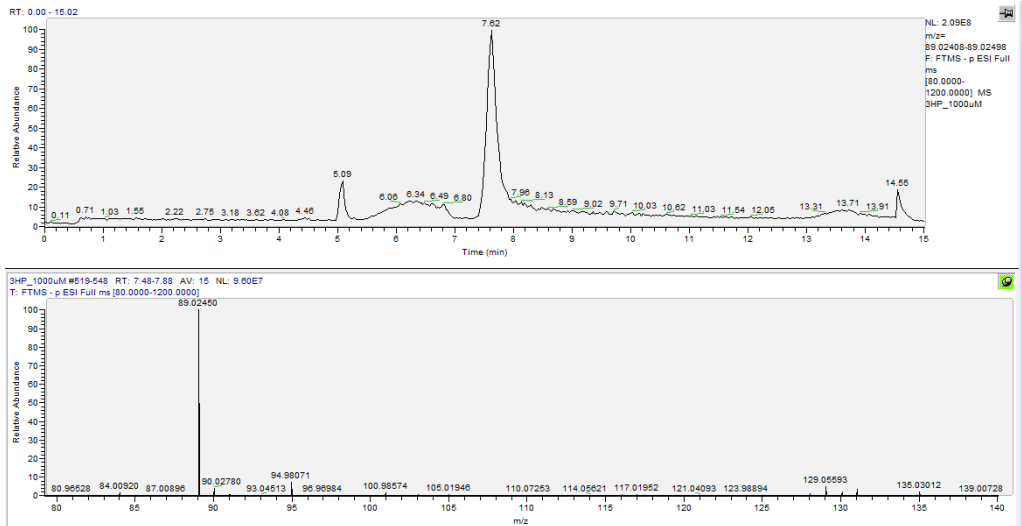


Figure A3 Mass spectrum of 1 mM 3-HP standard reagent

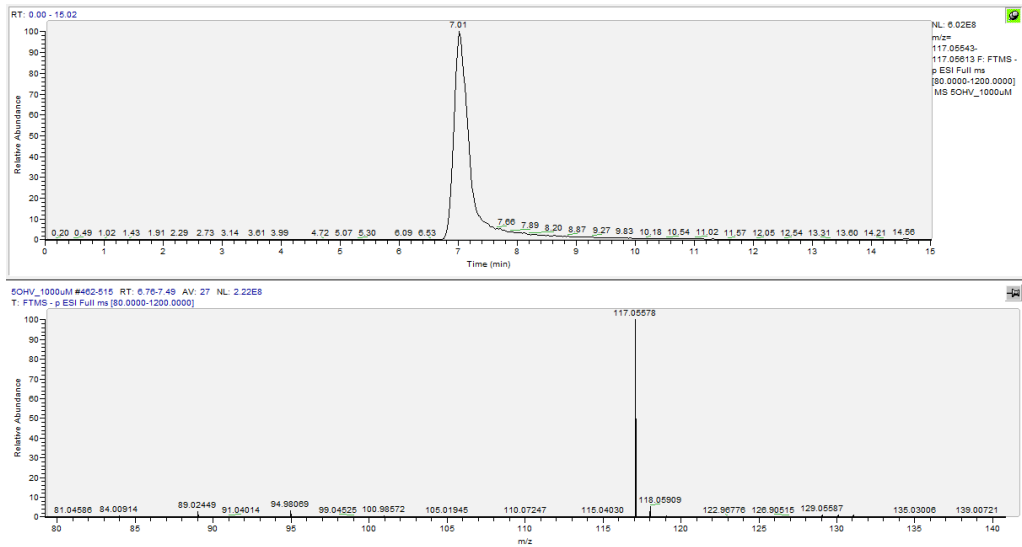


Figure A4 Mass spectrum of 1 mM 5-OHV standard reagent

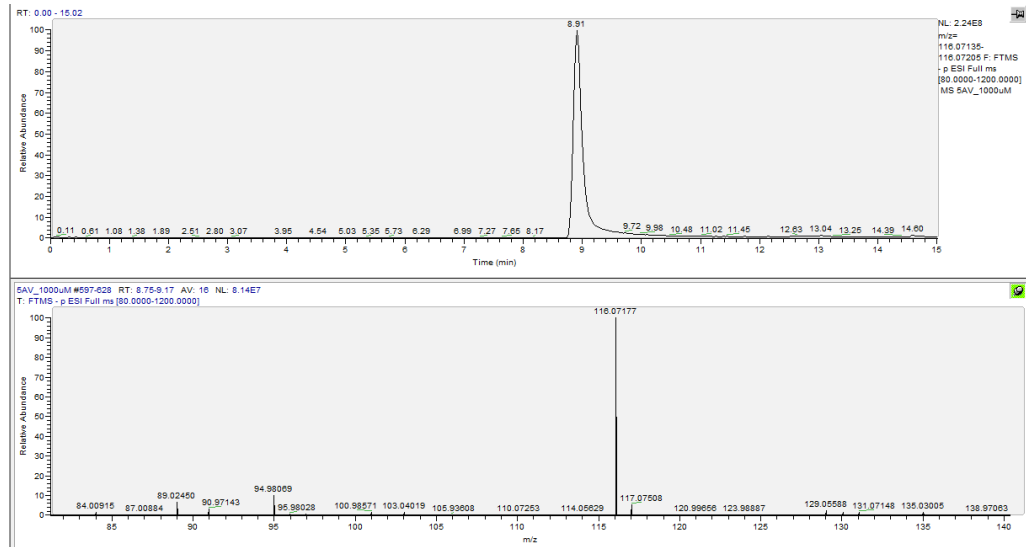


Figure A5 Mass spectrum of 1 mM 5-AV standard reagent

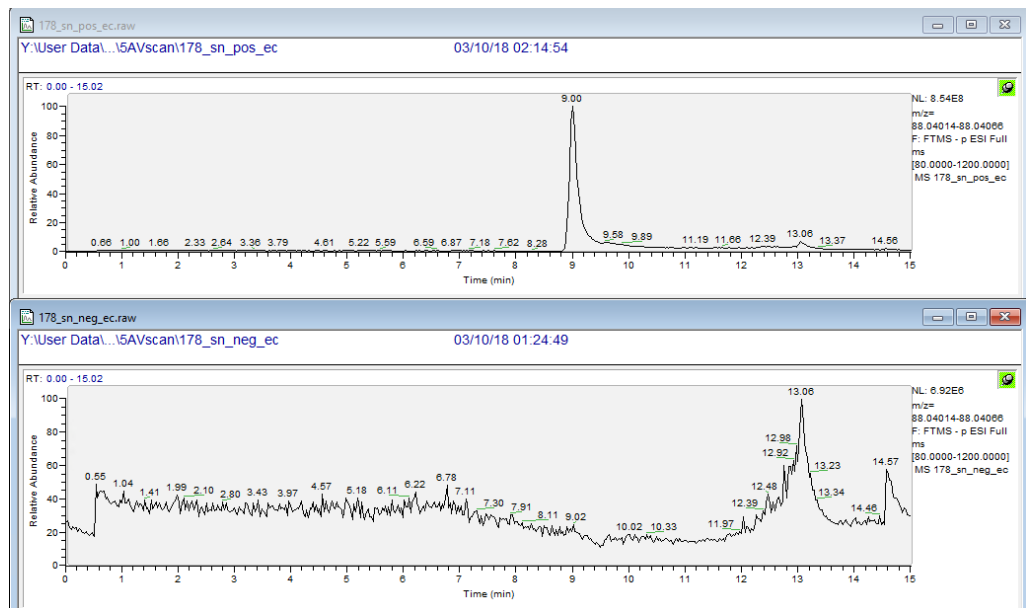


Figure A6 Alanine mass spectra of 50 mM β -alanine supplemented (top) and unsupplemented (bottom) EC21 (no plasmid control) *E. coli* fermentations, 48 h timepoint. RT β -alanine = 8.98. Measured: 9.00 (top); n.d. (bottom)

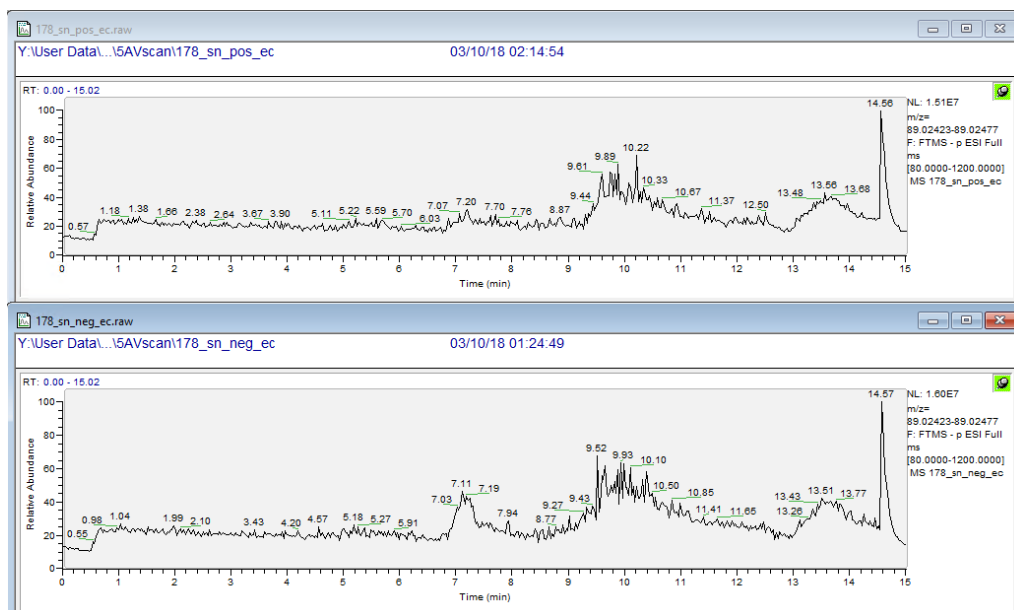


Figure A7 3-HP mass spectra of 50 mM β -alanine supplemented (top) and unsupplemented (bottom) EC21 (no plasmid control) *E. coli* fermentations, 48 h timepoint. RT 3-HP = 7.62. Measured: n.d. (top); n.d. (bottom)

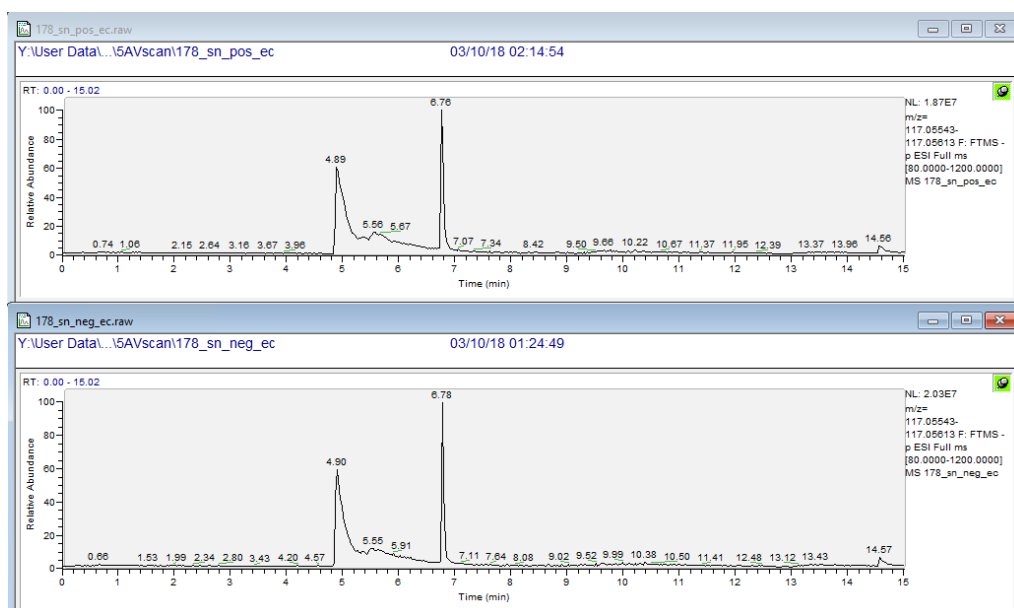


Figure A8 5-OHV mass spectra of 50 mM β -alanine supplemented (top) and unsupplemented (bottom) EC21 (no plasmid control) *E. coli* fermentations, 48 h timepoint. RT 5-OHV = 7.01. Measured: 4.89 and 7.76 (n.d.) (top); 4.90 and 6.78 (n.d.) (bottom)

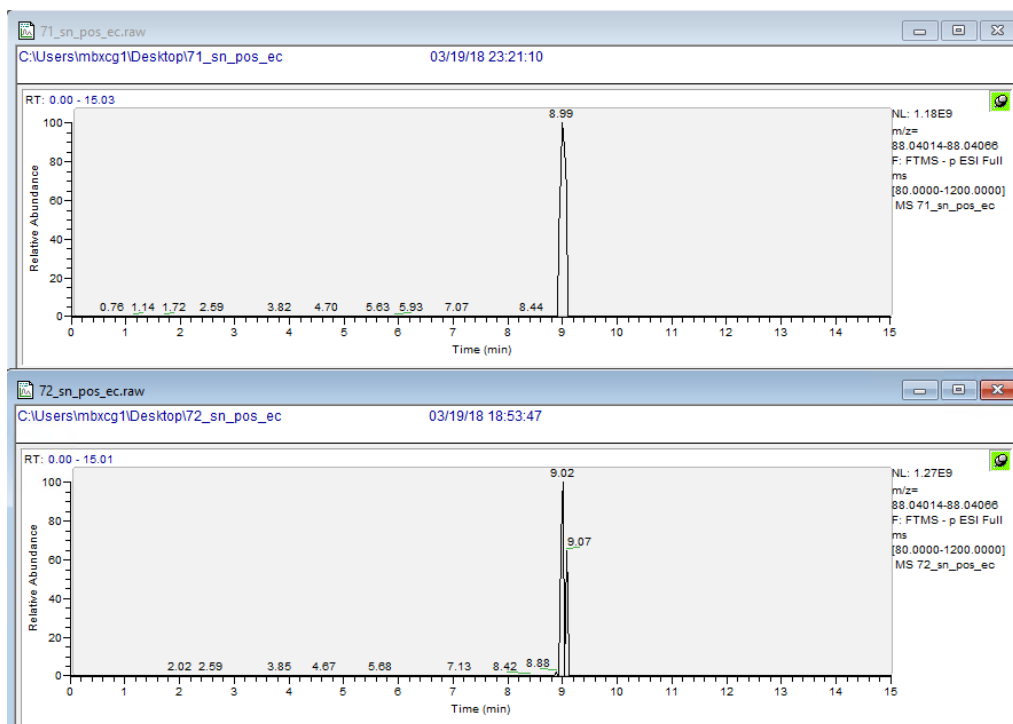


Figure A9 Alanine mass spectra of 50 mM β -alanine supplemented EC11 (top) and EC12 (bottom) *E. coli* fermentations, 48 h timepoint. RT β -alanine = 8.98. Measured: 8.99 (top); 9.02 (bottom)

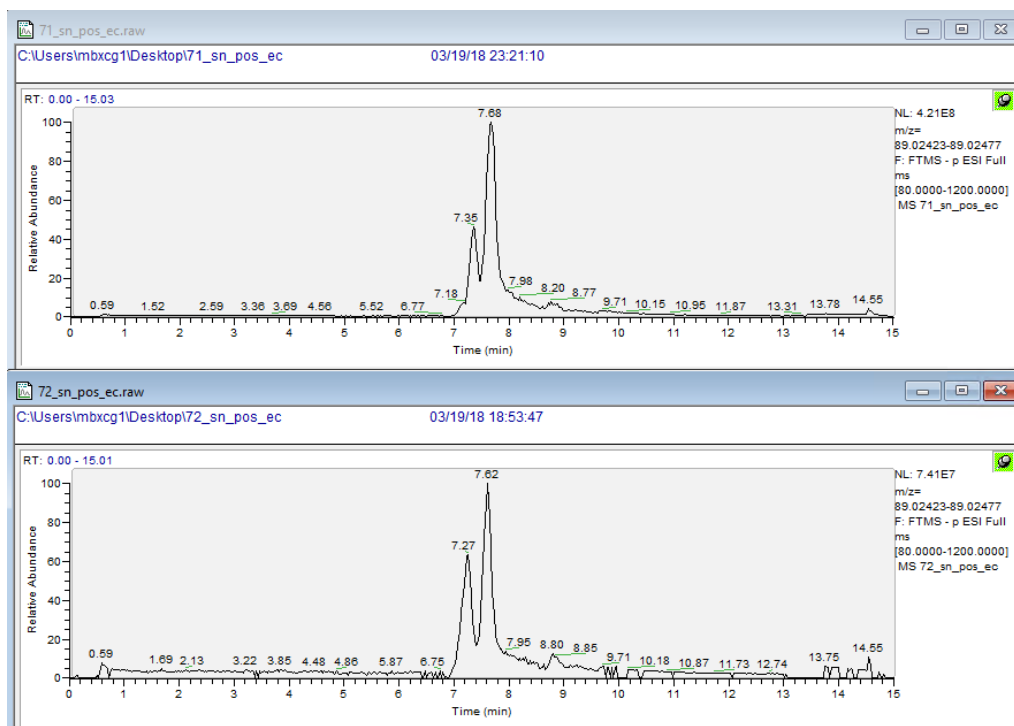


Figure A10 3-HP mass spectra of 50 mM β -alanine supplemented EC11 (top) and EC12 (bottom) *E. coli* fermentations, 48 h timepoint. RT 3-HP = 7.62 Measured: 7.68 (top); 7.62 (bottom).

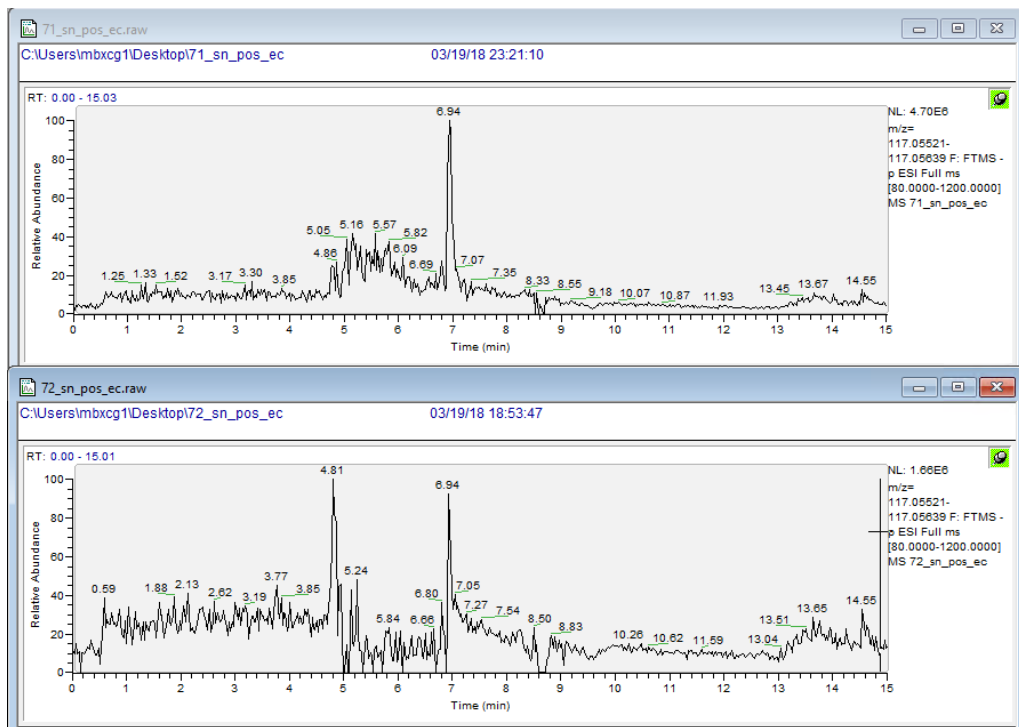


Figure A11 5-OHV mass spectra of 50 mM β -alanine supplemented EC11 (top) and EC12 (bottom) *E. coli* fermentations, 48 h timepoint. RT 5-OHV = 7.01. Measured: 6.94 (top); 6.94 (bottom)

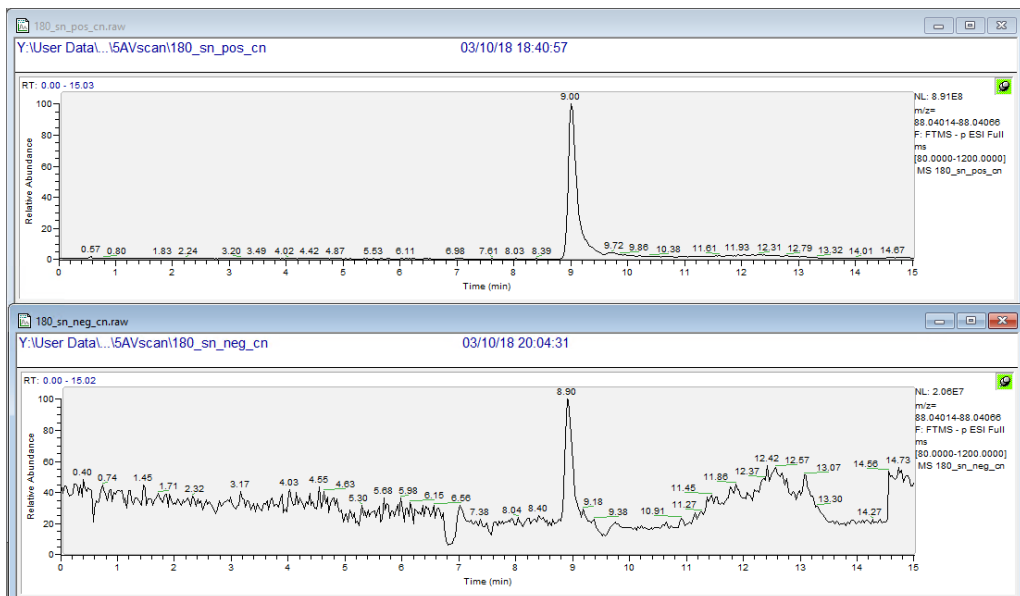


Figure A12 Alanine mass spectra of 50 mM β -alanine supplemented (top) and unsupplemented (bottom) CN21 Δ 4 (no plasmid control) fermentations, 48 h timepoint. RT β -alanine = 8.98. Measured: 9.00 (top); 8.90 (low signal) (bottom), n.d.

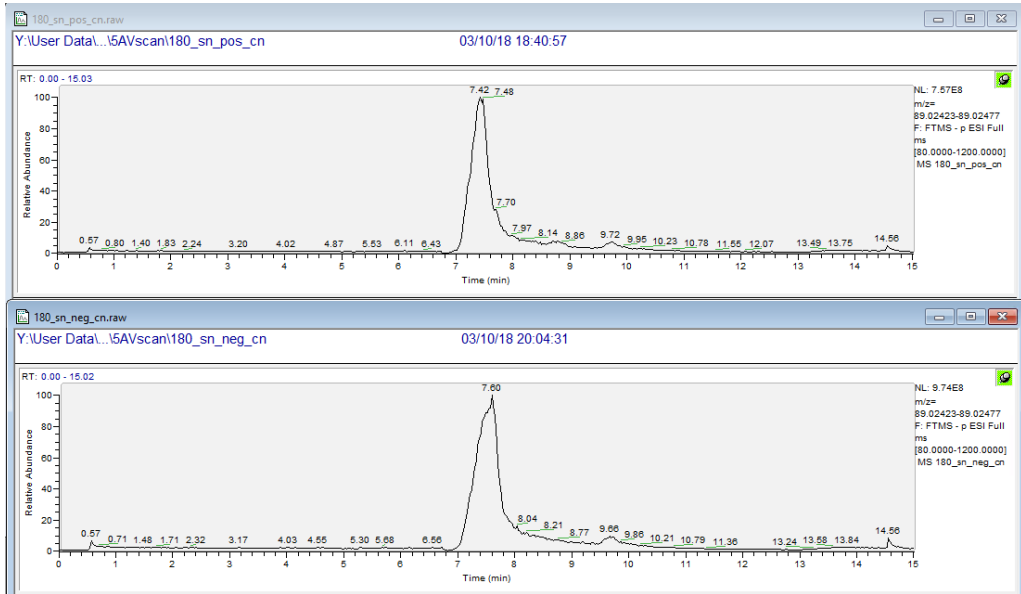


Figure A13 3-HP mass spectra of 50 mM β -alanine supplemented (top) and unsupplemented (bottom) CN21 Δ 4 (no plasmid control) fermentations, 48 h timepoint. RT 3-HP = 7.62 Measured: 7.42 (broad signal) (top); 7.60 (broad signal) (bottom). False positive peak, possible overlap with lactate. Slight peak shift.

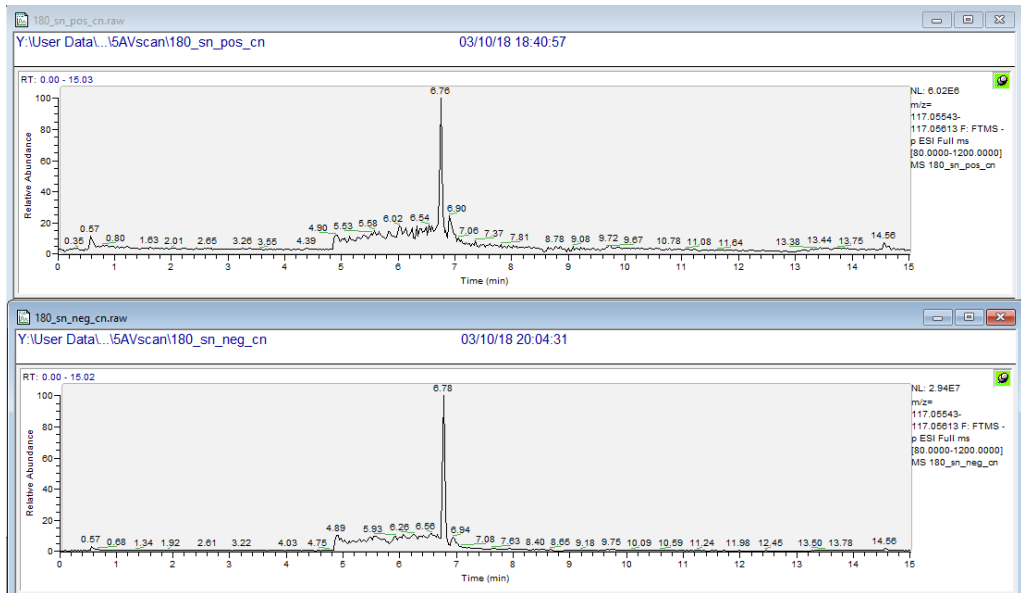


Figure A14 5-OHV mass spectra of 50 mM β -alanine supplemented (top) and unsupplemented (bottom) CN21 Δ 4 (no plasmid control) fermentations, 48 h timepoint. RT 5-OHV = 7.01. Measured: 6.76 (n.d.) (top); 6.78 (n.d.) (bottom)

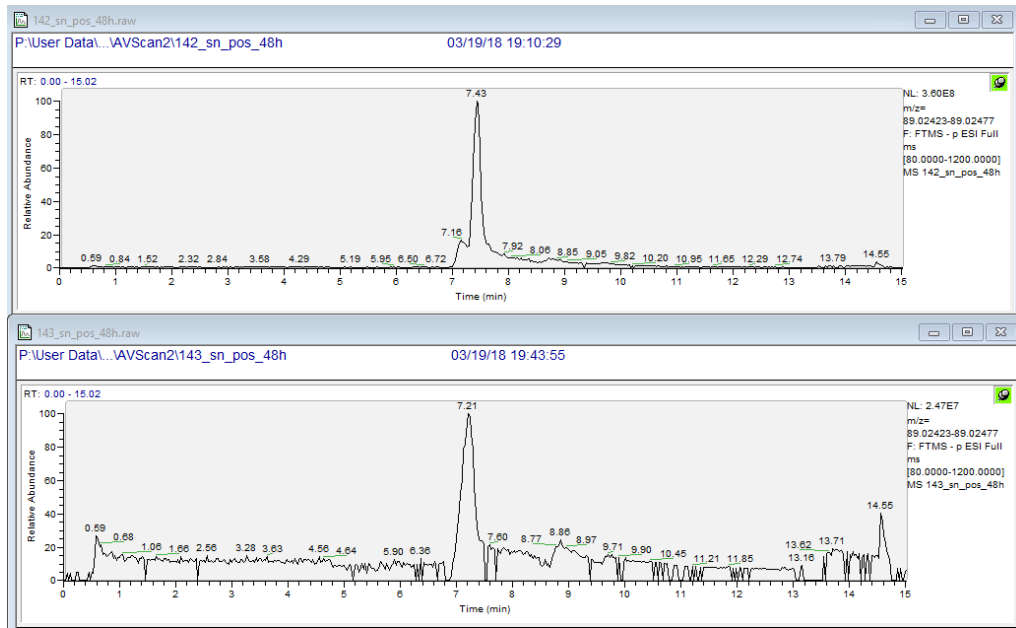


Figure A15 3-HP mass spectra of 50 mM β -alanine supplemented CN1 Δ 4 (top) and CN2 Δ 4 (bottom) fermentations, 48 h timepoint. RT 3-HP = 7.62 Measured: 7.43 (narrow signal) (top); 7.21 (broad signal) (bottom)(n.d.). Slight peak shift.

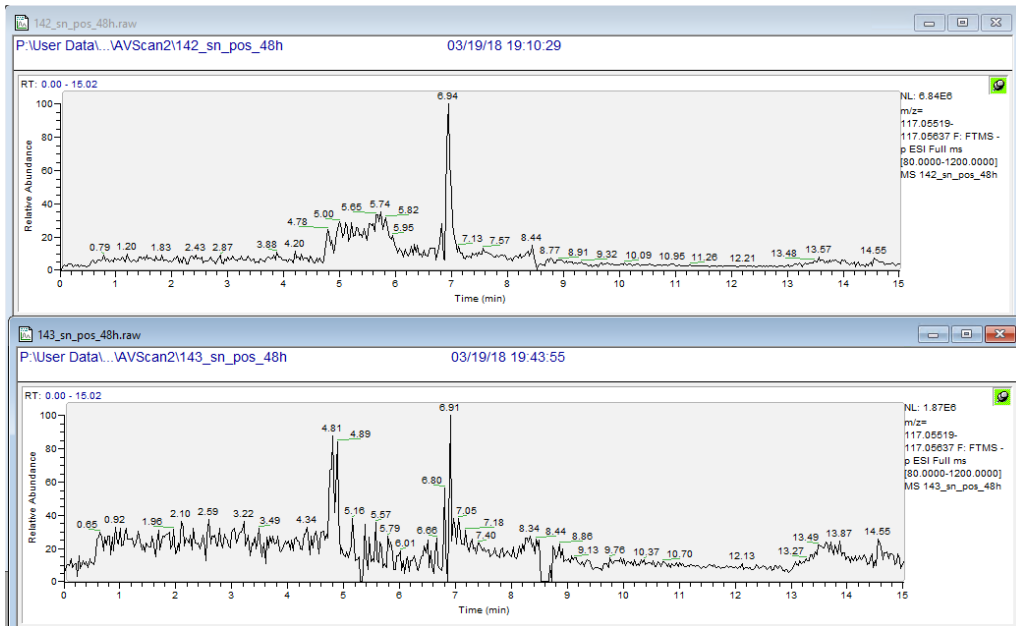


Figure A16 5-OHV mass spectra of 50 mM β -alanine supplemented CN1 Δ 4 (top) and CN2 Δ 4 (bottom) fermentations, 48 h timepoint. RT 5-OHV = 7.01. Measured: 6.94 (top); low S/N ratio for 6.91 peak, (n.d.) (bottom)

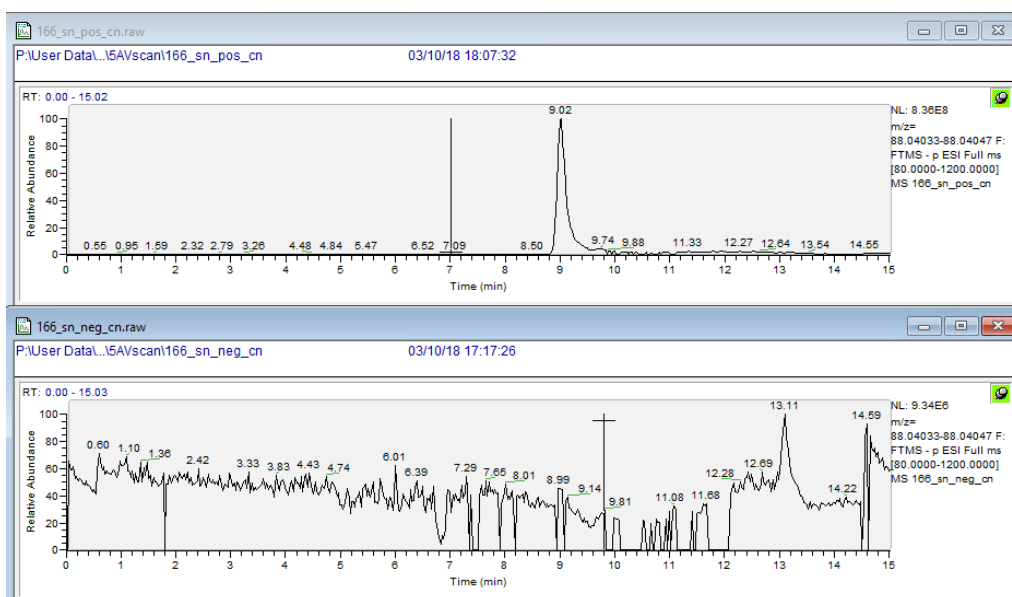


Figure A17 Alanine mass spectra of 50 mM β -alanine supplemented (top) and unsupplemented (bottom) CN11 Δ 4 fermentations, 48 h timepoint. RT β -alanine = 8.98. Measured: 9.02 (top); (n.d.) (bottom)

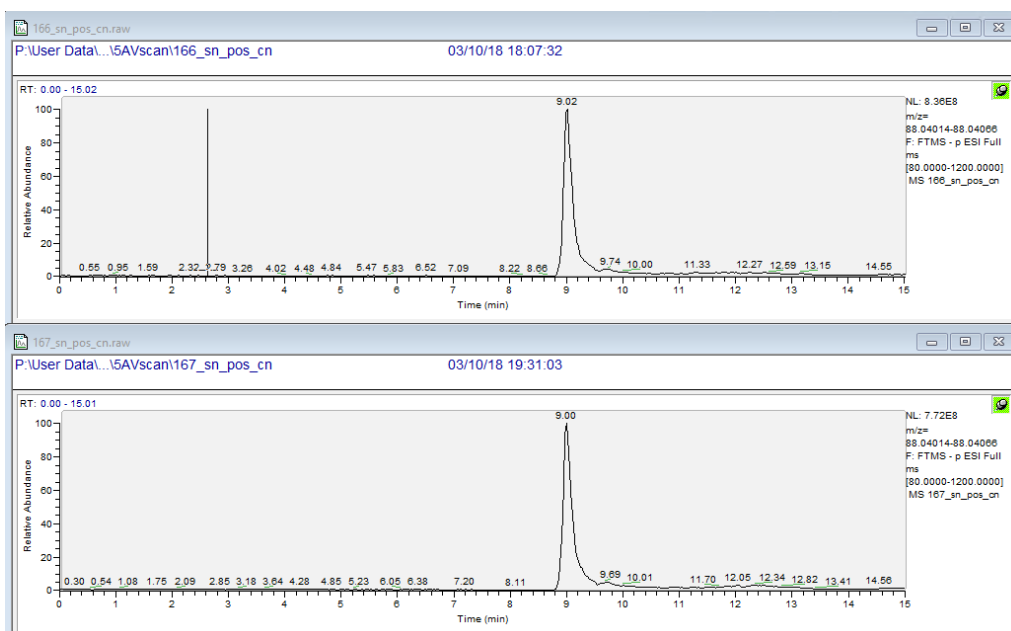


Figure A18 Alanine mass spectra of 50 mM β -alanine supplemented CN11 Δ 4 (top) and CN12 Δ 4 (bottom) fermentations, 48 h timepoint. RT β -alanine = 8.98. Measured: 9.02 (top); 9.00 (bottom)

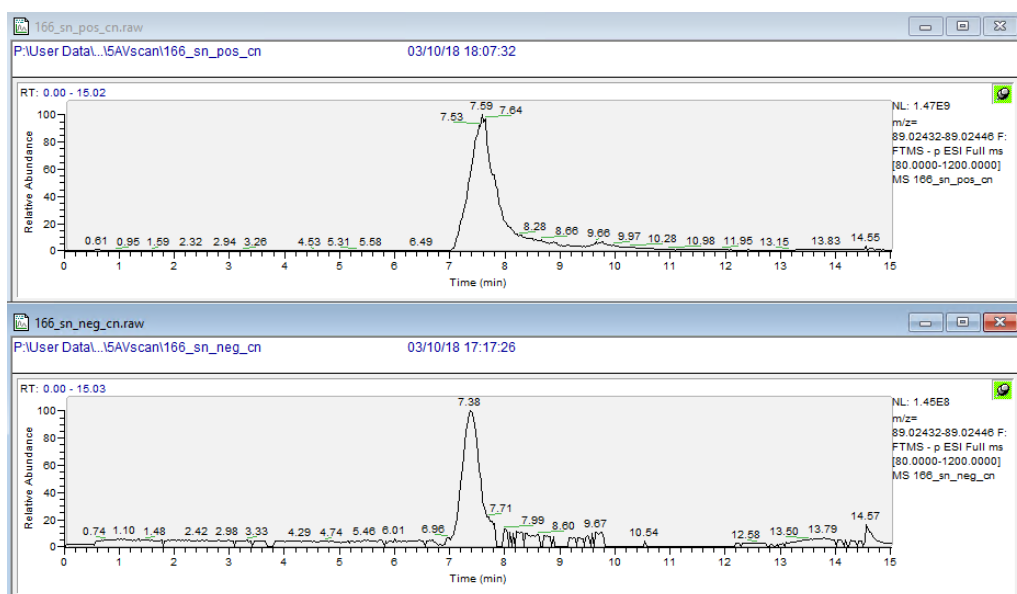


Figure A19 3-HP mass spectra of 50 mM β -alanine supplemented (top) and unsupplemented (bottom) CN11 Δ 4 fermentations, 48 h timepoint. RT 3-HP = 7.62 Measured: 7.59 (broad signal)(top); 7.38 (bottom)(ambiguous).

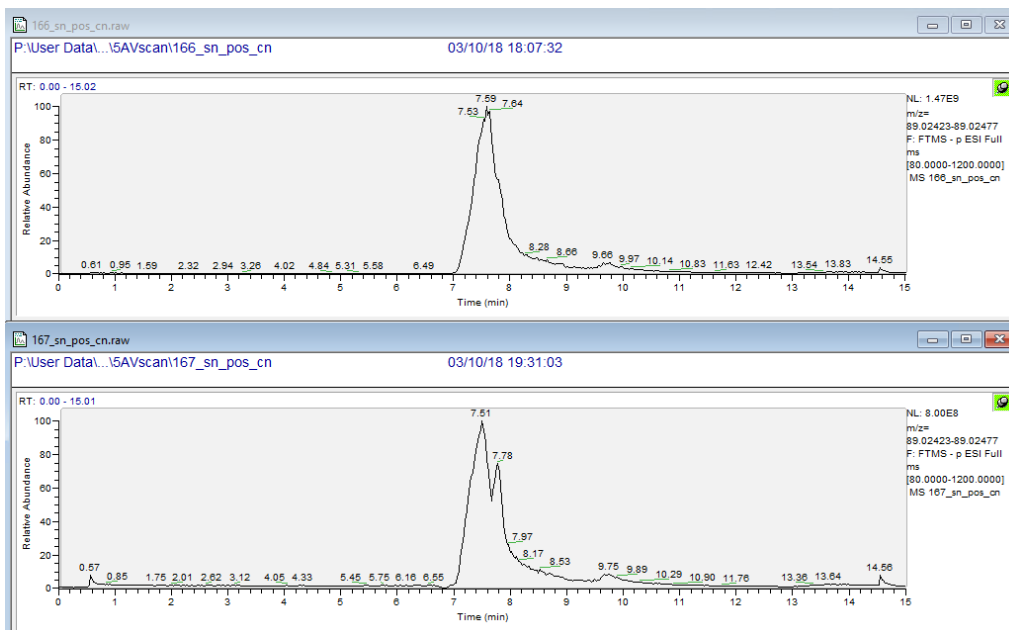


Figure A20 3-HP mass spectra of 50 mM β -alanine supplemented CN11 Δ 4 (top) and CN12 Δ 4 (bottom) fermentations, 48 h timepoint RT 3-HP = 7.62 Measured: 7.59 (broad signal)(top); 7.51 (broad signal).

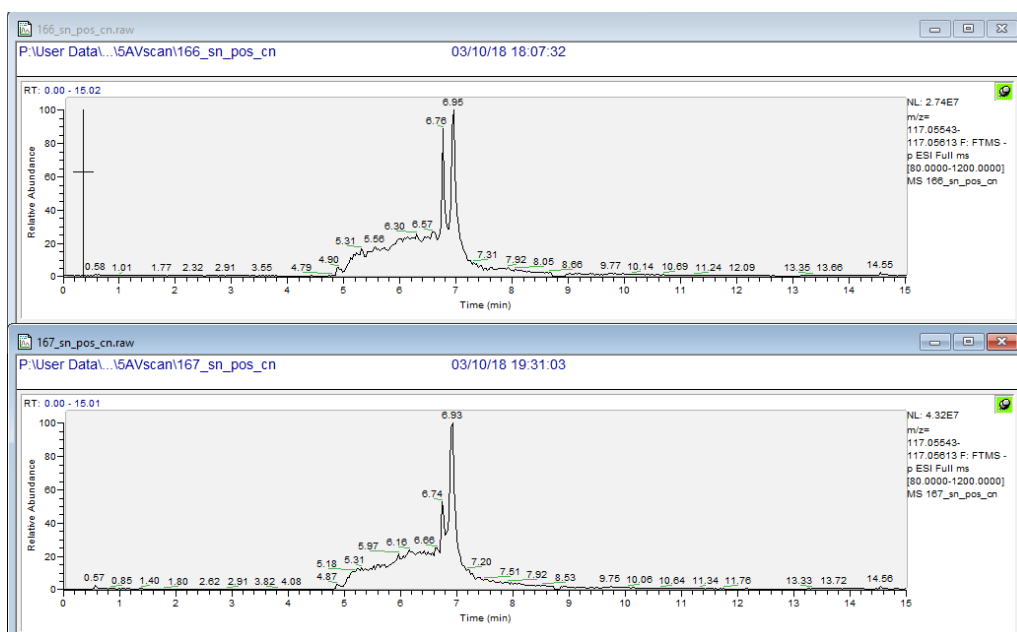


Figure A21 5-OHV mass spectra of 50 mM β -alanine supplemented CN11 Δ 4 (top) and CN12 Δ 4 (bottom) fermentations, 48 h timepoint . RT 5-OHV = 7.01. Measured: 6.95 (top); 6.93 (bottom)

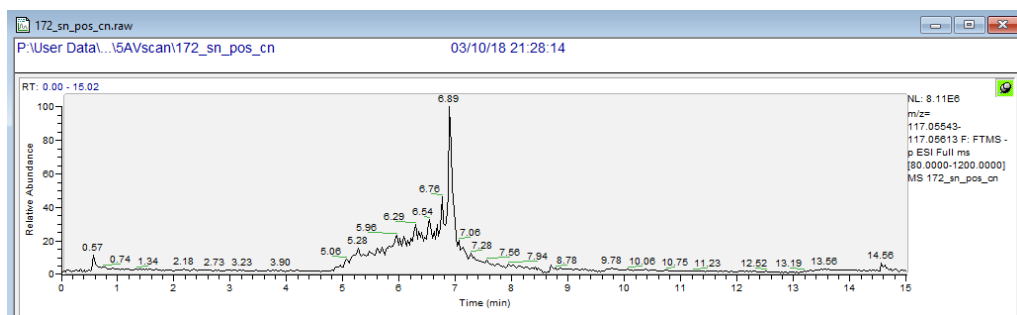


Figure A22 5-OHV mass spectra of 50 mM β -alanine supplemented CN17 Δ 4 fermentations, 48 h timepoint . RT 5-OHV = 7.01. Measured: 6.89

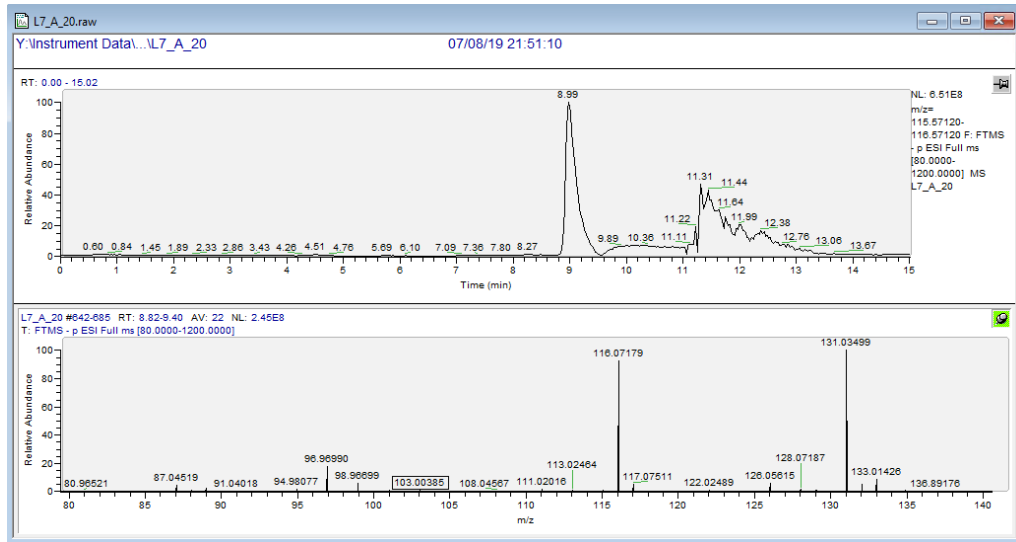


Figure A23 5-AV mass spectra of 20 mM L-lysine supplemented L7 fermentations, 20 h timepoint . RT 5-AV = 8.91. Measured: 8.99 (top)

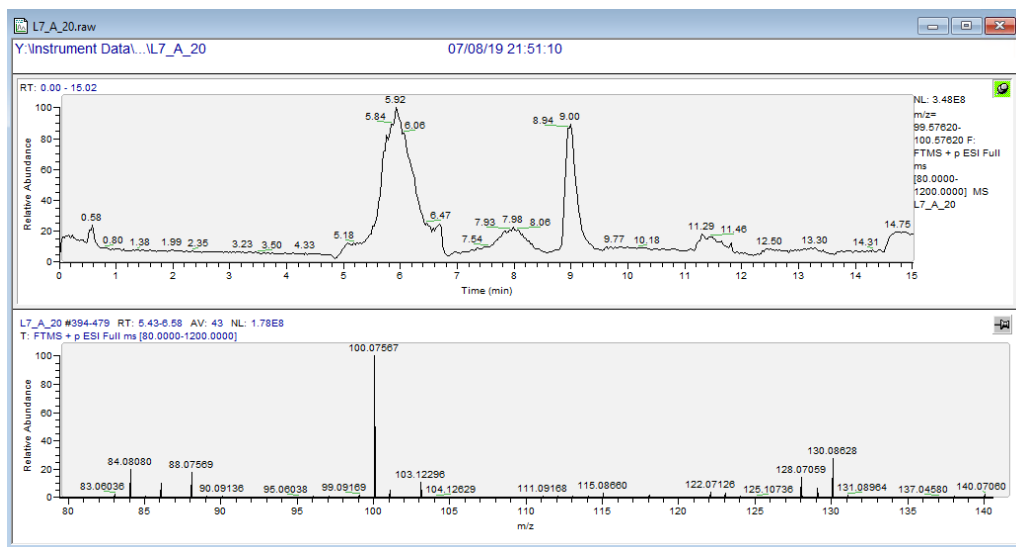


Figure A24 δ -valerolactam mass spectra of 20 mM L-lysine supplemented L7 + pBS2 fermentations, 20 h timepoint. RT δ -valerolactam = 6.00. Measured: 5.92

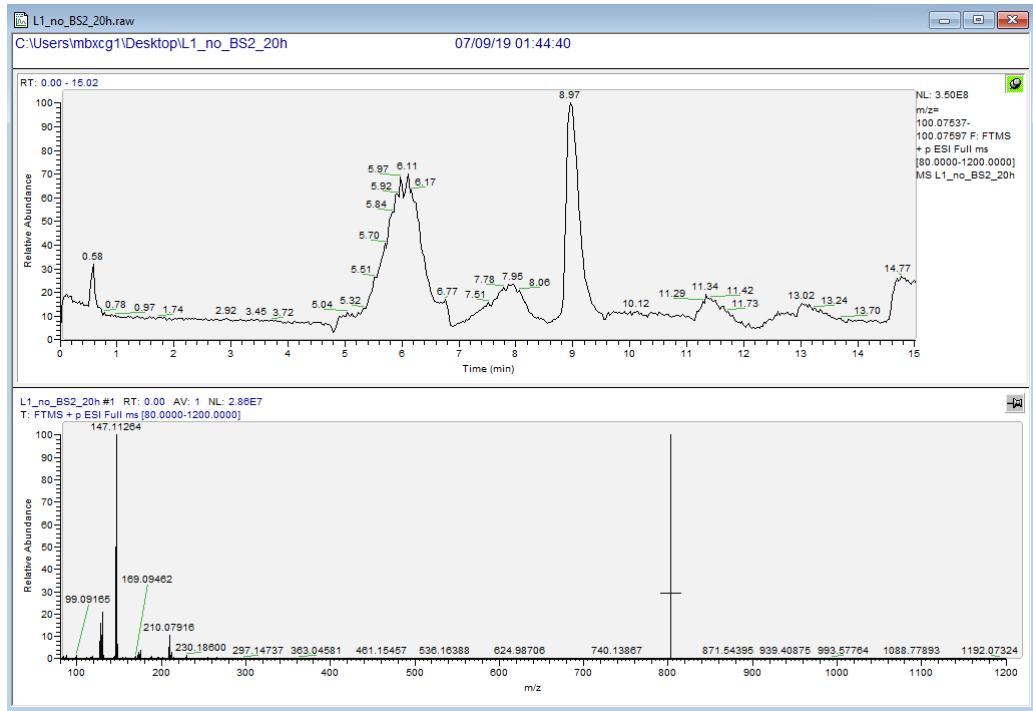


Figure A25 δ -valerolactam mass spectra of 20 mM L-lysine supplemented L1 without pBS2 fermentations, 20 h timepoint . RT δ -valerolactam = 6.00. Measured: 6.11

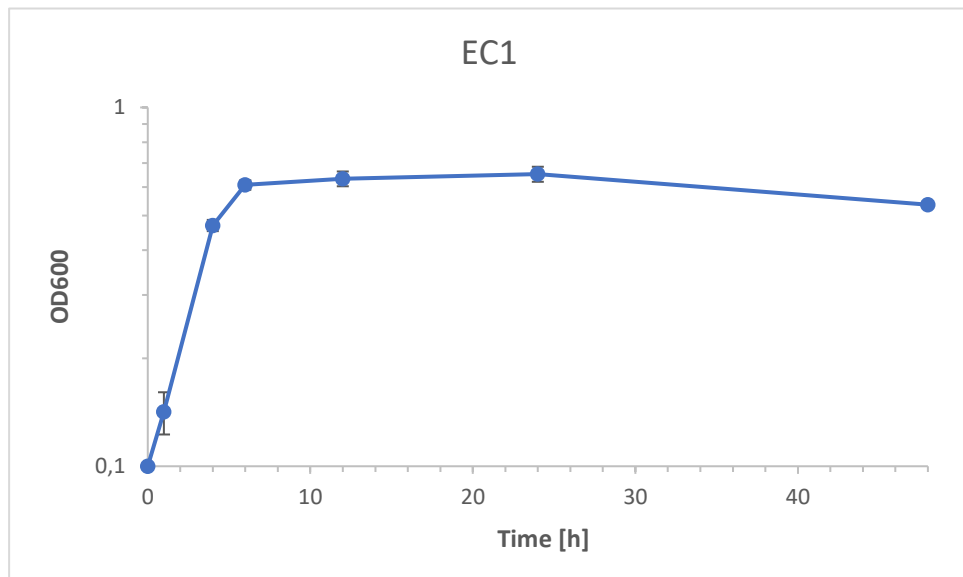


Figure A26 Growth curves of *E. coli* DH5 α EC1 in ECMM medium with 50 mM β -alanine supplementation over 48 h. *E. coli* EC1 was used to inoculate ECMM medium with 50 mM β -alanine at 0.1 OD₆₀₀ and grown for 48 hours. Blue curve: OD₆₀₀ of the supplemented cultures. All cultures were grown in biological triplicates and pH adjusted. $T_D = 2,200$ h.

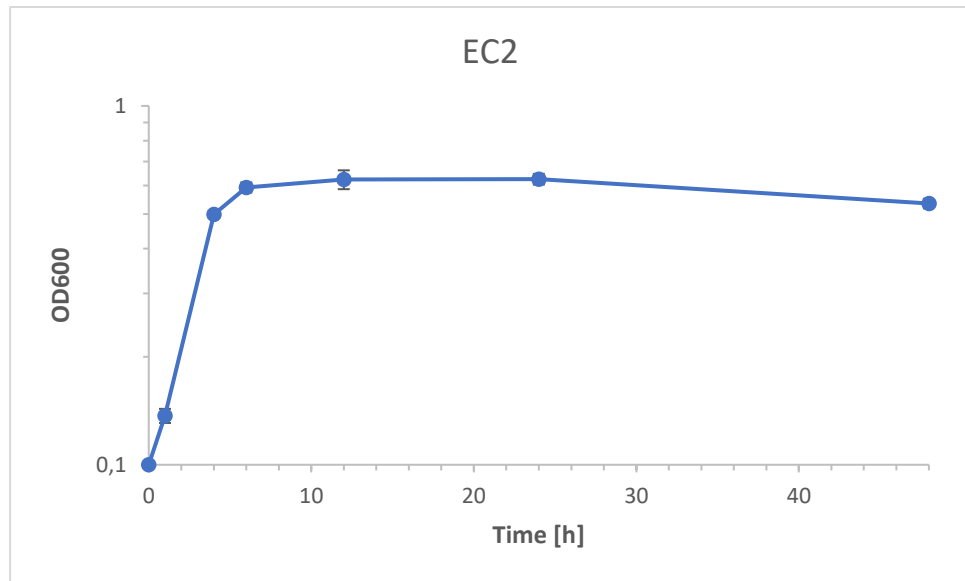


Figure A27 Growth curves of *E. coli* DH5α EC2 in ECMM medium with 50 mM β-alanine supplementation over 48 h. *E. coli* EC2 was used to inoculate ECMM medium with 50 mM β-alanine at 0.1 OD₆₀₀ and grown for 48 hours. Blue curve: OD₆₀₀ of the supplemented cultures. All cultures were grown in biological triplicates and pH adjusted. $T_D = 2,225$ h.

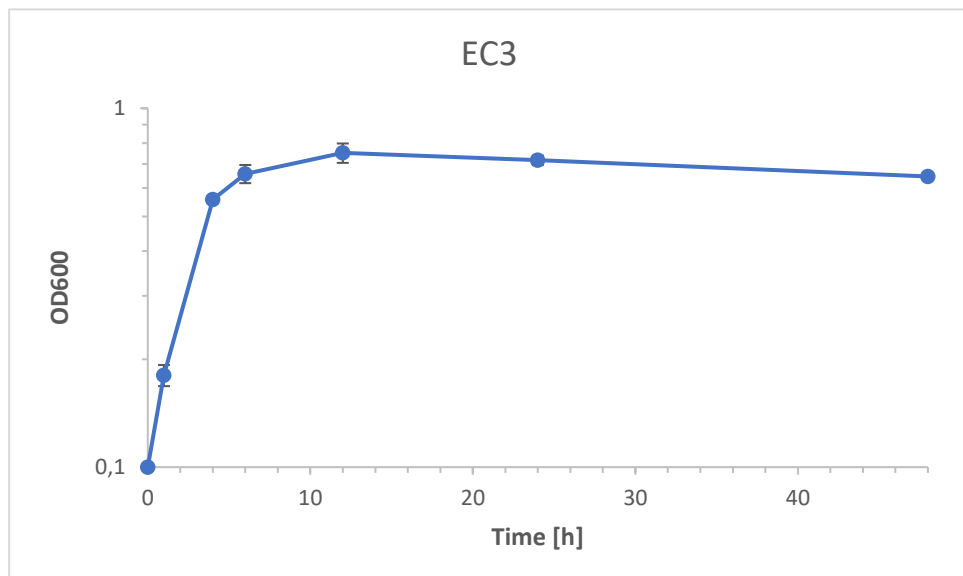


Figure A28 Growth curves of *E. coli* DH5α EC3 in ECMM medium with 50 mM β-alanine supplementation over 48 h. *E. coli* EC3 was used to inoculate ECMM medium with 50 mM β-alanine at 0.1 OD₆₀₀ and grown for 48 hours. Blue curve: OD₆₀₀ of the supplemented cultures. All cultures were grown in biological triplicates and pH adjusted. $T_D = 2,209$ h.

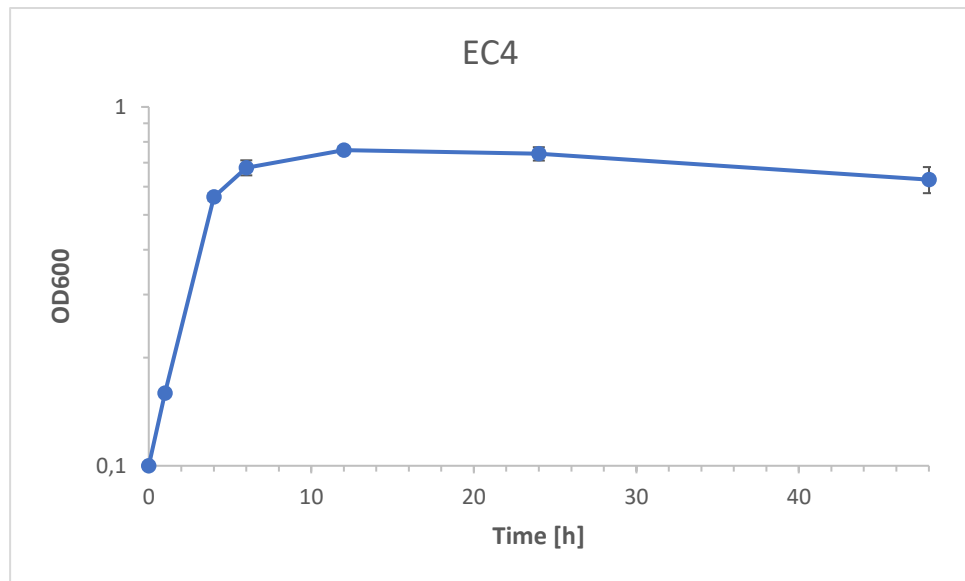


Figure A29 Growth curves of *E. coli* DH5α EC4 in ECMM medium with 50 mM β-alanine supplementation over 48 h. *E. coli* EC4 was used to inoculate ECMM medium with 50 mM β-alanine at 0.1 OD₆₀₀ and grown for 48 hours. Blue curve: OD₆₀₀ of the supplemented cultures. All cultures were grown in biological triplicates and pH adjusted. T_D = 2,173 h.

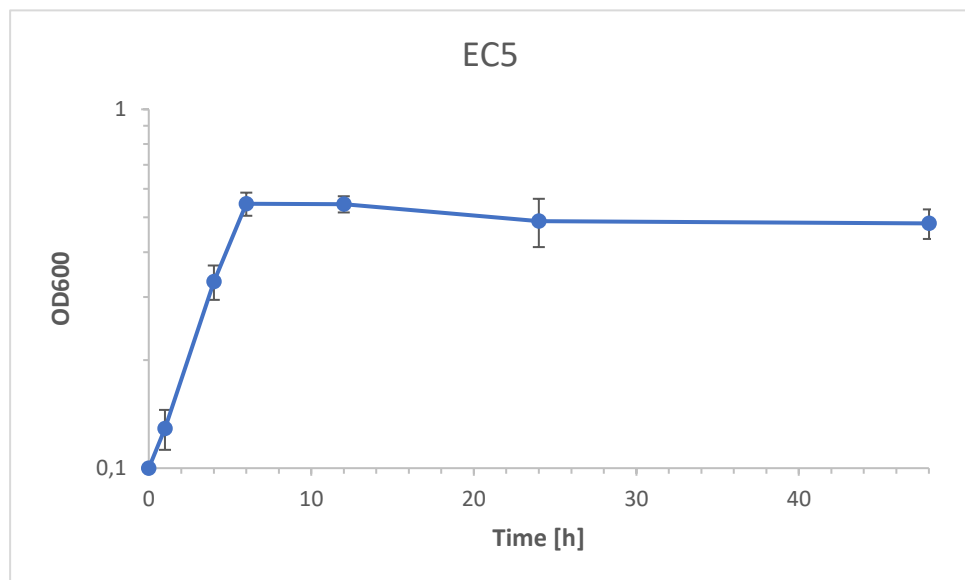


Figure A30 Growth curves of *E. coli* DH5α EC5 in ECMM medium with 50 mM β-alanine supplementation over 48 h. *E. coli* EC5 was used to inoculate ECMM medium with 50 mM β-alanine at 0.1 OD₆₀₀ and grown for 48 hours. Blue curve: OD₆₀₀ of the supplemented cultures. All cultures were grown in biological triplicates and pH adjusted. T_D = 2,541 h.

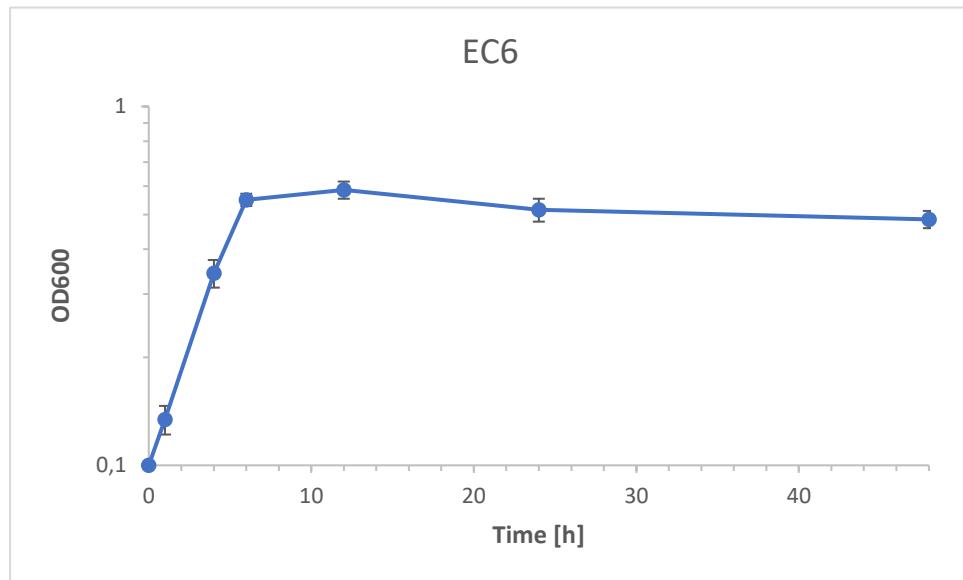


Figure A31 Growth curves of *E. coli* DH5α EC6 in ECMM medium with 50 mM β-alanine supplementation over 48 h. *E. coli* EC6 was used to inoculate ECMM medium with 50 mM β-alanine at 0.1 OD₆₀₀ and grown for 48 hours. Blue curve: OD₆₀₀ of the supplemented cultures. All cultures were grown in biological triplicates and pH adjusted. T_D = 2,440 h.

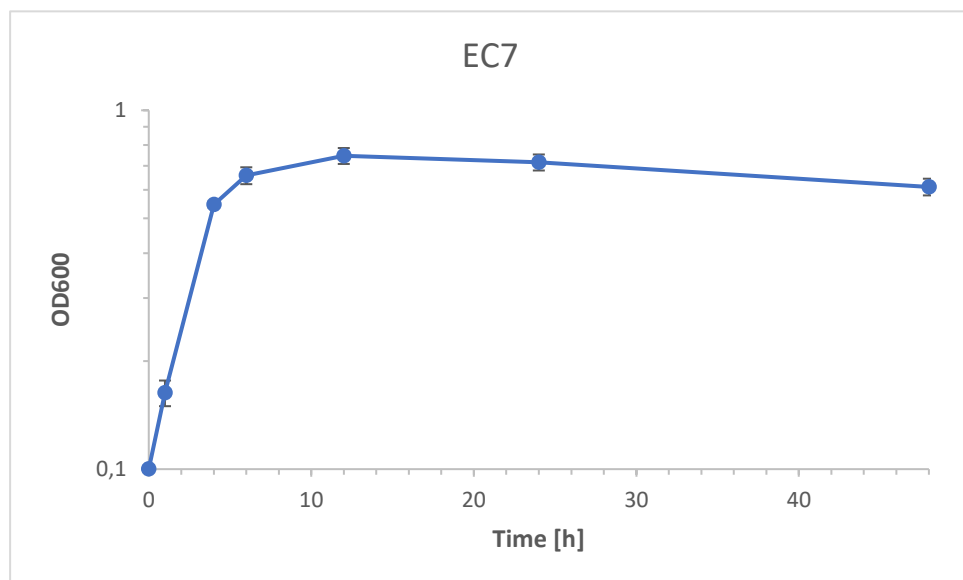


Figure A32 Growth curves of *E. coli* DH5α EC7 in ECMM medium with 50 mM β-alanine supplementation over 48 h. *E. coli* EC7 was used to inoculate ECMM medium with 50 mM β-alanine at 0.1 OD₆₀₀ and grown for 48 hours. Blue curve: OD₆₀₀ of the supplemented cultures. All cultures were grown in biological triplicates and pH adjusted. T_D = 2,207 h.

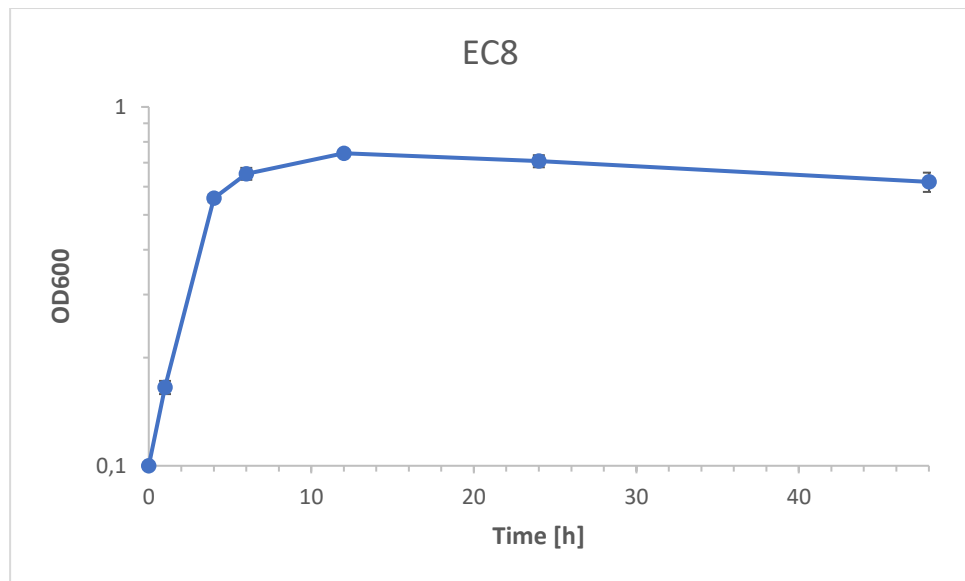


Figure A33 Growth curves of *E. coli* DH5α EC8 in ECMM medium with 50 mM β-alanine supplementation over 48 h. *E. coli* EC8 was used to inoculate ECMM medium with 50 mM β-alanine at 0.1 OD₆₀₀ and grown for 48 hours. Blue curve: OD₆₀₀ of the supplemented cultures. All cultures were grown in biological triplicates and pH adjusted. $T_D = 2,219$ h.

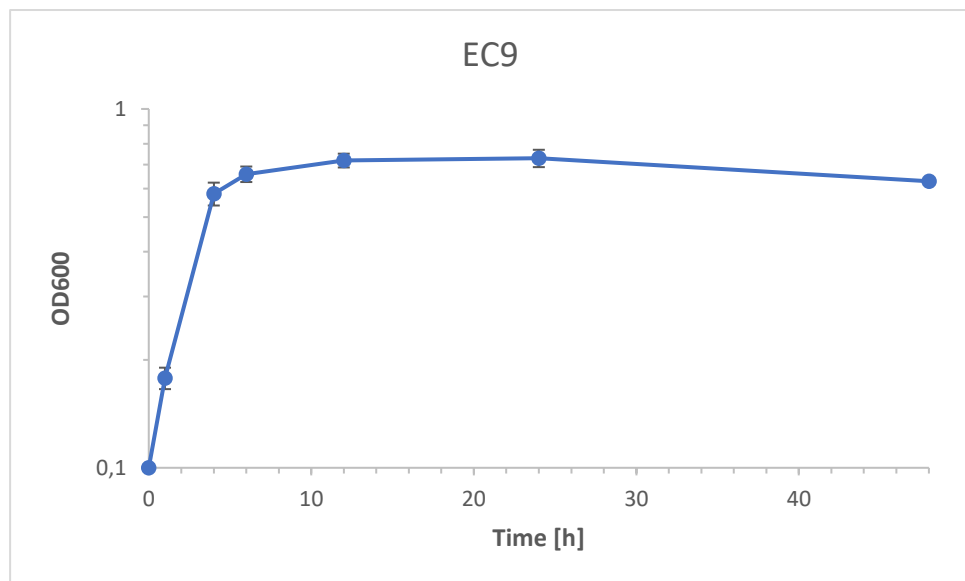


Figure A34 Growth curves of *E. coli* DH5α EC9 in ECMM medium with 50 mM β-alanine supplementation over 48 h. *E. coli* EC9 was used to inoculate ECMM medium with 50 mM β-alanine at 0.1 OD₆₀₀ and grown for 48 hours. Blue curve: OD₆₀₀ of the supplemented cultures. All cultures were grown in biological triplicates and pH adjusted. $T_D = 2,207$ h.

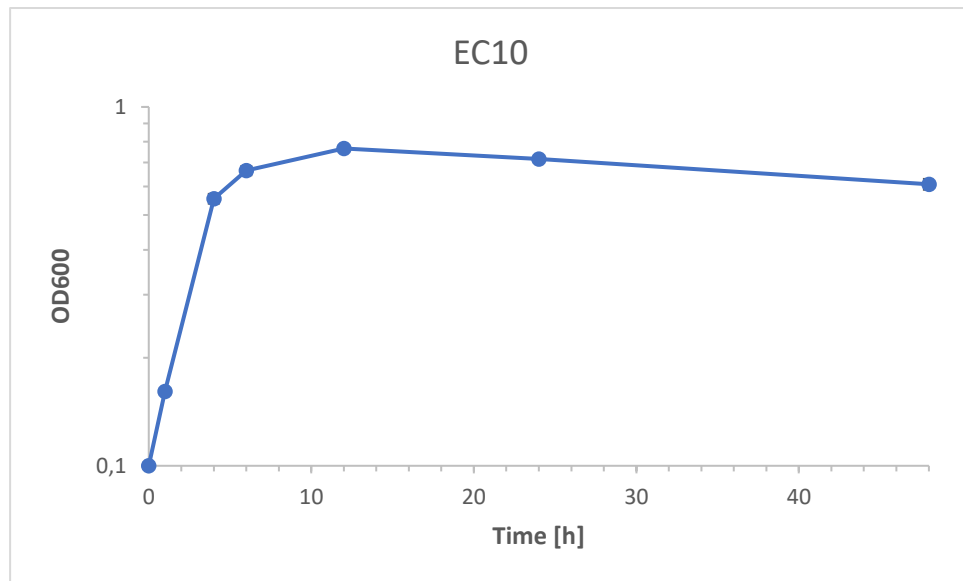


Figure A35 Growth curves of *E. coli* DH5α EC10 in ECMM medium with 50 mM β-alanine supplementation over 48 h. *E. coli* EC10 was used to inoculate ECMM medium with 50 mM β-alanine at 0.1 OD₆₀₀ and grown for 48 hours. Blue curve: OD₆₀₀ of the supplemented cultures. All cultures were grown in biological triplicates and pH adjusted. $T_D = 2,196$ h.

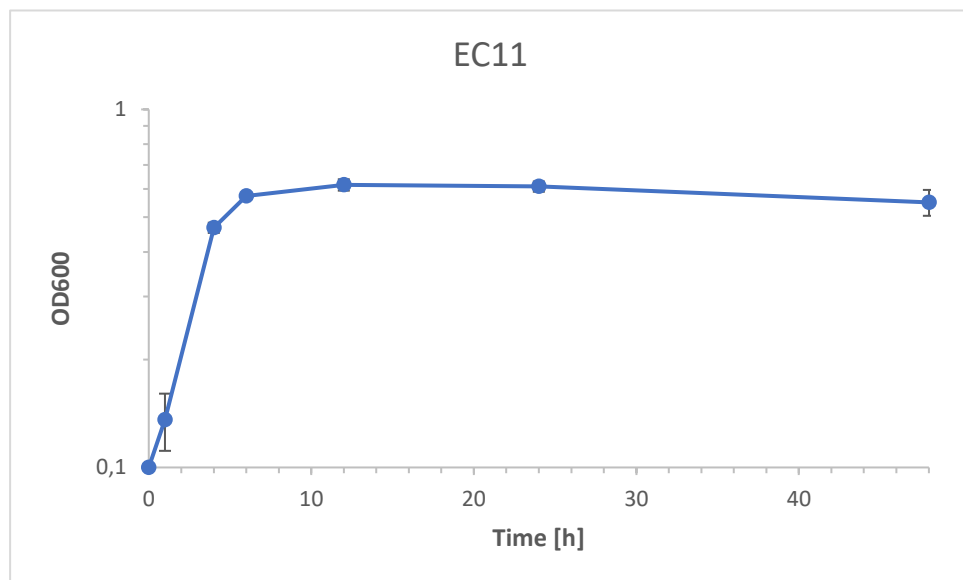


Figure A36 Growth curves of *E. coli* DH5α EC11 in ECMM medium with 50 mM β-alanine supplementation over 48 h. *E. coli* EC11 was used to inoculate ECMM medium with 50 mM β-alanine at 0.1 OD₆₀₀ and grown for 48 hours. Blue curve: OD₆₀₀ of the supplemented cultures. All cultures were grown in biological triplicates and pH adjusted. $T_D = 2,440$ h.

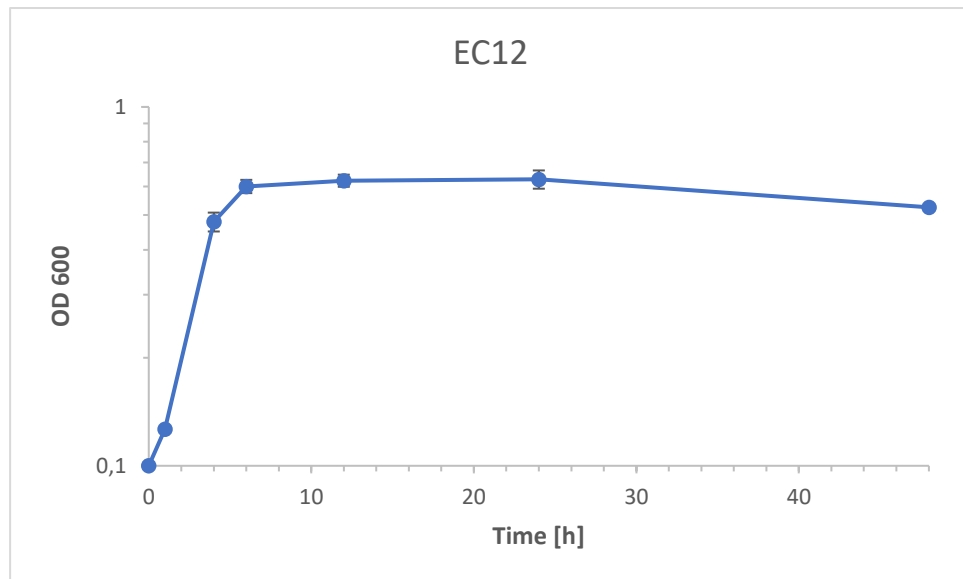


Figure A37 Growth curves of *E. coli* DH5α EC12 in ECMM medium with 50 mM β-alanine supplementation over 48 h. *E. coli* EC12 was used to inoculate ECMM medium with 50 mM β-alanine at 0.1 OD₆₀₀ and grown for 48 hours. Blue curve: OD₆₀₀ of the supplemented cultures. All cultures were grown in biological triplicates and pH adjusted. T_D = 2,319 h.

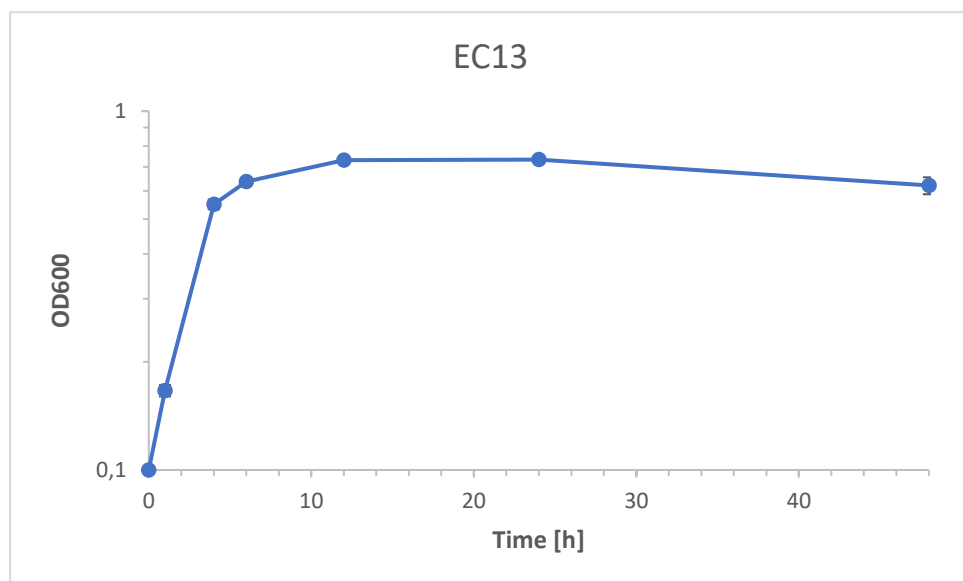


Figure A38 Growth curves of *E. coli* DH5α EC13 in ECMM medium with 50 mM β-alanine supplementation over 48 h. *E. coli* EC13 was used to inoculate ECMM medium with 50 mM β-alanine at 0.1 OD₆₀₀ and grown for 48 hours. Blue curve: OD₆₀₀ of the supplemented cultures. All cultures were grown in biological triplicates and pH adjusted. T_D = 2,246 h.

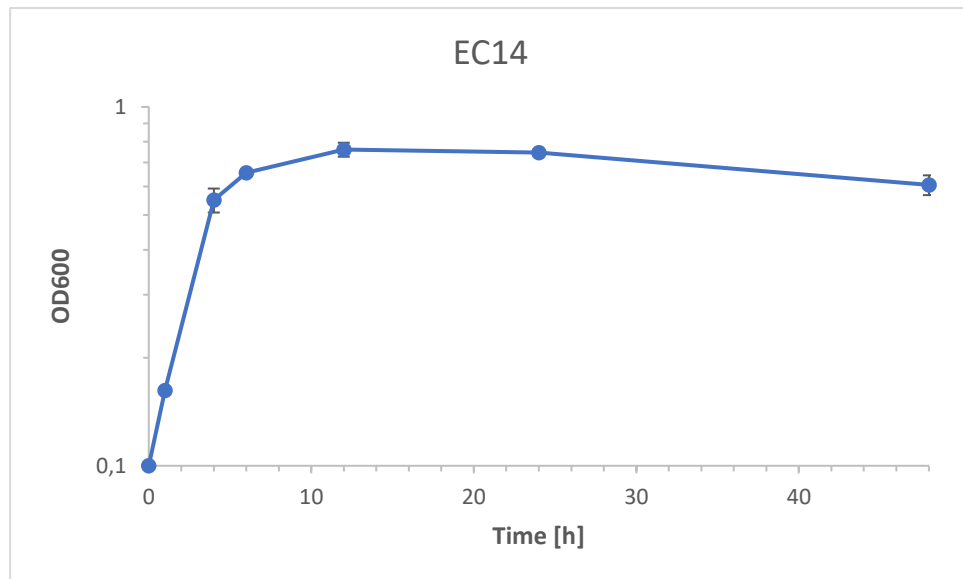


Figure A39 Growth curves of *E. coli* DH5α EC14 in ECMM medium with 50 mM β-alanine supplementation over 48 h. *E. coli* EC14 was used to inoculate ECMM medium with 50 mM β-alanine at 0.1 OD₆₀₀ and grown for 48 hours. Blue curve: OD₆₀₀ of the supplemented cultures. All cultures were grown in biological triplicates and pH adjusted. T_D = 2,211 h.

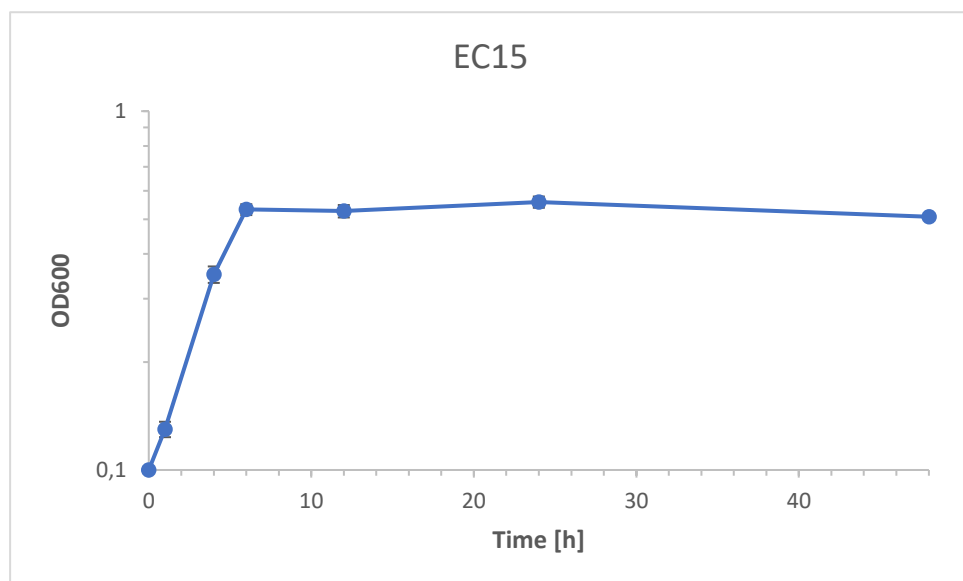


Figure A40 Growth curves of *E. coli* DH5α EC15 in ECMM medium with 50 mM β-alanine supplementation over 48 h. *E. coli* EC15 was used to inoculate ECMM medium with 50 mM β-alanine at 0.1 OD₆₀₀ and grown for 48 hours. Blue curve: OD₆₀₀ of the supplemented cultures. All cultures were grown in biological triplicates and pH adjusted. T_D = 2,488 h.

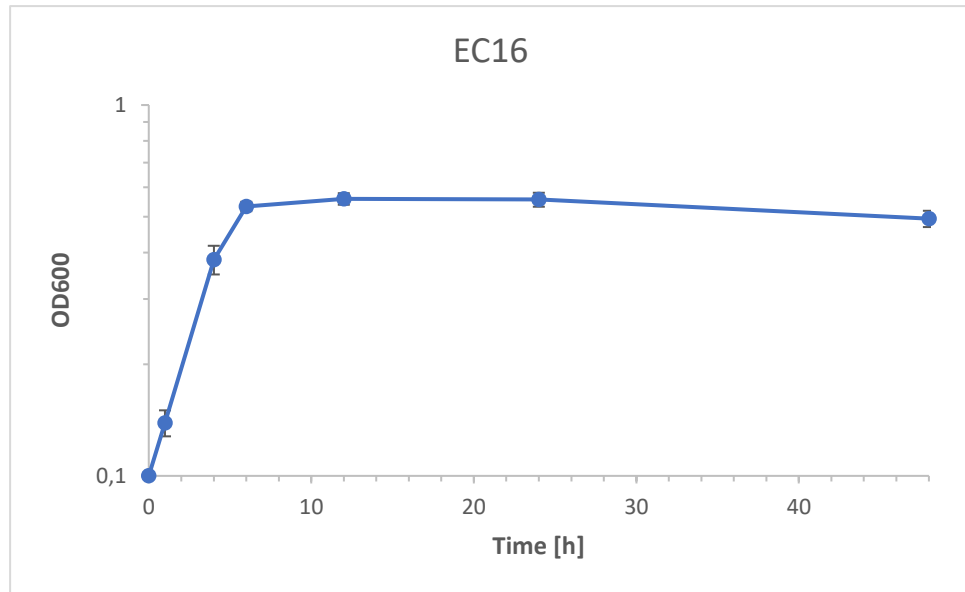


Figure A41 Growth curves of *E. coli* DH5α EC16 in ECMM medium with 50 mM β-alanine supplementation over 48 h. *E. coli* EC16 was used to inoculate ECMM medium with 50 mM β-alanine at 0.1 OD₆₀₀ and grown for 48 hours. Blue curve: OD₆₀₀ of the supplemented cultures. All cultures were grown in biological triplicates and pH adjusted. $T_D = 2486$ h.

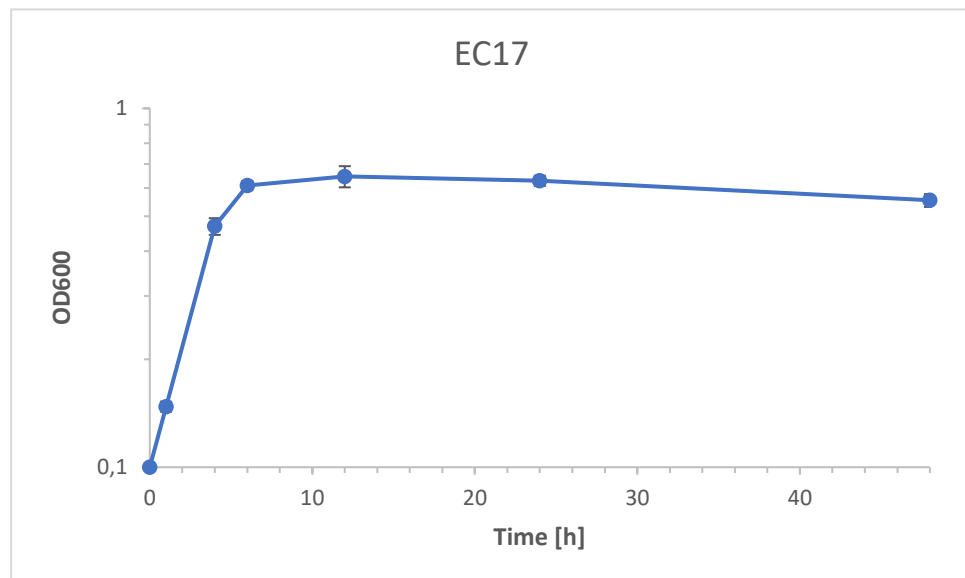


Figure A42 Growth curves of *E. coli* DH5α EC17 in ECMM medium with 50 mM β-alanine supplementation over 48 h. *E. coli* EC17 was used to inoculate ECMM medium with 50 mM β-alanine at 0.1 OD₆₀₀ and grown for 48 hours. Blue curve: OD₆₀₀ of the supplemented cultures. All cultures were grown in biological triplicates and pH adjusted. $T_D = 2,219$ h.

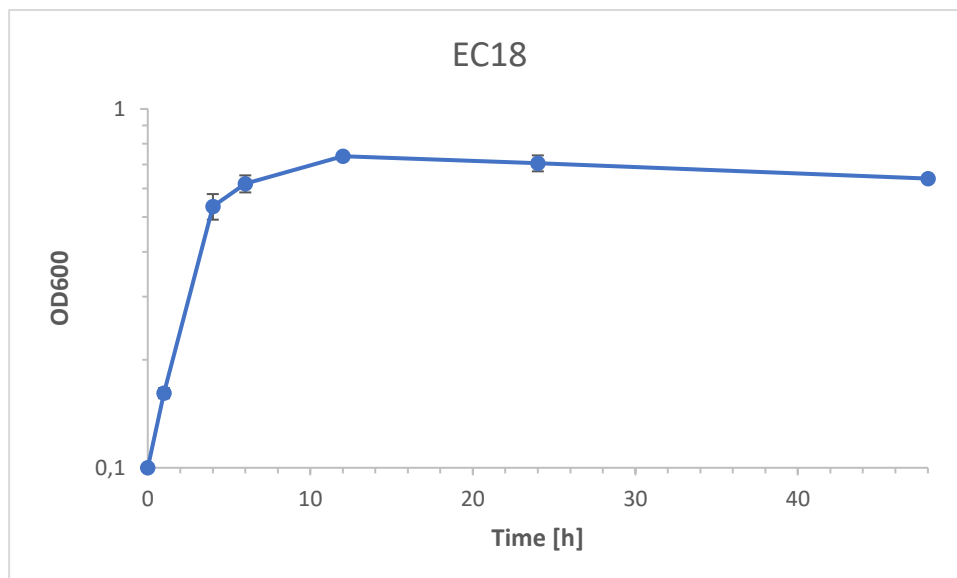


Figure A43 Growth curves of *E. coli* DH5α EC18 in ECMM medium with 50 mM β-alanine supplementation over 48 h. *E. coli* EC18 was used to inoculate ECMM medium with 50 mM β-alanine at 0.1 OD₆₀₀ and grown for 48 hours. Blue curve: OD₆₀₀ of the supplemented cultures. All cultures were grown in biological triplicates and pH adjusted. $T_D = 2,281$ h.

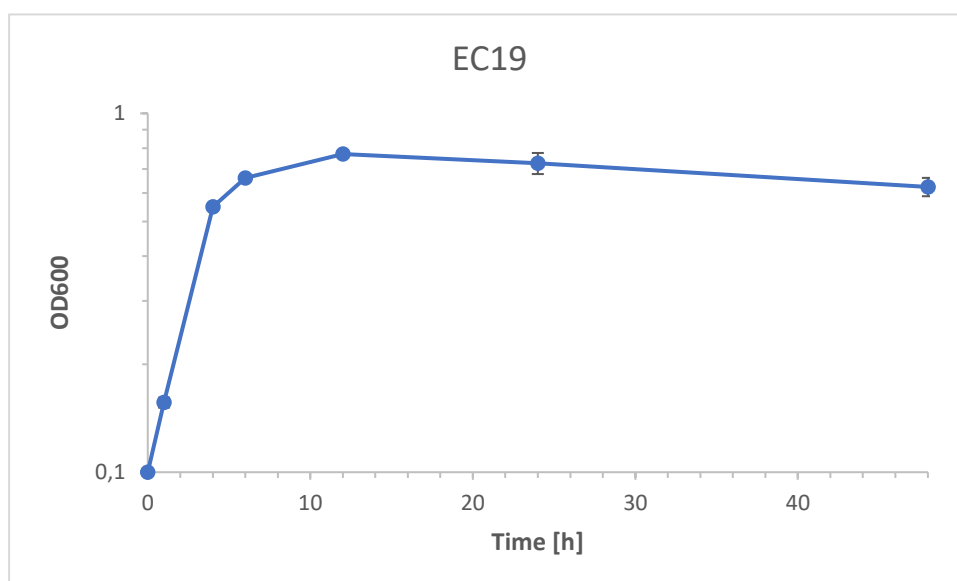


Figure A44 Growth curves of *E. coli* DH5α EC19 in ECMM medium with 50 mM β-alanine supplementation over 48 h. *E. coli* EC18 was used to inoculate ECMM medium with 50 mM β-alanine at 0.1 OD₆₀₀ and grown for 48 hours. Blue curve: OD₆₀₀ of the supplemented cultures. All cultures were grown in biological triplicates and pH adjusted. $T_D = 2,202$ h.

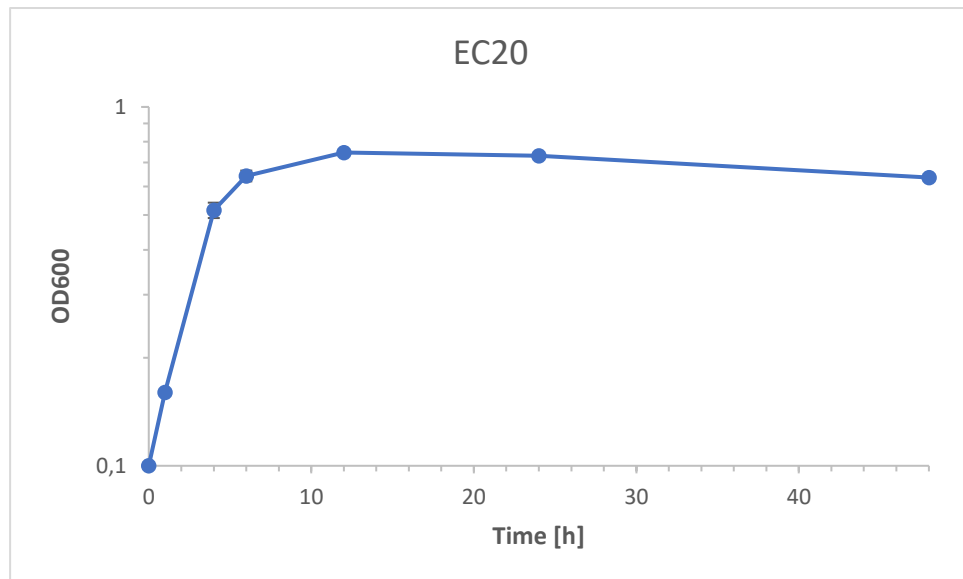


Figure A45 Growth curves of *E. coli* DH5α EC20 in ECMM medium with 50 mM β-alanine supplementation over 48 h. *E. coli* EC20 was used to inoculate ECMM medium with 50 mM β-alanine at 0.1 OD₆₀₀ and grown for 48 hours. Blue curve: OD₆₀₀ of the supplemented cultures. All cultures were grown in biological triplicates and pH adjusted. T_D = 2,236 h.

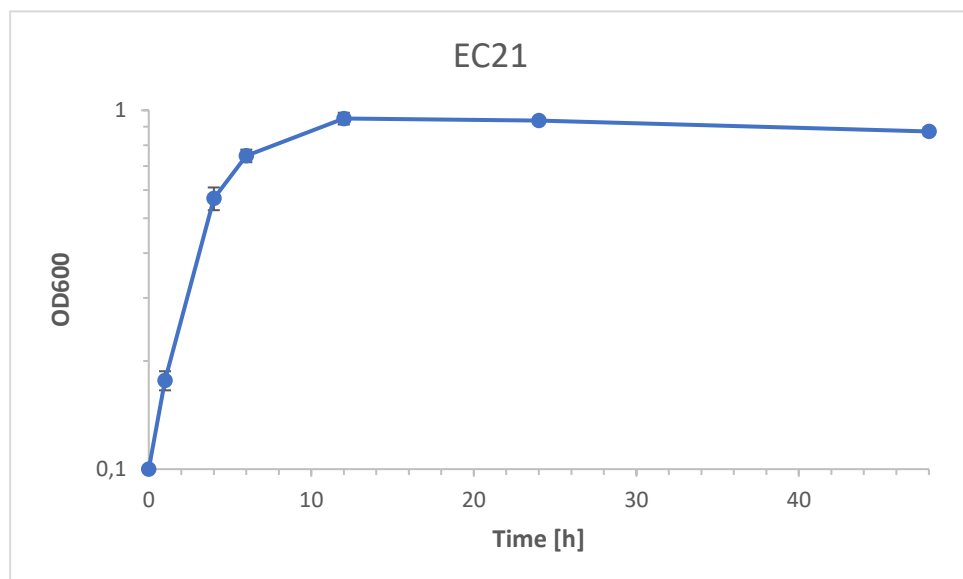


Figure A46 Growth curves of *E. coli* DH5α EC21 in ECMM medium with 50 mM β-alanine supplementation over 48 h. *E. coli* EC21 was used to inoculate ECMM medium with 50 mM β-alanine at 0.1 OD₆₀₀ and grown for 48 hours. Blue curve: OD₆₀₀ of the supplemented cultures. All cultures were grown in biological triplicates and pH adjusted. T_D = 2,068 h.

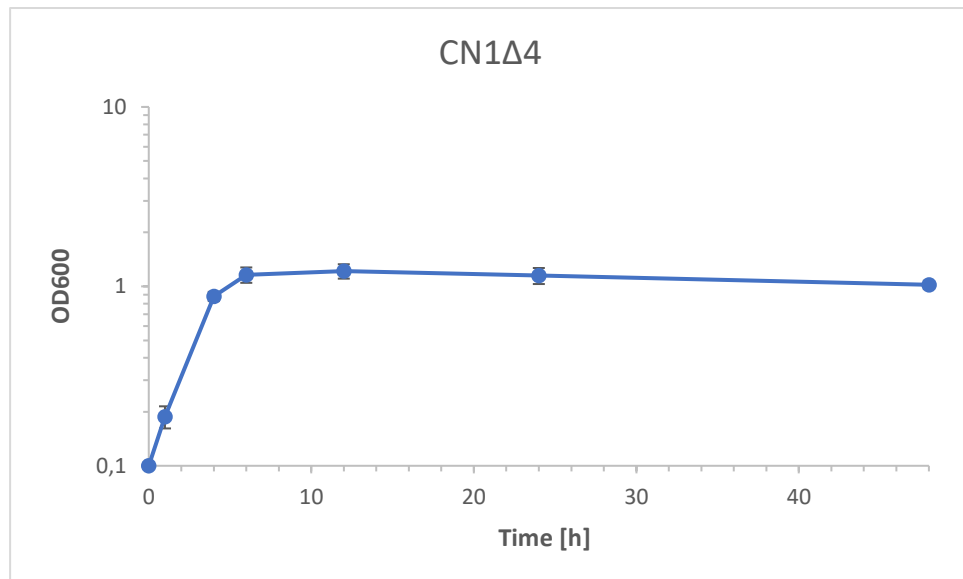


Figure A47 Growth curves of *C. necator* H16 CN1Δ4 in CNMM medium with 50 mM β-alanine supplementation over 48 h. CN1Δ4 was used to inoculate CNMM medium with 50 mM β-alanine at 0.1 OD₆₀₀ and grown for 48 hours. Blue curve: OD₆₀₀ of the supplemented cultures. All cultures were grown in biological triplicates and pH adjusted. T_D = 1,696 h.

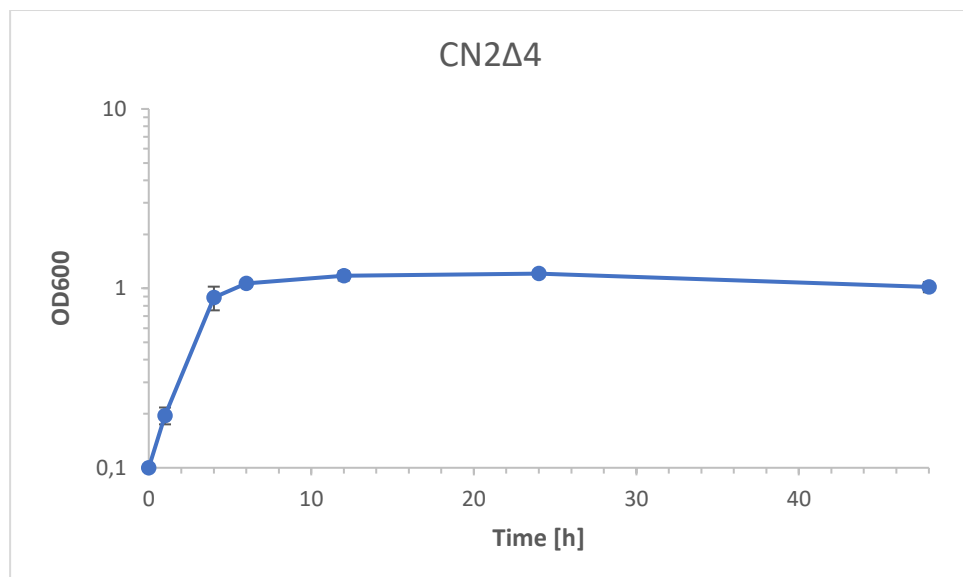


Figure A48 Growth curves of *C. necator* H16 CN2Δ4 in CNMM medium with 50 mM β-alanine supplementation over 48 h. CN2Δ4 was used to inoculate CNMM medium with 50 mM β-alanine at 0.1 OD₆₀₀ and grown for 48 hours. Blue curve: OD₆₀₀ of the supplemented cultures. All cultures were grown in biological triplicates and pH adjusted. T_D = 1,756 h.

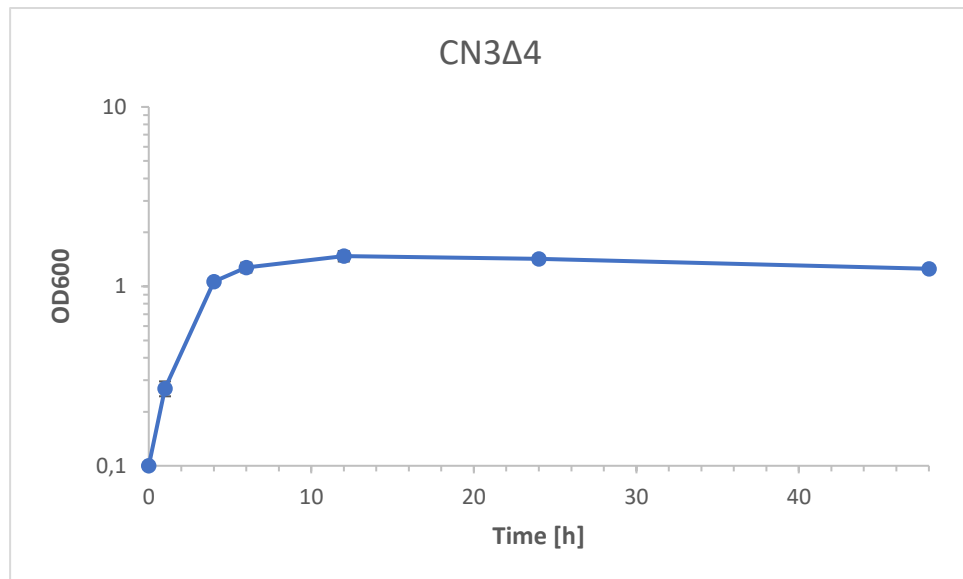


Figure A49 Growth curves of *C. necator* H16 CN3Δ4 in CNMM medium with 50 mM β-alanine supplementation over 48 h. CN3Δ4 was used to inoculate CNMM medium with 50 mM β-alanine at 0.1 OD₆₀₀ and grown for 48 hours. Blue curve: OD₆₀₀ of the supplemented cultures. All cultures were grown in biological triplicates and pH adjusted. T_D = 1,633 h.

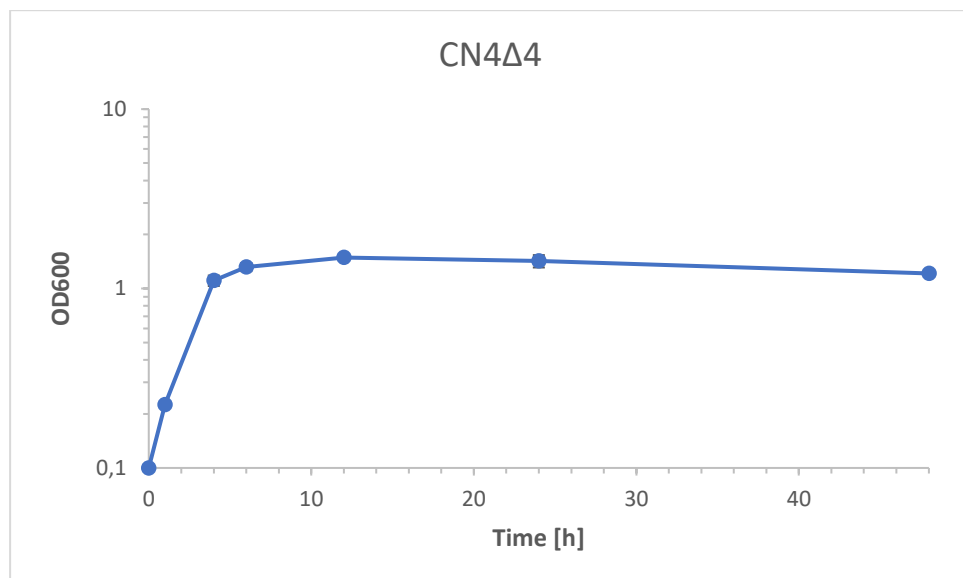


Figure A50 Growth curves of *C. necator* H16 CN4Δ4 in CNMM medium with 50 mM β-alanine supplementation over 48 h. CN4Δ4 was used to inoculate CNMM medium with 50 mM β-alanine at 0.1 OD₆₀₀ and grown for 48 hours. Blue curve: OD₆₀₀ of the supplemented cultures. All cultures were grown in biological triplicates and pH adjusted. T_D = 1,612 h.

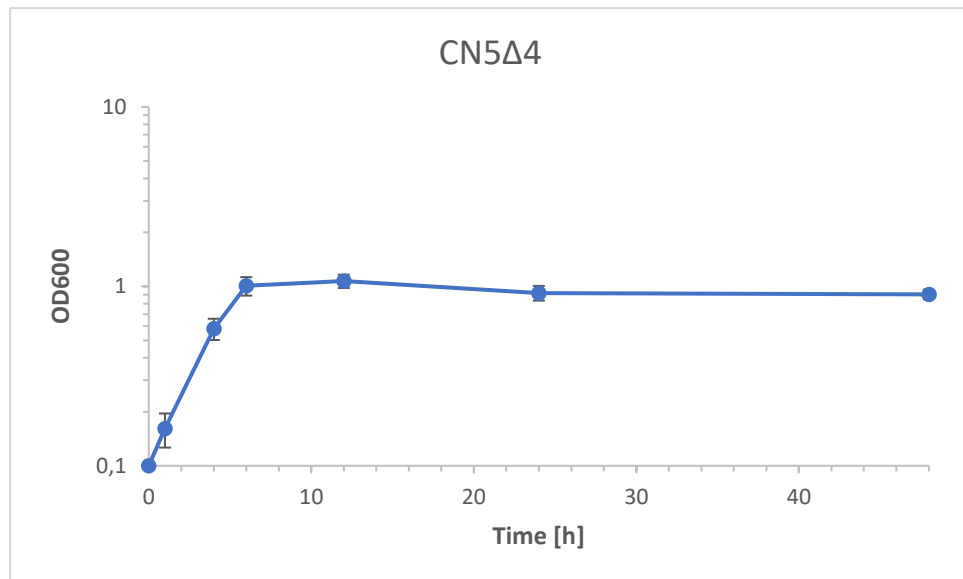


Figure A51 Growth curves of *C. necator* H16 CN5Δ4 in CNMM medium with 50 mM β-alanine supplementation over 48 h. CN5Δ4 was used to inoculate CNMM medium with 50 mM β-alanine at 0.1 OD₆₀₀ and grown for 48 hours. Blue curve: OD₆₀₀ of the supplemented cultures. All cultures were grown in biological triplicates and pH adjusted. T_D =1,800 h.

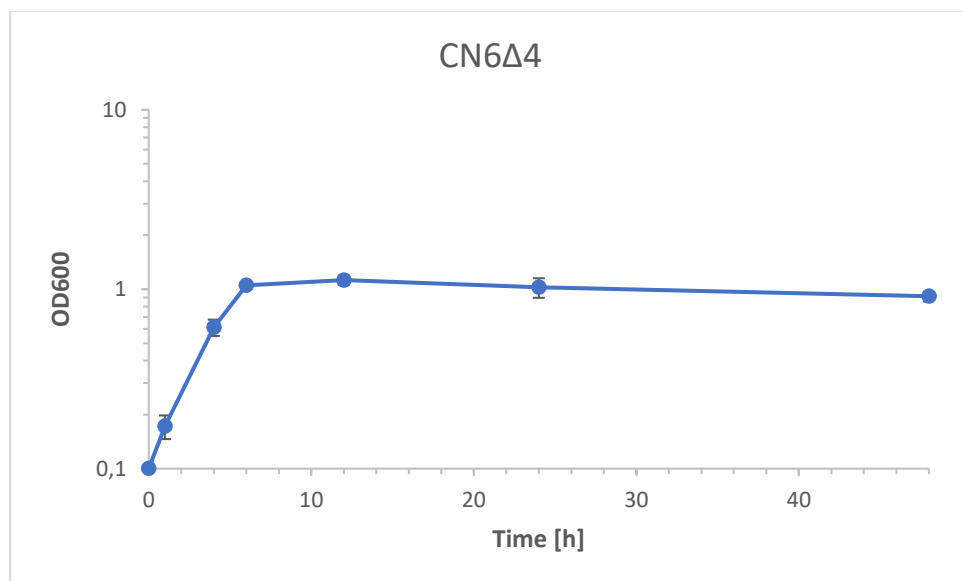


Figure A52 Growth curves of *C. necator* H16 CN6Δ4 in CNMM medium with 50 mM β-alanine supplementation over 48 h. CN6Δ4 was used to inoculate CNMM medium with 50 mM β-alanine at 0.1 OD₆₀₀ and grown for 48 hours. Blue curve: OD₆₀₀ of the supplemented cultures. All cultures were grown in biological triplicates and pH adjusted. T_D =1,760 h.

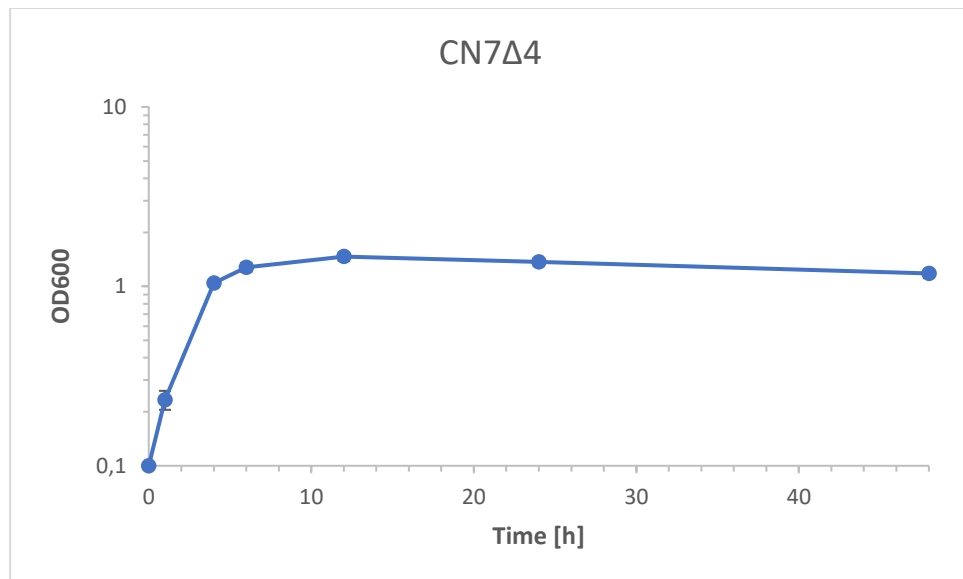


Figure A53 Growth curves of *C. necator* H16 CN7Δ4 in CNMM medium with 50 mM β-alanine supplementation over 48 h. CN7Δ4 was used to inoculate CNMM medium with 50 mM β-alanine at 0.1 OD₆₀₀ and grown for 48 hours. Blue curve: OD₆₀₀ of the supplemented cultures. All cultures were grown in biological triplicates and pH adjusted. $T_D = 1,632$ h.

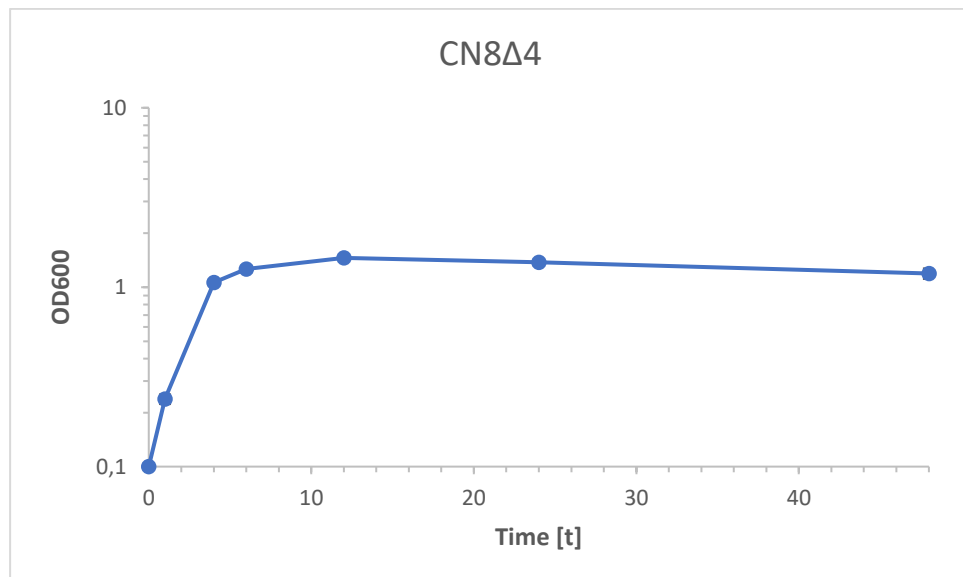


Figure A54 Growth curves of *C. necator* H16 CN8Δ4 in CNMM medium with 50 mM β-alanine supplementation over 48 h. CN8Δ4 was used to inoculate CNMM medium with 50 mM β-alanine at 0.1 OD₆₀₀ and grown for 48 hours. Blue curve: OD₆₀₀ of the supplemented cultures. All cultures were grown in biological triplicates and pH adjusted. $T_D = 1,639$ h.

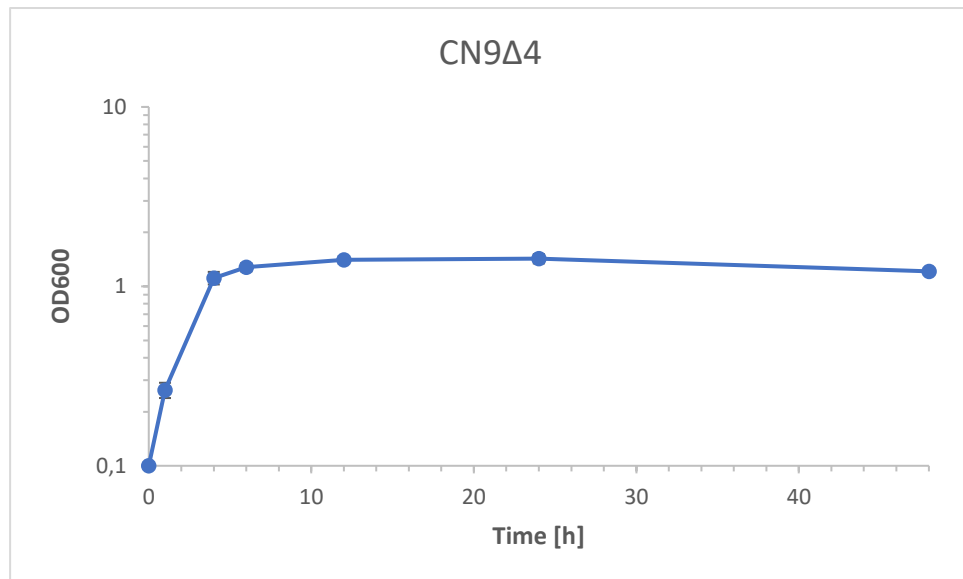


Figure A55 Growth curves of *C. necator* H16 CN9Δ4 in CNMM medium with 50 mM β-alanine supplementation over 48 h. CN9Δ4 was used to inoculate CNMM medium with 50 mM β-alanine at 0.1 OD₆₀₀ and grown for 48 hours. Blue curve: OD₆₀₀ of the supplemented cultures. All cultures were grown in biological triplicates and pH adjusted. $T_D = 1,632$ h.

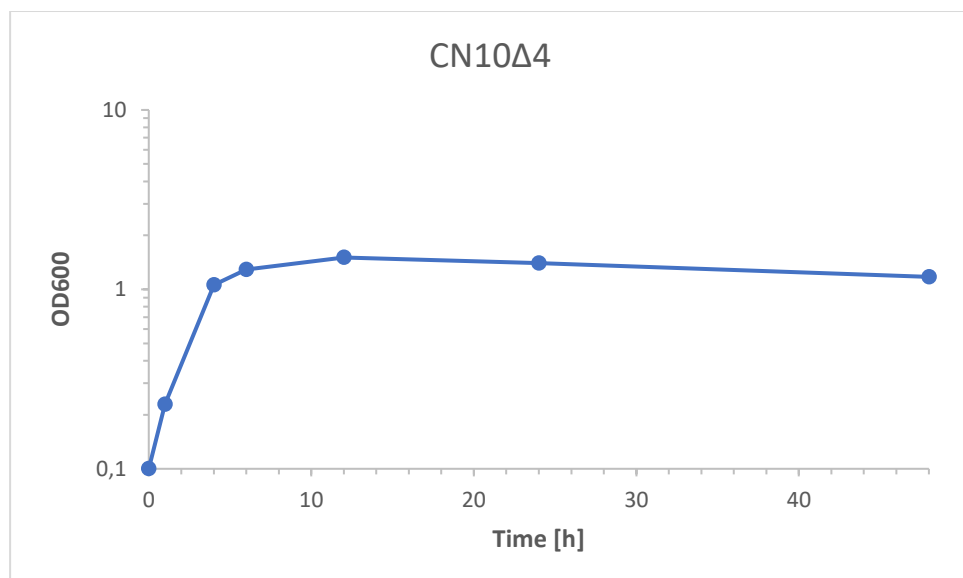


Figure A56 Growth curves of *C. necator* H16 CN10Δ4 in CNMM medium with 50 mM β-alanine supplementation over 48 h. CN10Δ4 was used to inoculate CNMM medium with 50 mM β-alanine at 0.1 OD₆₀₀ and grown for 48 hours. Blue curve: OD₆₀₀ of the supplemented cultures. All cultures were grown in biological triplicates and pH adjusted. $T_D = 1,626$ h.

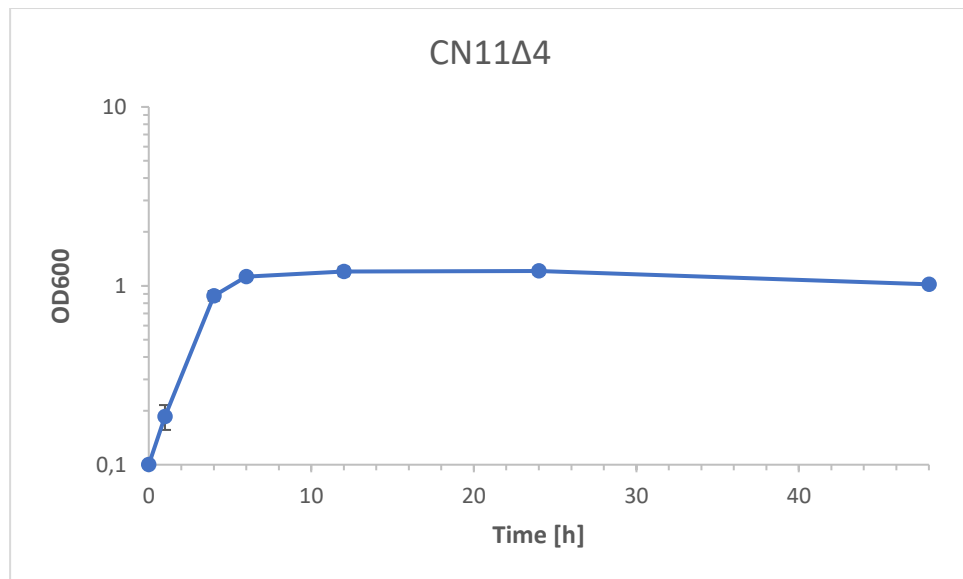


Figure A57 Growth curves of *C. necator* H16 CN11Δ4 in CNMM medium with 50 mM β-alanine supplementation over 48 h. CN11Δ4 was used to inoculate CNMM medium with 50 mM β-alanine at 0.1 OD₆₀₀ and grown for 48 hours. Blue curve: OD₆₀₀ of the supplemented cultures. All cultures were grown in biological triplicates and pH adjusted. T_D = 1,172 h.

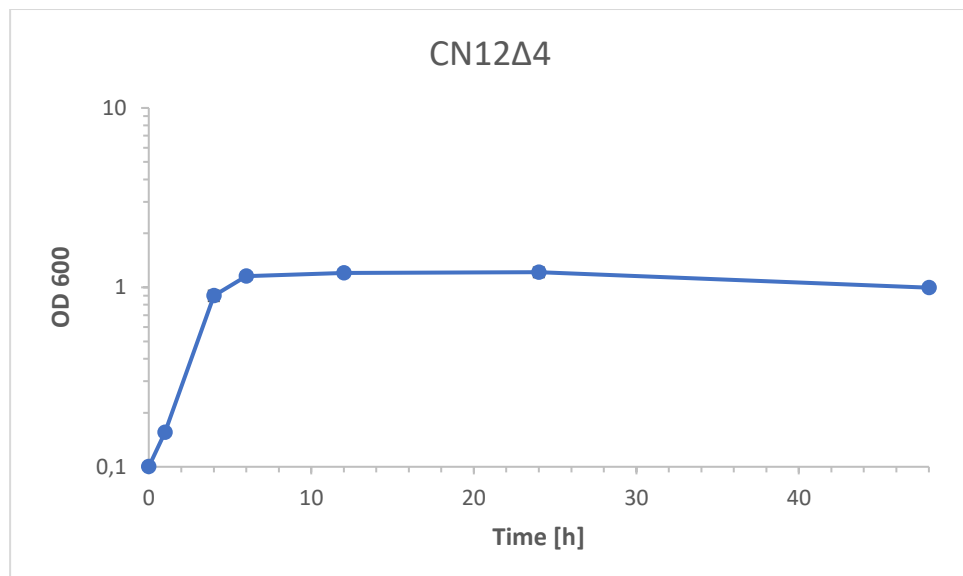


Figure A58 Growth curves of *C. necator* H16 CN12Δ4 in CNMM medium with 50 mM β-alanine supplementation over 48 h. CN12Δ4 was used to inoculate CNMM medium with 50 mM β-alanine at 0.1 OD₆₀₀ and grown for 48 hours. Blue curve: OD₆₀₀ of the supplemented cultures. All cultures were grown in biological triplicates and pH adjusted. T_D = 1,699 h.

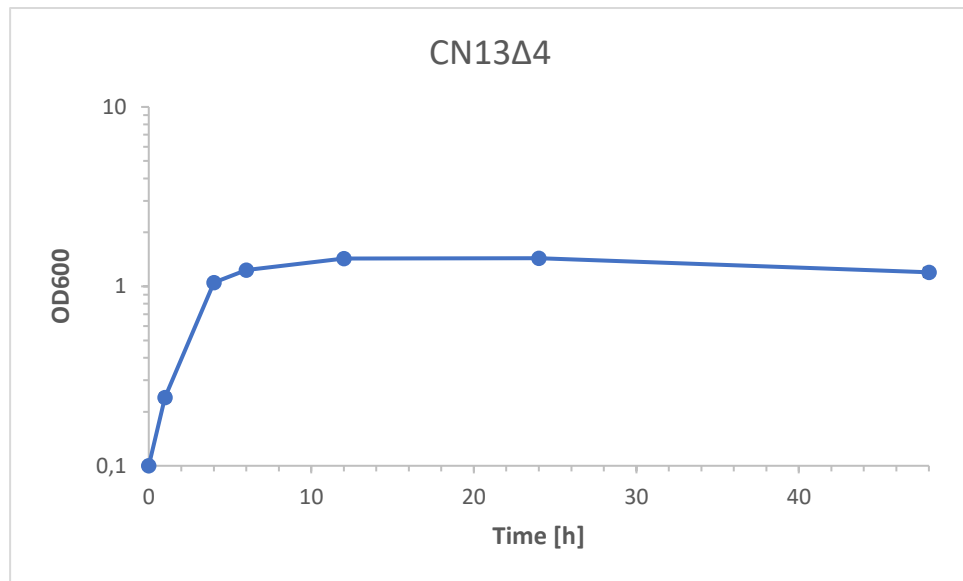


Figure A59 Growth curves of *C. necator* H16 CN13Δ4 in CNMM medium with 50 mM β-alanine supplementation over 48 h. CN13Δ4 was used to inoculate CNMM medium with 50 mM β-alanine at 0.1 OD₆₀₀ and grown for 48 hours. Blue curve: OD₆₀₀ of the supplemented cultures. All cultures were grown in biological triplicates and pH adjusted. T_D = 1,656 h.

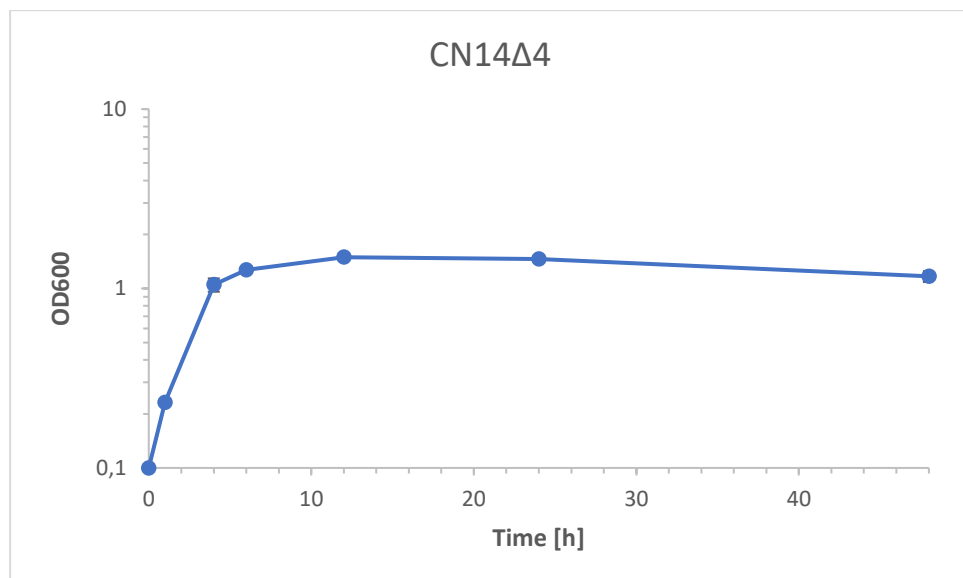


Figure A60 Growth curves of *C. necator* H16 CN14Δ4 in CNMM medium with 50 mM β-alanine supplementation over 48 h. CN14Δ4 was used to inoculate CNMM medium with 50 mM β-alanine at 0.1 OD₆₀₀ and grown for 48 hours. Blue curve: OD₆₀₀ of the supplemented cultures. All cultures were grown in biological triplicates and pH adjusted. T_D = 1,635 h.

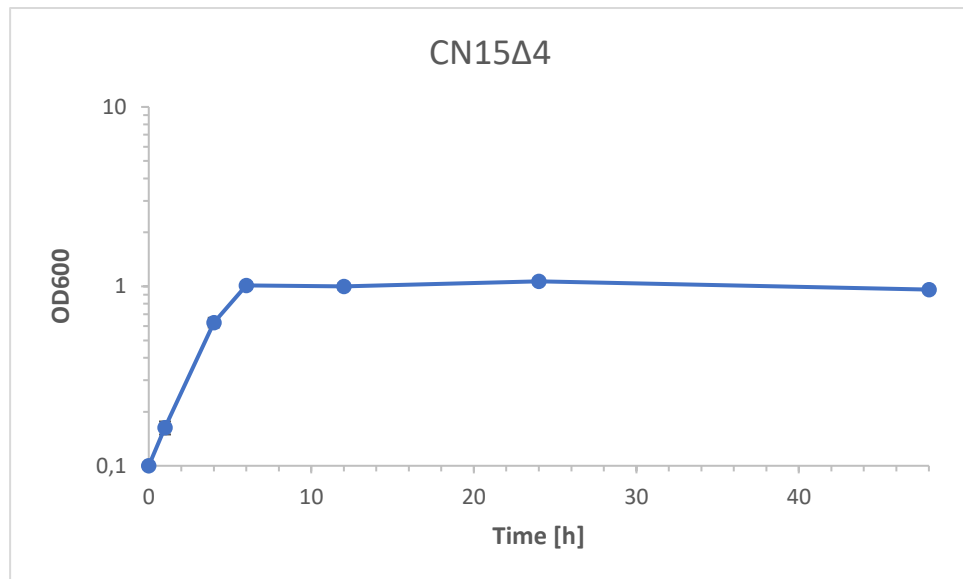


Figure A61 Growth curves of *C. necator* H16 CN15Δ4 in CNMM medium with 50 mM β-alanine supplementation over 48 h. CN15Δ4 was used to inoculate CNMM medium with 50 mM β-alanine at 0.1 OD₆₀₀ and grown for 48 hours. Blue curve: OD₆₀₀ of the supplemented cultures. All cultures were grown in biological triplicates and pH adjusted. T_D=1,797 h.

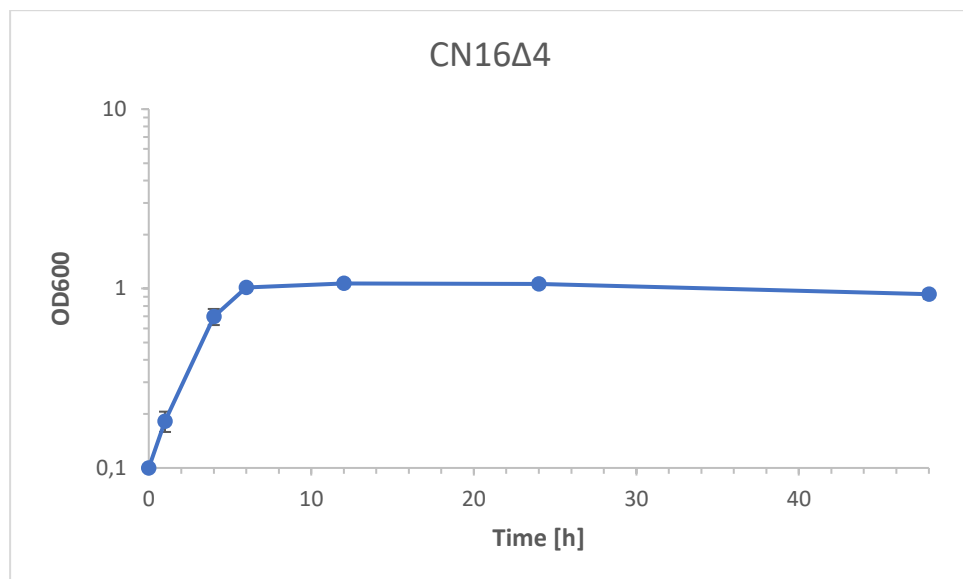


Figure A62 Growth curves of *C. necator* H16 CN16Δ4 in CNMM medium with 50 mM β-alanine supplementation over 48 h. CN16Δ4 was used to inoculate CNMM medium with 50 mM β-alanine at 0.1 OD₆₀₀ and grown for 48 hours. Blue curve: OD₆₀₀ of the supplemented cultures. All cultures were grown in biological triplicates and pH adjusted. T_D=1,796 h.

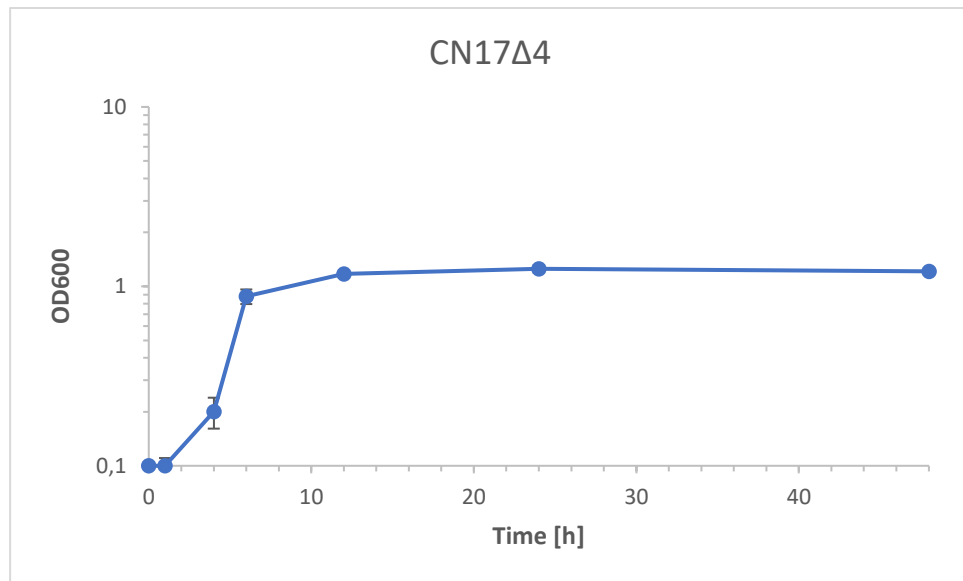


Figure A63 Growth curves of *C. necator* H16 CN17Δ4 in CNMM medium with 50 mM β-alanine supplementation over 48 h. CN17Δ4 was used to inoculate CNMM medium with 50 mM β-alanine at 0.1 OD₆₀₀ and grown for 48 hours. Blue curve: OD₆₀₀ of the supplemented cultures. All cultures were grown in biological triplicates and pH adjusted. $T_D = 1,687$ h.

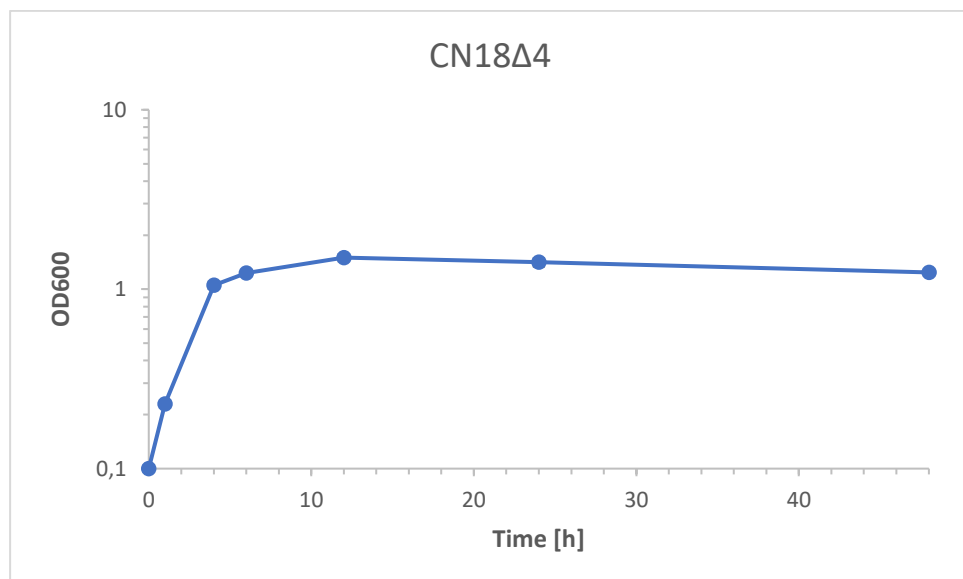


Figure A64 Growth curves of *C. necator* H16 CN18Δ4 in CNMM medium with 50 mM β-alanine supplementation over 48 h. CN18Δ4 was used to inoculate CNMM medium with 50 mM β-alanine at 0.1 OD₆₀₀ and grown for 48 hours. Blue curve: OD₆₀₀ of the supplemented cultures. All cultures were grown in biological triplicates and pH adjusted. $T_D = 1,656$ h

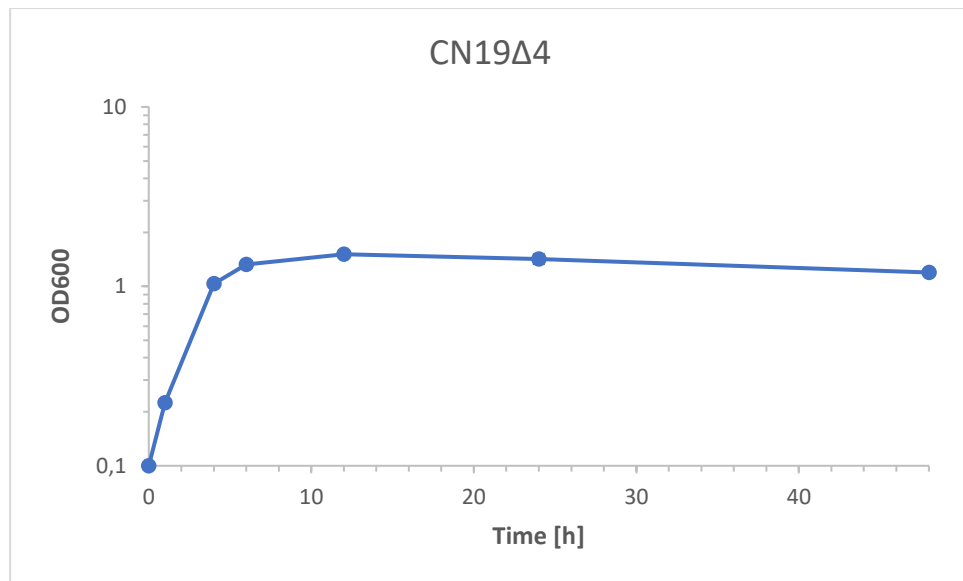


Figure A65 Growth curves of *C. necator* H16 CN19Δ4 in CNMM medium with 50 mM β-alanine supplementation over 48 h. CN19Δ4 was used to inoculate CNMM medium with 50 mM β-alanine at 0.1 OD₆₀₀ and grown for 48 hours. Blue curve: OD₆₀₀ of the supplemented cultures. All cultures were grown in biological triplicates and pH adjusted. $T_D = 1,610$ h

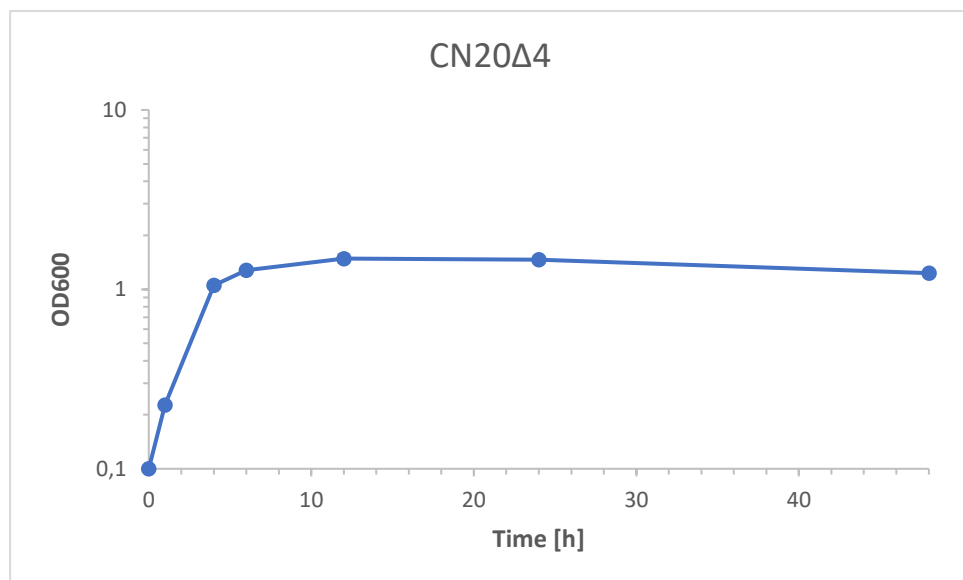


Figure A66 Growth curves of *C. necator* H16 CN20Δ4 in CNMM medium with 50 mM β-alanine supplementation over 48 h. CN20Δ4 was used to inoculate CNMM medium with 50 mM β-alanine at 0.1 OD₆₀₀ and grown for 48 hours. Blue curve: OD₆₀₀ of the supplemented cultures. All cultures were grown in biological triplicates and pH adjusted. $T_D = 1,632$ h

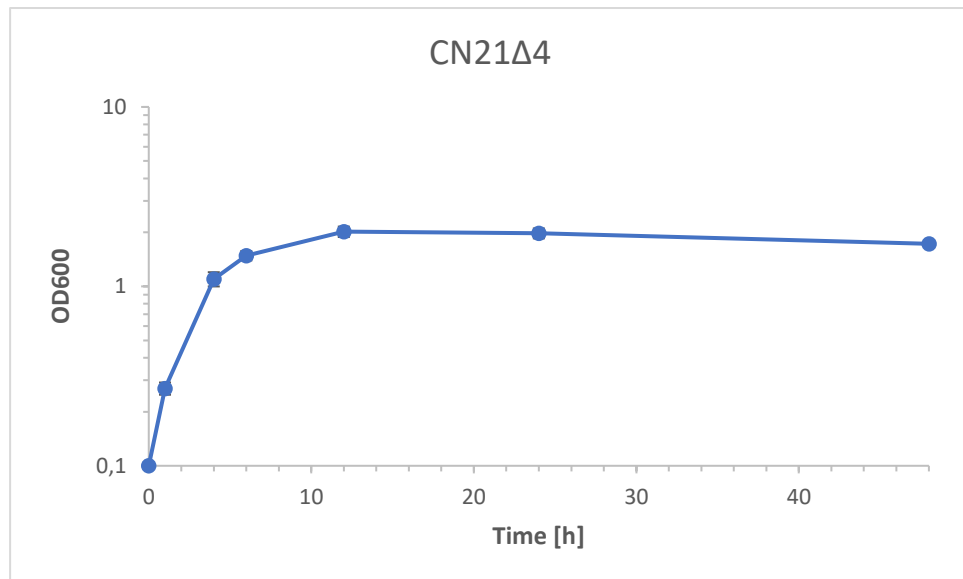


Figure A67 Growth curves of *C. necator* H16 CN21Δ4 in CNMM medium with 50 mM β-alanine supplementation over 48 h. CN21Δ4 was used to inoculate CNMM medium with 50 mM β-alanine at 0.1 OD₆₀₀ and grown for 48 hours. Blue curve: OD₆₀₀ of the supplemented cultures. All cultures were grown in biological triplicates and pH adjusted. $T_D = 1,542$ h

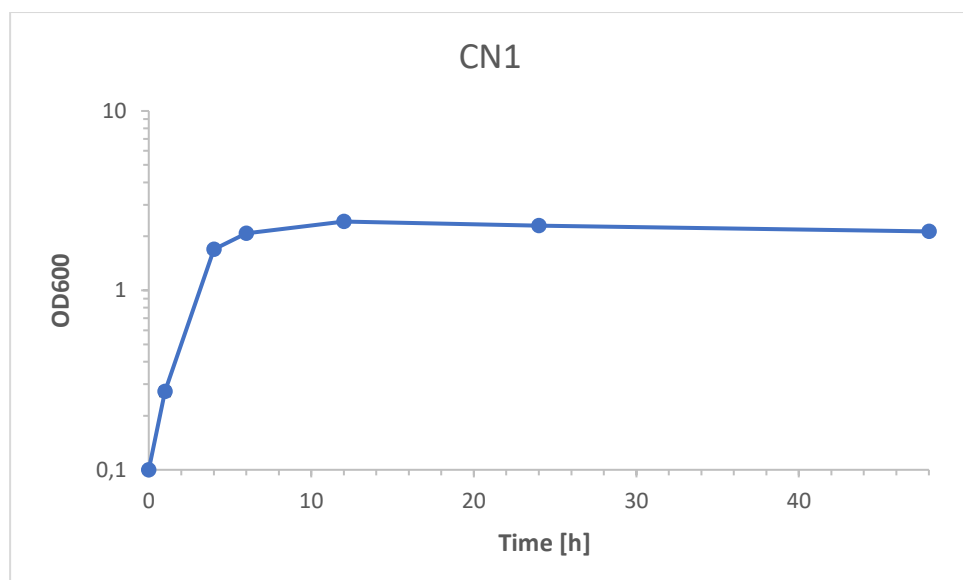


Figure A68 Growth curves of *C. necator* H16 CN1 in CNMM medium with 50 mM β-alanine supplementation over 48 h. CN1 was used to inoculate CNMM medium with 50 mM β-alanine at 0.1 OD₆₀₀ and grown for 48 hours. Blue curve: OD₆₀₀ of the supplemented cultures. All cultures were grown in biological triplicates and pH adjusted. $T_D = 1,374$ h

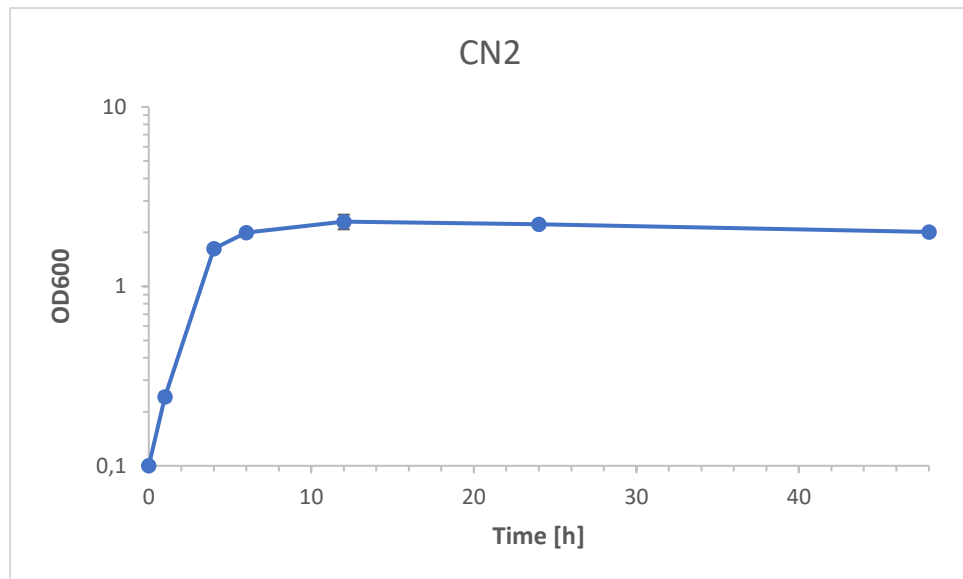


Figure A69 Growth curves of *C. necator* H16 CN2 in CNMM medium with 50 mM β -alanine supplementation over 48 h. CN2 was used to inoculate CNMM medium with 50 mM β -alanine at 0.1 OD₆₀₀ and grown for 48 hours. Blue curve: OD₆₀₀ of the supplemented cultures. All cultures were grown in biological triplicates and pH adjusted. $T_D = 1,366$ h

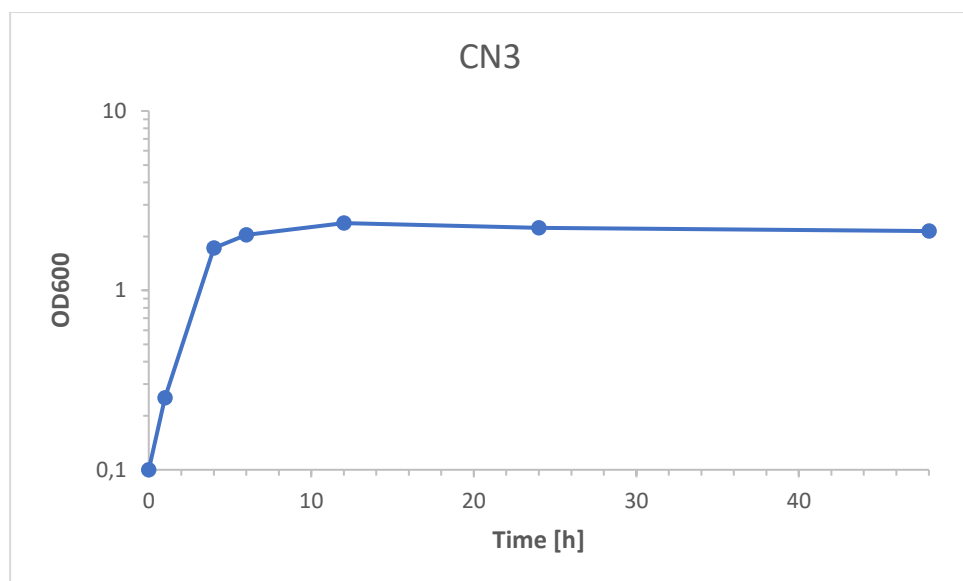


Figure A70 Growth curves of *C. necator* H16 CN3 in CNMM medium with 50 mM β -alanine supplementation over 48 h. CN3 was used to inoculate CNMM medium with 50 mM β -alanine at 0.1 OD₆₀₀ and grown for 48 hours. Blue curve: OD₆₀₀ of the supplemented cultures. All cultures were grown in biological triplicates and pH adjusted. $T_D = 1,374$ h

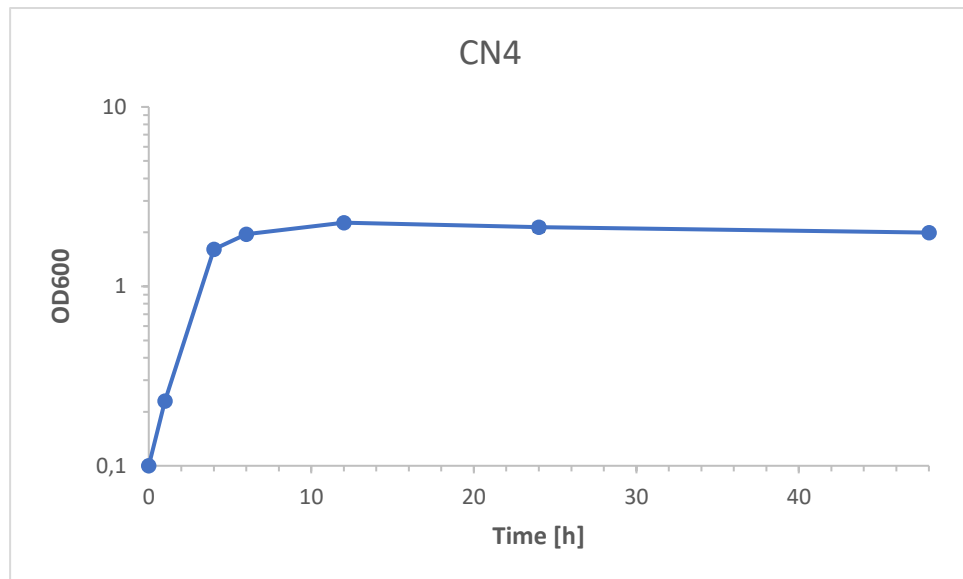


Figure A71 Growth curves of *C. necator* H16 CN4 in CNMM medium with 50 mM β -alanine supplementation over 48 h. CN4 was used to inoculate CNMM medium with 50 mM β -alanine at 0.1 OD₆₀₀ and grown for 48 hours. Blue curve: OD₆₀₀ of the supplemented cultures. All cultures were grown in biological triplicates and pH adjusted. $T_D = 1,346$ h

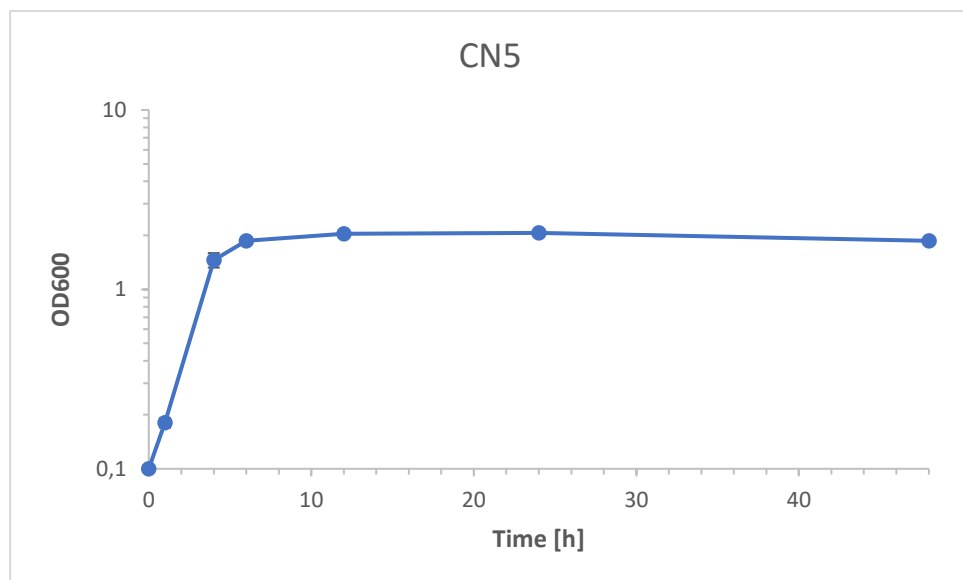


Figure A72 Growth curves of *C. necator* H16 CN5 in CNMM medium with 50 mM β -alanine supplementation over 48 h. CN5 was used to inoculate CNMM medium with 50 mM β -alanine at 0.1 OD₆₀₀ and grown for 48 hours. Blue curve: OD₆₀₀ of the supplemented cultures. All cultures were grown in biological triplicates and pH adjusted. $T_D = 1,421$ h

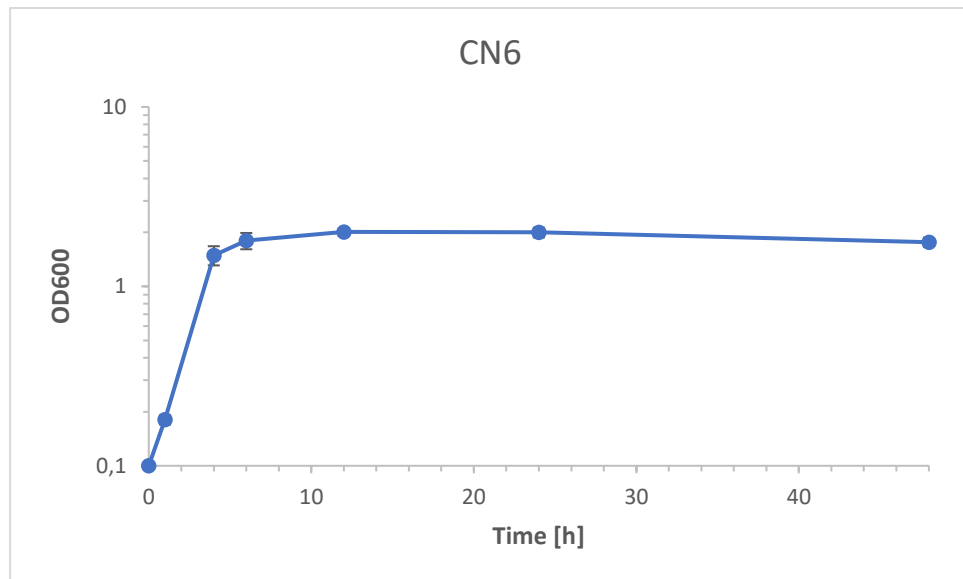


Figure A73 Growth curves of *C. necator* H16 CN6 in CNMM medium with 50 mM β -alanine supplementation over 48 h. CN6 was used to inoculate CNMM medium with 50 mM β -alanine at 0.1 OD₆₀₀ and grown for 48 hours. Blue curve: OD₆₀₀ of the supplemented cultures. All cultures were grown in biological triplicates and pH adjusted. $T_D = 1,440$ h

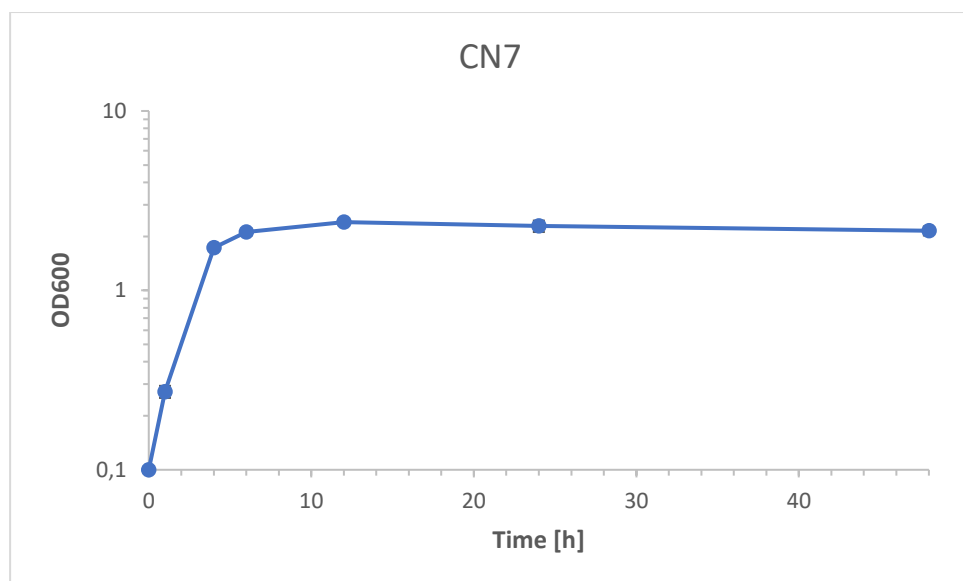


Figure A74 Growth curves of *C. necator* H16 CN7 in CNMM medium with 50 mM β -alanine supplementation over 48 h. CN7 was used to inoculate CNMM medium with 50 mM β -alanine at 0.1 OD₆₀₀ and grown for 48 hours. Blue curve: OD₆₀₀ of the supplemented cultures. All cultures were grown in biological triplicates and pH adjusted. $T_D = 1,362$ h

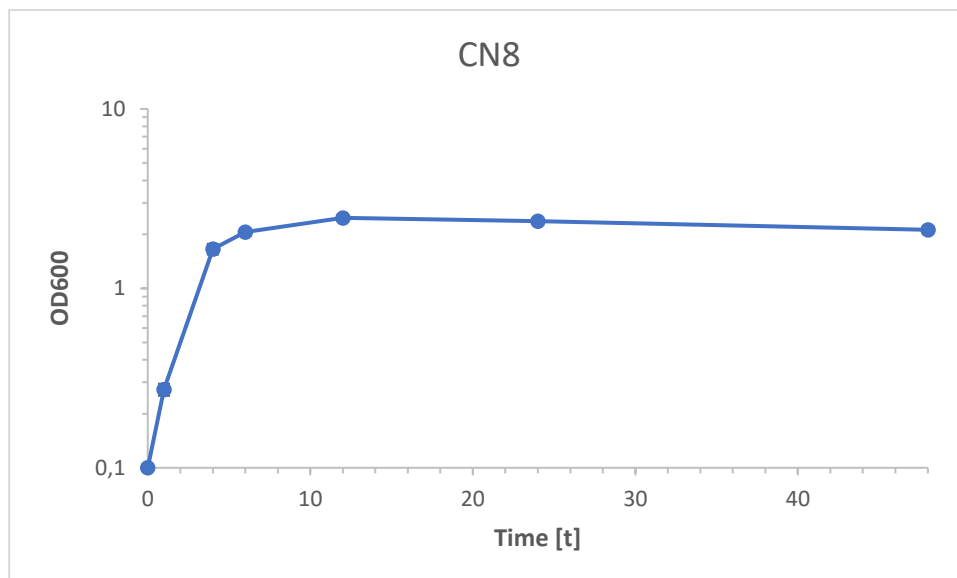


Figure A75 Growth curves of *C. necator* H16 CN8 in CNMM medium with 50 mM β -alanine supplementation over 48 h. CN8 was used to inoculate CNMM medium with 50 mM β -alanine at 0.1 OD₆₀₀ and grown for 48 hours. Blue curve: OD₆₀₀ of the supplemented cultures. All cultures were grown in biological triplicates and pH adjusted. $T_D = 1,375$ h

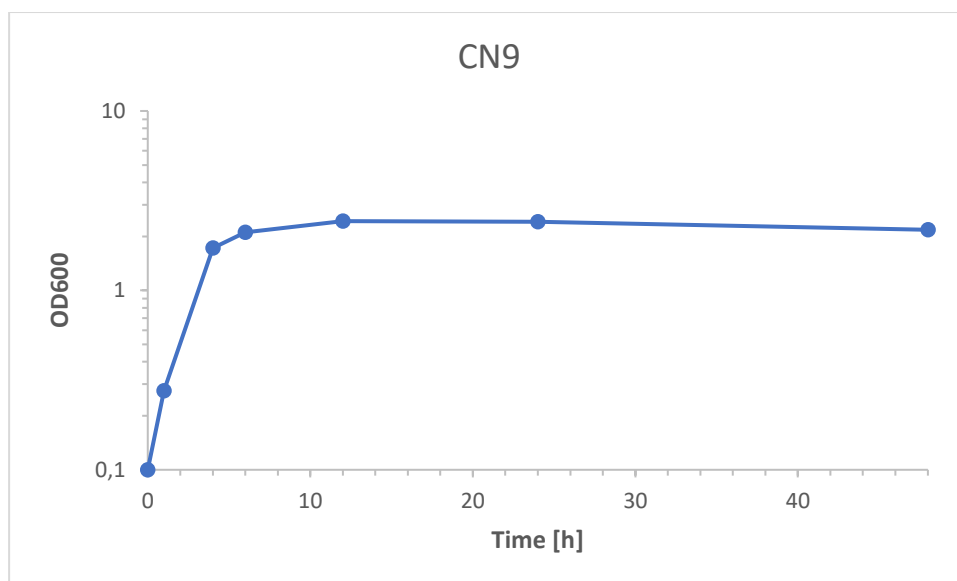


Figure A76 Growth curves of *C. necator* H16 CN9 in CNMM medium with 50 mM β -alanine supplementation over 48 h. CN9 was used to inoculate CNMM medium with 50 mM β -alanine at 0.1 OD₆₀₀ and grown for 48 hours. Blue curve: OD₆₀₀ of the supplemented cultures. All cultures were grown in biological triplicates and pH adjusted. $T_D = 1,365$ h

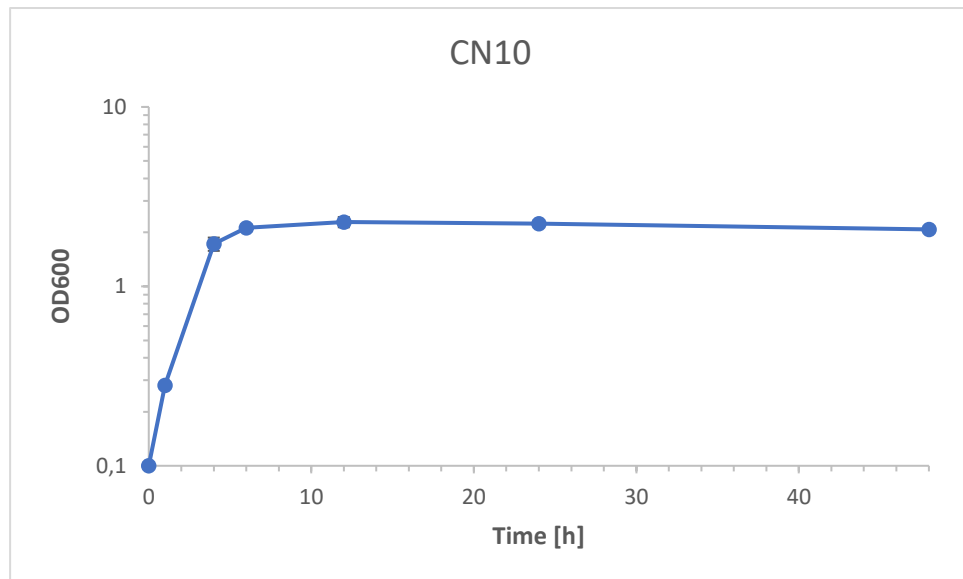


Figure A77 Growth curves of *C. necator* H16 CN10 in CNMM medium with 50 mM β -alanine supplementation over 48 h. CN10 was used to inoculate CNMM medium with 50 mM β -alanine at 0.1 OD₆₀₀ and grown for 48 hours. Blue curve: OD₆₀₀ of the supplemented cultures. All cultures were grown in biological triplicates and pH adjusted. $T_D = 1,362$ h

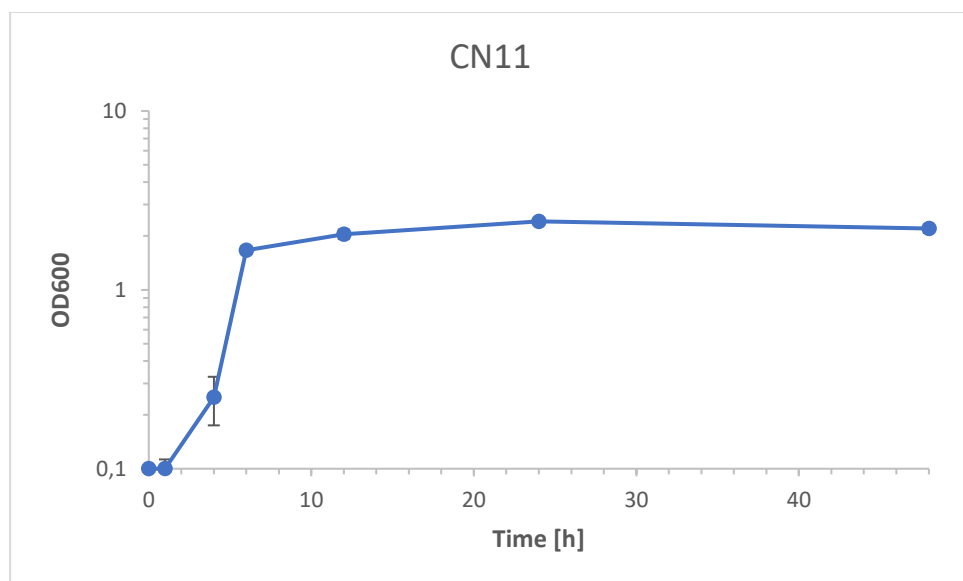


Figure A78 Growth curves of *C. necator* H16 CN11 in CNMM medium with 50 mM β -alanine supplementation over 48 h. CN11 was used to inoculate CNMM medium with 50 mM β -alanine at 0.1 OD₆₀₀ and grown for 48 hours. Blue curve: OD₆₀₀ of the supplemented cultures. All cultures were grown in biological triplicates and pH adjusted. $T_D = 1,377$ h

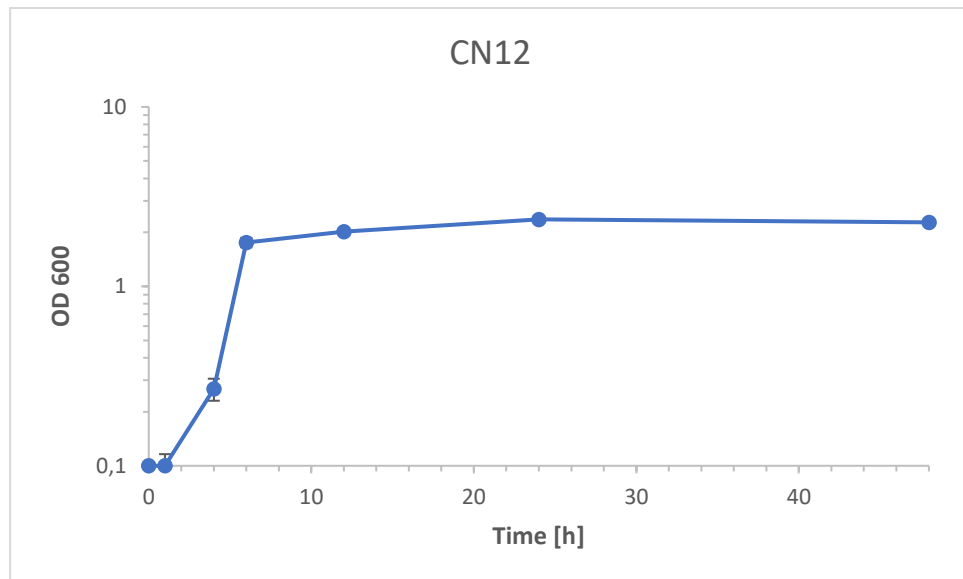


Figure A79 Growth curves of *C. necator* H16 CN12 in CNMM medium with 50 mM β -alanine supplementation over 48 h. CN12 was used to inoculate CNMM medium with 50 mM β -alanine at 0.1 OD₆₀₀ and grown for 48 hours. Blue curve: OD₆₀₀ of the supplemented cultures. All cultures were grown in biological triplicates and pH adjusted. $T_D = 1,383$ h

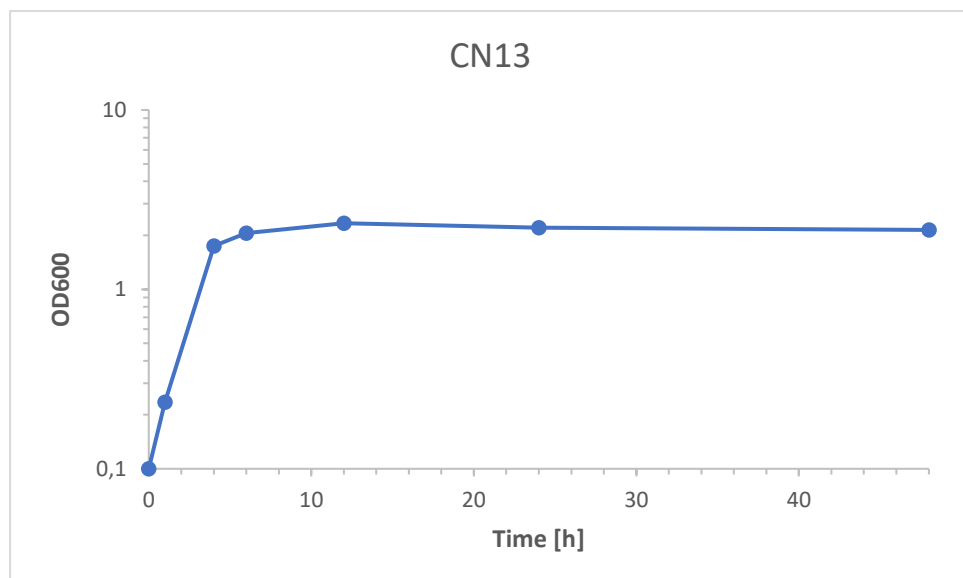


Figure A80 Growth curves of *C. necator* H16 CN13 in CNMM medium with 50 mM β -alanine supplementation over 48 h. CN13 was used to inoculate CNMM medium with 50 mM β -alanine at 0.1 OD₆₀₀ and grown for 48 hours. Blue curve: OD₆₀₀ of the supplemented cultures. All cultures were grown in biological triplicates and pH adjusted. $T_D = 1,375$ h

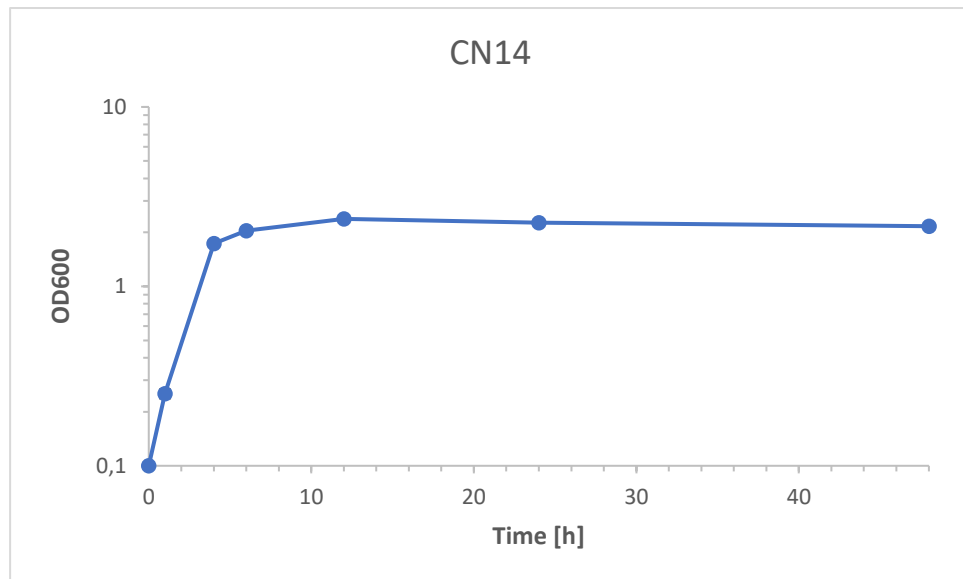


Figure A81 Growth curves of *C. necator* H16 CN14 in CNMM medium with 50 mM β -alanine supplementation over 48 h. CN14 was used to inoculate CNMM medium with 50 mM β -alanine at 0.1 OD₆₀₀ and grown for 48 hours. Blue curve: OD₆₀₀ of the supplemented cultures. All cultures were grown in biological triplicates and pH adjusted. $T_D = 1,378$ h

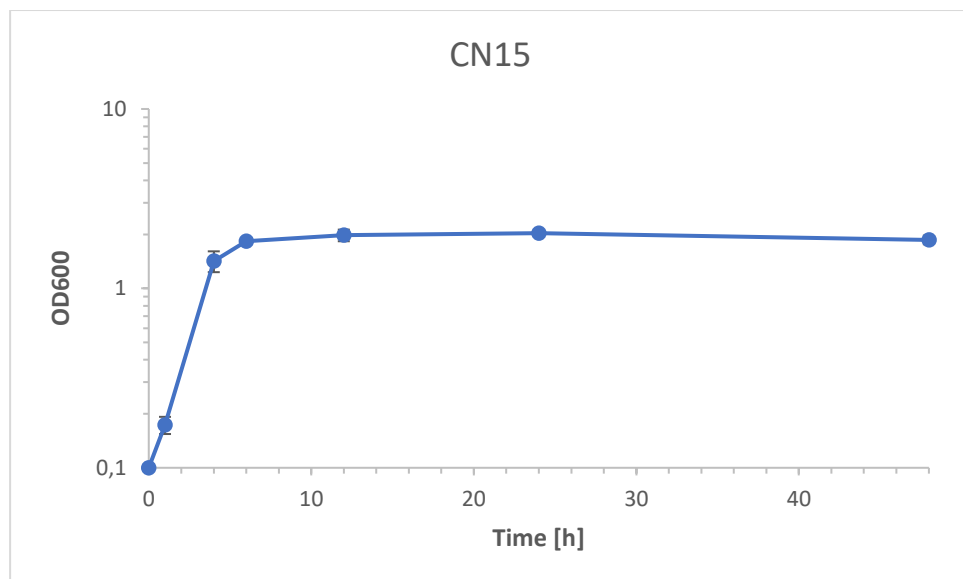


Figure A82 Growth curves of *C. necator* H16 CN15 in CNMM medium with 50 mM β -alanine supplementation over 48 h. CN15 was used to inoculate CNMM medium with 50 mM β -alanine at 0.1 OD₆₀₀ and grown for 48 hours. Blue curve: OD₆₀₀ of the supplemented cultures. All cultures were grown in biological triplicates and pH adjusted. $T_D = 1,430$ h

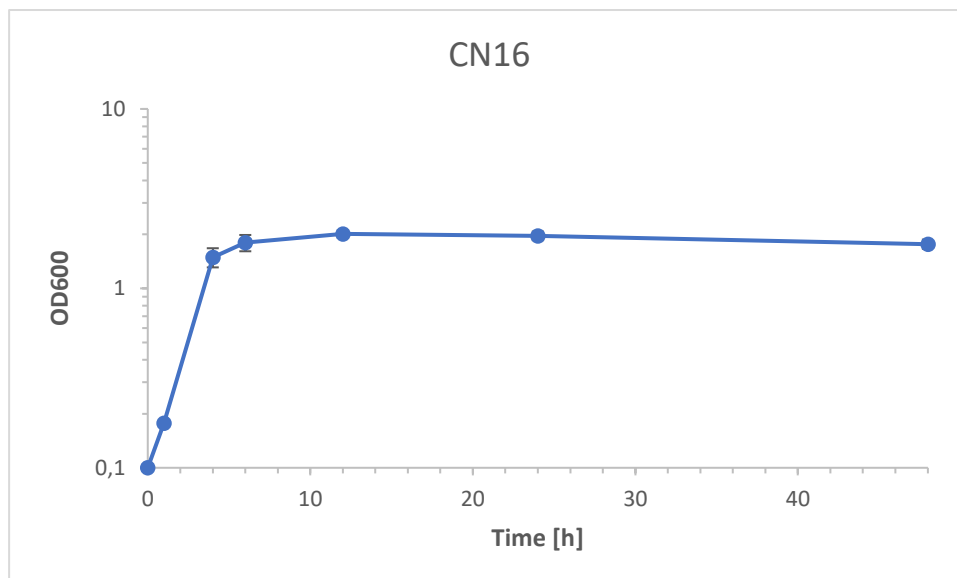


Figure A83 Growth curves of *C. necator* H16 CN16 in CNMM medium with 50 mM β -alanine supplementation over 48 h. CN16 was used to inoculate CNMM medium with 50 mM β -alanine at 0.1 OD₆₀₀ and grown for 48 hours. Blue curve: OD₆₀₀ of the supplemented cultures. All cultures were grown in biological triplicates and pH adjusted. $T_D = 1,440$ h

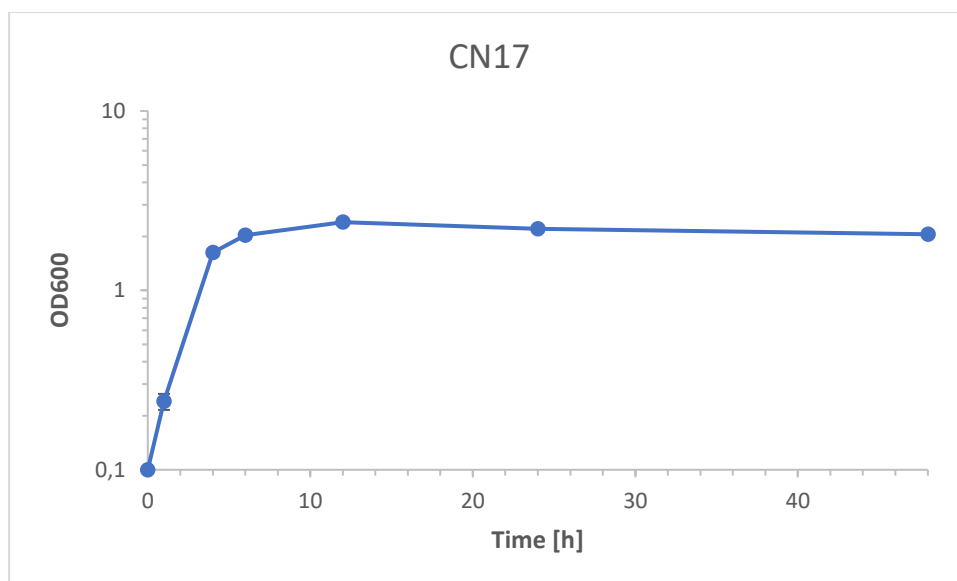


Figure A84 Growth curves of *C. necator* H16 CN17 in CNMM medium with 50 mM β -alanine supplementation over 48 h. CN17 was used to inoculate CNMM medium with 50 mM β -alanine at 0.1 OD₆₀₀ and grown for 48 hours. Blue curve: OD₆₀₀ of the supplemented cultures. All cultures were grown in biological triplicates and pH adjusted. $T_D = 1,380$ h

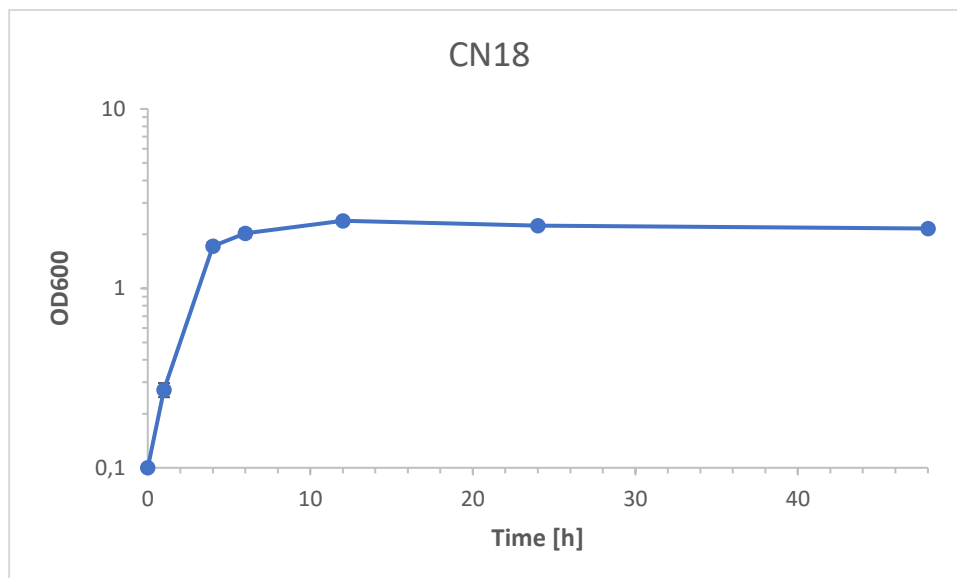


Figure A85 Growth curves of *C. necator* H16 CN18 in CNMM medium with 50 mM β -alanine supplementation over 48 h. CN18 was used to inoculate CNMM medium with 50 mM β -alanine at 0.1 OD₆₀₀ and grown for 48 hours. Blue curve: OD₆₀₀ of the supplemented cultures. All cultures were grown in biological triplicates and pH adjusted. $T_D = 1,381$ h

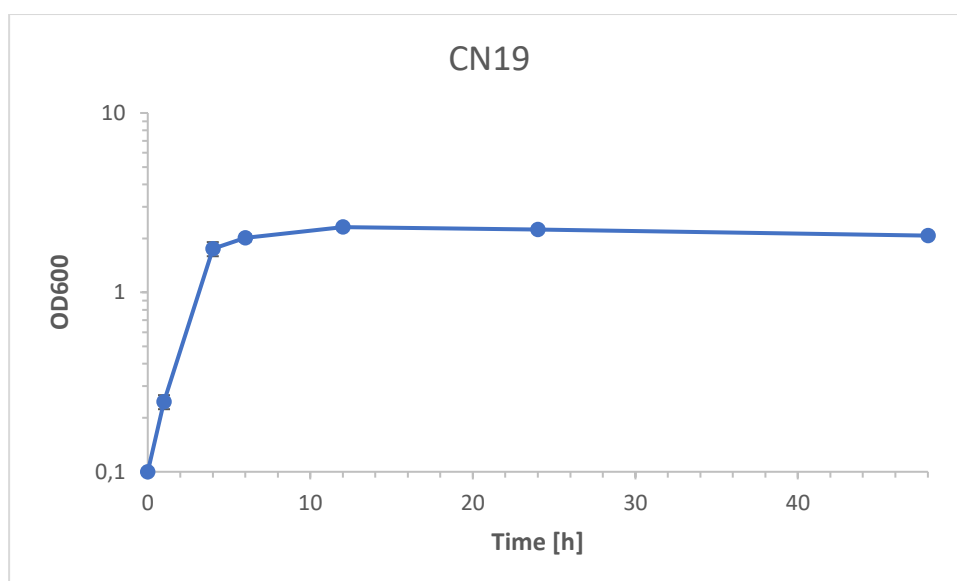


Figure A86 Growth curves of *C. necator* H16 CN19 in CNMM medium with 50 mM β -alanine supplementation over 48 h. CN19 was used to inoculate CNMM medium with 50 mM β -alanine at 0.1 OD₆₀₀ and grown for 48 hours. Blue curve: OD₆₀₀ of the supplemented cultures. All cultures were grown in biological triplicates and pH adjusted. $T_D = 1,385$ h

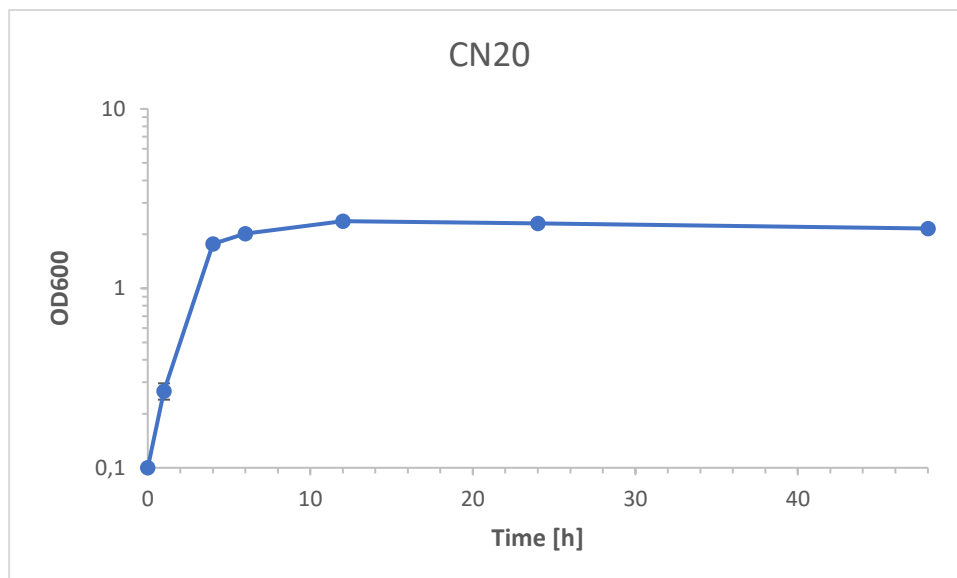


Figure A87 Growth curves of *C. necator* H16 CN20 in CNMM medium with 50 mM β -alanine supplementation over 48 h. CN20 was used to inoculate CNMM medium with 50 mM β -alanine at 0.1 OD₆₀₀ and grown for 48 hours. Blue curve: OD₆₀₀ of the supplemented cultures. All cultures were grown in biological triplicates and pH adjusted. $T_D = 1,383$ h

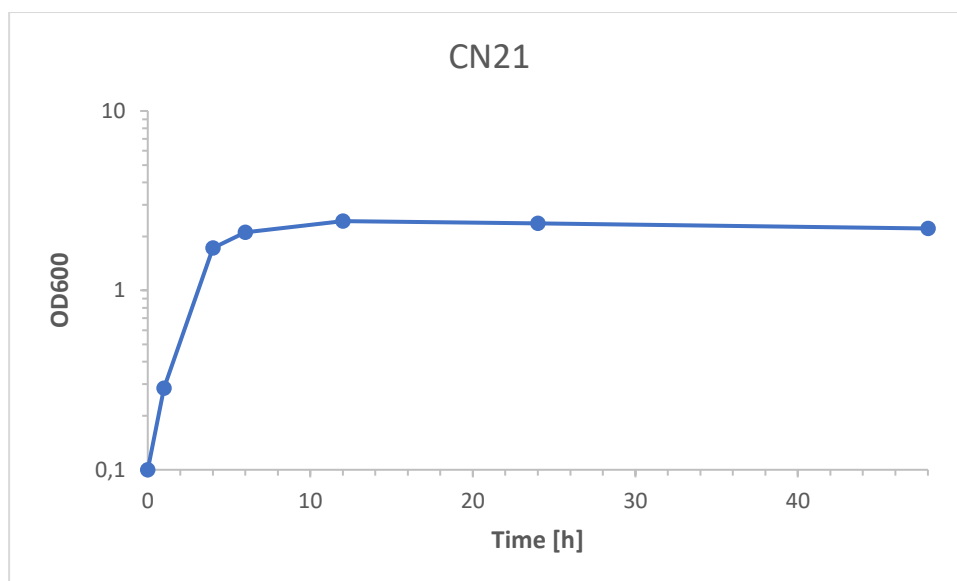


Figure A88 Growth curves of *C. necator* H16 CN21 in CNMM medium with 50 mM β -alanine supplementation over 48 h. CN21 was used to inoculate CNMM medium with 50 mM β -alanine at 0.1 OD₆₀₀ and grown for 48 hours. Blue curve: OD₆₀₀ of the supplemented cultures. All cultures were grown in biological triplicates and pH adjusted. $T_D = 1,364$ h

Plasmid maps

Plasmid maps of plasmid backbones used in this study:

pMTL71301

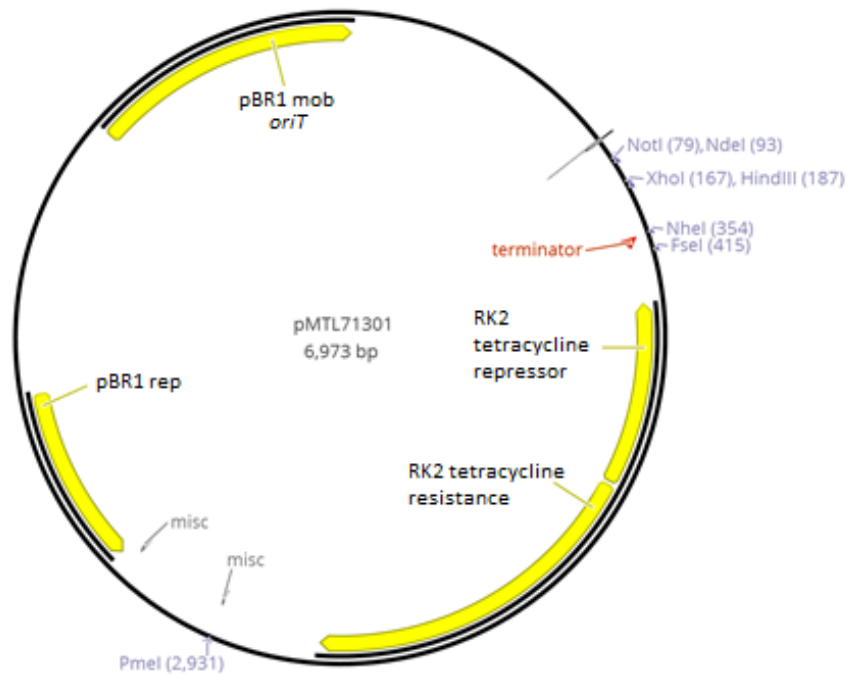


Figure A89 Plasmid map of vector pMTL71301. pMTL71301 uses the mob/rep replicon from pBR1. rep: replication region. mob/*oriT*: mobilisation module. RK2 tetracycline repressor and resistance: Confers tetracycline resistance. NotI, NdeI, XhoI, HindIII, NheI and FseI are restriction sites in the MCS. PmeI is a restriction site that can be used with FseI to cut out the tetracycline resistance module. Transcriptional terminators shown in red.

pMTL74111 (exemplified by pMTL74111-P_{BAD})

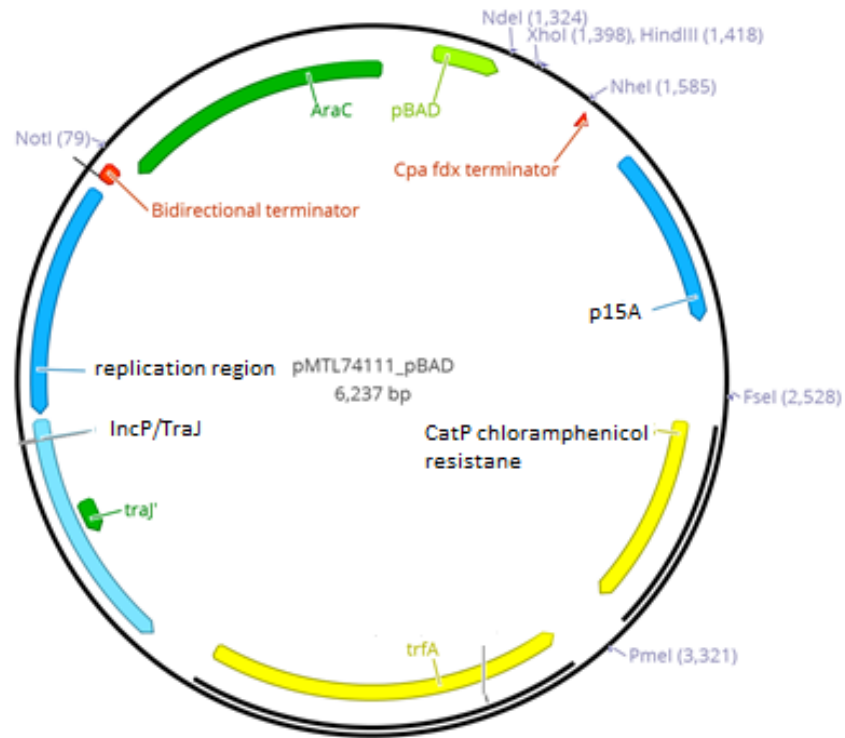


Figure A90 Plasmid map of vector pMTL4111. pMTL74111 uses the *traj/IncP* replicon from pCM62 and the *p15A* replicon from pACYC184. *CatP* confers chloramphenicol resistance. *trfA* is necessary for replication in several gram-negative hosts [435]. *NdeI*, *XhoI*, *HindIII* and *NheI* are restriction sites in the MCS. *PmeI* is a restriction site that can be used with *FseI* to cut out the chloramphenicol resistance module. Transcriptional terminators shown in red.

pET16b

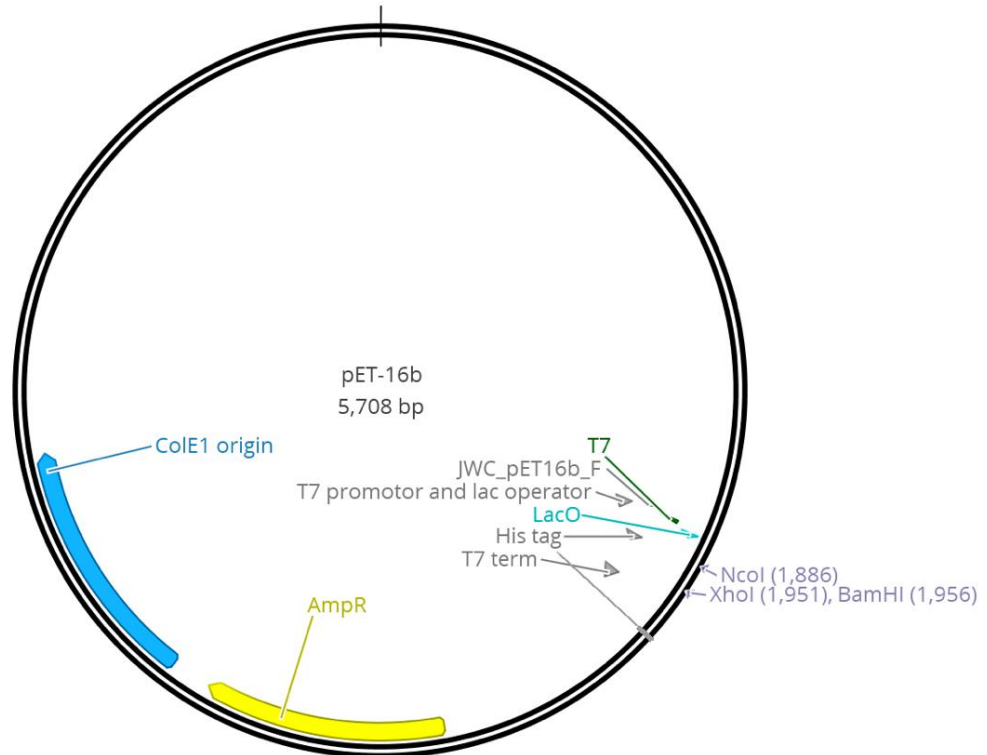


Figure A91 Plasmid map of vector pET-16b. pET16b uses the ColE1 replication module. AmpR confers ampicillin resistance. NcoI, XhoI and BamHI are restriction sites in the MCS. The vector contains a T7 promoter and T7 terminator for genes cloned in the MCS. Also, a N-terminal His-tag sequence is included. The T7 promoter is under lac operator control and IPTG can be used to induce transcription of genes cloned into the MCS.

Table A1 List of 5-AV N-adapted mutations. The table shows a list of mutations in the coding sequences of the 5-AV N-adapted *C. necator* H16 strain that was discussed in **Chapter 4.2.1**. The table shows the gene name, the locus tag and the type of mutation.

Chromosome 1	Locus tag	Type
Enoyl-CoA hydratase	H16_RS00680	No sufficient coverage
Unknown gene (coding CDS)	H16_RS33595	Multiple point mutations
Methylcrotonyl-CoA carboxylase	H16_RS00855	No sufficient coverage
GTP binding protein (inferred)	H16_RS00945	Multiple point mutations
GMC family oxidoreductase	H16_RS01135	SNP
Phenylacetic acid degradation protein	H16_RS01175	No sufficient coverage
Unknown gene (coding CDS)	H16_RS01290	SNP
ABC transporter ATP-binding CDS	H16_RS01905	SNP
Unknown gene (coding CDS)	H16_RS02580	SNP
Peptidase	H16_RS02655	SNP
Peptidase M48	H16_RS02745	No sufficient coverage
Multidrug transporter subunit MdtA	H16_RS02890	2 SNPs
tRNA epoxyqueuosine reductase QueG	H16_RS02940	1 deletion
Coproporphyrinogen III oxidase	H16_RS04705	SNP
Unknown gene (coding CDS)	H16_RS04885	2 SNPs
Unknown gene (coding CDS)	H16_RS33610	SNP
Allantoinase	H16_RS05000	SNP
Xanthine dehydrogenase subunit	H16_RS05050	SNP
RDD family protein	H16_RS05125	SNP
Unknown gene (coding CDS)	H16_RS05435	SNP
Bifunctional glutamin synthetase LuxR family transcriptional regulator (fatty acid biosynthesis)	H16_RS05595	Several SNPs
Unknown gene (coding CDS)	H16_RS06415	SNP
Unknown gene (coding CDS)	H16_RS34050	No sufficient coverage
Pyruvate dehydrogenase subunit	H16_RS06825	2 SNPs
Two-component sensor histidine kinase	H16_RS07260	SNP
Unknown gene (coding CDS)	H16_RS07990	No sufficient coverage
Unknown gene (coding CDS)	H16_RS34085	No sufficient coverage
Unknown gene (coding CDS)	H16_RS34090	No sufficient coverage
2-methylcitrate synthase	H16_RS09505	Several SNPs
Methylcrotonyl-CoA carboxylase	H16_RS09835	SNP
Unknown gene (coding CDS)	H16_RS10335	No sufficient coverage
Uracil-DANN glycosylase	H16_RS10565	SNP
Sulfate ABC transporter	H16_RS11180	No sufficient coverage
Copper-translocating P-type ATPase	H16_RS11600	No sufficient coverage
All genes between 2542695 and 2736508		No sufficient coverage
Unknown gene (coding CDS)	H16_RS13410	No sufficient coverage
Rieske (2Fe-2S) protein	H16_RS13635	No sufficient coverage
Transcriptional regulator (unknown function)	H16_RS14960	No sufficient coverage
Phosphoserine phosphatase	H16_RS15360	No sufficient coverage
Aminodeoxychorismate synthase	H16_RS15395	Deletion
All genes between 3361634 and 3434169		No sufficient coverage

tRNA Pro	H16_RS16210	SNP
Unknown gene (coding CDS)	H16_RS16215	No sufficient coverage
Unknown gene (coding CDS)	H16_RS16385	No sufficient coverage
Unknown gene (coding CDS)	H16_RS16590	No sufficient coverage
Multidrug efflux RND transporter permease subunit	H16_RS16735	SNP
Surface lipoprotein	H16_RS17080	Multiple point mutations
putA gene	H16_RS18130	2 point mutations
ABC transporter ATP-binding CDS	H16_RS18285	No sufficient coverage
Unknown gene (coding CDS)	H16_RS18505	No sufficient coverage
DNA binding response regulator	H16_RS18530	No sufficient coverage
Chromosome 2	Locus tag	Type
Tyrosine protein kinase	H16_RS18835	SNP
Unknown gene (coding CDS)	H16_RS19395	No sufficient coverage
IcIR family transcriptional regulator	H16_RS19420	No sufficient coverage
Flagellar biosynthesis regulator FlhF	H16_RS20005	SNP
ABC transporter (ATP binding)	H16_RS21240	Deletion
Flagellar motor switch protein FliM	H16_RS21555	SNP
Acyl-CoA dehydrogenase	H16_RS22105	SNP
Alpha/Beta hydrolase	H16_RS22790	SNP
Acetyl-coenzyme A synthetase	H16_RS22905	Several SNPs
Unknown gene (coding CDS)	H16_RS22925	No sufficient coverage
Acyl-CoA dehydrogenase	H16_RS22985	No sufficient coverage
S-adenosylhomocysteine deaminase	H16_RS23045	SNP
Fe-S-binding ATPase	H16_RS23550	SNP
Cytochrome C-550 PedF	H16_RS24045	No sufficient coverage
Unknown gene (coding CDS)	H16_RS34545	No sufficient coverage
Unknown gene (coding CDS)	H16_RS25290	No sufficient coverage
2-dehydropantoate 2-reductase	H16_RS27570	No sufficient coverage
MaoC family dehydratase	H16_RS27575	SNP
Unknown transcriptional regulator	H16_RS27585	Multiple SNPs
Branched-chain amino acid ABC transporter	H16_RS28925	SNP
Pyruvate dehydrogenase	H16_RS29860	SNP
Megaplasmid	Locus tag	Type
Ni-Fe hydrogenase	H16_RS31580	SNP
HoxI	H16_RS31960	No sufficient coverage

Sequences

Sequences of genes used in this study:

SEQ. ID1

bktB, encodes beta-ketothiolase BktB from *C. necator* H16. Locus name: H16_A1445.

```
ATGACGCGTGAAGTGGTAGTGGTAAGCGGTGTCCGTACCGCGATCGGGACCTTTGG
CGGCAGCCTGAAGGATGTGGCACCGGCGGAGCTGGGCGCACTGGTGGTGCGCGA
GGCGCTGGCGCGCGCAGGTGTGGGCGACGATGTGGCCACGTGGTATTCCGGC
AACGTGATCCAGACCGAGCCGCGCGACATGTATCTGGGCCGCGTCGCGGCCGTCAA
CGGCGGGGTGACGATCAACGCCCCGCGCTGACCGTGAACCGCCTGTGCGGCTCG
GGCCTGCAGGCCATTGTCAGCGCCGCGCAGACCATCCTGCTGGGCGATACCGACGT
CGCCATCGGCGGCGGCGCGAAAGCATGAGCCGCGCACCGTACCTGGCGCCGGCA
GCGCGCTGGGGCGCACGCATGGGCGACGCCGGCCTGGTCGACATGATGCTGGGTG
CGCTGCACGATCCCTTCCATCGCATCCACATGGGCGTGACCGCCGAGAATGTCGCCA
AGGAATACGACATCTCGCGCGCGCAGCAGGACGAGGCCGCGCTGGAATCGCACCG
CCGCGCTTCGGCAGCGATCAAGGCCGGCTACTTCAAGGACCAGATCGTCCCGGTGG
TGAGCAAGGGCCGCAAGGGCGACGTGACCTTCGACACCGACGAGCACGTGCGCCA
TGACGCCACCATCGACGACATGACCAAGCTCAGGCCGGTCTTCGTCAAGGAAAACG
GCACGGTACAGGCCGGCAATGCCTCGGGCCTGAACGACGCCGCCGCCGCGGTGGT
GATGATGGAGCGCGCCGAAGCCGAGCGCCGCGGCCTGAAGCCGCTGGCCCCGCTG
GTGTCGTACGGCCATGCCGGCGTGGACCCGAAGGCCATGGGCATCGGCCCGGTGC
CGGCGACGAAGATCGCGCTGGAGCGCGCCGGCCTGCAGGTGTGGACCTGGACGT
GATCGAAGCCAACGAAGCCTTTGCCGCACAGGCGTGCGCCGTGACCAAGGCGCTCG
GTCTGGACCCGGCCAAGGTTAACCCGAACGGCTCGGGCATCTCGCTGGGCCACCCG
ATCGGCCACCGGTGCCCTGATCACGGTGAAGGCGCTGCATGAGCTGAACCGCGT
GCAGGGCCGCTACGCGCTGGTGACGATGTGCATCGGCGGCGGGCAGGGCATTGCC
GCCATCTTCGAGCGTATCTGA
```

SEQ. ID2

phaB, encodes acetoacetyl-CoA reductase PhaB from *C. necator* H16. Locus name: H16_A1439.

```
ATGACTCAGCGCATTGCGTATGTGACCGGCGGCATGGGTGGTATCGGAACCGCCAT
TTGCCAGCGGCTGGCCAAGGATGGCTTTCGTGTGGTGGCCGGTTGCGGCCCAACT
CGCCGCGCCGCGAAAAGTGGCTGGAGCAGCAGAAGGCCCTGGGCTTCGATTCATT
GCCTCGGAAGGCAATGTGGCTGACTGGGACTCGACCAAGACCGCATTTCGACAAGGT
CAAGTCCGAGGTCGGCGAGGTTGATGTGCTGATCAACAACGCCGGTATCACCCGCG
ACGTGGTGTTCGCAAGATGACCCGCGCCGACTGGGATGCGGTGATCGACACCAAC
CTGACCTCGCTGTTCAACGTCACCAAGCAGGTGATCGACGGCATGGCCGACCGTGG
CTGGGGCCGCATCGTCAACATCTCGTCGGTGAACGGGCAGAAGGGCCAGTTCGGCC
AGACCAACTACTCCACCGCCAAGGCCGGCCTGCATGGCTTCACCATGGCACTGGCG
CAGGAAGTGGCGACCAAGGGCGTGACCGTCAACACGGTCTCTCCGGGCTATATCGC
CACCGACATGGTCAAGGCGATCCGCCAGGACGTGCTCGACAAGATCGTCGCGACGA
TCCCGGTCAAGCGCCTGGGCCTGCCGAAGAGATCGCCTCGATCTGCGCCTGGTTG
TCGTCCGAGGAGTCCGGTTTCTCGACCGGCGCCGACTTCTCGCTCAACGGCGGCCT
GCATATGGGCTGA
```

SEQ. ID3

crt3, encodes crotonase Crt3 from *C. necator* H16. Locus name: H16_B1843.

GTGTACGCAGCTAAGGACATCACCGTGGAGGAGCGCGCCGGCGGCGCGCTATGGA
TCACGATCGACCGGGCGCAGAAACACAATGCGCTGGCCCGCCACGTGCTGGCGGG
ATTGGCGCAGGTGGTGAGCGCCGCGGGCGGCGCAGCCCGGGGTGCGCTGCATCGTG
CTGACCGGCGCCGGCCAGCGCTTCTTTGCGGCAGGCGGCGATCTGGTCGAGCTGTC
CGGCGTGCGCGACCGGGAGGCTACGCTGGCCATGAGCGAGCAGGCGCGCGGTGCC
CTGGATGCGGTGCGCGACTGCCCGCTGCCGGTGCTGGCCTACCTGAACGGCGATGC
CATCGGCGGGCGGCCGAGCTGGCATTGGCCTGCGACATGCGGCTGCAGTCGGCG
AGCGCGCGCATCGGCTTTATCCAGGCGCGGCTGGCCATCACCTCGGCCTGGGGCGG
CGGCCCCGACCTGTGCCGGATCGTCGGCGCGGGCGCGGGCCATGCGCATGATGAGC
CGTTGCGAGCTTGTCGATGCGCAGCAGGCGCTGCAGTGGGGCTTGGCCGATGCGG
TGGTCACGGACGGACCCGCCGGAAGGACATCCACGCCTTCCTGCAACCGCTGCTG
GGCTGCGCCCCGAGGTGCTGCGCGGCATCAAGGCGCAGACCGCGGCCAGCCGGC
GCGGCGAGTCGCATGACGCTGCCCGCACCATCGAGCAGCAGCAACTGTTGCATACC
TGGCTCCATGCGGACCATTGGAACGCTGCCGAGGGCATCCTCTCCAGGAGGGCCCA
ATGA

SEQ. ID4

hbd3, encodes 3-hydroxybutyryl-CoA dehydrogenase Hbd3 from *Clostridium saccharoperbutylacetonicum* ATCC® 12472™. Locus name: Cspa_c22690.

ATGGCTAATTCAATTAGAAATATAACAGTATTTGGACCTGGAATGATGGGGAGTGG
AATCGCTCAAGTTTTGCAGGAAATGAAGATTTAAAAGTAACAATTTTTATTAGAGA
AAAATTTGAATATGAATGTATGGATAAAATAAAATCTAATCTTCAGGTATTTAAAAGA
AAATGGAGTGATAACTGAAGAAAAAATCAAAGGGATTTTGGATAGAATTGCTTTAA
CAGAGGATTTACAAGAAGCAGTTAAGGATGCTGATTTCATAGTAGAATGTATTCCA
GAAAATATGGAATTTAAACAAGATTTATTTAAAAGATTAGAACCTATCTGCAAGGAT
ACAACAATATTTGCAACAAATACTTCAGTAATGAGTATAACTGAAATTTGAGAAAAA
GTGAAAGATAAATCAAGACTTGTAGGTACTCATTTTTGGAATCCTCCATATTTAATAC
CACTAGTAGAAGTTATTAATCAGATTATACTTCAGATGAGATAATGGACAAGACAA
TGGAACTACTAAAGAAAGTAGAAAAACATCCAATAAGAGTAAATAAGGATGTACCA
GGTTTTGTTGCAAATAGATTACAACATGCTCTTTGGAGAGAAGCAATTTCTATAGTT
GAACATGATATAGCAGATGCAGCAACTGTTGATGAGGCAATAAAATATAGCTTTGG
ATTAAGACTTCCAGTACTTGGACCTATGGAGAATTCTGATATGGTTGGAAGTATTT
GACTTTATCTATTCACAGTTATATATTGAAGCATTTAGAAAATTCAACAGAACCTTCA
CCTATATTTAAAAGAAAAAGTGGAAAGCAGGAGATTTAGGCTTTAAAACAGGAAAGG
GCTTTCAAGAGTGGTCTGCCGATCAAGCTAAGAAATCAAATGAAAGACTTAGAGAT
TATTTAATTAAGTCCTATATAAAAAATAAATAA

SEQ. ID5

crt, encodes crotonase Crt from *Clostridium acetobutylicum* ATCC® 824™. Locus name: CA_C2712.

```
ATGGA ACTAAACAATGTCATCCTTGAAAAGGAAGGTAAAGTTGCTGTAGTTACCATT
AACAGACCTAAAGCATTAAATGCGTTAAATAGTGATACTAAAAGAAATGGATTAT
GTTATAGGTGAAATTGAAAATGATAGCGAAGTACTTGCAAGTAATTTAACTGGAGC
AGGAGAAAAATCATTGTAGCAGGAGCAGATATTTCTGAGATGAAGGAAATGAATA
CCATTGAAGGTAGAAAATTCGGGATACTTGGAATAAAGTGTTTAGAAAGATTAGAA
CTTCTTGAAAAGCCTGTAATAGCAGCTGTTAATGGTTTTGCTTTAGGAGGCGGATGC
GAAATAGCTATGTCTTGATATAAGAATAGCTTCAAGCAACGCAAGATTTGGTCAA
CCAGAAGTAGGTCTCGGAATAACACCTGGTTTTGGTGGTACACAAAGACTTTCAAG
ATTAGTTGGAATGGGCATGGCAAAGCAGCTTATTTACTGCACAAAATATAAAGG
CAGATGAAGCATTAAAGAATCGGACTTGTAATAAAGGTAGTAGAACCTAGTGAATTA
ATGAATACAGCAAAAAGAAATTGCAAACAAAATTGTGAGCAATGCTCCAGTAGCTGT
TAAGTTAAGCAAACAGGCTATTAATAGAGGAATGCAGTGTGATATTGATACTGCTTT
AGCATTTGAATCAGAAGCATTGGGAGAATGCTTTTCAACAGAGGATCAAAGGATG
CAATGACAGCTTTCATAGAGAAAAGAAAATTGAAGGCTTCAAAAATAGATAG
```

SEQ. ID6

terD, encodes trans-2-enoyl CoA reductase FadV from *Treponema denticola*. Locus name: TDE_0597. The shown sequence was codon-optimised by Biomatik Corp.

```
ATGATCGTCAAGCCAATGGTGC GCAATAATATCTGTCTGAACGCTCACCCGCAGGGT
TGTA AAAAGGGTGTAGAA GACCAGATTGAATACACTAAGAAACGCATCACCCGAGA
AGTTAAAGCAGGTGCCAAAGCACCGAAAAACGTCCTGGTGTGGGCTGCAGCAAC
GGCTACGGTCTGGCAAGCCGCATTACGGCTGCATTTCGGTTACGGCGCTGCTACTATT
GGTGTTAGCTTCGAAAAGGCGGGTTCTGAAACCAATACGGCACTCCAGGCTGGTA
CAACAACCTGGCATTTCGACGAAGCAGCGAAGCGTGAGGGTCTGTACTCTGTTACCA
TCGACGGTGACGCGTTCTCTGACGAGATCAAAGCTCAGGTTATCGAGGAAGCTAAA
AAGAAAGGTATCAAATTCGACCTGATTGTGTACTCCCTGGCCTCTCCGGTTCGTACC
GACCCGGATACCGGCATCATGCACAAAAGCGTACTGAAGCCGTTTGGCAAAACCTT
CACTGGTAAAACCGTTGATCCTTTACCCGGCGAGCTGAAGGAAATCTCCGCCGAGCC
AGCTAACGATGAGGAGGCTGCTGCGACCGTTAAAGTGATGGGTGGCGAAGACTGG
GAACGTTGGATCAAACA ACTGTCCAAGGAAGGTCTGCTGGAGGAGGGCTGTATTAC
TCTGGCATATTCTTACATCGGCCCGGAGGCGACTCAGGCACTGTATCGTAAGGGCA
CCATCGGTAAAGCGAAAGA ACATCTGGAGGCCACCGCTCACCGTCTGAACAAGGAA
AACCCGAGCATCCGTGCTTTTCGTGTCCGTTAACAAGGGCCTGGTTACGCGCGCTTCC
GCAGTAATCCGGTCATTCCGCTGTACCTGGCTTCCCTGTTTAAAGTCATGAAAGAA
AAAGGCAACCACGAAGGTTGTATCGAACA AATTA CTGCCTGTATGCGGAGCGCCT
GTACCGTAAGGATGGCACTATCCCGGTTGATGAAGAGA ACCGCATCCGCATTGACG
ATTGGGA ACTGGAAGAGGATGTACAGAAAGCGGTTTCCGCGCTGATGGAAAAAGT
GACGGGCGAAAACGCGGAATCCCTGACGGATCTGGCAGGTTACCGTCACGACTTTC
TGGCGTCTAATGGTTTCGACGTTGAGGGTATTA ACTACGAGGCAGAAGTTGAACGT
TTCGATCGTATTTAA
```

SEQ. ID7

terEG, encodes trans-2-enoyl CoA reductase TER from *Euglena gracilis*. Locus name: AY741582. The shown sequence was codon-optimised by Biomatik Corp.

```
ATGTCGTGCCCCGCCTCGCCGTCTGCTGCCGTGGTGTCTGCCGGCGCCCTCTGCCTG
TGGCTGGCAACGGTATTGTTGGCGACTGGATCCAACCCACCGCCCTGTCCACTGCT
TCCACTCGCTCTCCGACCTCACTGGTCCGTGGGGTGGACAGGGGCTTGATGAGGCC
AACCACTGCAGCGGCTCTGACGACAATGAGAGAGGTGCCCCAGATGGCTGAGGGA
TTTTCAGGCGAAGCCACGTCTGCATGGGCCGCCGCGGGGCCGAGTGGGCGGCGC
CGCTCGTGGCCGCGGCCTCCTCCGCACTGGCGCTGTGGTGGTGGGCCGCCCGGCGC
AGCGTGCGGCGGGCCGCTGGCAGCGCTGGCGGAGCTGCCACCGCGGTCACCCACC
TGGCCCCCGGATGGCGATGTTACCACCACAGCGAAGGTCATCCAGCCCAAGATTC
GTGGCTTCATCTGCACGACCACCCACCCGATCGGCTGTGAGAAGCGGGTCCAGGAG
GAGATCGCGTACGCCCGTGCCACCCGCCACCAGCCCTGGCCCGAAGAGGGTGT
GGTCATCGGCTGCAGTACCGGCTACGGGCTCTCCACCCGCATCACCGCTGCCTTCGG
CTACCAGGCCGCCACGCTGGGCGTGTTCTGGCGGGCCCCCGACGAAGGGCCGCC
CCGCCGCGGCGGGCTGGTACAACACCGTGGCGTTCGAGAAGGCCGCCCTGGAGGC
CGGGCTGTACGCCCGGAGCCTTAATGGCGACGCCTTCGACTCCACAACGAAGGCGC
GGACGGTCGAGGCGATCAAGCGGGACCTCGGCACGGTGGACCTCGTGGTGTACAG
CATCGCCGCCCGAAGCGGACGGACCCTGCCACCGGCGTCTCCACAAGGCCTGCC
TGAAGCCCATCGGCGCCACGTACACCAACCGCACTGTGAACACCGACAAGGCGGAG
GTGACCGACGTCAGCATTGAGCCGGCCTCCCCGAAGAGATCGCGGACACGGTGAA
GGTGATGGGCGGGGAGGACTGGGAGCTCTGGATCCAGGCGCTGTCCGAGGCCGG
CGTGCTGGCGGAGGGGGCCAAGACGGTGGCGTACTCCTACATCGGCCCCGAGATG
ACGTGGCCTGTCTACTGGTCCGGCACCATCGGGGAGGCCAAGAAGGACGTGGAGA
AGGCTGCCAAGCGCATCACGCAGCAGTACGGTGGCCGCGTACCCGGTGGTGGC
CAAGGCCTTGTCACCCAGGCCAGCTCCGCCATCCCGTGGTGCCGCTCTACATCTG
CCTGCTGTACCGCGTTATGAAGGAGAAGGGCACCCACGAGGGCTGCATCGAGCAG
ATGGTGCGGCTGCTACCACGAAGCTGTACCCGAGAACGGGGCCCCCATCGTCGA
TGAGGCCGACGTGTGCGGGTGGATGACTGGGAGATGGCGGAGGATGTGCAGCA
GGCTGTTAAGGACCTCTGGAGCCAGGTGAGCACTGCCAACCTCAAGGACATCTCCG
ACTTCGCTGGGTATCAAACCTGAGTTCCTGCGGCTGTTCCGGTTCGGCATTGACGGCG
TGGACTACGACCAGCCGTGGACGTGGAGGCGGACCTCCCCAGTGCTGCCAGCAG
```

SEQ. ID8

ydfG, encodes oxidoreductase YdfG from *Escherichia coli*. Locus name: JW1532.

```
ATGGCCGTTTTAGTAACTGGAGCAACGGCAGGTTTTGGTGAATGCATTA  
CTCGTCGT  
TTTATTCAACAAGGGCATAAAGTTATCGCCACTGGCCGTCGCCAGGAAC  
GGTTGCA  
GGAGTTAAAAGACGAACTGGGAGATAATCTGTATATCGCCCAACTGGAC  
GTTTCGCA  
ACCGCGCCGCTATTGAAGAGATGCTGGCATCGCTTCCTGCCGAGTGGT  
GCAATATT  
GATATCCTGGTAAATAATGCCGGCCTGGCGTTGGGCATGGAGCCTGCGC  
ATAAAGC  
CAGCGTTGAAGACTGGGAAACGATGATTGATACCAACAACAAAGGCCT  
GGTATATA  
TGACGCGCGCCGTCTTACCGGGTATGGTTGAACGTAATCATGGTCATAT  
TATTAACA  
TTGGCTCAACGGCAGGTAGCTGGCCGTATGCCGGTGGTAACGTTTACGG  
TGCGACG  
AAAGCGTTTGTTTCGTCAGTTTAGCCTGAATCTGCGTACGGATCTGCAT  
GGTACGGCG  
GTGCGCGTCACCGACATCGAACCGGTCTGGTGGGTGGTACCGAGTTTT  
CCAATGT  
CCGCTTTAAAGGCGATGACGGTAAAGCAGAAAAACCTATCAAATACCG  
TTGCAT  
TGACGCCAGAAGATGTCAGCGAAGCCGTCTGGTGGGTGTCAACGCTGC  
CTGCTCAC  
GTCAATATCAATACCCTGGAAATGATGCCGGTTACCCAAAGCTATGCC  
GGACTGAAT  
GTCCACCGTCAGTAA
```

SEQ. ID9

bapat, encodes β -alanine-pyruvate aminotransferase BAPAT from *Chromobacterium violaceum*. Locus name: NCTC8684_02560.

ATGAACCACCCGCTCACCACCCGTTCCGAATTCGACCATCTAGACCTGCGCGCGCAC
TGGATGCCGTTT CAGCGCCAACCGCAATTTCCAGCGCGATCCGCGGTTGATCGTGTCC
GGCGAGGGCAACTATCTGACCGACGCCGACGGCCGCCGCATCTTCGACAGCCTGTC
CGGCCTGTGGTGTGCGGCGCCGGCCACAGCCGCAAGGAGATCGCCGAGGCGGCC
TATCGCCAGCTGTCGACGCTGGATTATTCGCCC GGCTTCCAGTTCCGCCACCCGTTG
TCGTTCCGGCTGGCCGAGCGCGTGGCGGGCGATGGCGCCGGGCGCGCTGAACCACG
TGTTCTTCACCAACTCCGGCTCCGAATGCGCGGACACCGCGGTGAAGATGGCGCGC
GCCTACTGGCGGCTGAAGGGCCAGGCGTCCAAGACCAAGCTGATCGGCCGCGCCC
GCGGCTACCACGGCGTCAACATCGCCGGCACCAGCCTGGGCGGCATGAACGGCAA
CCGCAAATTATTCGGCCCCGCTGATGGACGCGGACCATCTGCCGCACACCTTGCTGCC
GGCCAACGCCTTCAGCCGCGGCCTGCCGGAGCAGGGCGCGGAGCTGGCGGACGAT
CTGCTGCGGCTGATCGAGCTGCACGACGCGTCCAATATCGCCGCGGTGATTGTGGA
GCCGATGGCCGGCTCCGCCGGCGTGATCGTGCCGCCGAGGGCTATCTGCAGCGCT
TGCGGGAGATTTGCACGCAGCACGGCATCCTGCTGATCTTCGACGAGGTGATCACC
GGTTTCGGCCGCACCGGCTCGCTGTTCCGGCGCCGACCACTTCGGCGTGACGCCGGA
CATCATGAATCTGGCCAAGCAGCTGACCAATGGCGCGGTGCCGATGGGCGCGGTG
GTGGCGAGCTCGGAGATCTACGACGCTTTCATGGCACAGGCCACGCCGGAGTACGC
GGTGGAATTCGCTCATGGTTATACCTATTCGGCACACCCGGTGGCCTGCGCGGCCG
CGCTGGCGGCGCTGGATGTGCTGGAGCAGGAAAACCTGGTGGCGAGAGCCGCGG
AGCTGGCACCCCACTTCGAGCGCGGCATTACGGCCTGAAAGGCTTGCCGCATGTG
ATCGACATCCGCAACTGCGGTCTGGCCGGCGCGGTGCAGATCGCGCCGAGCGGCCG
GCGACGCCATCGTGCGGCCCTACGAGGCGGCGATGGCGCTGTGGCGCAAGGGCTT
CTACGTCCGCTACGGCGGCGACGCGCTGCAGTTCCGGCCCCCGTTACCGCCACGC
CGCAGGAGCTGGACAGCCTGTTTCGACGCTGTCGGCGAGACGCTGGCCAAGCTGGC
CTGA

SEQ. ID10

pct, encodes propionate CoA transferase Pct from *C. necator* H16. Locus name: H16_A2718

ATGAAACCTGTAAAACCACTCGTATTAATGGACGAGTGCCGGTCCTGTCCGGCACA
GGAAGCGGTGAATTATATCCCGACGAAGCAACACTTTGTGTGTTAGGCGCTGGCG
GCGGTATTCTGGAAGCCACCACGTTAATTACTGCTCTTGCTGATAAATATAAACAGA
CTCAAACACCACGTAATTTATCGATTATTAGTCCAACAGGGCTTGCGCATCGCGCCG
ACCGTGGTATTAGTCCTCTGGCGCAAGAAGGTCTGGTGAAATGGGCATTATGTGGT
CACTGGGGACAATCGCCGCGTATTTCTGAACTCGCAGAACAAAATAAAATTATTGCT
TATAACTACCCACAAGGTGTACTTACACAAACCTTACGCGCCGCCGAGCCCACCAG
CCTGGTATTATTAGTGATATTGGCATCGGGACATTTGTCGATCCACGCCAGCAAGGC
GGCAAACCTGAATGAAGTCACTAAAGAAGACCTGATTAACCTGGTCGAGTTTGATAA
CAAAGAATATCTCTATTACAAAGCGATTGCGCCAGATATTGCCTTCATTCGCGCTACC
ACCTGCGACAGTGAAGGCTACGCCACTTTTGAAGATGAGGTGATGTATCTCGACGC
ATTGGTTATTGCCAGGCGGTGCACAATAACGGCGGTATTGTGATGATGCAGGTGC
AGAAAATGGTTAAGAAAGCCACGCTGCATCCTAAATCTGTCCGTATTCCGGGTTATC
TGGTGGATATTGTGGTGGTCGATCCGGATCAAACCCAACCTGTATGGCGGTGCACCG
GTTAACCGCTTTATTTCTGGTGACTTCACCCTTGATGACAGTACCAAACCTTAGCCTGC
CCCTAAACCAACGTAAATTAGTTGCGCGGCGCGCATTATTCGAAATGCGTAAAGGC
GCGGTGGGAATGTCGGCGTCGGTATTGCTGACGGCATTGGCCTGGTCGCCCGAG
AAGAAGGTTGTGCTGATGACTTTATTCTGACGGTAGAAACAGGTCCGATTGGCGGA
ATTACTTCACAGGGGATCGCCTTTGGCGCGAACGTGAATACCCGTGCCATTCTGGAT
ATGACGTCCCAGTTTGATTTTATCACGGTGGCGGTCTGGATGTTTGTTATTTGAGTT
TTGCTGAAGTCGACCAGCACGGTAACGTCCGGTGCATAAATTCAATGGTAAAATC
ATGGGCACCGGTGGATTTATTGATATCAGTGCCACTTCGAAGAAAATCATTTTCTGC
GGCACATTAACCTGCGGGCAGTTTAAAAACAGAAATTACCGACGGCAAATTAATAT
CGTCCAGGAAGGACGGGTGAAGAAATTTATTCGGGAACTACCGGAAATTAATTTCA
GCGGAAAAATCGCTCTCGAGCGAGGGCTGGATGTTTCGTTATATCACTGAGCGCGCA
GTATTCACGCTGAAAGAAGACGGCCTGCATTTAATCGAAATCGCCCCTGGCGTCGAT
TTACAAAAAGATATTCTCGACAAAATGGATTTACCCCCAGTGATTTGCCAGAACTC
AAACTGATGGACGAAAGATTATTTATCGATGCGGCGATGGGTTTTGTCTGCCTGAA
GCGGCTCATTA

SEQ. ID11

prpE, encodes propionate CoA synthetase PrpE from *E. coli*. Locus name: JW0326.

ATGTCITTTAGCGAATTTTATCAGCGTTCGATTAACGAACCGGAGCAGTTCTGGGCC
GAGCAGGCCCGGCGTATTGACTGGCAGACGCCCTTTACGCAAACGCTCGATCACAG
CAATCCGCCGTTTGGCGTTGGTTTTGTGAAGGCCGAACCAACTTGTGCCACAACGC
CATCGACCGCTGGCTGGAGAAACAGCCAGAGGCGCTGGCGCTGATTGCCGTCTCTT
CGGAAACAGAAGAAGAGCGCACCTTTACCTTTGTCAGCTGCATGACGAAGTGAAC
GCGGTGGCCTCAATGTTGCGTTCATTGGGTGTGCAGCGCGGCGATCGGGTGCTGGT
GTATATGCCGATGATTGCCGAAGCGCATATTACTCTGCTGGCCTGCGCGCGCATTGG
CGCTATCACTCGGTGGTGGTTGGTGGATTTGCCTCGCACAGCGTGGCGGCGCGAA
TTGATGACGCTAAACCGGTGCTGATTGTCTCGGCTGATGCCGGAGCGCGCGGTGGC
AAAATCATTCCCTATAAAAAATTGCTCGACGATGCGATAAGTCAGGCGCAGCACCA
GCCACGCCATGTTTTGCTGGTGGATCGCGGGCTGGCGAAAATGGCGCGCGTCAGCG
GGCGGGATGTCGATTTGCGTCTGTTGCGCCATCAACACATCGGCGCGCGGGTACCG
GTGGCGTGGCTGGAATCCAACGAAACCTCTGCATTCTCTACACTTCCGGCACGACC
GGCAAACCTAAAGGCGTGCAGCGTGACGTCGGCGGATATGCGGTGGCGCTGGCGA
CCTCGATGGACACCATTTTTGGCGGCAAAGCGGGCAGCGTGTCTTTTTGCGCATCGG
ATATCGGCTGGGTGGTGGGGCATTTCGTATATCGTTTACGCGCCGCTGCTGGCGGGG
ATGGCGACTATCGTTTACGAAGGATTGCCGACCTGGCCGACTGCGGCGTGTGGTG
GACAATCGTCGAGAAATATCAGGTTAGCCGGATGTTCTCAGCGCCGACCGCCATTC
GCGTGCTGAAAAAATTCCCTACCGCTGAAATTCGAAACACGATCTCTCGTCGCTGG
AAGTGCTCTATCTGGCTGGAGAACCCTGGACGAGCCGACCGCCAGTTGGGTGAGC
AATACGCTGGATGTGCCGGTTCATCGACAACACTGCGCAGACCGAATCCGGCTGGCC
GATTATGGCGATTGCTCGCGGTCTGGACGACAGGCCGACGCGTCTGGGAAGCCCCG
GTGTGCCGATGTATGGCTATAACGTGCAGTTGCTTAATGAAGTCACCGGCGAACCG
TGTGGCGTCAACGAGAAAGGGATGCTGGTGGTGGAAAGGGCCGCTGCCCGCGGGT
GTATTCAGACCATCTGGGGCGACGACGGCCGCTTTGTGAAGACTTACTGGTCGCTG
TTTTCCCGCCCGGTGTACGCCACCTTTGACTGGGGCATCCGTGACGCTGACGGTTAT
CACTTTATTCTCGGGCGCACTGACGATGTAATTAACGTTGCCGGGCATCGGCTGGG
GACGCGCGAGATTGAAGAGAGTATCTCCAGCCATCCGGGCGTTGCCGAAGTGCGG
GTGGTTGGGGTGAAGATGCGCTGAAAGGGCAGGTGGCGGTGGCCTTGTGATTC
CGAAAGAGAGCGACAGTCTGGAAGATCGTGATGTGGCGCACTCGCAAGAGAAGGC
GATTATGGCGCTGGTGGACAGCCAGATTGGCAACTTTGGCCGCCCGGCGCACGCTC
GGTTTGTCTCGCAATTGCCAAAACCGATCCGGAAAATGCTGCGCCGCACGATC
CAGGCGATTTGCGAAGGACGCGATCCTGGAGATCTGACGACCATTGATGATCCTGC
GTCGTTGGATCAGATCCGCCAGGCGATGGAAGAGTAG

SEQ. ID12

fadAB, encodes 3-hydroxyacyl-CoA dehydrogenase/enoyl-CoA hydratase FadAB from *C. necator* H16. Locus name: H16_A0461

ATGTCCAATTTTCATCGTCAAGAAGGTCGCCGTGCTGGGTGCCGGCGTCATGGGGGC
GCAGATCGCCGCCACCTGATCAATGCGCGCTGCCGGTGGTGTGTTGACCTTCC
CGCCAAGGAAGGCCCAAGAACGGCATCGCGCTGCGGCCATCGAGAACCTGAAG
AAGCTCTCGCCCGCGCCGCTGGGCATCAAGGAAGAGGCCGGCCTGATCCAGGCGG
CCAACACTACGAGGACGACATCGCGCTGCTCAAGGAATGCGACCTGGTGTGATCGAGGCG
ATCGCCGAGCGCATGGACTGGAAGCACGACCTGTACAAGAAGGTCGCGCCGCACCT
GGCCTCGCACGCGATCTTCGCGACCAACACCTCGGGCCTGTGATCACAGCGCTGTC
CGACGGGTTTGATGCGGACCTGAAGTCGCGCTTCTGCGGCGTGCACTTCTCAACCC
GCCGCGCTACATGCACCTGGTGGAACTGATCCCGACCGCGACCACGCAGCCGCAGA
TCCTCGACCAGCTGGAAGCCTTCTGACCACCAGCTCGGCAAGGGCGTGGTACGC
GCCAAGGACACGCCAACTTCATCGCCAACCGCGTCGGCATCTTCTCGATCCTGGCC
GTGTTTGCCGAAGCCGAGAAGTTCGGCATCCCGTTGACGTGGTGTGATGACCTGAC
CGGCTCCAAGCTGGGCGCGCCAAGTCCGCCACCTTCCGCACCGCGGACGTGGTGC
GCCTGGACACCATGGCGCACGTGATCAAGACCATGCAGGACACCCTGCACGACGAC
CCGTTTCGCGCCGGTGTACAAGACCCCGGCCGTACTIONAAGGGCCTGGTGCACGCGG
CGCGCTGGGCCAGAAGACCGGTGCCGGCTTCTACAAGAAGGAAGGCAAGGCCATC
AAGGTGCTCGACGCCAAGACCGGCCAGTACGTGATGCCGGAAGAAGGCCGACG
AGATCGTGGTGCGCATGCTGAAGAAGGATGCGGCCGAGCGCATCAAGCTGCTGCG
CGAGTCGACCAACCCGAGGCGCAGTTCCTGTGGGCGGTGTTCCGCGACGTGTTCC
ACTACATCGCCGTCTACCTGGAGCAGATCGCAGGCTCCGCCCGGACATCGACCTG
GCGATCCGCTGGGGCTTCGGCTGGAACCTCGGGTCCGTTGAAAGACTGGCAGTCGGC
CGGCTGGAAGCAGGTGGCCGAGTGGGTCAAGGAAGACGTGGAAGCCGGCAAGGC
GCTGTGCGCCGCGCCGCTGCCGGCATGGGTATTGAGGGCCCGGTGGCAGAGAAC
CAGGGCGTGACGCGCTGCCGGTTCGTGGTCCGCGGCGACGCAGTCTTTCGTGCG
GCGCAGCAAGCTGCCGGTGTACCAGCGCCAGGCATTCCGTGCCGCGATCAAGGGC
ACTGCCGCGCCGATCCGCGCAAGGCCGGCCGACCGTCAAGAGAACGACGCCG
TGCGCATCTGGGTGAGCGAAGGCCAGGACGACGTGCTGGTGGTCTCGTTCAAGAG
CAAGATGAACACCATCGGGCCGACGTGATCGACGGCCTGACCCGCGCCATCGACC
TGGCCGAAGCCGGCTACAAGGGGCTGGTGGTGTGGCAGCCGACTTCGCTGCAGCT
GGGCGCACCGGGTGGCCGTTCTCCGCCGGCGCCAACCTGGAAGCGGCCATGCC
GCCTTCATGATGGGCGGCGCCAAGGGCATCGAACCGTTCTGTAAGAGGTTCCAGG
ACGGCATGATGCGCGTGAAGTACGCCTCGGTGCCGGTGGTGTCCGCGGCGTCCGG
CATTGCGCTGGGCGGCGGCTGCGAGCTGATGCTGCATTGCGCTTCGCGCGTGGCCG
CGCTGGAGACGTATATCGGCCTGGTGAAGTGGGCGTGGGCTGGTGCAGGCGCCGG
CGGCGGCCTGAAGGAAGCCGCGCTGGCGGCCGCGCGCGGCGCAGGCCGCGGG
CAGCACCACATCCTGCAGTTCCTGACCAGCCGCTTCCAGAGCGCGGCCATGGCCAA
GGTCTCGGCCTCGGCGCTGGAAGCGCGCCAGATGGGCTACCTGCAGCCGTCCGACA
AGATCGTCTTCAACGTGCACGAGCTGCTGTACGTGGCGCAGAACGAAGTGCAGCGG
CTGGCCAGCGCCGGCTACCGCGCGCCGCTGCCGACGCTGGTCCCGGTGGCCGCGCCG
CTCGGGCATTGCCACCATCAAGGCATCGCTGGTCAATATGCGCGACGGCGGCTTTAT
CTCGACGCACGACTTCTGATCGCCAGCCGCATCGCCGAGGCGGTGTGCGGCGGGC
ACGTCGAGGCCGGCTCGCTGGTGAAGCGAGGACTGGCTGCTGGCGCTGGAGCGCAA
GGCCTTTGTGACCTGCTCGGCACCGGCAAGACGCAGGAGCGCATCATGGGCATGC
TGCAGACCGGCAAGCCGGTGCCTAACTAA

SEQ. ID13

paaJ, encodes 3 3-oxoadipyl-CoA thiolase PaaJ from *E. coli*. Locus name: JW1392

ATGCGTGAAGCCTTTATTTGTGACGGAATTCGTACGCCAATTGGTCGCTACGGCGG
GGCATTATCAAGTGTTCCGGGCTGATGATCTGGCTGCTATCCCTTTGCGGGAAGTCT
GGTGCGAAACCCGCGTCTCGATGCGGAGTGTATCGATGATGTGATCCTCGGCTGTG
CTAATCAGGCGGGAGAAGATAACCGTAACGTAGCCCGGATGGCGACTTTACTGGCG
GGGCTGCCGCAGAGTGTTCCGGGCACAACCATTAACCGCTTGTGTGGTTCCGGGCT
GGACGCACTGGGGTTTGCCGCACGGGCGATTAAAGCGGGCGATGGCGATTTGCTG
ATCGCCGGTGGCGTGGAGTCAATGTCACGGGCACCGTTTGTATGGGCAAGGCAGC
CAGTGCATTTTCTCGTCAGGCTGAGATGTTGATACCACTATTGGCTGGCGATTTGT
GAACCCGCTCATGGCTCAGCAATTTGGAAGTACAGCATGCCGAAACGGCAGAGA
ATGTAGCTGAACTGTAAAAATCTCACGAGAAGATCAAGATAGTTTTGCGCTACGCA
GTCAGCAACGTACGGCAAAAGCGCAATCCTCAGGCATTCTGGCTGAGGAGATTGTT
CCGGTTGTGTTGAAAAACAAGAAAGGTGTTGTAACAGAAATACAACATGATGAGCA
TCTGCGCCCGAAACGACGCTGGAACAGTTACGTGGGTAAAAGCACCATTTCTGTG
CCAATGGGGTGATTACCGCAGGCAATGCTTCCGGGGTGAATGACGGAGCCGCTGC
GTTGATTATTGCCAGTGAACAGATGGCAGCAGCGCAAGGACTGACACCGCGGGCG
CGTATCGTAGCCATGGCAACCGCCGGGGTGAACCGCGCCTGATGGGGCTTGGTCC
GGTGCCTGCAACTCGCCGGGTGCTGGAACGCGCAGGGCTGAGTATTCAGATATGG
ACGTGATTGAACTGAACGAAGCGTTCGCGGCCAGGCGTTGGGTGTAACGCGAA
TTGGGGCTGCCTGATGATGCCCCACATGTTAACCCCAACGGAGGCGCTATCGCCTTA
GGCCATCCGTTGGGAATGAGTGGTGCCCGCCTGGCACTGGCTGCCAGCCATGAGCT
GCATCGGCGTAACGGTCGTTACGCATTGTGCACCATGTGCATCGGTGTCGGTCAGG
GCATCGCCATGATTCTGGAGCGTGTGTTGA

SEQ. ID14

davA, encodes 5-aminopentanamidase DavA from *Pseudomonas putida*. Locus name: PP_0382. The shown sequence was codon-optimised by Biomatik Corp.

CGGGCCGATCGCCCTGGCGGATTGAGACAAGGAGGCACCATGCGCATCGCTCTGTA
CCAGGGCGCACCCAAGCCACTGGATGTGCCCGGCAACCTGCAACGGCTGCGCCACC
AGGCGCAGCTGGCAGCCGAACGCGGCGCACAGTTGCTGGTGTGCCCGGAGATGTT
CCTGACCGGCTACAACATCGGCCTGGCCCAGGTTCGAGCGCCTGGCCGAGGCCGCCG
ATGGCCCGGCAGCCATGACCGTGGTAGAGATCGCCAGGCGCACCGCATCGCCATT
GTCTATGGCTACCCGGAGCGCGGTGACGACGGGGCGATCTACAACAGCGTGCAGTT
GATCGATGCGCATGGCCGAGCCTGAGCAATTACCGCAAGACGCACCTGTTCCGGTG
AACTGGACCGCTCGATGTTCCAGCCCTGGTGC GGACCACTTCCCGGTGGTGAACTG
GAAGGCTGGAAGGTTGGCCTGCTGATCTGCTACGACATCGAGTTCCCGGAGAACGC
CCGACGCCTAGCGCTGGACGGCGCCGAGCTGATCCTGGTGCCGACGGCGAACATG
ACGCCGTACGACTTTACCTGCCAGGTGACCGTGAGAGCGAGGGCACAGGAAAACC
AGTGCTACCTGGTATATGCCAACTACTGCGGTGCGGAAGACGAGATTGAGTATTGC
GGCAGAGCAGCATCATCGGCCCGGATGGCAGCTTGCTGGCCATGGCCGGGCGGG
ATGAGTGCCAGTTGTTGGCAGAGCTTGAACATGAGCGGGTGGTGCAGGGGCGCAC
GGCGTTTCCCTACCTGACCGATTTGCGCCAGGAGCTGCACCTGCGTAAAGGCTGA

SEQ. ID15

davB, encodes L-lysine 2-monooxygenase DavB from *Pseudomonas putida*. Locus name: PP_0383. The shown sequence was codon-optimised by Biomatik Corp.

```
ATGAACAAGAAGAACCGCCACCCCGCCGACGGCAAGAAGCCGATCACCATTTTCGG
CCCGGACTTCCCTTTTGCTTCGACGACTGGCTGGAACACCCGGCAGGCCTGGGCAG
CATTCCGGCTGAGCGCCATGGGGAAGAGGTGGCCATTGTCGGTGCCGGTATCGCCG
GCCTGGTAGCGGCCTACGAGCTGATGAAGCTGGGCCTCAAGCCGGTGGTGTACGA
GGCTTCCAAGCTGGGCGGCCGGCTGCGCTCGCAAGCCTTCAATGGCACTGACGGGA
TCGTTGCCGAACTGGGTGGCATGCGCTCCCGGTGTCGTCCACCGCCTTCTACCACT
ACGTCGACAAGCTGGGCCTGGAACCAAGCCCTTCCCAACCCGCTGACCCCGGCTT
CGGGCAGCACGGTGATCGACCTGGAAGGCCAGACCTACTACGCCGAGAAGCCCAC
CGACCTGCCACAACCTGTTTCATGAGGTAGCCGACGCCTGGGCCGATGCGCTGGAGA
GCGGTGCGCAGTTCGCCGATATCCAGCAGGCCATCCGCGACCGTGATGTACCGCGC
CTGAAGGAACTTTGGAACAAGCTGGTGCCGCTGTGGGACGACCGCACCTTCTACGA
CTTCGTGCGCACCTCGCGCTCTTTTGCCAAGCTGAGCTTCCAGCACCGCGAAGTGTT
GGCCAGGTTCGTTTCGGCACCGGCGGTTGGGACTCGGACTTCCCAACTCGATGCT
GGAAATCTTCCGCGTGGTGATGACCAACTGCGACGACCACCAGCACCTGGTGGTGC
GGGGCGTGGAACAAGTGCCACAAGGCATCTGGCGCCACGTACCGGAACGCTGCGT
GCATTGGCCAGAGGGCACCAAGCCTGAGCACGCTGCATGGCGGCGCACCGCGTACC
GGTGTCAAGCGCATTGCCCGCGCCTCCGATGGCCGCTGGCGGTACCGACAACCTG
GGGCGATACCCGCCACTACAGCGCAGTACTCGCCACCTGCCAGACCTGGTTGCTGA
CCACCCAGATCGACTGCGAAGAATCGCTGTTCTCGCAAAAGATGTGGATGGCCCTG
GACCGTACCCGCTACATGCAGTCGTGAAAACCTTCGTCATGGTTCGACCGCCGTT
TGGAAGGACAAGGACCCGGAAACCGGCCGTGACCTGCTGAGCATGACCCTCACCG
ATCGCCTCACCCGCGGCACTTACCTGTTTCGACAACGGCAACGACAAGCCCGGGGTG
ATCTGCCTGTCATACTCGTGGATGAGCGACGCGCTGAAGATGCTGCCGCACCCGGT
GGAGAAGCGCGTACAACCTGGCCCTGGATGCGCTGAAGAAGATCTACCCGAAGACC
GATATCGCCGGCCACATCATCGGCGACCCGATCACGGTTTCCTGGGAGGCCGACCC
GTACTTCCTCGGCGCCTTCAAAGGCGCGCTTCCGGGCCATTACCGCTACAACCAGCG
CATGTACGCGCACTTCATGCAGCAGGACATGCCGGCAGAGCAGCGCGGTATCTTCA
TTGCTGGTGACGACGTGTCATGGACCCCGCCTGGGTTGAAGGCGCGGTGCAGACG
TCGCTGAATGCAGTGTGGGTATCATGAACCACTTTGGTGGCCACACCCACCCCGAC
AACCCGGGCCCCGGGCGATGTGTTCAACGAAATCGGCCCGATCGCCCTGGCGGATTG
A
```

SEQ. ID16

lysC_{CG}, encodes aspartate kinase AK from *Co. glutamicum*. Locus name: Cgl0251. The shown sequence was codon-optimised by Biomatik Corp.

```
GTGGCCCTGGTCGTACAGAAATATGGCGGTTCTCGCTTGAGAGTGCGGAACGCAT
TAGAAACGTCGCTGAACGGATCGTTGCCACCAAGAAGGCTGGAATGATGTCGTGG
TTGTCTGCTCCGCAATGGGAGACACCACGGATGAACTTCTAGAATTGCAGCGGCA
GTGAATCCCGTTCCGCCAGCTCGTGAAATGGATATGCTCCTGACTGCTGGTGAGCGT
ATTTCTAACGCTCTCGTCGCCATGGCTATTGAGTCCCTTGCGCAGAAGCCCAATCTT
TCACGGGCTCTCAGGCTGGTGTGCTCACACCGAGCGCCACGGAAACGCACGCATT
GTTGATGTCACTCCAGGTCGTGTGCGTGAAGCACTCGATGAGGGCAAGATCTGCAT
TGTTGCTGGTTTCCAGGGTGTTAATAAAGAAACCCGCGATGTCACCACGTTGGGTCG
TGGTGGTTCTGACACCACTGCAGTTGCGTTGGCAGCTGCTTTGAACGCTGATGTGTG
TGAGATTTACTCGGACGTTGACGGTGTGTATACCGCTGACCCGCGCATCGTTCCTAA
TGCACAGAAGCTGGAAAAGCTCAGCTTCGAAGAAATGCTGGAACCTTGCTGCTGTTG
GCTCCAAGATTTTGGTGCTGCGCAGTGTTGAATACGCTCGTGCATTCAATGTGCCAC
TTCGCGTACGCTCGTCTTATAGTAATGATCCCGCACTTTGATTGCCGGCTCTATGGA
GGATATTCCTGTGGAAGAAGCAGTCCTTACCGGTGTCGCAACCGACAAGTCCGAAG
CCAAAGTAACCGTTCTGGGTATTTCCGATAAGCCAGGCGAGGCTGCGAAGGTTTTT
CGTGCGTTGGCTGATGCAGAAATCAACATTGACATGGTTCTGCAGAACGTCTCTTCT
GTAGAAGACGGCACCAACCGACATCACCTTACCTGCCCTCGTTCGACGGCCGCCGC
GCGATGGAGATCTTGAAGAAGCTTCAAGTTCAAGGCAACTGGACCAATGTGCTTTA
CGACGACCAGGTCGGCAAAGTCTCCCTCGTGGGTGCTGGCATGAAGTCTACCCAG
GTGTTACCGCAGAGTTCATGGAAGCTCTGCGCGATGTCAACGTGAACATCGAATTG
ATTTCCACCTCTGAGATTCGATTTCCGTGCTGATCCGTGAAGATGATCTGGATGCTG
CTGCACGTGCATTGCATGAGCAGTTCAGCTGGGCGGCGAAGACGAAGCCGTCGTT
TATGCAGGCACCGGACGCTAA
```

SEQ. ID17

ddh_{CG}, encodes *m*-diaminopimelate dehydrogenase DAPDH from *Co. glutamicum*. Locus name: Cgl2617.

ATGACCAACATCCGCGTAGCTATCGTGGGCTACGGAAACCTGGGACGCAGCGTCGA
AAAGCTTATTGCCAAGCAGCCCGACATGGACCTTGTAGGAATCTTCTCGCGCCGGG
CCACCCTCGACACAAAGACGCCAGTCTTTGATGTCGCCGACGTGGACAAGCACGCC
GACGACGTGGACGTGCTGTTCTGTGCATGGGCTCCGCCACCGACATCCCTGAGCA
GGCACC AAAGTTCGCGCAGTTCGCCTGCACCGTAGACACCTACGACAACCACCGCG
ACATCCCACGCCACCGCCAGGTCATGAACGAAGCCGCCACCGCAGCCGGCAACGTT
GCACTGGTCTCTACCGGCTGGGATCCAGGAATGTTCTCCATCAACCGCGTCTACGCA
GCGGCAGTCTTAGCCGAGCACCAGCAGCACACCTTCTGGGGCCCAGGTTTGTACA
GGGCCACTCCGATGCTTTGCGACGCATCCCTGGCGTTCAAAGGCAGTCCAGTACA
CCCTCCCATCCGAAGACGCCCTGGAAAAGGCCCGCCGCGGCGAAGCCGGCGACCTT
ACCGGAAAGCAAACCCACAAGCGCCAATGCTTCGTGGTTGCCGACGCGGCCGATCA
CGAGCGCATCGAAAACGACATCCGCACCATGCCTGATTACTTCGTTGGCTACGAAGT
CGAAGTCAACTTCATCGACGAAGCAACCTTCGACTCCGAGCACACCGGCATGCCACA
CGGTGGCCACGTGATTACCACCGGCGACACCGGTGGCTTCAACCACACCGTGGAAT
ACATCCTCAAGCTGGACCGAAACCCAGATTTACCGCTTCCTCACAGATCGCTTTCG
GTCGCGCAGCTCACCGCATGAAGCAGCAGGGCCAAAGCGGAGCTTTCACCGTCCTC
GAAGTTGCTCCATACCTGCTCTCCCCAGAGAACTTGGACGATCTGATCGCACGCGAC
GTCTAA

SEQ. ID18

lysC^{A279T}_{CG} encodes a feedback-resistant A279T mutant of aspartate kinase AK from *Co. glutamicum*. Original locus name: Cgl0251. The shown sequence was codon-optimised by Biomatik Corp.

```
ATGGCCCTGGTCGTACAGAAATATGGCGGTTCTCGCTTGAGAGTGCGGAACGCAT
TAGAAACGTCGCTGAACGGATCGTTGCCACCAAGAAGGCTGGAATGATGTCGTGG
TTGTCTGCTCCGCAATGGGAGACACCACGGATGAACTTCTAGAATTGCAGCGGCA
GTGAATCCC GTTCCGCCAGCTCGTGAAATGGATATGCTCCTGACTGCTGGTGAGCGT
ATTTCTAACGCTCTCGTCGCCATGGCTATTGAGTCCCTTGCGCAGAAGCCCAATCTT
TCACGGGCTCTCAGGCTGGTGTGCTCACACCGAGCGCCACGGAAACGCACGCATT
GTTGATGTCACTCCAGGTCGTGTGCGTGAAGCACTCGATGAGGGCAAGATCTGCAT
TGTTGCTGGTTTCCAGGGTGTTAATAAAGAAACCCGCGATGTCACCACGTTGGGTCCG
TGGTGGTTCTGACACCACTGCAGTTGCGTTGGCAGCTGCTTTGAACGCTGATGTGTG
TGAGATTTACTCGGACGTTGACGGTGTGTATACCGCTGACCCGCGCATCGTTCCTAA
TGCACAGAAGCTGGAAGCTCAGCTTCGAAGAAATGCTGGAATTGCTGCTGTTG
GCTCCAAGATTTTGGTGTGCGCAGTGTTGAATACGCTCGTGCATTCAATGTGCCAC
TTCGCGTACGCTCGTCTTATAGTAATGATCCCGGCACCTTGATTGCCGGCTCTATGGA
GGATATTCCTGTGGAAGAAGCAGTCCTTACCGGTGTCGCAACCGACAAGTCCGAAG
CCAAAGTAACCGTTCTGGGTATTTCCGATAAGCCAGGCGAGACTGCGAAGGTTTTCC
GTGCGTTGGCTGATGCAGAAATCAACATTGACATGGTTCTGCAGAACGTCTCTTCTG
TAGAAGACGGCACCACCGACATCACCTTACCTGCCCTCGTTCGACGGCCGCCGCG
CGATGGAGATCTTGAAGAAGCTTCAGGTTCCAGGGCAACTGGACCAATGTGCTTTAC
GACGACCAGGTCGGCAAAGTCTCCCTCGTGGGTGCTGGCATGAAGTCTCACCCAGG
TGTTACCGCAGAGTTCATGGAAGCTCTGCGCGATGTCAACGTGAACATCGAATTGAT
TTCCACCTCTGAGATTTCGATTTCCGTGCTGATCCGTGAAGATGATCTGGATGCTGCT
GCACGTGCATTGCATGAGCAGTTCAGCTGGGCGGCGAAGACGAAGCCGTCGTTTA
TGCAGGCACCGGACGCTAA
```

SEQ. ID19

dapA_{CG} encodes the feedback-resistant 4-hydroxy-tetrahydrodipicolinate synthase DHDPR from *Co. glutamicum*. Locus name: Cgl1971.

```
ATGAGCACAGGTTTAAACAGCTAAGACCGGAGTAGAGCACTTCGGCACCGTTGGAGT
AGCAATGGTTACTCCATTCACGGAATCCGGAGACATCGATATCGCTGCTGGCCGCG
AAGTCGCGGCTTATTTGGTTGATAAGGGCTTGGATTCTTTGGTTCTCGCGGGCACCA
CTGGTGAATCCCCAACGACAACCGCCGCTGAAAACTAGAAGTCTCAAGGCCGTT
CGTGAGGAAGTTGGGGATCGGGCGAAGCTCATCGCCGGTGTGCGAACCAACAACA
CGCGGACATCTGTGGAAGTTGCGGAAGCTGCTGCTTCTGCTGGCGCAGACGGCCTT
TTAGTTGTAAGTCTTATTACTCCAAGCCGAGCCAAGAGGGATTGCTGGCGCACTTC
GGTGCAATTGCTGCAGCAACAGAGGTTCCAATTTGTCTCTATGACATTCCTGGTCGG
TCAGGTATTCCAATTGAGTCTGATACCATGAGACGCCTGAGTGAATTACCTACGATT
TTGGCGGTCAAGGACGCCAAGGGTGACCTCGTTGCAGCCACGTCATTGATCAAAGA
AACGGGACTTGCCTGGTATTCAGGCGATGACCCACTAAACCTTGTGGCTTGCTTT
GGGCGGATCAGGTTTCATTTCCGTAATTGGACATGCAGCCCCACAGCATTACGTGA
GTTGTACACAAGCTTCGAGGAAGGCGACCTCGTCCGTGCGCGGGAAATCAACGCCA
AACTATCACCGCTGGTAGCTGCCCAAGGTCGCTTGGGTGGAGTCAGCTTGGCAAAA
GCTGCTTCGCGTCTGCAGGGCATCAACGTAGGAGATCCTCGACTTCCAATTATGGCT
CCAAATGAGCAGGAAGTGTGAGGCTCTCCGAGAAGACATGAAAAAGCTGGAGTTCT
ATAA
```

SEQ. ID20

orf26 encodes the 4-aminobutyryl-CoA ligase ORF26 *Streptomyces aizunensis*. Locus tag: AY899214.1. The shown sequence was codon-optimised by Biomatik Corp.

```
ATGGGCAGCAGCCATCATCATCATCATCACAGCAGCGGCCTGGTGCCGCGCGGCAG
CCATATGCGCCAATGACCGCTAAAATCTTCGCCGTCGACTCCGTCCGTCCGATCGA
CGAGTTTGAGCAGGACGCACTGCGCGTTGCGGATGTGATTTCGCGAACGTGGCGTGT
GTCTGGGTGACCGTGTGATGTTGAAGGCGGGCAACAGCGCGTCGTACGTTTTCGTT
TTGTATGCGCTGATGCACATCGGTGCGAGCATCGTTTTGGTCGATCAGCAAGAGCAT
AAAGAGGAAACCCGTCGTATCGCGCTGCGTACCGGCGTAAAAGTCACGTTTGTGGA
TGATGAAACCCCGATTGATCAAGATGCGGACCCGATTCACCTGTACGAGCTGATGG
TGGCTACCCAGAACCGTCCTCCGATGGACAGCGCACTGAGCTTCGACGCGTGGGGT
GAACTGTCTGACGGTCTGATTATGTGGACGAGCGGCAGCACCGGTAGCCCGAAGG
GTGTCGTGAAGAGCGGTGGTAAATTCCTGGCGAATCTGCGCCGTAACGCGCATCAA
GTGGGTATCGTCCGGATGACGTGCTGATGCCGCTGCTGCCGTTTCGCGCACCAAGTA
CGGTCTGTCTATGGTGCTGATTGCATGGCTGACGCGCTGCTCCCTGGTTATTGCGCC
ATACCGCCGTCTGGATCGTGCTTTGCGTATGGCCCGTGACAGCGGCACGACCGTTAT
CGATGCCACGCGGAGCAGCTATCGCAGCATCCTGGGCCTGGTCACGCGTAAACCGG
CCCTGCGTGACACCTGGCCGGCACCCGCATGTTCTGTGTGGGCGCAGCGCCGTTG
GATGCGCCGCTGGTCGAAAGCTACGTTCAAGAGTTTGGTCTGCCGCTGTTGGACAG
CTATGGTTCTACCGAGCTGAACAATATCGCTTTTCGCGACCCTGGATAATCCGTTTTCC
TGTGGTCGCGCAATGGAAGGTATCGGTCTGCGTATTGTTGACGAAGATGGTCGTGA
AGTTGCGGCAGGCCAACCGGGCGAAATCGAGGTTGACACTCCGGATGCCCTGGAG
GGTCAAATCGCCGAGGATGGTAGCATTATCCGGCACCGACCGGCTGGCAGCGTAC
GGGCGATCTGGGTCACTTGGACGCCGACGGCAACCTGTATGTCCTGGGTGCGTAAGT
TTGCGGTCCACCGCATGGGTTATACTTTGTACCCAGAGCTGATTGAGCGCAAAGTG
GCCGCTGAGGGCTGCCCGACCCGCATTGTTCCGCTGCCGGACGAGCTGCGTGGTAG
CCAATGGTCTTTTTTCGTGGAAGATGATGAACAGCGTGACGCAGGTTACTGGCGTG
AACGTCTGTGCGGTTTGTGCGCGGCTTCGAGCAGCCGAACAAGGTGGTCGTTCTG
GAGCAGTTTCTCTGAATCGCAATGGCAAGCCGGACAAGAAAGAGCTGACCCGTAT
GGCGGCAGAATGA
```

SEQ. ID21

caiC encodes the Crotonobetaine/carnitine--CoA ligase CaiC from *E. coli*. Locus tag: JW0036

ATGGATATCATTGGCGGACAACATCTACGTCAAATGTGGGACGATCTTGCGGACGT
TTACGGTCATAAAACGGCGCTGATTTGTGAATCCAGCGGCGGAGTCGTTAACCGGT
ATAGTTATCTTGAGTTAAATCAGGAGATTAACCGCACGGCAAACCTGTTTTATACGC
TGGGGATTGCAAAGGCGACAAGGTTGCACTACATCTCGACAACCTGCCCGGAATTT
ATCTTTTGCTGGTTCGGGCTGGCAAAAATTGGCGCGATTATGGTGCCGATTAACGCC
CGCCTGTTGTGCGAGGAAAGCGCGTGGATCCTGCAAATAGCCAGGCGTGCCTGCT
GGTGACCAGTGCGCAATTCTATCCTATGTATCAACAGATTCAGCAGGAAGATGCCAC
TCAATTGCGGCACATTTGCCTGACAGATGTGGCACTTCCCGCTGATGATGGCGTGAG
TTCGTTTACTCAACTGAAAAATCAACAACCTGCCACCTTGTGCTATGCACCGCCGCTA
TCGACTGACGATACGGCGGAAATTCTTTCACCTCCGGCACCACCTCCCGACCGAAA
GGTGTGGTGATTACCCATTACAACCTGCGCTTCGCTGGATATTACTCCGCTGGCAG
TGTGCACTGCGTGACGATGACGTCTACCTGACGGTAATGCCTGCGTTTCATATCGAT
TGCCAGTGTACTGCGGCGATGGCGGCGTTTTCTGCCGGGGCCACCTTTGTGCTGGTC
GAGAAATACAGCGCCCGCGCCTTCTGGGGACAGGTACAGAAGTACCGCGCCACCGT
TACCGAATGTATTCCGATGATGATCCGTACGTTGATGGTACAGCCGCCTTCAGCGAA
CGATCAGCAACACCGCCTGCGGGAAGTGATGTTTTATCTCAACTTGTGCGGAGCAGG
AAAAAGATGCGTTTTGTGAACGCTTCGGCGTTCGCTTGCTGACGTCTTATGGGATGA
CGGAAACCATTGTGGGCATTATCGGCGATCGTCCTGGCGATAAACGACGCTGGCCG
TCGATTGGTCGGGTGGGGTTTTGCTACGAAGCGGAGATCCGCGACGATCACAATCG
CCCGCTCCCGGCTGGTGAGATCGGTGAAATCTGCATTAAGGCATACCTGGGAAAA
CCATCTTCAAAGAGTACTTTCTCAACCCACAAGCCACTGCGAAAGTGCTGGAAGCCG
ATGGCTGGCTGCATACCGGCGATACCGGATACCGCGACGAAGAGGACTTTTTTTATT
TCGTGATCGCCGCTGCAATATGATTAACGTGGCGGCGAGAATGTCTCCTGCGTG
GAGCTGGAAAATATTATCGCCGCGCACCCGAAAATTCAGGACATCGTGGTTGTGGG
TATTAAGATTCGATTCGCGATGAAGCCATCAAAGCATTTGTGGTGCTGAATGAAG
GTGAAACATTGAGCGAAGAGGAATTTTTCCGCTTCTGCGAACAAAATATGGCGAAA
TTTAAAGTGCCTCTTATCTGGAGATCAGAAAAGATCTGCCACGTAATTGCTCGGGG
AAAATAATTAGAAAGAATCTGAAATAA

SEQ. ID22

chnR encodes Xyls/AraC-type transcriptional activator ChnR in *Acinetobacter* sp. Locus tag: AB006902.3. The shown sequence was codon-optimised by Biomatik Corp.

```
ATGAGCACAGACAAAGCAAATACGCTGATCAAACCCGAAGATGTCGTGTTATGGAT
TCCGGGTAATGTCACAATTGACAGCATGAATGCCGGTTGGGAAAACATTGCAATCA
GAGGGTACGAATATACCAACCTCGATGTGCATATTCCTGCCATGCGTGACTACATGA
TCGTCAACTATAAAAAAAGTGCGGCGGAAATGCGTAGAAAAGGCGATGCCTCTTG
GATACCCAAGTGGTTAAGCCGGGTTATGTCTCCTTGTGACCTGTGGTGAAGATTCC
CGCTGGGCGTGGAATGACCATATTGCCGTCACCCATGTCTACATTTGCGATGACTCC
ATCACCTCAATGGCGAATAAGGTGTTTGATTATGATATCGCTTCGATCCGAATCAGA
GACGAAGTCGGTGTGGAAGATCATGTTTTACCTGCTCTGACTTCACTTTTAGAACTA
GAATTAAGCAAGGTGGTTTAGGTGGAAACCTGTATTTAGAGAGCATTAAAAACCA
GATCGCCCTGCATTTACTCCGTCAGTATGCCAAATTAGATTTAAGGAAGGACAGTG
CCGTTCTGGTTTTACTCCCCTACAACGCAGACTGTTATTAGAATTTATCAATGAAAC
ATGAGCATTAAAATTACCCTCGAAGATTTAGCGGGATTAGTCAAGATGAGCGTGCCT
CATTTAATGAGAAAATTTAAAGTCGATTTTGGTAATTCCTGCTGCCTACATCATGA
ATCTCAGGGTGCAATTTGCTAAACGTTTGCTCACTTCAAAAAAAGAAATCCACTGA
AAGTGATTGCCAGTGAAGCCGGTTTTTGGGATCAGAGCCATATGACCCGAGTATTC
AAAAATTTTTTGGGAAAACACCCATCGAAATCAGACAGGAACACACCAATCTCGTGT
CTGAAAATTCAGTCTCCTCTATTGTTTTTTGA
```

SEQ. ID23

P_{ChnB} is the promoter for *chnB* in *Acinetobacter* sp. Locus tag: AB006902.1.

GATAATCTCCATTACGACATGTGAATTTATTCAAATCTGCAGTGCTGGTTATTCATT
GCTGATTAATAGCATTGCTTATTCATTGAATAAAGAATCGCAGGAATGCAATCACAA
GGCTTGGATGGGGTGAACCTAAAAATTGTACATAATGATCATTGTAGAAAAAAAC
AAACTCCAAATAAAAAATTCTATTTTTATTGTAATCTTATGTTTTAATTAATAATATAT
TTATATATTGTATGTTTTATTTGCATTGAACAATTTGTCATTCGTGTTGGAATAACT
TAAATTTTTAATCCTAGCCCCGAGAGGGCTAGGATTACCTAAAAATAAAAAATCG
AAGAGTTAAATCTTTCAACGATTTGGGTAAGTATCCAAACAATCTCTTTAGTT
GCAAGCTTCTTCATCTGCTAGAAAGAAGGGAAATGGGAAACCTCTCCTTGAAGTG
ATTAGACTTACATATTCGGATAGTTTGGACCACCACCACC